Robust Computational Frameworks for Power Grid Reliability, Vulnerability and Resilience Analysis

Thesis submitted in fulfilment of the requirements of the University of Liverpool for the degrees
of Doctor of Philosophy in Engineering

by

Roberto Rocchetta

B.Eng, Energy Engineering
M.Sc(Eng), Energy Engineering
MRes(Eng), Decision Making Under Risk and Uncertainty

Supervised by
Prof. Edoardo Patelli (primary)
Dr. Matteo Broggi (secondary)
Prof. Dr. Sven Schewe (secondary)

November 2018

Acknowledgement

The author would like to acknowledge the gracious support of this work through the EPSRC and ESRC Centre for Doctoral Training on Quantification and Management of Risk & Uncertainty in Complex Systems & Environments Grant number (EP/L015927/1).

I would like acknowledge the kind participation to this work of the industrial group ARAMIS srl, the academic research group LASAR at Politecnico Milano and the Risk Engineering Lab at Institute of Energy Technology in ETH, Zurich. I spent overall 7 months visiting/placement during my PhD years.

Finally, the author would like to point out that the article "*On-line Bayesian Model Updating for Structural Health Monitoring*" which have been recently published in the Journal *Mechanical Systems and Signal Processing* and is co-authored by E. Patelli, M. Broggi and Q. Huchet has not been included in this dissertation. Unfortunately, due to lack of space and little adherence to the power grid topic we decided to remove this journal publication from the thesis body.

Special Thanks

I wish to thank my primary supervisor Edoardo Patelli and all the other supervisors and academic/industrial partners for their valuable help and support during this project. I also want to express my gratitude to my relatives and to all my friends. A very special thank goes to my mother, Elisabetta, for helping me and hosting me when I was back in Italy. A big thank you goes to my dad, Bruno, for the numerous lunches and dinners together and for its valuable assistance in sending and fixing bikes. I thank my 'little' brother, Tobia, and my grandmother Maria. She is always saying that she misses me so much, and I miss her too. Also, thank you to all my friends from Italy (too many to name them all) Arturo, Manuel, Matteo, Martino, Riccardo, Laura, Giulia, Luca, Andrea and all the guys from Liverpool. Finally, a big thanks to Petra, for all the nice time spent together, good experiences, her kindness and for staying the closest to me during those years.

Declaration

I declare that this thesis was composed by myself and that the results contained herein have not been submitted for any other degree or professional qualification. I confirm that the work submitted is mine, except where it forms part of a jointly-authored publication. In which case, my contribution and the names of the other authors have been explicitly indicated below. I confirm also that appropriate credit is given where reference is made to others' work and that the thesis contains 202 pages, 56 figures, and 29 tables.

I declare that the Chapter 4 of this dissertation has been recently published in the Journal *Applied Mathematical Modelling* as "*Do we have enough data? Robust reliability via uncertainty quantification*" co-authored by E. Patelli (my primary supervisor) and M. Broggi (my secondary supervisor) and it is an extension of a work initially developed during the MRes in Decision Making Under Uncertainty successfully completed at the University of Liverpool.

The Chapter 5 has been accepted for publication in the *International Journal of Electric Power and Energy Systems* as "*Assessment of power grid vulnerabilities accounting for stochastic loads and model imprecision*" with co-authors, E. Patelli (primary supervisor).

Chapter 6 has been published in the Journal *Allied Energy* as "*A power-flow emulator approach for resilience assessment of repairable power grids subject to weather-induced failures and data deficiency*" with co-authors, E. Zio (Academic Advisor) and E. Patelli (primary supervisor) and E. Zio (academic partner). This is the final result of a secondment period at the Politecnico di Milano under direct supervision of Professor Enrico Zio.

Chapter 7 summarise the results carried out during 1 month visiting to the Reliability and Risk Engineering Lab, Institute of Energy Technology, at ETH Zurich. This work has been recently published with title "*Effect of Load-Generation Variability on Power Grid Cascading Failures*" in the proceeding of the annual European Safety and Reliability Conference, ESREL, held in Trondheim 2018, co-authored by Li Bing,

Giovanni Sansavini and Edoardo Patelli. In the next months we are planning to extend the works presented in chapter 7 targeting a high quality journal publication.

Finally, Chapter 8 summarise a work developed in the ARAMIS s.r.l. group. This work has been recently published in the proceedings of the workshop Reliable Engineering Computing (REC 2018) as "*A Reinforcement Learning Framework for Optimisation of Power Grid Operations and Maintenance*", co-authored by Michele Compare, Edoardo Patelli and Enrico Zio. A refined version of this work has been recently accepted for publication in the international journal Applied Energy (Volume 241, 1 May 2019, Pages 291-301).

1^{st} November 2018

List of Publications

Peer-reviewed Journal Publications

1. Roberto Rocchetta, Matteo Broggi, and Edoardo Patelli. Do we have enough data? robust reliability via uncertainty quantification. *Applied Mathematical Modelling*, 54(Supplement C):710 – 721, 2018

2. Roberto Rocchetta and Edoardo Patelli. Assessment of power grid vulnerabilities accounting for stochastic loads and model imprecision. *International Journal of Electrical Power & Energy Systems*, 98:219 – 232, 2018

3. Roberto Rocchetta, Enrico Zio, and Edoardo Patelli. A power-flow emulator approach for resilience assessment of repairable power grids subject to weather-induced failures and data deficiency. *Applied Energy*, 210:339 – 350, 2018

4. Roberto Rocchetta, Matteo Broggi, Quentin Huchet, and Edoardo Patelli. On-line bayesian model updating for structural health monitoring. *Mechanical Systems and Signal Processing*, 103:174 – 195, 2018

5. R. Rocchetta, L. Bellani, M. Compare, E. Zio, and E. Patelli. A reinforcement learning framework for optimal operation and maintenance of power grids. *Applied Energy*, 241:291 – 301, 2019

Peer-reviewed Conference Publications

1. R. Rocchetta, M. Broggi, and E. Patelli. Efficent epistemic-aleatory uncertainty quantification: Application to the nafems challenge problem. In *NAFEMS World Congress 2015, At San Diego, CA*, 2015

2. R. Rocchetta and E. Patelli. A simulation-based probabilistic risk assessment of electric vehicles control strategies accounting for renewable energy sources. In *13th International Probabilistic Workshop (IPW 2015)*, pages 183–198, Nov 2015

3. R. Rocchetta, M. Broggi, Q. Huchet, and E. Patelli. Likelihoods comparison in a bayesian updating procedure for fatigue crack detection. In *Safety and Reliability of Complex Engineered Systems (ESREL 2015)*, Sep 2015

4. R. Rocchetta and E. Patelli. Power grid robustness to severe failures: Topological and flow based metrics comparison. In *ECCOMAS Congress 2016 - Proceedings of the 7th European Congress on Computational Methods in Applied Sciences and Engineering*, volume 3, pages 6121–6135, 2016

5. R Rocchetta and E Patelli. Imprecise probabilistic framework for power grids risk assessment and sensitivity analysis. In *Risk, Reliability and Safety: Innovating Theory and Practice*, pages 2789–2796, 2016

6. R. Rocchetta and E. Patelli. An efficient framework for reliability assessment of power networks installing renewable generators and subject to parametric p-box uncertainty. In *Safety and Reliability. Theory and Applications (ESREL 2017)*. Taylor and Francs, 2017

7. R. Rocchetta and E. Patelli. Stochastic analysis and reliability-cost optimization of distributed generators and air source heat pumps. In *2017 2nd International Conference on System Reliability and Safety (ICSRS)*, pages 31–35, Dec 2017

8. R. Rocchetta, E. Patelli, B. Li, and G. Sansavini. Effect of load-generation variability on power grid cascading failures. In *European Safety and Reliability Conference (ESREL 2018)*, 2018

9. R. Rocchetta, M. Compare, E. Patelli, and E. Zio. A reinforcement learning framework for optimisation of power grid operations and maintenance. In *workshop on Reliable Engineering Computing 2018*, 2018

10. O. Cangul, R. Rocchetta, E. Patelli, and M. Fahrioglu. Financially optimal solar power sizing and positioning in a power grid. In *2018 IEEE International Energy Conference (ENERGYCON)*, pages 1–6, June 2018

11. E. Patelli, S. Tolo, H. G. Williams, J. Sadeghi, R. Rocchetta, M. de Angelis, and M. Broggi. Opencossan 2.0: an efficient computational toolbox for risk, reliability and resilience analysis. In *Proceedings of the joint ICVRAM ISUMA UNCERTAINTIES conference Florianopolis, SC, Brazil*, April 8-11 2018

Summary

The power grid was originally designed to forward electric power from large and isolated power production units to residential, commercial and industrial end-users. Due to recent trends such as the increasing allocation of uncertain in output renewable and broadly distributed generators (leading to a two-way flow of electricity, from isolated power production units to the grid and from the end-users to the grid) and environmental changes which are drifting weather scenarios towards extremes, the traditional grid design is radically changing. In order to respond promptly and safely to those important changes, reliability and resilience are becoming major concerns for the future power grid. Improve overall resilience of future infrastructures is of primary importance and, to do so, power grid computational models and associated frameworks for the system assessment have to be improved, better designed, robustly validated and updated. This is necessary to clearly understand which are the key factors affecting the system risk and which are the main hazards with the potential to undermine a reliable delivery of electric power. Enhance the future power grid reliability and resilience is paramount.

In the power grid literature, reliability is a well-defined concept and is sometimes referred to as the probability of power grid satisfactory operation over the long run. Similar to reliability, network vulnerability is a power grid security-related concept. If compared to power network reliability, vulnerability rather focuses on low-probability-high-consequence events and on assessing the inherent structural weaknesses and robustness of the power system. Differently, the concept of power grid resilience tries to merge both the reliability and vulnerability ideas in a unified assessment framework, but also further extending the scope of the analysis. The resilience concept has been recently introduced for power grids, although a generally accepted definition still has to be formulated. It is sometimes defined as '*the power grid ability to anticipate extraordinary, high-impact, low-probability scenarios, promptly reacting and quickly recovering from these disruptive events, reorganizing its structure and operation to mitigate the impact of similar events in the future*'. We believe that much research has to be carried out to provide a robust definition of network resilience and introduce a set of well-accepted metrics for resilience quantification and a standardized framework for its evaluation.

The Author's also belief is that a robust resilience framework should account for the following key concepts, which are extensively discussed in this dissertation:

1 Assure a robust quantification of all the relevant sources of uncertainty, which can be due to inherently variable inputs, small sample sizes (e.g. rare events), qualitative, vague and incomplete information (e.g. due to data protection, expert opinions or non-collaborative agents); (addressed in Chapters 2- 4 and in Ref. [131])

2 Distinguish between epistemic and aleatory uncertainty, therefore highlighting how much of the uncertainty on the resilience metric is reducible; (addressed in Chapters 2 and 4 and in Ref. [131])

3 Include an evaluation of structural vulnerability and the consequence of low-probability-high-consequence events such as multiple-components outages;(addressed in Chapter 5 and in Ref. [132])

4 Account for domino effects, cascading failures and weather effects (e.g. interdependencies weather-grid, weather-induced failures, delays, renewable production, etc); (addressed in Chapters 6- 7 and in Ref. [133]- [129])

5 Embed an economic component, i.e. should be usable in a cost-resilience optimisation; (addressed in Chapter 8 and in Ref. [121]- [24]- [127])

6 Should discern between different learning capabilities of different systems, i.e. given that a new piece of information is provided, a resilience metric should discern between systems which are capable of learning faster and better policies (i.e. minimising costs and maximising resilience); (addressed in Chapter 8 and [121])

Problems of uncertainty

Uncertainty affects complex systems, critical infrastructures and the simulation tools adopted for their analysis. For power grid systems, the problem of uncertainty is particularly interesting because of the many factors involved such as renewable sources, weather scenarios, etc. Uncertainty is affecting the power network in many ways. For instance, uncertainty affects the complex interaction between the network fundamental constituents (e.g. components and subsystems) and heterogeneous weather conditions, which can potentially trigger multiple failures, cascading outages, repairing crew delays and can alter the operative state of the system (e.g. the power produced by renewable energy sources, the electric heating load demand, etc.). Uncertainty is affecting simulation models, weather models and the collected data, thus, it has to be addressed consciously. A proper characterization and quantification of all the

relevant uncertainties is a necessary step to guarantee a high system resilience performance and at the same time assure economic gain for both grid operator and customers.

A review of the most recent and advanced uncertainty quantification methods is proposed in Chapter 2 and testing on 2 novel case study is proposed in Chapter 4.

Definition of quantitative metrics

Due to the complexity of the network and critical role played by the asset, it is generally not possible to check the power grid reliability trough analytical analysis or experimental testing. Commonly, the only viable way to evaluate and check the system safety is to rely on high-fidelity simulators, which are reproducing realistically all the relevant network behaviours. Once defined, power grid computational models can be then embedded within a resilience assessment framework, which is dedicated to the assessment of the grid performance in terms of safety, reliability and vulnerability. One of the critical steps to develop a resilience assessment framework is the definition of a robust and comprehensive quantitative resilience metric. Traditionally, reliability indices have been adopted as reference metrics, although they miss some of the key features of the resilience concept. Metrics for structural/topological vulnerability assessment have been recently introduced and provide a different perspective on the system security. Chapter 3 of this thesis proposes a state-of-the-art review of security-related concepts for the analysis of power grid (such as reliability, vulnerability, risk and resilience) as well as a review of power flow methods for a high-fidelity or approximated modelling and simulation of the system.

Topological vulnerability metrics provide a computationally efficient way of dealing with low-probability-high-consequence events and can be considered as additional metrics for measuring the system security (e.g. to be combined with traditional reliability metrics). In the Chapter 5 of this dissertation, we analyse classical and novel vulnerability metrics and reliability metrics, pointing out strength, weaknesses and similarities. The vulnerability metrics are generally computed adopting graph theoretical approaches to analyse topologically the network. This is done to try quantifying what are the consequences of severe contingencies on the system (e.g. terrorist threats, targeted attacks or extreme weather events). Uncertainty is indeed affecting these metrics and it has to be addressed through all the phases of the calculations.

Weather-driven effects, cascading failures and repairs

Nowadays, it is generally well-known that external environmental factors are intimately linked to the power grid operative behaviour and structure. High penetration of

weather-dependent renewable energy sources, seasonal variability in the electric heating and electric cooling of houses and commercial facilities, increasing penetration of electric mobility which usage pattern depends on human behaviour (also affected by the weather conditions) are few examples of how external environmental factors affect power grid operations and structure.
Furthermore, the vast majority of blackout events are caused by extreme weather phenomena such as, for instance, lightning strikes, extreme wind gusts, heavy wet snow, ice storms, trees branches and so on. To develop and improve realistic simulation frameworks for critical infrastructures, it is a necessity to consider and model extreme weather as well as weather-system interactions. A reliable indicator of the associated uncertainties should be also provided in the process.

Chapter 6 analyses the effect of weather-induced failures and repairs on power grids. It also introduces a computationally efficient framework for lack of data quantification on the coupled weather-grid model. Weather extremes are also known to have the potential to trigger severe cascading events and are extensively analysed. Cascading failures are dangerous failure mechanisms which can affect a large portion of the grid and, although several computational models for the assessment of cascading failure have been proposed, many do not account for relevant uncertainties. Uncertainty affects cascading failure models and one of the most prominent issues is the lack of statistical failure samples associated with large blackout events, undermining the validity of the cascading models to evaluate large cascading events. Chapter 7 of this dissertation further investigates the robustness of a realistic cascading failure model by analysing its sensitivity to variable and uncertain input factors.

Learning capability and optimal decision-making under uncertainty

Finally, to assure high resilience, the system should have a capacity to learn from past occurrences, i.e. some learning capabilities. The power grid should be able to efficiently, effectively and, if possible, autonomously process new data, information, events. New sensors and monitoring technologies, e.g. Prognostic Health Management devices, can enlarge the quantity of information gathered. Thus, equip the system with automatic learning capabilities could allow for a substantial improvement in existing operational routines, maintenance actions and decision policies in general. Reinforcement learning and agent-based learning frameworks offer an interesting opportunity to tackle this issue. For this reason, Reinforcement Learning framework for the optimization and maintenance and operations of power grid systems has been investigated in Chapter 8.

Research questions

Concluding this summary, the modelling aspect of the project proposed several challenges and posed a variety of research questions. The goal of this dissertation is to provide some answers to the following challenging questions:

- When the available information suffice to answer a basic reliability, vulnerability and resilience question?
- How to maintain computational tractability when advanced uncertainty quantification methods are adopted?
- What is the contribution of a good network topology and good operations in the overall power grid security?
- How to properly select quantitative metrics for reliability, vulnerability and resilience assessment?
- How to realistically model cascading failures and domino effects?
- How to model extreme environmental conditions and interaction to the power grid resilience? How these environmental conditions link to components failures?
- How to learn better policies when gathering new data from a stochastic system-environment?

Contents

List of Figures

List of Tables

Chapter 1

Introduction

1.1 Abstract

The power grid is one of the largest man-made critical infrastructures. It has been designed to distribute electric power from generating units to residential, commercial and industrial end-users. Due to the continuous increasing of electrical penetration, the availability and reliability of network is of paramount importance. In addition, the continuous increasing of renewable generators posed a further challenges to the stability of the network due to their dependencies on environmental changes, which are drifting weather scenarios towards extremes. Hence, resilience is becoming a major concern for the future power grid. In order to respond promptly to those important changes, the resilience of the such critical infrastructure has to be augmented. This can only be achieved with the availability of robust computational models that allow to design a better network, robustly validated and updated the results. Ideally, a computational framework for the assessment of power grid resilience should capture all the relevant physical interactions between components, subsystems and the system as a whole. Furthermore, uncertain and heterogeneous environmental factors have to be accounted for and their effect on safety-related metrics explicitly modelled and quantified. This is necessary to reveal power grid risks, hazards and identity situation for which an immediate safety and resilience enhancement is necessary. In this thesis, the existing power grid safety-related concepts (i.e. reliability, risk, vulnerability and resilience) and ancillary uncertainty quantification methods are analysed. The major weakness in existing quantification frameworks has been identified as the way a lack of data required by the frameworks and the treatment of such imprecise information. To overcome this limitation, a novel and robust methods for the uncertainty quantification in power grid safety-critical evaluations has been developed. The main contributions of this dissertation are a set of novel tools for the assessment of power grid reliability, vulnerability and resilience and accounting for a rigorous treatment of lack of data uncertainty. These methods have a limited need for artificial model assumptions, which might alter the quality of the available information and, with it, the validity of safety-critical decisions. One of the key elements for a resilient grid is the system ability to learn from past events, improving the grid structure, operations and policies. For this reason, a Reinforcement Learning framework for optimal decision-making under uncertainty has been investigated. This allows to equip the systems with learning capabilities, which is a fundamental component of the resilience concept, and it optimizes operation and maintenance decisions. The developed frameworks can be used to investigate the effect of threatening scenarios (such as extreme weather conditions, multiple contingencies and cascading events) on the grid safety performance. The validity of the approaches has been tested on scaled-down power grids and prognostic health management as well on realistic models of existing systems (e.g. the IEEE reliability test system). These tools provide a valuable contribution to the research community and industrial practitioners

as they can help to discern whether the available information suffices to answer a reliability, vulnerability or resilience related question. If the information is limited and additional data has to be gathered, the method informs the decision-maker with the most relevant and sensitive factors, i.e. a basic indication on where to start collecting data so that an expected reduction in uncertainty is maximised.

1.2 Context

Nowadays, complex systems and highly interconnected critical infrastructures are integrating part of our existence and of the society, we all live in. Safeguard their physical and functional integrity is uttermost important as these systems provide indispensable services to local industry and citizens. Virtual models and simulation tools offer a viable way to test the safety and reliability of the system, under the occurrence of threats and disturbances, in a protected digital environment.

Realistic (high-fidelity) simulators are necessary tools to test the system capacity to respond to unexpected events. The computational model (i.e. a digital copy of the real system) has to be verified and the outcomes of the analysis validated against historical data of the physical system. Ideally, a computational model should capture all the relevant physical interactions between system, subsystems, components and dynamic external environments where sub-systems are operated. Once a high-fidelity simulator of the physical system is generated, it has to be embedded within robust assessment frameworks aiming at evaluating the system robustness against contingency scenarios (e.g. reliability, vulnerability and resilience assessment frameworks). It goes without saying, the modelling part of the system is a challenging task on its own and attempt to embed the computational model within a broader, more general framework (e.g. for reliability, vulnerability and resilience assessments) poses additional questions and challenges for the modellers and analysts.

In particular, relevant sources of uncertainty affecting the system should be considered in all the phases of the analysis. Uncertainty should be quantified, not just in the virtual modelling phase, but throughout the whole life of the system, from the digital verification of its safety performance to the real actions and operations performed on the physical system, all the way to its decommissioning.

In this thesis, we review and apply uncertainty quantification methods to analyse computational models of power grid critical infrastructures. Novel generalised uncertainty quantification methods have been developed to better analyse reliability, vulnerability and resilience of power grid systems. The power grid system has been adopted as a representative case study due to its inherent complexity, large size, non-trivial inter-dependencies between sub-systems and components and due to the

many uncertainties affecting its structure, operations and external environment.

The concepts of reliability, vulnerability and resilience are presented in the power grid security analysis literature and are defined based on different concepts. Broadly speaking, reliability assess power grid ability (likelihood or probability) to correctly operate in the long-run, vulnerability assess its innate structural robustness against low-probability-high-consequence events, resilience investigates the grid ability to promptly and adequately react to a variety of contingency scenarios (e.g. common failures and also low-probability events), rapidly recovering and also learning from the new data and experiences. These security-related concepts have been reviewed and novel frameworks have been proposed by adopting a generalised probabilistic framework for the quantification of the uncertainties.

1.3 A generalised framework for uncertainty quantification

Many challenges are associated with the modelling of a complex system. One of the most prominent issues is probably the necessity to cope with the unavoidable uncertainty affecting both the model of the system and the collected data. Uncertainty has to be properly characterised and quantified to improve confidence in the model and its results. In general, uncertainty can affect the data and the model in several ways. For instance:

- noises can affect signals;
- privacy issues can lead to a partial censoring of the data;
- lack of data, small sample sizes, e.g. due to time-economic constraints;
- low image/signal resolutions;
- tolerances imprecision and measurement tools limitations;
- gaps in the data or missing points in the data;
- qualitative or subjective information;
- limited numerical/computational precision;
- linguistic vagueness;
- inherent variability;
- low-fidelity models (surrogates, reduced, simplified models);
- conflicting evidence (e.g from sensors or experts).

In some situation, when data is scarce or at all available, expert elicitation (i.e. expert guessing) may be the only viable way of carrying on with the analysis.

In the last decades, generalised uncertainty quantification methods have been developed to better cope with the combination of epistemic and aleatory uncertainty in a unified mathematical framework. In particular, characterise lack of data and imprecision (i.e. epistemic uncertainty) using only classical probability is particularly challenging as, for its treatment, strong artificial assumptions are often required (and are generally hardly justifiable). Generalised probabilistic methods have been recently developed to better cope with the uncertain quantification tasks when problems affected by a combination of epistemic and aleatory uncertainties are challenging the analyst. Generalised methods are generally non-intrusive and applicable to any computational model. These methods do not require (or require less) unwarranted, hard-to-justify assumptions compared to their classical probabilistic counterpart, thus better preserving the real information content in the data, and can quantify the effect of both aleatory and epistemic uncertainty without mixing them. Their capability to differentiate between aleatory and epistemic uncertainty offer several advantages from a modeller and analyst perspective. First, this allows modellers to clearly defined which among the input factors uncertainties can be, theoretically, reduced (i.e. the one for which can be economically viable to collect more data). Secondly, the output of a generalised probabilistic framework points out if the uncertainty in the system performance is mainly due to lack of knowledge or inherent variability.
This is valuable information for decision makers which will have quantitative evidence to discuss:

1) A necessity to achieve higher precision in the results;

2) The inability/ability to take a decision based on the assessed uncertainty;

3) The need to invest in further data gathering;

4) On which uncertain factors focus the data collection;

5) Uncertainty reduction (precision-cost) trade-off;

Although those methods are powerful and flexible, thse find a limited application in real world industrial environments. This is possibly due to lack of clear guidance for practitioner, relatively new and not fully developed theory and to the few applications needed to display capability of the methods. Moreover, generalised probabilistic approaches are very intensive computationally speaking and, in many cases, this restricts their applicability.

Figure 1.1 presents the generalised framework for uncertainty quantification adopted in this work. Figure 1.1 presents some of the key components of the framework which can be summarised as follows:

1: **High-Fidelity Computational Model:** The high-fidelity model is a realistic representation of a system or a process. For the goals of uncertainty quantification it can be conveniently regarded as a black-box model. This can include a digital twin of the real physical system, but it can also be a combination of models (e.g. system-environment models coupled) or an entire work-flow, e.g. different pieces of software, physical experiments, framework for the reliability, vulnerability, resilience assessment.

2: **Uncertainty Characterisation (Epistemic):** The epistemic uncertainty characterization goal is to model the uncertainty associated to features for which the information is limited, imprecise, vague, qualitative or affected by any mixture of lack of data and variability. Mathematical tools deriving from imprecise probability theory (such as P-boxes, Possibility distributions, Credal Sets, Fuzzy Variables or Dempster-Shafer structures) can be used for the modelling as described in Chapter 2.

3: **Uncertainty Characterisation (Aleatory):** Aleatory uncertainty can be effectively characterised by e.g. cumulative distribution function, probability masses, probability distributions etc. Classical probability theory is commonly used to characterise aleatory uncertainty.

4: **Uncertainty Propagation (Aleatory):** The propagation of aleatory uncertainty deals with the effect of inherent variability of model inputs to the quantities of interest in the model outputs. Aleatory uncertainty propagation can be performed using classical sampling methods, e.g. Monte Carlo (MC), Lathing Hypercube Sampling (LHS), or if appropriate, more efficient methods such as subset simulation, line sampling, importance sampling, etc.

5: **Uncertainty Propagation (Generalised):** Generalised propagation of the uncertainties consists of a combined analysis of the effect of epistemic and aleatory uncertainty (without mixing them) on the model output quantities of interest. This is generally performed using time costly double loop methods and optimization methods.

6: **Emulators/Surrogates:** In case of time-consuming codes, a low-fidelity, computationally cheap substitute of the high-fidelity model can be adopted. This model will act as an approximated model (also known as emulator or surrogate model) on top of which uncertainty quantification can be performed efficiently. Some

representative examples are the Response Surfaces models, Polynomial Chaos Expansions, Gaussian Process Emulator (GPE), Artificial Neural Networks (ANN), Extreme Learning Machines.

7: **Aleatory feedback loops:** When new information is made available to the analyst (e.g. new information which comes from the propagation/quantification of aleatory uncertainty), it can be used to update and refine the model and produce better inferences on output quantities of interest. For instance, sensitivity analysis and dimensionality reduction can be performed on the aleatory space (e.g. by applying screening methods or variance-based sensitivity analysis) or Bayesian inference used to refine the model.

8: **Epistemic feedback loop:** Analogously to the aleatory feedback loop, the epistemic feedback loop adopts the new information to improve the model but also to reduce the extent of the epistemic uncertainty by a better characterisation of the imprecise inputs. The uncertainty model can be update and refine in this phase, imprecisely defined parameters can be better specified and also sensitivity analysis can be performed (e.g. epistemic space pinching, Bayesian updating of the epistemic space, etc.).

1.4 International standards

The 'Guide to the expression of Uncertainty in Measurement' (GUM) is a book of standards intended to guide the reader in uncertainty evaluation tasks. Complementary documents such as the one provided by the Working Group 1 of the JCGM (and has bene[U+FB01]ted from detailed reviews undertaken by member organizations of the JCGM and National Metrology Institutes) provides additional guidance in the uncertainty-related topic not explicitly treated in the GUM [60]. These standards provide good guidance to perform uncertainty quantification analysis. However, a probabilistic treatment of uncertain is generally recommended. This treatment is suggested independently from the amount of data available to characterize the probabilistic model and, thus, it substantially different from the the proposed this work. In this work, imprecise quantities will be considered affected by both aleatory and epistemic uncertainty and a non-probabilistic treatment of epistemic uncertainty is proposed. On the other hand, the GUM and JCGM books refer to the term imprecision in an aleatory uncertainty sense. To give an example, the JCGM 101:2008 document states that "If the only available information regarding a quantity X is a lower limit a and an upper limit b with $a < b$, then, according to the principle of maximum entropy, a rectangular distribution $R(a, b)$ over the interval $[a, b]$ would be assigned to X", [60]. This assumption seems reasonable and can be used to carry on with classical probabilistic analysis. However, this can be a strong assumption, with the potential to lead to an underestimation of the

uncertainty, which is potentially dangerous in a reliability/resilience assessment context. In fact, it is challenging to model uncertainty arising from poor quality data, e.g. interval-valued information, using classical probability theory. This has the potential to undermine the goodness of the analysis and even worst induce a sense of over-confidence in the results (e.g. confidence that a safe/reliable/resilience design has been found for a system to be built). Further examples are provided in the remaining of this Ph.D. thesis. The author believes there is a need to update the international UQ standards to include a more robust treatment of uncertainties arising from lack of knowledge, vague information, conflicting pieces of evidence, etc. Generalized UQ methods, when compared to classical probabilistic methods, can provide a valuable perspective on the real quality of the available information.

1.5 Problem statement, open issues and objectives

Power grid reliability is a well-defined mathematical concept and several frameworks to assess power grid reliability have been proposed in the last decades. Reliability generally focuses on known threats and assess the power grid capacity to withstand a predefined list of contingencies. Similarly, power network vulnerability assesses the capacity of the network to withstand unexpected scenarios. However, it differs from the reliability concept as the unexpected disturbances considered in vulnerability analysis are generally low-probability-high-consequences scenarios. Moreover, vulnerability commonly assesses the grid robustness only from a structural perspective (e.g. structural integrity after a targeted attack or an extreme $N - k$ contingency).
As mentioned, power grid resilience can be regarded as a unifying concept, extending both classical reliability and vulnerability definitions. It broadens the reliability and vulnerability concepts by evaluating both high-probability threats, low-probability-high-consequence events (such as severe weather conditions or targeted attacks) but also accounting for the system ability to quickly recover, self-healing and learning from those occurrences. To provide a comprehensive definition of network resilience, the system ability to learn from past occurrences is one of the key elements and has to be properly accounted for and an example of resilience definition is '*the network ability to withstand high impact low probability events, rapidly recovering and improving operations and structures to mitigate the impact of similar events in the future*'.

Thus, it can be argued that the main difference between a reliable power grid and a resilient power grid is that, in the latter, low-probability-high-consequence events are specifically considered and handled, with the ability to learn from past occurrences. To achieve this, a comprehensive analysis of the relevant sources of uncertainty should be provided. In particular, lack of data is generally affecting low probability events and computational tractability is an issue for advanced uncertainty quantification methods.

To improve overall robustness of the analysis, it is uttermost important to develop and improve frameworks capable of tackling (effectively and efficiently) data deficiency issues. A rigorous quantification of the lack of data affecting extreme low-probability-high-consequence events, vulnerability, reliability and resilience frameworks is necessary. Following those considerations, the research questions motivating this work and dissertation can be summarised as follows:

1 How to quantify the effect of epistemic and aleatory uncertainties in power grid reliability, vulnerability and resilience frameworks without mixing them?

2 How does the choice of a specific vulnerability metric affect the result of power grid robustness analysis? What is the uncertainty associated with this selection and what are the effects on the contingency ranking results?

3 How does extreme weather affect power grid failures, repairs and overall resilience?

4 How to efficiently handle computationally demanding simulations? How to speed up uncertainty quantification tasks for power grid analysis?

5 How do variability and uncertainty in the electric demand and production affect the consequences of cascading failures?

6 A resilient grid is a grid capable of self-healing and autonomously learn from past experience. How to tackle decision-making tasks in an automatic way? How to provide self-healing and learning capabilities to power grid systems?

1.5.1 Outline of the dissertation

Table 1.1 presents an overview of the chapters which constitute this dissertation. The chapter novelty, or state of the art (SoA), is highlighted and key words introducing the contextual area investigated is presented. Chapters 4 to 8 present novel methods and frameworks for the analysis of power grid systems whilst Chapters 2 and 3 review state of the art concepts for probability analysis and power grid security analysis.

The rest of this thesis is organized as follows: Chapter 2 reviews methods for advanced uncertainty characterisation and propagation, In Chapter 3 an overview of power flow methods and a state-of-the-art review of reliability, vulnerability and resilience concepts for power grids is proposed. In Chapter 4 lack of data issues are discussed and 2 case study are proposed to test the generalised uncertainty quantification framework. In Chapter 5 vulnerability and robustness concepts are further reviewed and a novel vulnerability assessment framework is proposed for the assessment of spectral vulnerability metrics and components ranking under uncertainty. Chapter 6 introduces a computationally efficient framework for the resilience assessment of power grid. A combined

Table 1.1: Outline of the thesis: each row presents the chapter index, if it contains new material or belongs to the State-of-the-Art (SoA), Also, a few keywords are included to guide the reader.

Chap.	Novelty	Key Words
2	SoA	Review
3	SoA	Review
4	New	Uncertainty quantification, Information quality, Probability boxes, Dempster-Shafer, Computational tool, Reliability
5	New	Vulnerability assessment, Contingency ranking, Power grid, Uncertainty, Overload cascading failures, Spectral graph metrics
6	New	Load curtailing, Severe weather, Power grids, Resilience, Global sensitivity, Artificial neural network, Credal sets
7	New	Resilience, Reliability, Cascading failures Morris' sensitivity, Sobol's sensitivity, Given data sensitivity
8	New	Reinforcement Learning, Prognostic and health management, Operation and maintenance, Degradation, Power grid, Uncertainty, Resilience,

weather-grid model is proposed and a novel emulator of the power-flow solver allows computational tractability of imprecise probabilistic analysis. Chapter 7 presents an application of sensitivity analysis and screening methods used to validated and verify a computational model for power grid cascading failures. In Chapter 8, a Reinforcement Learning framework is investigated for optimal operations and maintenance scheduling in a scaled-down power grid case study. The final Chapter 9 conclude the dissertation with a summary and a discussion on the need for future research.

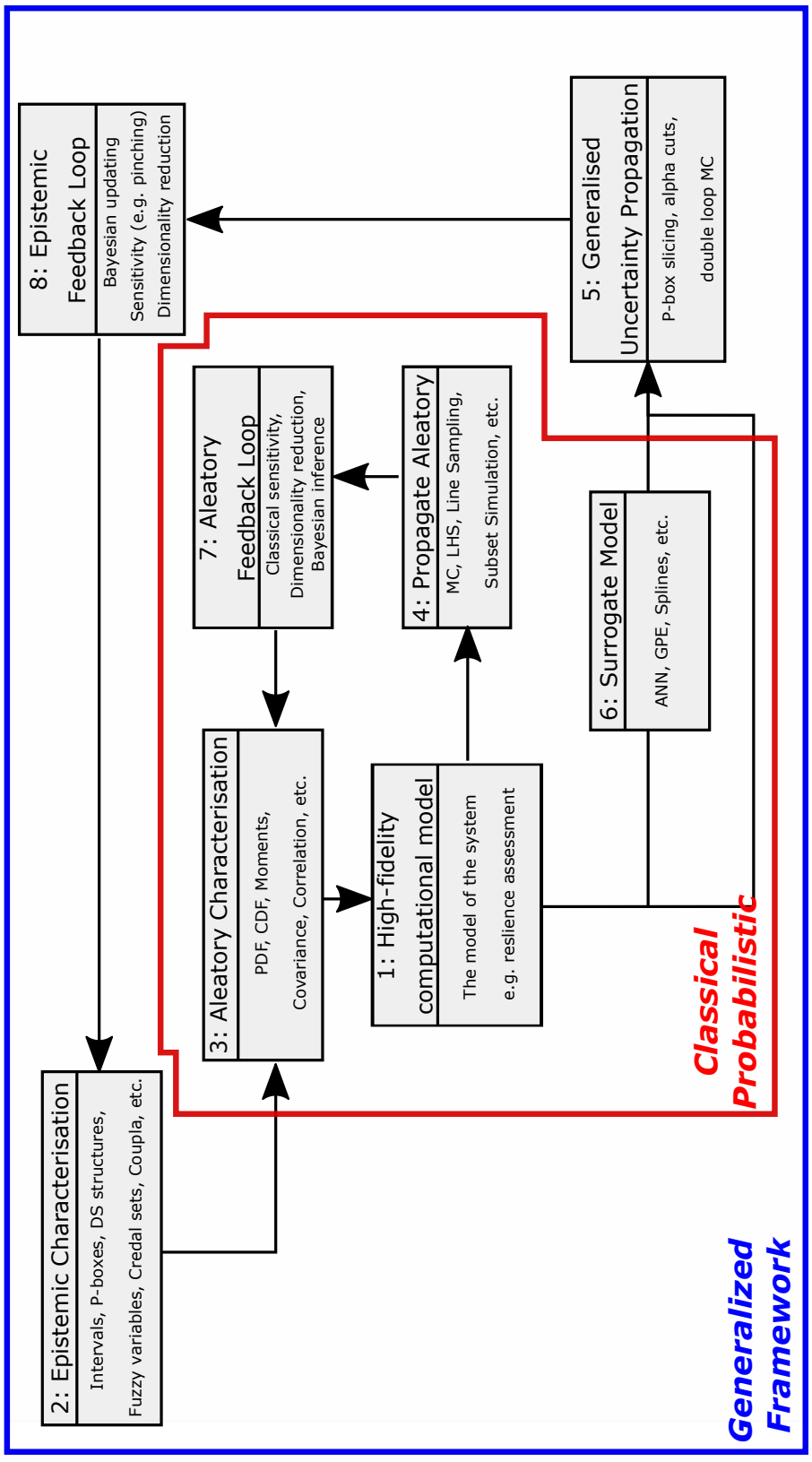

Figure 1.1: A conceptual framework for generalised uncertainty quantification on top of any computational model.

Chapter 2

Probability Theory and Stochastic Analysis

2.1 Abstract

In this chapter, we briefly review probability theory axioms, modeling tools, and uncertainty quantification methods. Advanced tools for generalized uncertainty quantification and modeling of quantities affected by mixed aleatory-epistemic uncertainty is also presented. Evidence theory, Probability boxes, Dempster-Shafer structures, and Credal sets are introduced and their interchangeability discussed. Slicing method and double loop Monte Carlo methods for mixed aleatory-epistemic uncertainty propagation are introduced and used to quantify the effect of the uncertainty on any outputs of interest in computational models. Finally, traditional variance-based sensitivity analysis methods are reviewed and compared to generalized methods for sensitivity analysis on Probability boxes. An introduction to widely applied surrogate models for uncertainty quantification is also proposed.

2.2 Classical probability theory

2.2.1 Axioms

First, let define the probability space $(\Omega, \mathcal{F}, \mathbb{P})$, where Ω is an event space (or sample space) equipped with a σ-algebra $\mathcal{F}$ and $\mathbb{P}$ is a probability measure. A probability measure is a real-valued function mapping $\mathbb{P} : \Omega \rightarrow \mathbb{R}$ and satisfying the followings axioms:

1. $\mathbb{P}(E) \geqslant 0 \ \forall \omega \in \Omega$ (non-negativity)
2. $\mathbb{P}(\omega) + \mathbb{P}(\omega^c) = 1 \ \forall \omega \in \Omega$ and $\omega^c \cap \omega = \varnothing$ (unitarity)
3. for any set of mutually exclusive events $\{\omega_1, .., \omega_i, .., \omega_n\} \in \Omega$ (σ-additivity)

$$\mathbb{P}(\bigcup_{i=1}^{\infty} \omega_i) = \sum_{i=1}^{\infty} \mathbb{P}(\omega_i)$$

In the traditional Kolmogorov's probability theory, a probability $\mathbb{P}(\omega)$ associated to an event $\omega \in \Omega$ is defined to satisfy the above mentioned Kolmogorov's axioms.

2.2.2 Random variables, CDFs and method of moments

Given a probability space $(\Omega, \mathcal{F}, \mathbb{P})$, a random variable X is defined as a map $X : \omega \in \Omega \rightarrow X(\omega) \in \mathcal{I}_X \subset \mathbb{R}$, which relates basic events ω in the event space Ω to a value $X(\omega)$ included in the random variable support $\mathcal{I}_X$, subset of the real line. If X is discrete, then it is generally associated with a probability mass function $f_X(x)$ defined as $f_X(x) = \mathbb{P}(X = x) = \mathbb{P}(\{\omega \in \Omega : X(\omega) = x\})$. If X is continuous, then is associated with a probability density function (PDF) $f_X(x)$, where $f_X(x)$ is non-negative Lebesgue-integrable function such that:

$$\mathbb{P}(a \leqslant x \leqslant b) = \int_a^b f_X(x)dx \tag{2.1}$$

where the PDF express how likely is to have the random va in the interval $[a, b]$.

A cumulative distribution functions (CDFs) $F_X(x)$ is a non decreasing mapping from $\mathbb{P}$ to [0,1] such that for a probability measure $\mathbb{P}$ and for each $x \in \mathbb{R}$, the followings $F_X(x) = \mathbb{P}((-\infty, x])$ and $f_X(x) = \frac{dF_X(x)}{dx}$ hold. An empirical CDF can be used to estimate the CDFs of a random variable X given data. In particular, given a set of realisations $\{\mathcal{X}_1, .., \mathcal{X}_i, .., \mathcal{X}_N\}$, the empirical CDF is defined as:

$$F_X^e(x) = \frac{1}{N} \sum_{i=1}^{N} \mathbb{I}_{x \geqslant \mathcal{X}_i}(x) \tag{2.2}$$

where $\mathcal{X}_i$ is the i^{th} realization of the random variable X and the indicator function $\mathbb{I}_{x \geqslant \mathcal{X}_i}$ is equal 1 if $x \geqslant \mathcal{X}_i$ and 0 otherwise.

The n^{th} moment of a real-valued continuous density function associated to a random variable is defined as:

$$\mu_n = \int_{-\infty}^{+\infty} (x - c)^n f_X(x) dx \tag{2.3}$$

Given a population of X samples, it is possible to estimate the row moments and central moments of the underlying $F_X(x, \mathbf{p})$ where $\mathbf{p}$ is the parameter vector identifying a specific distribution family. The first raw moment is named expectation (or sample mean) and the second central moment is named variance, both can be estimated from samples of $F_X(x, \mathbf{p})$ as follows:

$$\mathbb{E}[\mathcal{X}] = \frac{1}{N} \sum_{i=1}^{N} \mathcal{X}_i \quad Var[\mathcal{X}] = \frac{1}{N-1} \sum_{i=1}^{N} (\mathcal{X}_i - \mathbb{E}[\mathcal{X}])^2 \tag{2.4}$$

where for a sufficiently large number of samples the 2 moments will correctly estimate the true mean μ and standard deviation σ of the underlying distribution family. One of the limitations of classical probability theory, is that the measure $X(\omega)$ is a crisp (precise) value, which is obtained assuming exact knowledge of the underlying PDF and cumulative probability distribution function. Especially for cases affected by a lack of data, where imprecise information or expert judgement are utilised, and there is a poor understanding of all the relevant underlying process, strong initial assumptions may be needed to characterize $X(\omega)$ is a crisp (precise) way, i.e. using classical probabilistic methods.

2.2.3 Limitations: Do we have enough data?

From a pragmatic preservative, uncertainty can be conveniently classified into two categories, one is the aleatory uncertainty and the other is the so-called epistemic uncertainty. Aleatory uncertainty (also known as Type I or irreducible uncertainty), represents stochastic behaviours, inherent variability and randomness of events and variables. Hence, due to its intrinsic random nature it is normally regarded as irreducible. Some examples of aleatory uncertainty are future weather conditions, stock market prices or chaotic phenomenon. On the other hand, epistemic uncertainty (sometimes named Type II or reducible uncertainty), is commonly associated with lack of knowledge about phenomena, imprecision in measurements and poorly designed models. It is considered to be reducible since further data can decrease the level of uncertainty, although this might not always be practical or feasible. This classification

is often considered very useful as it allows do discuss and understand if there is hope for a better determined of a model output quantity of interest (e.g. by further data gathering to reduce the epistemic uncertainty) and to which extent this quantity is inherently variable (i.e. affected by aleatory uncertainty and thus not better defined but just quantified).

Generally speaking, traditional probability methods rely upon a good characterisation of variables as well as distribution moments to be estimated through samples data. This usually requires a considerable body of empirical information in order to properly define probability distributions or to accurately estimate expectation, variance or higher moments. Furthermore, prior assumptions can be necessary to define the shape distribution family $F_X(x, \mathbf{p})$ (e.g. Gaussian, Beta, Exponential), even if no prior knowledge on the shape of family type is actually available. More importantly, probability theory provides only single measure for the uncertainty. This makes the uncertainty analyst unable to grasp how much of the uncertainty is due to inherent variability and to what extent the uncertainty is due to poor data quality (therefore suitable to be reduced in principle).

In recent decades, efforts were focused on the explicit treatment of imprecise knowledge, non-consistent information and both epistemic and aleatory uncertainty [9]. The methodologies have been proposed and discussed in literature by different mathematical concepts: Dempster-Shafer theory of Evidence [136]- [37], interval probabilities [8], Bayesian approaches [106], Fuzzy-based approaches [150], info-gap approaches [16], probability boxes [49] and Credal sets [63] are some of the most intensively applied concepts and will be briefly reviewed in the following sections.

2.3 Evidence theory

The Dempster-Shafer (DS) theory of evidence is a well-suited framework to represent both aleatory and epistemic uncertainty. The main difference between the axioms of classical probability theory and the DS theory of evidence is that the latter slacken the strict assumption of a single probability measure for an event. It can be seen as a generalisation of Bayesian probability [37].

2.3.1 Dempster-Shafer structures

Mathematically, a Dempster-Shafer structure on the real line $\mathbb{R}$ is identified with a basic probability assignment, that is a map as follows:

$$m : 2^{\mathbb{R}} \rightarrow [0, 1] \tag{2.5}$$

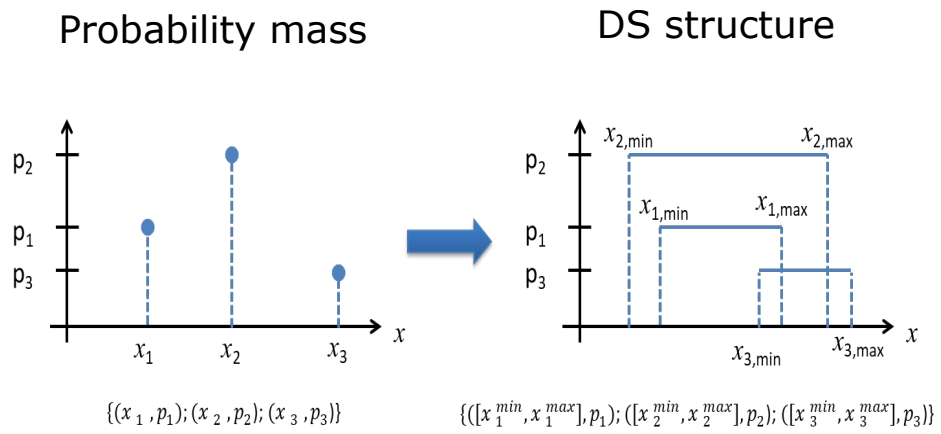

Figure 2.1: A comparison between a probability mass function associated to 3 point-valued data and DS structure associated to 3 interval-valued data.

where the probability mass is $m([\underline{x}_i, \overline{x}_i]) = p_i$ for each focal element $[\underline{x}_i, \overline{x}_i] \subseteq \mathbb{R}$ with $i = 1, .., n$ and n is the number of interval-valued data available on the quantity x. The probability mass associated with the the empty set $S = \varnothing$ and to any set $S \neq [\underline{x}_i, \overline{x}_i]$ is $m(S)$ =0, such that $p_i > 0 \ \forall i$ and $\sum_{1}^{n} p_i = 1$. Dempster-Shafer structures are similar to discrete distribution but probability mass is no longer associated to precise points or events, but rather to sets of real values, i.e. focal elements. An example of Dempster-Shafer structure is the following:

$$\{([\underline{x}_1, \overline{x}_1], m_1), ([\underline{x}_2, \overline{x}_2], m_2), ..., ([\underline{x}_n, \overline{x}_n], m_n)\} \tag{2.6}$$

where $([\underline{x}_i, \overline{x}_i], m_i)$ represents the i^{th} focal element with upper bound $\overline{x}_i$ and lower bound $\underline{x}_i$, m_i is the probability mass associated. Figure 2.1 presents the difference between probability mass functions and DS structures.

In the literature, the upper bound on probability is generally referred as plausibility and the lower bound as belief. The cumulative plausibility function $Pl(x)$ and cumulative belief function $Bel(x)$ are computed as:

$$Pl(x) = \sum_{\underline{x}_i \leqslant x} m_i \tag{2.7}$$

$$Bel(x) = \sum_{\overline{x}_i \leqslant x} m_i \tag{2.8}$$

Compute cumulative $Bel(x)$ and $Pl(x)$ is a straightforward way of transforming a Dempster-Shafer structure in a distribution-free probability box.

2.4 Credal sets

Set-theoretical methods are often used to deal with epistemic uncertainty. The set-theoretical models [91] use set-valued descriptors (e.g. intervals) to model epistemic uncertainty, e.g. intervals [93], random sets [146] or fuzzy sets [92]. Intervals are used when variables are only known to be bounded within lower and upper limits whereas Fuzzy Sets can be used to simultaneously analyse different bounded sets. This is particularly helpful if the bounds are not precisely known [124]- [36]. Credal sets theory [63] provides strong mathematical foundation to express sets of probability distributions. A Credal set ($\mathfrak{C}$) is defined as a set of probability distribution functions. The hyper-parameters $\mathbf{p}$ defining the joint probability distribution $F_X(\mathbf{x};\mathbf{p})$ can be given as intervals (i.e. an n-orthotope also called hyper-rectangle). A Credal set is then defined as follows:

$$\mathfrak{C} = \{F_X(\mathbf{x};\mathbf{p}) | \underline{\mathbf{p}} < \mathbf{p} < \overline{\mathbf{p}}\} \tag{2.9}$$

where $\mathbf{x}$ is the random variable vector and $\underline{\mathbf{p}}$ and $\overline{\mathbf{p}}$ are the lower and upper bounds of the parameter vector defining the joint probability distribution $F_X(\mathbf{x};\mathbf{p})$, respectively.

2.4.1 Expectations in generalised uncertainty models

When the probabilistic model input is precisely defined, i.e. $\underline{\mathbf{p}} = \mathbf{p} = \overline{\mathbf{p}}$, its output will also be precisely specified, i.e. a crisp probability distribution and expectation. The *precise* expectation of the probabilistic model $F_X(\mathbf{x};\mathbf{p})$ is defined as:

$$\mathbb{E}[F_X(\mathbf{x};\mathbf{p})] = \int_\Omega F_X(\mathbf{x};\mathbf{p}) d\eta \tag{2.10}$$

When imprecision is affecting the problem, the expectation becomes imprecise and can be obtained as follows:

$$\begin{bmatrix} \overline{\mathbb{E}}[F_X(\mathbf{x};\mathbf{p})] \\ \underline{\mathbb{E}}[F_X(\mathbf{x};\mathbf{p})] \end{bmatrix} = \begin{bmatrix} \sup \\ \underline{\mathbf{p}} < \mathbf{p} < \overline{\mathbf{p}} \\ \inf \\ \underline{\mathbf{p}} < \mathbf{p} < \overline{\mathbf{p}} \end{bmatrix} \int_{\Theta(\mathbf{p})} F_X(\mathbf{x};\mathbf{p}) dx \tag{2.11}$$

where Ω is the probability space, Θ is the space of epistemic uncertainty dependent on the vector $\mathbf{p}$, $\overline{\mathbb{E}}$ and $\underline{\mathbb{E}}$ are the upper and lower expectations, respectively. In order to compute bounds for the expectation, a minimisation (inf) maximisation (sup) problem constrained by the hyper-parameter space bounds $\underline{\mathbf{p}}, \overline{\mathbf{p}}$ has to be solved [3]. For the solution, different approaches can be used, for instance vertex methods [40], global optimisation techniques [110]- [25], sampling or interval arithmetic methods [153].

2.5 Probability boxes

Mathematically, a P-box is defined as a pair of lower and upper cumulative distribution functions $[\underline{F}_X, \overline{F}_X]$ from the epistemic space Θ to [0,1] such that $\underline{F}_X(x) \leqslant F_X(x) \leqslant \overline{F}_X(x)\ \forall\ x \in \Omega$ and Ω is a classical event space, i.e. such that $\underline{F}_X$ stochastically dominates $\overline{F}_X$ [49]. The upper and lower bounds for the CDFs are $\overline{F}_X = \overline{P}(X \leqslant x)$ and $\underline{F}_X = \underline{P}(X \leqslant x)$, respectively. A P-box can be viewed as a continuous form of random sets and Dempster-Shafer structure. Note that the probability distribution family associated with the random variable x can be either specified or not specified. The former are generally named distributional P-boxes, or parametric P-boxes, the latter are named distribution-free P-boxes, or non-parametric P-boxes [106].

2.5.1 Distributional P-boxes

In general distributional P-box can be defined as follows:

$$\{P \in \mathbb{P}\,|\forall p \in \mathbb{R}, \underline{F}_X(x) = P((-\infty, x]) \leqslant \overline{F}_X(x)\} \tag{2.12}$$

where equation (2.12) defines the Credal set induced by the p-box $[\underline{F}_X, \overline{F}_X]$.

Figure 2.2 shows a distributional P-box, the parent distribution is the normal distribution and the mean and standard deviation are defined as intervals. The lower bound $\underline{F}_X(x, \mu, \sigma)$ and the upper bound $\overline{F}_X(x, \mu, \sigma)$ are obtained combining the bounds on the distribution parameters.

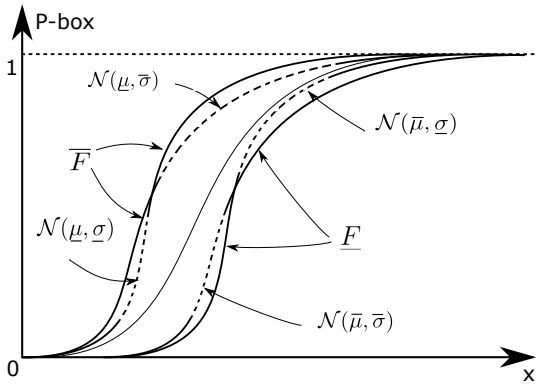

Figure 2.2: Illustrative example of distributional P-box. The parent distribution is the normal distribution with mean and standard deviation defined as intervals. The figure displays the lower bound on the probability, also named $Bel(x)$, and the upper bound, also named $Pl(x)$, which can be constructed as combination of lower and upper bounds on the distribution parameters.

2.5.2 Distribution-free P-boxes

Distribution-free P-boxes are defined only through bounds and the underlying probability distribution family is not known and not defined, i.e. $[\underline{F}_X, \overline{F}_X]$. Distribution-free P-boxes are closely related to Dempster-Shafer structures as they can be always translated to a DS and vice versa [49]. Probability boxes (P-boxes) are powerful and versatile

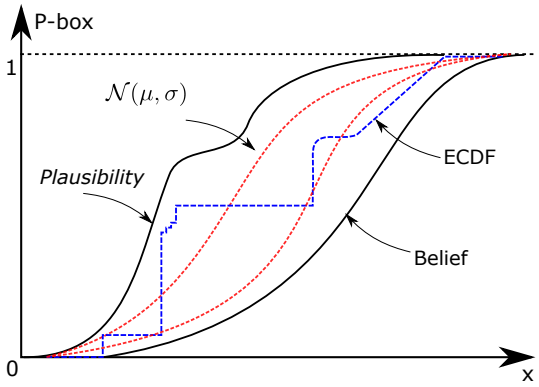

Figure 2.3: Illustrative example of distribution-free P-box and 3 sample distributions enclosed between lower and upper bounds. Two CDF for which probability family is known (e.g. normal) are shown in dashed smooth red lines. In dashed discontinuous blue line an empirical cumulative distribution functions, e.g. an ECDF obtained from samples.

tools to characterise quantities affected by both aleatory and epistemic uncertainty [14] and they have a very intuitive way of distinguish between those two types of uncertainty. The wider the distance between the upper and the lower bound is, the higher the incertitude associated to the random variable. Fig.2.4 shows two examples of distribution-free P-boxes. The distance between the upper and lower CDFs represents the amount of epistemic uncertainty associated with the quantity of interest (e.g. vulnerability in the figures). It can be observed that the P-box on the right-hand side is strongly affected by epistemic uncertainty. Conversely, the P-box on the left-hand side has a stronger aleatory component and the epistemic uncertainty appear to be less relevant.

2.6 Constructing P-boxes from data

2.6.1 Kernel density estimation

It is in general difficult to identify the true distribution from a small number of samples using parametric methods. This is because in general, there is not enough information to properly estimate the PDF when only a few data points are available. Then Kernel density estimator is a non-parametric approach that can be used to construct the probability density function associated to data samples [115]. The approach does not need to assume an underlying distribution. However, samples need to be assumed indepen-

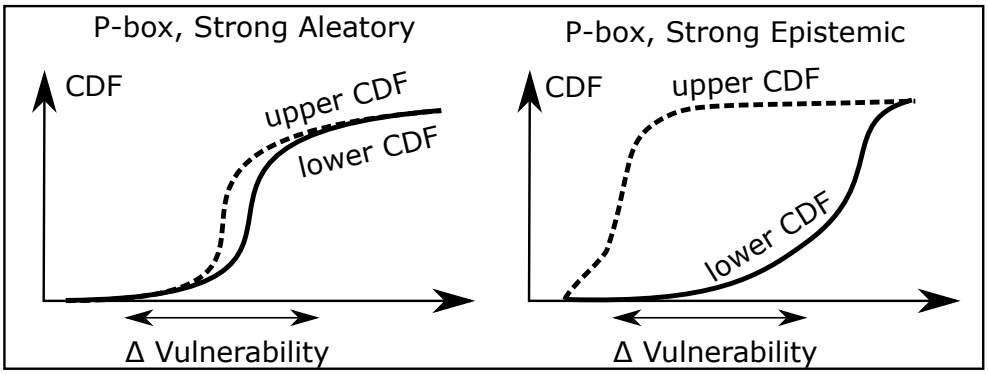

Figure 2.4: A comparison of two P-box used to characterize the uncertainty affecting a factor (vulnerability in this example). The one on the right-hand side has a strong epistemic component.

dent and identically distributed (*iid*) and some 'smoothness' condition, i.e. continuity or differentiability, have to be satisfied (or assumed). A commonly used univariate parametric kernel is the Gaussian or normal Kernel, defined as follows:

$$\hat{f}(x) = \frac{1}{n\sigma\sqrt{2\pi}} \sum_{i=1}^{n} \left(\frac{-(x - x_i)^2}{2\sigma^2} \right) \tag{2.13}$$

where $\hat{f}_X(x)$ represents the estimated probability density function of n samples $\mathcal{X}_i$ drawn from an unknown density function $f_X(x)$. The variance (or bandwidth) σ^2 is the only parameter that needs to be estimated. The best bandwidth can be estimated using, for instance, the Silverman's rule of thumb [138] or in case of very small sample sizes the approach proposed by [115]. One way of construct probability boxes by using Kernel density estimator method is to obtain confidence bounds $[\underline{\sigma},\overline{\sigma}]$ for the estimated parameter σ (e.g. by Bootstrapping). The set of $\sigma \in [\underline{\sigma},\overline{\sigma}]$ will correspond to a set of Kernel densities, which are in turn equivalent to a set of CDFs (i.e. distributional P-box).

2.6.2 Kolmogorov-Smirnov test

The Kolmogorov-Smirnov (KS) statistical test [81] is a non-parametric test that used to compute bounds on empirical CDFs given N samples. The test is based on the maximum distance between an empirical CDF and a hypothetical CDF, as follows:

$$T = sup_x |F_X^e(x) - F_X(x)| \tag{2.14}$$

where sup_x is the supermum of the set of distances and $F_X^e(x)$ and $F_X(x)$ are the empirical CDF (built using the N samples) and an hypothetical CDF, respectively. The

KS test can be used to assess whether a given $F_X(x)$ is a plausible underlying probability distribution of $F_X^e(x)$, thus obtaining confidence limits on $F_X(x)$ given sample and a predefined confidence level. The bounds of the distribution-free P-box can be computed as follows [161]:

$$[\underline{F}_X(x)] = [max\,(0, F_X^e(x) - D(\alpha, N))] \tag{2.15}$$

$$[\overline{F}_X(x)] = [min\,(1, F_X^e(x) + D(\alpha, N))] \tag{2.16}$$

where $D(\alpha, N)$ is the one-sample KS critical statistic for the α significance level and the N number of samples. Different α and sample sizes N lead to different confidence bounds on the CDFs, see for instance Miller's tables [90]. Those bounds when propagated, produce boarder or narrow bounds on the resulting P-boxes, which have to be regarded as a statistical claim for the selected significance level α.

2.6.3 P-boxes and Dempster-Shafer structures interchangeability

A Dempster-Shafer structure can be always converted into a distribution-free P-box by constructing cumulative plausibility and belief functions ($Pl(x)$ and $Bel(x)$). Similarly, a P-box can be translated into a Dempster-Shafer structure by performing the so-called α-slicing of the P-box (i.e. a discretization procedure). The Dempster-Shafer structure is constructed as follows: 1) n α-cuts $(0, .., \alpha_i, .., 1)$ are selected; 2) one interval is obtained for each α_i inverting P-box bounds (equations-2.17-2.18) and a probability mass $m_i = \underline{F}_X(\alpha_{i+1}) - \underline{F}_X(\alpha_i)$ is assigned to the interval:

$$\overline{F}_X(\alpha)^{-1} = \{x | \overline{F}_X(x) = \alpha\}\ \forall \alpha \in [0, 1] \tag{2.17}$$

$$\underline{F}_X(\alpha)^{-1} = \{x | \underline{F}_X(x) = \alpha\}\ \forall \alpha \in [0, 1] \tag{2.18}$$

where the interval $[\underline{F}_X(\alpha_i)^{-1}, \overline{F}_X(\alpha_i)^{-1}]$ is the support of the focal element i. Figure 2.5 shows an example of DS and P-box interchangeability. It is important to mention that Dempster-Shafer structures can be always translated into P-boxes although that is not a biunivocal transformation. More specifically, a Dempster-Shafer structure can be associated to a single Probability box, while a Probability box can be associated to more than one Dempster-Shafer structure depending on the number of the number n in the α-slicing procedure (e.g. a low n will correspond to a coarse discretization) [49]. Probability boxes and Dempster-Shafer structures offer a straightforward way to deal with multiple and overlapping intervals, inconsistent sources of information and small sample sizes.

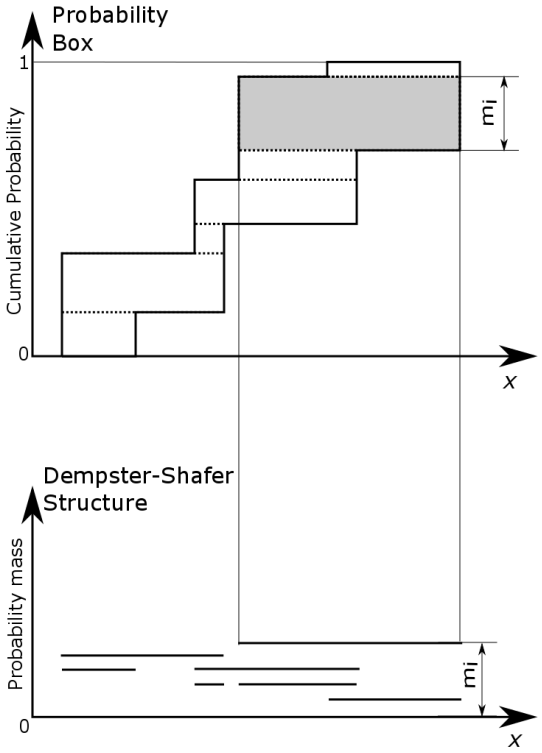

Figure 2.5: Illustrative example of how to construct P-box (top figure) using DS structure (bottom figure) and vice versa.

2.7 Generalized methods for uncertainty propagation

2.7.1 Black-box models

Consider a (deterministic) computational model $M_{\mathcal{V}}$, is a map from a m-dimensional input space $\mathbf{x}$ to a o-dimensional output space of a multidimensional quantity $\mathbf{V}$. Formally, it is:

$$M_{\mathcal{V}} : \mathbf{x} \in \mathcal{I}_X \subset \mathbb{R}^m \rightarrow \mathbf{V} = M_{\mathcal{V}}(\mathbf{x}) \in \mathbb{R}^o \tag{2.19}$$

where input and output vectors are $\mathbf{x} = (x_1, ..., x_M)$ and $\mathbf{V} = (\mathcal{V}_1, ..., \mathcal{V}_O)$, respectively. In order to perform uncertainty quantification, this computational model can be treated as a black-box of which only the input and output vectors can be processed. If $\mathbf{x}$ is affected by aleatory uncertainty, it will be characterised using appropriate probability distribution function (and corresponding CDF). Once propagated through $M_{\mathcal{V}}$ (e.g. using classical Monte Carlo method) the output will result in a well-defined CDF. If $\mathbf{x}$ is affected by epistemic or mixed aleatory-epistemic uncertainty, generalised probabilistic tools (e.g. DS, P-boxes) will be suitable for the characterisation. After uncertainty propagation, the outputs will produce bounds on the vulnerability CDFs (i.e. P-boxes).

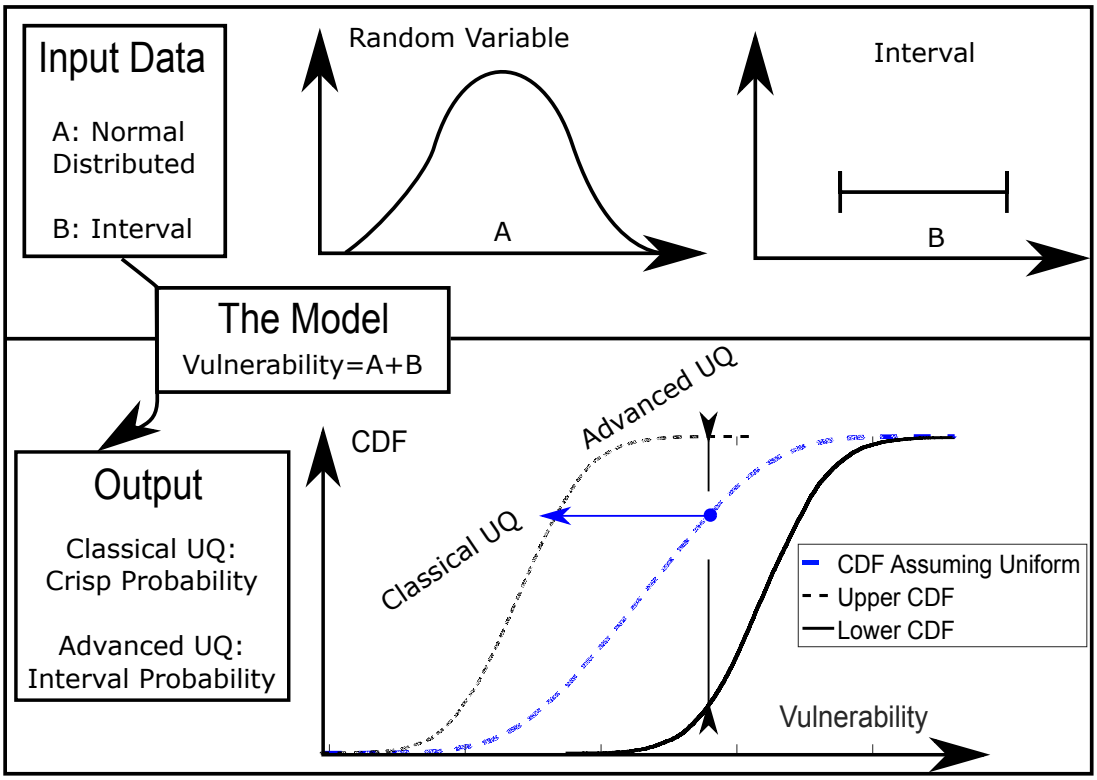

Figure 2.6: A conceptual comparison between advanced uncertainty quantification and classical uncertainty quantification methods applied to a simple vulnerability model.

2.7.2 Classical versus generalized uncertainty propagation

Fig.2.6 presents a simple comparison between a classical probabilistic method to an advanced uncertainty quantification (UQ) method. In the example, a vulnerability measure is the output quantity computed using the model $M_{\mathcal{V}}$ (sum of quantity A and quantity B), where input A has a well-known aleatory behaviour (e.g. it is distributed as a normal PDF) and the B is a parameter affected by purely epistemic uncertainty (e.g. a tolerance interval). The parameter B does not have a stochastic behaviour, but it is rather imprecisely defined. This is due, for instance, to a limited precision in the available measurements for B. This interval can be narrowed down by providing better instruments for the measurements, i.e. reducing the epistemic uncertainty associated. In order to run a classical Monte Carlo method, a PDF should be assumed to characterize the uncertainty for B. Commonly, uniform distribution is assumed within the interval, adopting the so-called Laplace's principle of indifference. Once the probabilistic model is well-defined and uncertainty propagated, the output will have a precise probabilistic description (i.e. a crisp CDF in long-dashed line). This might result inappropriate for two main reasons. First, assumptions might be difficult to justify and might produce wrong results. Secondly and perhaps most importantly, the system analysts will be unable to distinguish between the contribution

of epistemic uncertainty and aleatory uncertain to the output [14]. To overcome this limitation, classical probabilistic approaches can be coupled to advanced uncertainty quantification which allows differentiating between epistemic and aleatory uncertainty in the output without introducing assumptions (i.e. uniform random behaviour of a parameter within a tolerance interval) and with weaker or fewer assumptions compared to the classical counterpart. Resulting output will be described by e.g. intervals or by lower and upper bounds on the CDF, see for instance Fig.2.6 in solid and dashed line, respectively. The drawback of those methods is the generally higher computational cost [109]- [41] and an imprecise probabilistic description of the output [14], which is the price to pay for slaking the assumptions on the probabilistic model. Nevertheless, generalised probabilistic frameworks provide a valuable perspective on the result and, being non-intrusive, are applicable to any computational model [109].

2.7.3 Monte Carlo method

The Monte Carlo (MC) method is a numerical procedure which can be used to quantify the uncertainty associated with the output of a computational model $M_{\mathcal{V}}$ by propagating the uncertainty in inputs factors. Monte Carlo is flexible, unbiased and one of the most well-established methodologies to propagate uncertainty. Moreover, MC method is not heavily affected by the curse of dimensionality as, by the central limit theorem, this method displays $1/\sqrt{N}$ convergence, i.e. quadrupling the number of sampled points halves the error, regardless of the number of dimensions.
However, the classical MC implementation does not differentiate between aleatory and epistemic uncertainty. In fact, a clear definition of input CDFs and dependencies have to be provided for the method to be applicable.

The idea behind the MC method is that it is possible to approximate the output CDF (and PDF) of a black-box model by sampling realisations from the input distributions, i.e. by using a random numbers generator (pseudo random numbers), then, evaluating the corresponding model outputs. The set of output samples will provide a statistical description of the outputs variability, moment and correlation.
The MC procedure can be summarised as follows:

1. **Inverse transform sampling**: (1) Sample M random numbers rn_i distributed uniformly distributed in [0,1], one for each input i. (2) Obtain the j^{th} input vector realisation $\mathbf{x}$ by calculating the values of the inverted CDFs at random numbers values, $\mathbf{x}_j = (F^{-1}_{X_1}(rn_1), ..., F^{-1}_{X_M}(rn_M))$;

2. **Model Evaluation**: run the computational model to obtain the corresponding output vector $\mathbf{V}_j = M_{\mathcal{V}}(\mathbf{x}_j)$;

3. **Loop and post-process**: Save $\mathbf{V}_j$ and repeat step 1. and 2. for several j until the output CDF is approximated;

2.7.4 Dempster-Shafer structures propagation

Figure 2.7 introduces a simple procedure for Dempster-Shafer structures propagation given any black-box computational model. The procedure works as follows:

1. First, n "Parameter cells" are constructed by Cartesian product of the focal elements. Then, each parameter cell $\mathcal{I}_{X,i}$ is an hypercube $\mathcal{I}_{X,i} : \{\underline{\mathbf{x}} \leqslant \mathbf{x} \leqslant \overline{\mathbf{x}} \ \forall \ \mathbf{x}\}, i = 1, .., n$.

2. The minimum and maximum value for each entry i of the model output vector $\mathbf{V}$ is calculated based on optimization technique:

$$\overline{\mathcal{V}}_i = \max_{\mathbf{x} \in \mathcal{I}_{X,i}} M_{\mathcal{V}}(\mathbf{x}) \tag{2.20}$$

$$\underline{\mathcal{V}}_i = \min_{\mathbf{x} \in \mathcal{I}_{X,i}} M_{\mathcal{V}}(\mathbf{x}) \tag{2.21}$$

   where equations 2.20-2.21 define constrained maximization and minimization problems, respectively. The optimisation are, therefore problem specific and might be relatively hard to solve efficiently and/or effectively.

3. Each min-max interval is used to construct a focal element $([\underline{\mathcal{V}}_i, \overline{\mathcal{V}}_i], m_i)$ by associated to the interval a probability mass equal to the product of the probability masses associated to the focal elements in $\mathcal{I}_{X,i}$, i.e. $m_i = \prod_j m_j$ where j indicates the j^{th} focal element used to build $\mathcal{I}_{X,i}$.

4. The n focal elements (i.e.result of the propagation of the focal elements) are used to construct Dempster-Shafer structures for each $\mathcal{V}$, i.e. $\{([\underline{\mathcal{V}}_1, \overline{\mathcal{V}}_1], m_1), \cdots, ([\underline{\mathcal{V}}_i, \overline{\mathcal{V}}_i], m_i), \cdots, ([\underline{\mathcal{V}}_n, \overline{\mathcal{V}}_n], m_n)\}$

The computational cost of the procedure is proportional to the number of input intervals to be propagated and the time needed to simulate the system. Applicability for complex systems with highly non-regular behaviour, which are hence computationally expensive, can require a meta-modelling approach to speed-up the propagation procedure (e.g. Polynomial Chaos, Artificial Neural Networks).

2.7.5 P-boxes propagation

P-boxes can propagated using several different strategies, examples are the double loop Monte Carlo algorithm or the slicing method [124]. Fig.2.8 presents graphically the two methods.

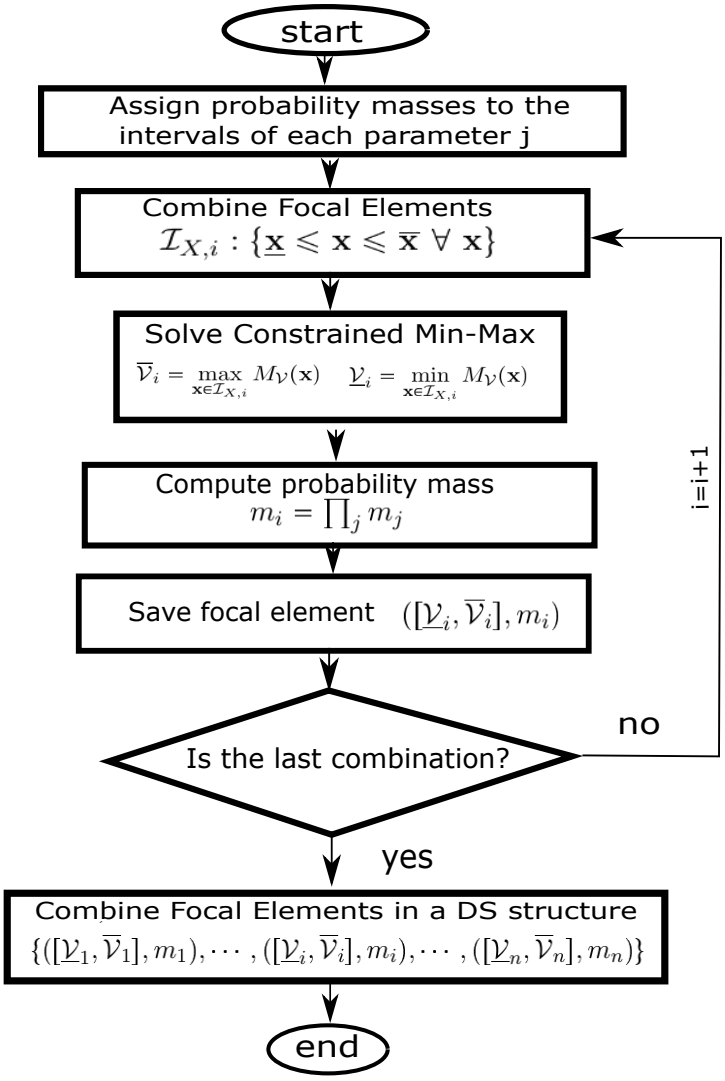

Figure 2.7: Dempster-Shafer structures propagation procedure.

Double loop Monte Carlo method

A simple and effective (but not efficient) way of propagating both aleatory and epistemic uncertainties without mixing them is the double loop MC [109] method. A first loop (outer loop) samples from the epistemic uncertainty space Θ, e.g. sampling P-boxes parameters uniformly in the given intervals. Each epistemic space realisation corresponds a traditional probabilistic uncertainty quantification problem (i.e. inputs CDFs are specifically defined) for which only aleatory type of uncertainty has to be accounted. Then, a traditional MC simulation can be used (inner loop) to propagate aleatory uncertainty. The quantity N_e is the number of realisations in the epistemic space and N_a is the number of samples from the aleatory space. θ_j is the set of uncertain parameters of the epistemic space realizations j, sampled from a known set of intervals $[\underline{\theta}, \overline{\theta}]$. The quantity $x_{k,i}$ is the sample i of the random variable k obtained from the inverse trans-

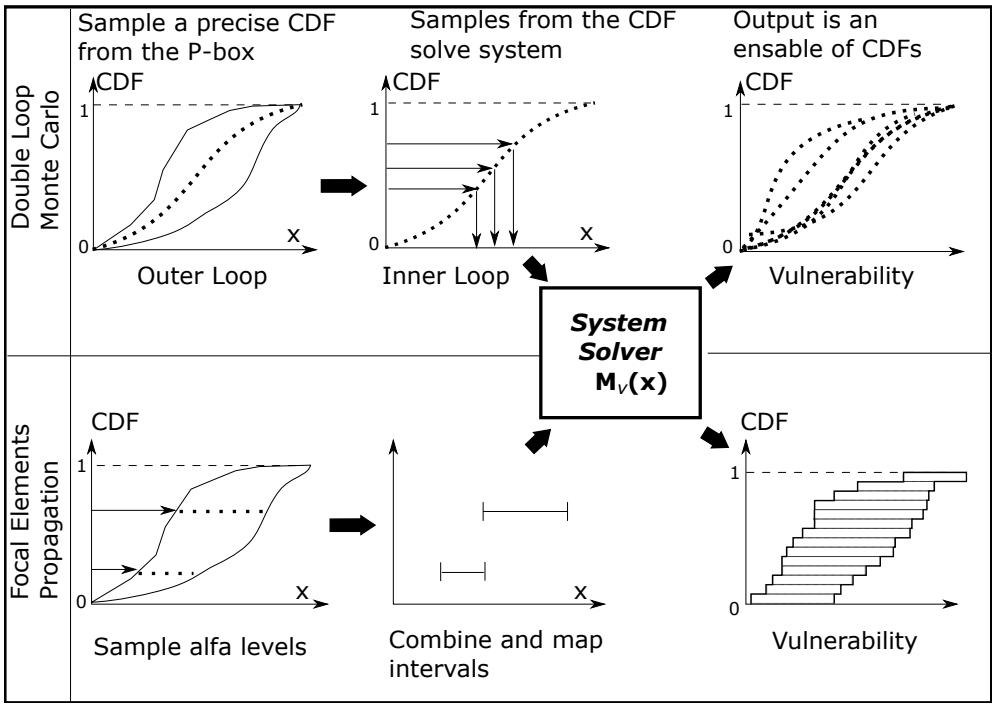

Figure 2.8: A conceptual comparison of the double loop Monte Carlo (in the top panel) method and the slicing method (in the bottom panel) [124].

form of the associated CDF $F_{X_k|\theta_j}(x)$, which depends on the epistemic realization θ_j. The cumulative distribution $F_{Y|\theta_j}(y)$ of the model output can be used for instance to compute $P_{f,j}$, which is the system failure probability given the epistemic realization j. The probability results of the inner loop are not to be averaged over the outer loop but only collected. Then the minimum and maximum can be selected to obtain bounds on the quantity of interest.

Slicing method

The slicing method (or focal element propagation) a total of N_s independent samples are directly obtained from the P-box bounds. For each input P-box a so-called 'alpha-cut' α is generated by sampling from the uniform probability distribution $U(0,1)$. Then, the bounds of the P-boxes are inverted to obtain an interval $[\overline{F}_X(\alpha)^{-1}, \underline{F}_X(\alpha)^{-1}]$ as described in equations 2.17-2.18. The Cartesian product of the input intervals defines the $\mathcal{I}_X$ of the α-slice and corresponds to a parameter cell which is defined by the m-orthotope:

$$\mathcal{I}_{X,i} : [\underline{F}_{X1}(\alpha_1)^{-1}, \overline{F}_{X1}(\alpha_1)^{-1}] \times ... \times [\underline{F}_{Xm}(\alpha_m)^{-1}, \overline{F}_{Xm}(\alpha_m)^{-1}] \tag{2.22}$$

Once the support $\mathcal{I}_X$ is sampled, minimum and maximum of the output are obtained as in equations 2.20-2.21. The procedure stops when a total of N_s hyper-rectangles $\mathcal{I}_X$

are sampled and empirical upper and lower CDF bounds computed as:

$$\underline{F}_e(\mathcal{V}) = \frac{1}{N_s}\sum_{i=1}^{Ns} 1_{\mathcal{V}\leqslant\overline{\mathcal{V}}_i} \qquad \overline{F}_e(\mathcal{V}) = \frac{1}{N_s}\sum_{i=1}^{Ns} 1_{\mathcal{V}\leqslant\underline{\mathcal{V}}_i}$$

In order to obtain $\overline{\mathcal{V}}_i$ and $\underline{\mathcal{V}}_i$, different methods can be used. For instance, bounds can be approximated by sampling within $\mathcal{I}_X$, using vertex methods [116] or by global optimisation approaches [109].

2.8 Feedback loop: Surrogates, sensitivity and Bayesian model updating

2.8.1 Sensitivity analysis

This section proposes a brief introduction to uncertainty quantification and methods for sensitivity analysis. Sensitivity analysis are often connected to uncertainty analysis (propagation and quantification), which ideally, should run in a looped fashion.

An uncertainty quantification analysis generally starts by characterizing the uncertainty in the model input factors (i.e. assiging probability distributions to variables and parameters). Once the uncertainty has been characterized, it is propagated into the simulation code via, for instance, Monte Carlo method. First, uncertain factors are characterised by assigning joint probability distributions describing the uncertainty, this is an important step which has to be performed adequately to assure high quality and consistency of results [111]. Then, samples are obtained from the joint probability distribution of the input factors, e.g. by Latin hypercube sampling, quasi-random sequences or crude Monte Carlo inverse transform sampling [107]. Once the i^{th} input realisation is obtained $\mathbf{X}_i = [X_i(0), .., X_i(m)]$, the sample is forwarded to the computational model $M(X)$. This allows obtaining information about the input-output mapping defined by the computational model as follows:

$$M : \mathcal{X} \rightarrow \mathcal{Y}, \quad \mathbf{X} \rightarrow Y = M(\mathbf{X}) \tag{2.23}$$

where Y is the model output, for simplicity assumed 1-dimensional and without loss of generality.

Sensitivity analysis is, in essence, the study of how an uncertain output Y of a mathematical or numerical model M can be apportioned to different sources of uncertainty in its inputs $\mathbf{X} = [X(1), X(2), ..., X(m)]$. There are a large number of approaches to performing a sensitivity analysis, many of which have been developed to address specific issues. Some of the prominent constraints and issues often faced when performing sen-

sitivity analysis are for instance computationally expensive model M, correlated inputs (most sensitivity analysis methods assume independence, but sometimes inputs can be strongly correlated), model interactions, multiple output, given data (e.g. unavailable model M).

From a general perspective, sensitivity analysis method can be devised in local and global methods. Local methods generally involve taking the partial derivative of the output Y with respect to the j^{th} input factor $X_i(j)$ in a specific point i of the variable support: $\left|\frac{\partial Y}{\partial X(j)}\right|_{\mathbf{X}_i}$ Few examples of local method are the elementary effect method and automated differentiation method. Local method are computationally light, the results quite easy to interpret. One of the main drawback is that the sensitivity information is valid only locally. On the other hand, global sensitivity analysis methods try to identify the most and the least relevant factors over the whole input space, not just locally in $X_i(j)$. Global method are usefull tool to gain additional knowledge of the input-output mapping defined in equation 2.23. Several global methods have been developed in the last decades. For instance, screening methods, such as the Morris method [95], variance-based methods and density-based methods are some of the most intensively applied concepts.

Variance-based Sensitivity Analysis

Variance-based sensitivity analysis is a form of global sensitivity analysis. It works by decomposing the variance of the output into fractions which can be attributed to inputs or groups of inputs.

Let define Y as a chosen univariate output of a model M (multiple outputs can be analysed by multiple independent sensitivity analyses) and be $X(i) \in [0,1], i = 1,2,..,d$ a set of independent model inputs uniformly distributed in the unit hypercube. The model can be decomposed as:

$$Y = M_0 + \sum_{i=1}^{d} M_i(X(i)) + \sum_{i<j}^{d} M_{ij}(X(i), X(j)) + \cdots + M_{1,2,\ldots,d}(X(1), X(2), \ldots, X(d))$$

whereM_0 is a constant and M_i is a function of the variable i, M_{ij} is a function of $X(i)$ and $X(j)$, etc. Being all the terms in the functional decomposition orthogonal, the functional decomposition can be rewritten in terms of conditional expected values:

$$M_0 = \mathbb{E}[Y]$$

$$M_i(X(i)) = \mathbb{E}[Y|X(i)] - M_0$$

$$M_{ij}(X(i), X(j)) = \mathbb{E}[Y|X(i), X(j)] - M_0 - M_i - M_j$$

where M_i is the effect of varying $X(i)$ alone (also referred as the main effect of the factor i), and M_{ij} is the effect of varying $X(i)$ and $X(j)$ simultaneously, additional to the effect of their individual variations. This is known as a second-order interaction. Higher-order terms have analogous definitions. Further assuming that the $M(\mathbf{X})$ is square-integrable, the functional decomposition may be squared and integrated to give the popular variance decomposition equation as follows:

$$Var(Y) = \sum_{i=1}^{d} V_i + \sum_{i<j}^{d} V_{ij} + \cdots + V_{12\ldots d}$$

where the term on the right hand side are:

$$V_i = Var_{X_i}\left[\mathbb{E}_{\mathbf{X}_{\sim i}}[Y \mid X_i]\right]$$

$$V_{ij} = Var_{X_{ij}}\left[\mathbb{E}_{\mathbf{X}_{\sim ij}}[Y \mid X(i), X(j)]\right] - V_i - V_j$$

$$\ldots$$

$$V_{12\ldots d} = \ldots$$

The $\mathbf{X}$ i notation indicates the set of all variables except $X(i)$. The above variance decomposition shows how the variance of the model output can be decomposed into terms attributable to each input, as well as the interaction effects between them. Together, all terms sum to the total variance of the model output.

Sobol's indices

A variance-based statistic, commonly referred to as the first order sensitivity coefficient, quantifies the (additive) effect of each input factor on the model output as follows [76]:

$$S_i = \frac{Var_{X_i}\left[\mathbb{E}_{\mathbf{X}_{\sim i}}[Y|X(i)]\right]}{Var\left[Y\right]} \tag{2.24}$$

where $Var\left[Y\right]$ is the total variance of the output Y, $X(i)$ is the i^{th} uncertain input factor, $\mathbf{X}_{\sim i}$ is the matrix of all uncertain factors but $X(i)$, $\mathbb{E}_{\mathbf{X}_{\sim i}}[Y|X(i)]$ is the expectation of the model output Y taken over all possible values of $\mathbf{X}_{\sim i}$ while removing the $X(i)$ uncertainty (i.e. keeping X_i fixed) and $Var_{X_i}[]$ is the variance taken over all possible values of $X(i)$. The indices S_i can be used to reveal the importance of the input factor $X(i)$ on the variance of the output and it is a normalized index, that is $\sum_i S_i = 1$.

The main effect index reveals what is the importance of each uncertain input factor on the uncertainty in the model output. It is relatively cheap to compute, especially by employing given data methods, e.g. using input-output data retrived from a plain Monte Carlo or by scatter plot decomposition [114]. The main drawback of the main

effect index is that it does not account for interactions between input factors (e.g. inherently to the structure of the model M) nor it accounts for correlation between inputs. Higher order Sobol's effects (second and higher order interactions) compose the so-called total effect index S_{Ti}. This is a variance-based measure of the influence of an input i accounting for all the interactions with other uncertain factors. It is defined as follows:

$$S_{Ti} = \frac{\mathbb{E}_{\mathbf{X}_{\sim i}}\left[Var_{X_i}[Y|\mathbf{X}_{\sim i}]\right]}{Var\left[Y\right]} = 1 - \frac{V_{\mathbf{X}_{\sim i}}\left[\mathbb{E}_{X_i}[Y|\mathbf{X}_{\sim i}]\right]}{Var\left[Y\right]} \tag{2.25}$$

where S_{Ti} account for all the contribution to the total variance of the output $Var\left[Y\right]$ when the first order effect of $\mathbf{X}_{\sim i}$ is removed. On the contrary of S_i, we have in general $\sum_i S_{Ti} \geqslant 1$ as the input factor effects are accounted multiple times because of interactions within the model (we have $\sum_i S_{Ti} = 1$ only in case of purely additive models).

Elementary effects and Morris diagram

The Elementary Effects (EEs) is a screening method used identify the effect of input factors $X(i)$ with $i = 1, 2, .., m$ on the output Y of a mathematical or computational model $M(\mathbf{X})$. The method consists in the calculation of m incremental ratios, also called Elementary Effects, which are used to assess the influence of the input variables and parameters and are somehow analogous to partial derivatives of a dependent variable Y with respect to x. The i^{th} elementary effect of the m-dimensional input vector $\mathbf{X}_0$ is defined as follows:

$$\delta_i(\mathbf{X}_0) = \frac{Y(X_0(1), ., X_0(i) + \Delta, ., X_0(m)) - Y(\mathbf{X}_0)}{\Delta} \tag{2.26}$$

where the quantity Δ is a given variation in the input factor whose effect has to be evaluated. Intuitively speaking, the input factors leading to the higher incremental ratios $\delta_i(\mathbf{X}_0)$ have to be considered as the most relevant for the output quantity Y. Of curse, this relevance metric is valid only locally, in $\mathbf{X}_0$, where Y has been evaluated. Repeated One-At-a-Time (OAT) evaluations of random vector configurations provide the elementary effect method with global sensitivity analysis features [147]. The mean and standard deviation of the EEs, resulting from random input vector configurations, can be plotted in the well-known $\mu(\delta) - \sigma(\delta)$ plot proposed by Morris [95]. If a factor X_i results in a small absolute value of the mean and small variance, it should be considered less relevant for the model. On the other hand, a factor X_i resulting in a high $|\mu(\delta_i)|$ has to be considered highly relevant for the model, i.e. it leads to the average higher variation in the output. Similarly, a factor X_i resulting in a high $\sigma(\delta_i)$ is also of interest for the model output. In fact, high $\sigma(\delta_i)$ probably indicate a non-linear relation between the factor i and the output and/or a relevant interaction with other factors. Figure 2.9 presents an example of Morris diagram. The standard error of the mean (SEM) is

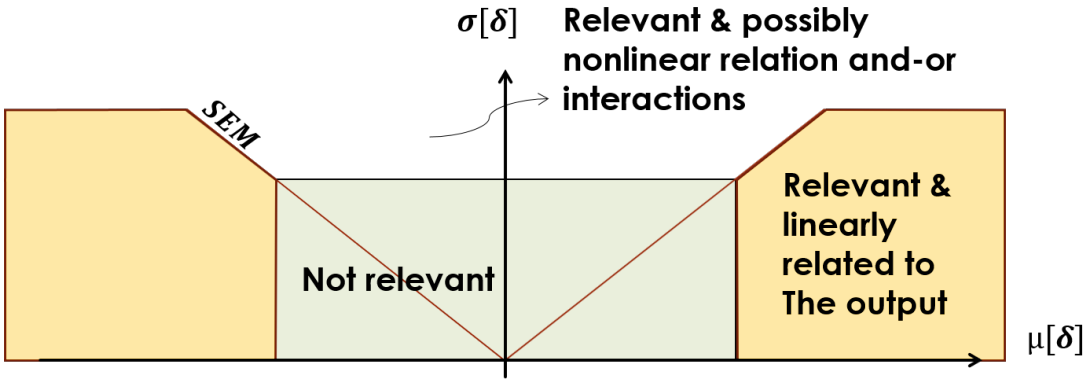

Figure 2.9: An example of Morris diagram and how to discern between important and non-important factors.

used to partition the plot in different areas of interest. The method has some points of strength, worth highlighting:

1. It is relatively easy to implement;
2. Computationally cheap compared to other global sensitivity methods, also for a high number of factors;
3. It uses a sensitivity measure which is simple to communicate (similarity between incremental rations and partial derivatives) to non-experts;
4. Compared to variance/based measures, shows if the input factors are (in average) positively or negatively correlated to the output;

P-boxes sensitivity and epistemic space pinching

Sensitivity analysis is performed to systematically investigate how input variables influence the output of the model. In many cases, it is possible to reduce the dimensionality of an input space and understand which among the input estimates should be improved to improve the most the output estimate [109]. Sensitivity analysis is common practice in Monte Carlo based approaches but it has been proposed also for non-parametric input P-boxes trough pinching and focal elements propagation [50]. Classically, variance-based sensitivity analysis of the output is done by fixing the uncertain input variables to precise values and quantifying its effect on the uncertainty in the output (e.g. reduction in variance) before and after reducing the input uncertainty [111]. For P-boxes sensitivity analysis, this procedure is referred to as "pinching" of the epistemic-aleatory space. The pinching can be done in several ways, for instance, a P-box can be pinched to a precise distribution, can be replaced with a precise point value, or pinched to an interval with zero variance (i.e. removing the aleatory uncertainty but not the epistemic uncertainty). Figure 2.10 shows input P-boxes pinched to point values and

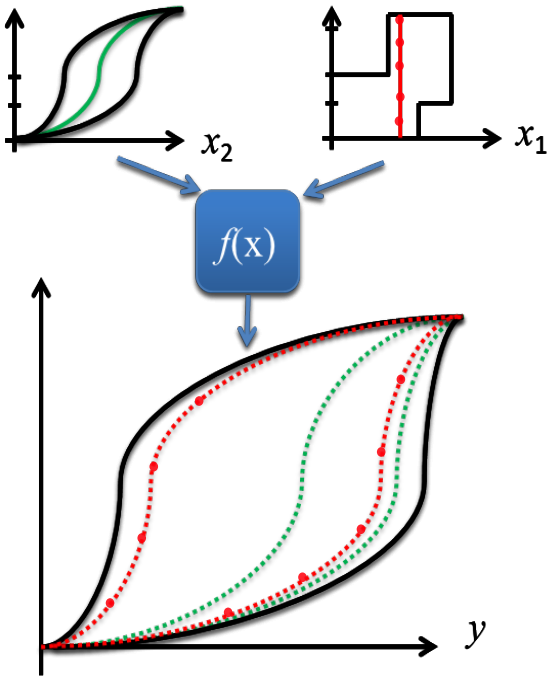

Figure 2.10: This figure presents 2 examples of P-box "pinching" and sensitivity analysis. The variable x_2 is pinched to a specific CDF, whilst X_1 to a precise point-value. The former leads to the higher reduction in the P-box area.

to a precise CDF. The uncertainty in the output of a model $f(x)$ is reduced accordingly.

Analogously to variance-based methods used in a global sensitivity analysis, a sensitivity index $Sidx$ can be computed as, for instance, a percentage of reduction in a measure of uncertainty of the output δ. An example of a sensitivity measure can be as follows:

$$Sidx = 100\left(\frac{\delta - \delta_i}{\delta}\right) \tag{2.27}$$

where δ_i is the uncertainty after pinching of input variable i. A straightforward indicator of the epistemic uncertainty in the P-box is the area between upper and lower bounds. The measure δ is computed as follows:

$$\delta = \int_{-\infty}^{+\infty} |\overline{F}_X(x) - \underline{F}_X(x)|dx \tag{2.28}$$

This index can be used to rank the epistemic uncertain inputs with respect to their effect on the uncertainty in the output.

2.8.2 Surrogates models

Surrogate models, also known in the literature as meta-models or emulators, are mathematical models used to mimic the input-output relation of the computational expensive numerical model $\mathcal{M}$. This is generally done by replacing the high-fidelity model with a cheaper analytical model $\hat{\mathcal{M}}$. Some examples of surrogate models are Artificial Neural Networks (ANN) [166], Poly-Harmonic Splines [78], Extreme Learning Machines [58], Kriging models and response surfaces.

Artificial neural networks

An ANN is a mathematical model defining a function $\hat{\mathcal{M}} : \mathbf{I} \rightarrow \mathbf{Y}$ where $\hat{\mathcal{M}}(g)$ is a composition (e.g. non-linear weighted sum) of other weighted functions $g_i(x)$. The basic architecture for a feed-forward ANN consists of one input layer, one or more hidden layers and one output layer [166]. Each layer employs several artificial neurons, also known as nodes, which are connected to the neurons of the adjacent layers by weighted links. In each neuron, the inputs are first weighted and, then, summed as follows:

$$g(x) = \sum_{i=1}^{n} \omega_i \cdot g_i(x) + b$$

where ω_i are the weights, $g_i(x)$ is the output of the node i in the previous layer and b is the bias, which is generally introduced in the hidden and output layers and acts as a threshold for the argument of the activation function. The sum $g(x)$ is processed by an activation function K to produce the neuron's output. An example of commonly employed activation function is the sigmoidal function, defined as follow:

$$K(g) = \frac{1}{(1 + e^{-g})}$$

Figure 2.12 exemplifies a neural network architecture and node functionality is depicted.

Select a suitable ANN topology is a problem specific task and it can be useful to maximise the emulator performance. Advanced optimisation approaches can be employed for the selection. A simple but computationally demanding method consists of a heuristic testing of different architectures, exploring different combinations of hidden neurons and hidden layers. Then, the best ANN architecture is selected based on a performance indicator. The coefficient R^2 can be used as the performance index of the ANN regression and used to select the most suitable ANN architecture. The R^2 coefficient is expressed as follows:

$$R^2 = 1 - \frac{\sum_i (y_i - \hat{y}_i)^2}{\sum_i (y_i - \bar{y})^2}$$

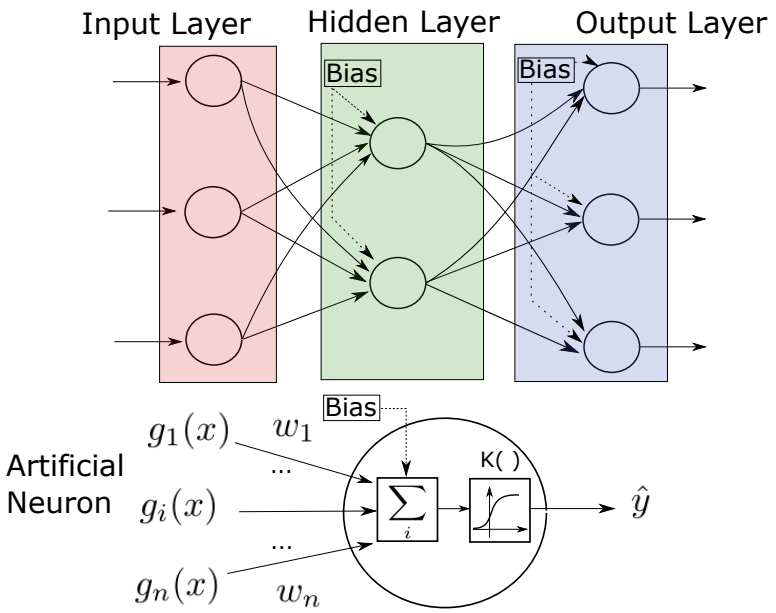

Figure 2.11: Conceptual scheme of an Artificial Neural Network architecture and the function of an artificial neuron.

where y_i is the i^{th} output of the high-fidelity model, $\hat{y}_i$ is the output predicted by the surrogate model, $\bar{y}$ is the average of the output of the high-fidelity model.

Gaussian process emulators

A Gaussian Process Emulator (GPE), also known as Kriging emulator, is a stochastic process (i.e. a collection of random variables in the time and/or space domains), such that every finite linear combination of them is normally distributed. The concept of Gaussian processes is named after Carl Friedrich Gauss because it is based on the notion of the Gaussian distribution (normal distribution). Gaussian processes can be seen as an infinite-dimensional generalization of multivariate normal distributions. The distribution of a Gaussian process is the joint distribution of all those (infinitely many) random variables, and as such, it is a distribution over functions with a continuous domain, e.g. time or space. Algorithms that involve GPs use a measure of the similarity between points also known as the kernel function. The kernel is used to forecast the value for an unvisited data point in the input domain (i.e. a point not available in the training data). One of the main advantages of GPEs is that the predicted output has a measure of uncertainty which is automatically associated with it (i.e.the marginal distribution at that point). Gaussian processes are useful in statistical modelling, benefiting from properties inherited from the normal and to replace computationally expensive models.

Let $f(\mathbf{x})$ be a function or a computer model mapping a multidimensional input on the real line, $f : \mathbb{R}^m \rightarrow \mathbb{R}$. Let $\mathbf{X} = \{\mathbf{x}_1, .., \mathbf{x}_n\}$ be a set of n design points (i.e. the

set of points in the input space) and corresponding set of outputs $\mathbf{Y} = \{y_1, .., y_n\}$, such that $\mathbf{x}_i \in \mathbb{R}^m \forall i = 1..., n$ denotes a given input configuration and each output reads $y_i = f(\mathbf{x}_i) \forall i = 1..., n$. Then, each pair $(\mathbf{x}_i, y_i)$ denotes a training run for the Gaussian Process Emulator, which is assumed to be an interpolation model $y_i = \hat{f}(\mathbf{x}_i)$. If a fully parametrised Gaussian process prior is assumed for the outputs of the simulator, then the set of design points has a joint Gaussian distribution. The general assumption is that the simulator satisfies the statistical model for the output with the following structure:

$$f(\mathbf{x}) = h(\mathbf{x})^T \beta + Z(\mathbf{x}|\sigma^2, \phi) \tag{2.29}$$

where $h(\cdot)$ is a vector of known basis (location) functions of the input, β is a vector of regression coefficients, and $Z(\mathbf{x}|\sigma^2, \phi)$ is a Gaussian process with zero mean and covariance function $cov(x, x'|\phi, \sigma^2) = \sigma^2 k(x, x'|\phi)$ where σ^2 is the signal noise and $\phi \in \mathbb{R}^m$ denotes the length-scale parameters of the correlation (kernel) function $k(\cdot, \cdot)$. The kernel function is capable of measuring the distance between different input (and corresponding output) configurations are. The base of such measure is related to the Euclidean distance in such a way that it weights differently each input variable.

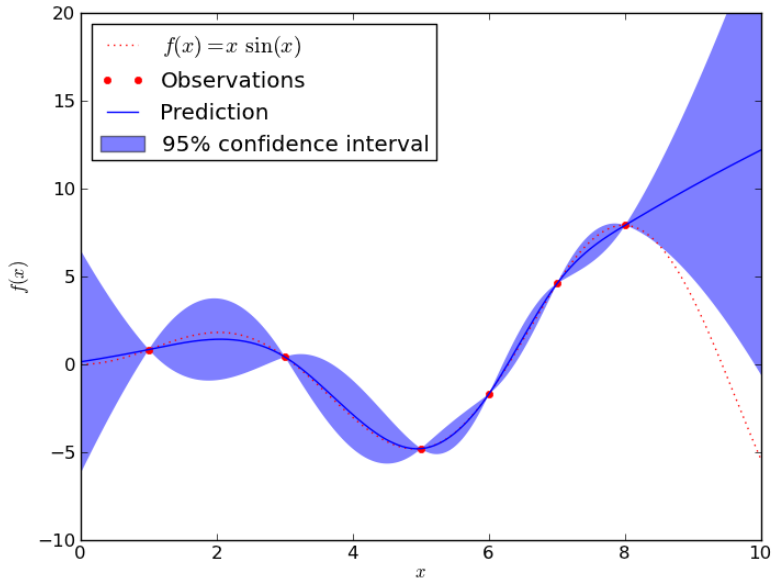

Figure 2.12: An example of Gaussian process regression using 6 data points gnerated by an unknown function $f(x)$. The uncertainty (confidence interval) is larger in the area of the input spaced where data is not provided and is zero in correspondence of the training points.

2.8.3 Bayes' theorem and model updating

A Bayesian model updating procedure is based on the well-known Bayes' theorem [13]. The general formulation is the following:

$$P(\boldsymbol{\theta}|D,I) = \frac{P(D|\boldsymbol{\theta},I)\,P(\boldsymbol{\theta}|I)}{P(D|I)} \tag{2.30}$$

where $\boldsymbol{\theta}$ represents any hypothesis to be tested, e.g. the value of the model parameters, D is the available data (i.e. observations), and I is the background information. Main terms can be identified in the Bayes' theorem:

- $P(D|\boldsymbol{\theta},I)$ is the likelihood function of the data D;
- $P(\boldsymbol{\theta}|I)$ is the prior probability density function (PDF) of the parameters;
- $P(\boldsymbol{\theta}|D,I)$ is the posterior PDF;
- $P(D|I)$ is a normalization factor ensuring that the posterior PDF integrates to 1;

The equation (2.30) introduces a way to update some a priori knowledge on the parameters $\boldsymbol{\theta}$, by using data or observations D and conditional to some available information or hypothesis I.

In a model updating framework, the initial knowledge about the unknown adjustable parameters, e.g. from prior expertise, is expressed through a prior PDF. A proper prior distribution can be a uniform distribution in the case when only a lower and upper bound of the parameter is known, or a Gaussian distribution when the mean and the relative error of the parameter are known. The likelihood function gives a measure of the agreement between the available experimental data and the corresponding numerical model output [168]. Particular care has to be taken in the definition of the likelihood, and its choice depends on the type of data available, e.g. whether the data is a scalar or a vector quantity. Different likelihood leads to different accuracy and efficiency in the results of the updating procedure and should be selected with caution; as an example, the use of unsuitable likelihood function might cause that the model updating does not produce any relevant variation in the prior [119].
Finally, the posterior distribution expresses the updated knowledge about the parameters, providing information on the most plausible ranges of values, based on the initial knowledge and on the collected experimental data.

2.8.4 Transitional Markov-Chain Monte-Carlo

The Bayesian updating expressed in equation (2.30) needs a normalizing factor $P(D|I)$, that can be very complex to obtain or not treatable. An effective stochastic simulation algorithm, called Transitional Markov Chain Monte Carlo (TMCMC) [28], has been

used in this analysis. This algorithm allows the generation of samples from the complex shaped unknown posterior distribution through an iterative approach. In this algorithm, m intermediate distributions P_i are introduced:

$$P_i \propto P\left(D|\boldsymbol{\theta}, I\right)^{\beta_i} P\left(\boldsymbol{\theta}|I\right) \tag{2.31}$$

where the contribution of the likelihood is scaled down by an exponent β_i, with $0 = \beta_0 < .. < \beta_i < .. < \beta_m = 1$, thus the first distribution is the prior PDF, and the last is the posterior distribution. The value of these exponents β_i is automatically selected to ensure that the dispersion of the samples at each step meet a prescribed target. For additional information, the reader is reminded to [28]. These intermediate distributions show a more gradual change in the shape from one step to the next when compared with the shape variation from the prior to the posterior.
In the first step, samples are generated from the prior PDF using direct Monte-Carlo. Then, samples from the P_{i+1} distribution are generated using Markov chains with the Metropolis-Hasting algorithm [55], starting from selected samples taken from the P_i distribution, and β_i is updated. This step is repeated until the distribution characterized by $\beta_i = 1$ is reached. By using the Metropolis-Hasting algorithm, samples are generated from the posterior PDF without the necessity of ever computing the normalization constant. By employing intermediate distributions, it is easier for the updating procedure to generate samples also from posterior showing very complex distribution, e.g., very peaked or multi-modal. The Bayesian model updating procedure solved using TMCMC requires many model evaluations and the overall computational time for the detection can result very high. To reduce computational time, a surrogate model approach can be adopted.

Chapter 3

Power Grid Reliability, Vulnerability and Resilience

3.1 Abstract

In this chapter we introduce some of the basic concepts for the analysis of complex systems and critical infrastructures. In particular, resilience-related concepts such as risk, safety, reliability and vulnerability are reviewed and discusses. Quantitative metric are reviewed and load-flow solvers used to analyse power grid systems are introduced. It is worth pointing out that, although definitions, metrics and analysis tools introduced here come from the power grid literature, this shouldn't be regarded as a lost of generality. In fact, many of the resilience-related ideas and load-flow analysis methods naturally translates to wider class of complex systems and critical infrastructures which power grids well-represent.

Table 3.1 presents two definitions of complex systems and critical infrastructures. It is fair to argue that power grid is an extremely complex systems and it has a crucial role in the society, i.e. is a critical infrastructure. Power grid includes many highly interconnected components which are operated to provide a service/utility to the customers and society as a whole. Maximising the system productivity, minimizing the costs while assuring a safe and reliable delivery of electric power is of uttermost import. This requires robust uncertainty quantification and decision-making frameworks, capable of outperforming existing experience-based methods while accounting for uncertainty affecting system operational conditions, components health states and interactions with the external environment. Power grids are generally complex, heterogeneous, with

Complex System	A complex system can be defined as an ensemble of components, functionally and physically interconnected as in a network structure. Often heterogeneous and showing complex dynamic and complex structural behaviours [167].
Critical infrastructure	An infrastructure is called critical if its incapacity or destruction has a significant impact on health, safety, security, economics and social well-being (Council Directive 2008/114/EC) [167]. Another definition is 'infrastructure whose unavailability or destruction would have a extensive impact on economy, Infrastructure Government services and, in general, on everyday life, with severe consequences for a nation [34].

Table 3.1: Definition of Complex Systems and Critical Infrastructure

many highly interconnected components connected in a network-like fashion. Also, even a partial disruption of the grid would cause significant damage to the society and economy of the affected state. The power grid is probably the most representative example of a complex system and critical infrastructure and, thus has been selected in this work as the reference system for the testing and verification of novel methods for generalised quantification of uncertainty. In this chapter, an in-depth review of probabilistic methods for power grid safety analysis and a concise introduction to safety-related terminology is presented. In this chapter we introduce some of the basic concepts for the analysis of complex systems and critical infrastructures safety and reliability and with particular regard to power grid systems. Two literature definitions of complex systems and critical infrastructures are presented within Table 3.1.

3.2 Power grid background information: Reliability, risk, vulnerability and resilience

Table 3.2 reviews some of the most widely applied concepts often used within safety-related power grid analysis.

Reliability usually refers to the ability of the system to satisfying operational criteria over the long run (or to perform a given function over a given time interval). Similarly, but with a slightly different meaning, probabilistic risk assessments in power grids focus on providing satisfactory operations accounting for the consequences of unwarranted events and the probability of facing those events. Different metrics are generally used to quantify different risks and probabilistic risk metrics are more commonly adopted when the analysts are interested in short-term (operational) scenarios [84]- [157], although these metrics have been effectively employed also to perform long-term maintenance and planning evaluations [122]. Table 3.3 and Table 3.4 present two (non-exhaustive) lists including some the most widely applied indices for power grid reliability and risk analysis, respectively. The list includes the metrics proposed within the IEEE reliability standards [59] and other reliability and risk indices which have been recently defined to match specific analysis goals.

The term robustness (sometimes defined as the opposite of vulnerability for power grids) is used to quantify network damages after unexpected events occur. It is closely linked to the system reliability and risk concepts but it primarily focuses on extremely rare events with, in general, very high consequences for the system (e.g. malicious terrorist attacks or targeted outages). Vulnerability assessments generally focus on the network structure rather on the system operations (i.e. its topology/architecture rather than the safe operations) although some works have been proposed to extend this type of analysis with information from the operational state of the system. Power network robustness is generally assessed by using complex network theoretical concepts and graph theory. This is going to be discussed in more details in Chapter 5 of this thesis. The definition of suitable metrics for robustness and vulnerability assessment of power grid is an open topic of research and Table 3.5 presents a sample of vulnerability metrics adopted to analyse power grid systems.

Tables 3.3 and 3.4 show the equations for the indices calculation (the third column). For the reliability indices, the term $\mathfrak{p}_i$ is the likelihood/probability of loss of capacity, t_i the duration of loss (load greater than capacity) in percent, E is the total energy in the period considered, n is the number of units, N_i is the number of customers interrupted by each incident i, N_T is the total number of customers in the system, r_i is the restoration time for each interruption, P_i is the average load interrupted by each interruption i, N_c is the total number of customers that have experienced at least one interruption during the reporting period, $N_{c,k>n}$ is the number of customers who experienced more than n sustained interruption and monetary interruption events during the observed period, T is the time interval or observed period (e.g. 8760 hours).

Reliability	The probability of satisfactory operation over the long run [67].
Risk	Product of the probability (or frequency) of disturbances to system operation and their consequences [122].
Robustness	Degree to which a network is able to withstand an unexpected event without degradation in performance. It quantifies how much damage occurs as a consequence of such unexpected perturbation [34].
Vulnerability	The lack of robustness. Vulnerability is often used to score low reliability of power grids [34].
Resilience	The ability to withstand high impact-low probability events, rapidly recovering and improving operations and structures to mitigate the impact of similar events in the future [104].
Adequacy	Reliability criteria in terms of violations of static failure conditions are called adequacy criteria [85].
Security	Reliability criteria in terms of violations of dynamic failure conditions are called security criteria [85].
Contingency	Unexpected failure (outage) of grid component (e.g. generator, line, transformer) [122] [27].
Disturbance	An unexpected event that produces an anomalous system condition [34].
N-k Contingency	'Simultaneous' failure of k components in the system. [27].

Table 3.2: State of the art definitions of safety related concepts for power grids.

3.2.1 Reliability metrics

Power grid reliability assessments have been traditionally performed by using analytical methods or by using simulation-based methods. Table 3.3 presents some of the most widely applied reliability metrics.

Recently, the Council of European Energy Regulators (CEER) proposed an accurate review of the historical trend for the power grid reliability scores of countries belonging to the European power network. The Benchmarking Report [99] on the continuity of electricity and gas supply presents reliability trend for the European grids in the last 10-15 years is presented and mainly focusing on SAIFI, SAIDI, ENS and CAIDI. Figure 3.1, taken from [99], shows an example of historical trends for the SAIDI indices of different countries, from 2002 until 2016. This study further highlights the need to account for uncertainty, in fact, it can be observed a high variability of the reliability score. State-specific policies, energy diversification, grid topological robustness, exceptional events, etc. will lead to a very different values of the SAIDI for different countries and different years. For instance in the year 2016, Switzerland and Germany resulted as the most stable (approximately 10 minutes interruptions per customer over the year) and reliable whilst Romania and Poland (about 300 and 200 minutes per customer over the year, respectively) score as the less reliable in terms of SAIDI index within the European network. In [99], an estimation of the total ENS for several European countries is also presented. These estimations include only unplanned events and neglect extraordinary contingencies (e.g. major power outages). Similarly to

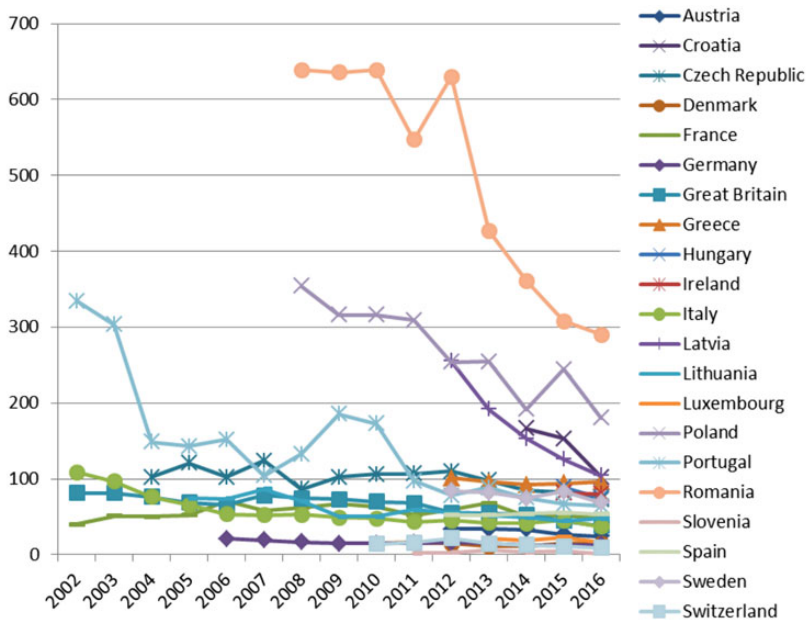

Figure 3.1: Unplanned SAIDI scores, without including exceptional events (in minutes per customer) – time series and min-max [99]

the SAIDI, also the ENS shows large variability among different networks and between different years. For instance, the Italian grid ENS score ranges from values as low as 1.5 to values higher than 3.5 MWh (between years 2006 and 2015). On the other hand, the Romanian power grid ENS ranges from 30 to about 390 between 2004 and 2014 [99].

It can be noticed that some of the reviewed indices can be computed analytically. In some cases, however, use Monte Carlo method may be necessary to calculate statistical moments of the reliability indices (e.g. expectation and variance). The moments are generally obtained by simulating different time histories/trajectories for the system and by a realistic simulation of e.g. failures, load variability. The Loss-of-Load-Probability (LOLP) is probably one of the most popular reliability measures for power grids. It is commonly used for the definition and dosing of generation capacity as a standard reliability criterion. The unreliability of a system in this context is viewed as its inability to meet the daily peak load. A loss of load occurs whenever the system load exceeds the available generating capacity. The overall probability that there will be a shortage of power (loss of load) is called the Loss-of-Load-Probability. It is usually expressed terms of days per year, hours per day, hours per year or as a percentage of time. When expressed as the expected accumulated amount of time during which a shortage of power is experienced, the measure is more correctly referred to as the loss of load expectation (LOLE). A common practice is to plan the power system to achieve an LOLP of one-day-in-ten-years.

The CAIDI gives the average outage duration that any given customer would experience, it can also be viewed as the average restoration time and measured in units of time, often minutes or hours. The System Average Interruption Duration Index (SAIDI) indicates the total duration of interruption for the average customer during a predefined period of time. It is commonly measured in customer minutes or customer hours of interruption. The Customer Average Interruption Duration Index (CAIDI) represents the average time required to restore service. The Customer Total Average Interruption Duration Index (CTAIDI) represents the total time in the reporting period that average customers who actually experienced an interruption were without power. This index is a hybrid of CAIDI and is similarly calculated, except that those customers with multiple interruptions are counted only once. The Average Service Availability Index (ASAI) represents the fraction of time (often in percentage) that a customer has received power during the defined reporting period. The System Average Interruption Frequency Index (SAIFI) indicates how often the average customer experiences a sustained interruption over a predefined period of time. The Customers Experiencing Multiple Sustained Interruption and Momentary Interruption Events Index (CEMSMIn) is the ratio of individual customers experiencing n or more sustained interruptions or/and momentary interruption events to the total customers served. Its purpose is to help identify customer issues that cannot be observed by using averages.

3.2.2 Risk metrics

Risk is defined as the product of the probability (or frequency) of disturbances to system operation and their consequences. Probability of face an event and the consequences of this event, i.e. the severity, are to be computed to quantify the system risk. Generally speaking, risk is defined as the product of probability of occurrence of a threatening event (i.e. a contingency/failure event) and the related consequences (i.e. severity). In order to account for multiple events in an integral way, the definition can be extended by summing all the contributions as follows:

$$R = \sum_{i=1}^{n} \mathcal{P}(E_i) Sev(E_i) \tag{3.1}$$

where $\mathcal{P}(E_i)$ is the probability of occurrence of the undesired event E_i and $Sev(E_i)$ quantify the consequences or severity if the event happens.

Also for power grids, risk indices generally include a probabilistic term and a severity term. In the last decades, many severity metrics have been proposed to evaluate different consequences on different system features. Table 3.4 presents a short list of some of the most commonly adopted risk metrics to analyse the power grid. In the Table 3.4, the term $\mathcal{P}(C_k|\zeta)$ defines the probability to face the contingency C_k under the

LOLP	Loss-of-Load-Probability	$\sum_{i=1}^{n} \mathfrak{p}_i \cdot t_i$	[h/yr]
LOLE	Loss-of-Load-Expectation	$\sum_{i=1}^{n} \mathfrak{p}_i \cdot t_i \cdot T$	[h/yr]
LOEE	Loss-of-Energy-Expectation	$\sum_{i=1}^{n} \frac{\mathfrak{p}_i \cdot P_i}{E}$	[kWh/yr]
ENS	Energy Not Supplied	$\sum_i P_i \cdot r_i$	[kWh/yr]
AENS	Average Energy Not Supplied	$\sum_i \frac{P_i \cdot r_i}{\sum_i N_i}$	[kWh/yr cust]
SAIFI	System average interruption frequency index	$\sum_i \frac{N_i}{N_T}$	[int/yr cust]
SAIDI	System average interruption duration index	$\sum_i \frac{N_i \cdot r_i}{N_T}$	[h/yr cust]
CAIDI	Customer average interruption duration index	$\sum_i \frac{N_i \cdot r_i}{\sum_i N_i}$	[h/yr cust]
CTAIDI	Customer total average interruption duration index	$\sum_i \frac{N_i \cdot r_i}{N_c}$	[h/yr cust]
CAIFI	Customer average interruption frequency index	$\sum_i \frac{N_i}{N_c}$	[h/cust]
ASAI	Average service availability index	$\sum_i \frac{N_i \cdot r_i}{N_T \cdot T}$	[h/yr cust]
CEMI$_n$	Customers experiencing multiple interruptions	$\frac{N_{c,k>n}}{N_T}$	[int/yr cust]

Table 3.3: Definition of reliability indices for power grid analysis. Reliability indices are taken form the IEEE summary in reference [59]. The unit of measure refers to an observed period T of 1 year (yr).

$\mathbf{R}_{OL}$	Over Load Risk	$\sum_j \sum_k \mathcal{P}(C_k\|\zeta) \cdot S_{OL,j}(C_k, \zeta)$
$\mathbf{R}_{LV}$	Low Voltage Risk	$\sum_b \sum_k \mathcal{P}(C_k\|\zeta) \cdot S_{LV,b}(C_k, \zeta)$
$\mathbf{R}_{VI}$	Voltage Instability Risk	$\sum_k \mathcal{P}(C_k\|\zeta) \cdot S_{VI}(C_k, \zeta)$
$\mathbf{R}_{COL}$	Cascading Over Load Risk	$\sum_j \sum_k \mathcal{P}(C_j\|C_k, \zeta) \cdot S_{OL,j}(C_k, \zeta)$
$\mathbf{R}_{LoL}$	Loss of Load Risk	$\sum_k \mathcal{P}(C_k, \zeta) \cdot S_{LoL,j}(C_k, \zeta)$

Table 3.4: Definition of risk indices for power grid analysis. Indices have been taken from references [122]- [85].

environmental-operational conditions ζ, C_k refers to the k^{th} contingency listed (e.g. the k^{th} line, generator or transformer failure). The overload severity function for the line j under the contingency k and grid-environment condition ζ is $S_{OL,j}(C_k, \zeta)$; $S_{LV,b}(C_k, \zeta)$ is the low voltage severity of the node (bus) b; $S_{VI}(C_k, \zeta)$ is the voltage instability severity function, defined for the whole system under contingency k, $\mathcal{P}(C_j|C_k, \zeta)$ is a probabilistic indicator for cascading failures (i.e. probability of face failure C_j after failure C_k) and $S_{LoL,j}(C_k, \zeta)$ is the loss of load severity (i.e. overall load curtailed after failure C_k). The severity functions can be defined focusing on different consequences and with several mathematical expressions, as explained in [156] (e.g. step-discrete, continuous linear, continuous exponential, etc.). As mentioned, each severity function is defined to extract specific system features, grid behaviours or physical limits. For instance, the overload severity function relates to the thermal limit of transmission and distribution lines, the low voltage severity is connected to the stability of the system and to the reactive power consumption at each bus, thus to the possibility of facing generators tripping. Both overload and low voltage severity function are specifically defined for each component in the power network and thanks to the additive propriety of risk can be summed to provide an overall risk index for the grid as a whole. Conversely, the voltage instability severity function is specifically defined for the system as a whole and it is computed as the percentage of margin from the loadability point in the nose curve (i.e. Power-Voltage curve), thus, providing an indicator of how adequate is the given system state to satisfy the power need of the customers. The cascading index, similarly to overload risk, relates to the lines thermal limits but accounts also for the conditional probability of failure after previous contingencies such as the $N-1-1$ contingency (i.e. secondary single failure after the first $N-1$ contingency).

An example of a risk model for power grid analysis

In traditional deterministic risk assessment, the impact of each failure is considered but the likelihood of facing the contingency is not. In probabilistic risk assessment, the probability of components failure is estimated based on the available information and historical data. In this example, the probability of each contingency takes into account

the failure of a distribution line by, for instance, a Poison distribution function as in [97]:

$$\mathcal{P}(C_l) = [1 - \exp(\lambda_l l_l)] \exp(-\sum_{j \neq l} \lambda_j l_j) \tag{3.2}$$

where $\mathcal{P}(C_l)$ is the probability of line contingency l in the next 1 h, λ_l is the failure rate of the distribution line l per unit time and length and l_l source is the length of the l^{th} line. The expression 3.2 holds if the contingencies list include all the single line failures, considered as mutually exclusive events in the model.

Severity functions are used to quantify the extent of the failure, several types of severity expressions have been introduced in literature. The continuous type for overload is specifically defined for each circuit (distribution lines and transformers) and it measures the extent of violation in terms of excessive power flow as the percentage of rating PR_l. The PR_l value is obtained as the ratio between active power flowing in the line f_l and its emergency rating $f_{emerg,l}$. The expression for the continuous severity due to overload of a line l is:

$$S_{OL,l} = d * PR_l + c \quad for \quad PR_l \geqslant PR_l^{min} \tag{3.3}$$

where the severity $S_{OL,l}$ is zero for PR_l values less than a safety limit PR_l^{min}=0.9. The deterministic limit for the violation of line l is PR_l=1, the near violation region is 0.9$\leqslant PR_l <$1, and the value PR_l under 0.9 is regarded as safe, d=10 and c=-9.

3.2.3 Vulnerability metrics

An interesting field of research to analyse power grid vulnerability is the one employing topological models based on network theory. Graph-theoretic models are particularly valuable for assessing the robustness/vulnerability of critical infrastructures as most systems are naturally organised as networks. Pure topological models disregard physical proprieties of the system (e.g. flows, electrical parameters), instead representing the system abstractly as an unweighted graph $\mathcal{G} = \{\mathcal{N}, \mathcal{L}\}$, i.e. a collection of nodes $n \in \mathcal{N}$ and edges $l \in \mathcal{L}$ [20]- [73]- [47]- [38]. In the simplest category of topological models, there is no differentiation between components in the system; that is, different functions within the set of nodes or edges are ignored [69]. For power systems, this means that substations, buses, generators are equally treated as nodes and transmission cables, underground or overhead distribution cables are equally treated as edges.

Those approaches have been criticised as they seem to be unable to capture entirely the complexity of the network. However, these can be computationally very cheap and offer a fast way to analyse efficiently large size systems. These can be used to provide an ancillary point of view on the gird by analysing only its structure and trying

to extrapolate collective systemic behaviours and weaknesses rather than analyse its detailed operations. More recently, extended topological approaches were attempted by including information from the electrical engineering field. Extended topological approaches can be used to differentiate between e.g. substations and generators or adopting weighted graphs $\mathcal{G} = \{\mathcal{N}, \mathcal{L}, \mathbf{w}\}$ to include electrical proprieties of the system within the analysis (e.g. reactive and active flows, line lengths, susceptances, thermal limits, etc.) [20]- [73]- [47]- [38].

M. Ouyang et al. [100] analysed the correlation of six topology-based vulnerability metrics respect to single and multiple component failures. E. Bompard et al. [20] compared two hybrid metrics (i.e. extended betweenness and net-ability) by ranking components with respect to the system vulnerability. Recently, Lucas Cuadra et al. [34] reviewed power grid robustness metrics computed adopting complex network theory approaches. Authors of reference [145] show a method to perform power grid partitioning (best islands section) clustering spectral proprieties of the power grid associated graph. A relatively new field of research deals with the spectral graph analysis of power grid, where vulnerability metrics have been obtained from the spectral decomposition of the weighted adjacency matrix and the Laplacian of the adjacency matrix. Examples are the spectral radius ($\rho_{\mathcal{G}}$) [148], the algebraic connectivity (μ_2) [65]- [122], the natural connectivity $\overline{\lambda}_{\mathcal{G}}$ [112] and effective graph resistance $R_{\mathcal{G}}$ [65] (see Chapter 5 for further details).
Table 3.5 review some of the most applied vulnerability indices based on network theory and analysis of the power grid associated graph. The diameter of a network is defined as the 'longest shortest path' in the network, where $d_{i,j}$ is the minimum number of edges (i.e. geodesic distance) between node i and node j. The shortest path between node i and j is called geodesic path and the number of geodesic paths passing through a node n and a edge l are named $\sigma_{ij}(n)$ and $\sigma_{ij}(l)$, respectively. Connectivity loss describes the ability of distribution substations to receive power from the generators, where N_g is the total number of generators, N_D is the total number of distribution substations, and N_G^i is the number of generators connected to substation i. The Spectral radius is the largest eigenvalue of adjacency matrix associated to the graph λ_1 whilst μ_2 is the second smallest eigenvalue of the Laplacian of the adjacency matrix.

3.2.4 Resilience metrics

The first influential quantitative resilience metric based on the functionality recovery curve was proposed by Bruneau et al. [22], where resilience is quantified as a loss in functional (or resilience) performance as follows:

$$R_L = \int_{t_0}^{t_f} [100\% - Q(t)]dt \tag{3.4}$$

D	Diameter	$max_{i,j}\ d_{i,j}$
E	Efficiency	$\frac{1}{N(N-1)} \sum_{i,j} \frac{1}{d_{i,j}}$
CL	Connectivity loss	$1 - \frac{1}{N_D} \sum_{i}^{N_D} \frac{N_g^i}{N_G}$
C_n	Node Centrality	$\frac{deg(n)}{n-1}$
$\overline{\lambda}_{\mathcal{G}}$	Natural connectivity	$\ln\left(\frac{1}{N} \cdot \sum_{1=1}^{N} e^{\lambda_i}\right)$
$R_{\mathcal{G}}$	Effective resistance	$N \cdot \sum_{i}^{N} \frac{1}{\mu_i}$
$\rho_{\mathcal{G}}$	Spectral radius	λ_1
μ_2	Algebraic connectivity	μ_2
$\mathcal{B}(n)$	Node betweenness	$\sum_i \sum_j \frac{\sigma_{ij}(n)}{\sigma_{ij}}$
$\mathcal{B}(l)$	Edge betweenness	$\sum_i \sum_j \frac{\sigma_{ij}(l)}{\sigma_{ij}}$

Table 3.5: A non-comprhensive list of vulnerability indices for power grid robustness analysis [20]- [64]- [69].

where $Q(t)$ is the system functionality/utility at time t; t_0 is the time when the event strikes; t_f is the time when the system utility fully recovers and R_L is positive definite. It has the advantage of being easily generalized to different structures, infrastructures, and communities. This definition assumes that the functionality is 100% pre-event and will eventually be recovered to a full functionality of 100%, although this may not be true in practice. A system may be partially functional when a hurricane strikes and may not be fully recovered due to uneconomic cost-benefit ratio.

Resilience index can be obtained normalized metric between 0 and 1, computed from the functionality recovery curve:

$$R = \frac{\int_{t_0}^{t_h} Q(t)dt}{t_h - t_0} \tag{3.5}$$

where t_h is the time horizon of interest. In the power grid reliability and resilience analysis context, the ENS reliability metric has been used to measure resilience of power grids, e.g. [43]- [102]- [104], it directly quantifies the power grid loss in functionality as the area between a power demand curve and a power supply curve. Figure 3.2 shows an example of Energy-Not-Supplied due to unexpected system disturbances.

The ENS and its robust estimation (i.e the Expected ENS which accounts for relevant sources of uncertainty sources), are commonly adopted to assess power grids reliability. Nonetheless, they are also suitable to describe key features of the resilience concept when calculated in a broader framework which accounts for degradation, recovery during an event, as well as the comparison of system's resilience performance in different scenarios and stress by different hazards [43].

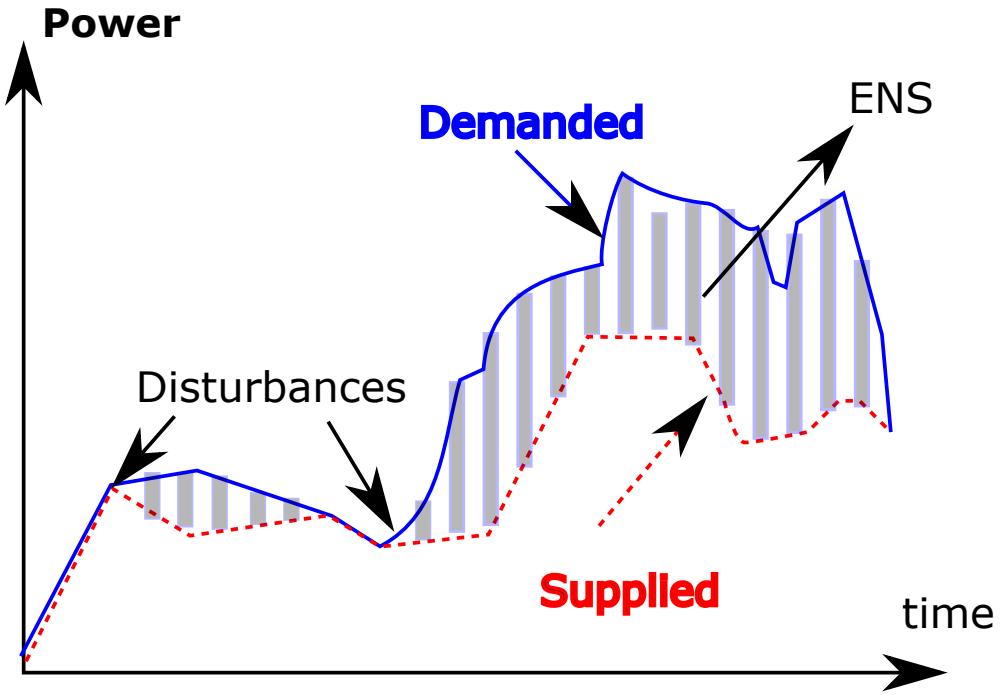

Figure 3.2: An example of ENS quantification. The Energy-not-supplied index is calculated as the area intercepted by the overall power demand curve and the overall power supply over time

3.3 Introduction to Power Flow methods

Power-flow or load-flow studies are important for planning the future expansion of power systems as well as in determining the best operation of existing systems. The principal information obtained from the power-flow study is the magnitude and phase angle of the voltage at each bus, and the real and reactive power flowing in each line. Power flow methods are commonly used in several power grid evaluation frameworks and their applicability is scope/goal dependent. Generally, power flow methods are used to simulate/approximate/reproduce a realistic system behaviours and to assess a variety of system features such as, operational costs, design costs, stability, adequacy, etc.
Power flow methods can be used to simulate the power grid performance in the long run (e.g. design problems) or for short-term and medium-term time frames (e.g. operational policies, control strategies, different power market structures, etc.). Different problems will define tight or weak constraints on the computational cost of the analysis. For instance, economic dispatch problems compared to design problems will result in tighter constraints on the computational cost as they often deal with 1-day ahead, 1-h ahead, or even real-time scheduling of the power produced by the controllable generators. The generalized uncertainty quantification methods proposed in this dissertation mainly focuses over problems for which the computational cost of the analysis is not a restrictive constraint (e.g. maintenance problems or design problems such as topological enhancements). Nonetheless, their applicability is theoretically extendable to short-term medium-term decision processes, this is considered beyond the scope of this work. Applicability to short-term time frame would require a substantial reduction in computational complexity. This issue will be further discussed in the remaining of this dissertation. The rest of this chapter presents a summary of power flow problems, acronyms and associated system constraints. Table 3.6 presents a list of some of the most widely applied methods.

3.3.1 AC and DC Power Flow (PF)

Alternating-Current (AC) and the Direct-Current (DC) are the most widely-used power-flow models to analyse power grid. AC-PF and DC-PF are commonly used in both the academic research environment and in the industrial sectors, a simple but representative example of everyday life industrial use of those technologies is the energy dispatch problem, which is the scheduling of the production from generators so that the overall cost of the network is minimised and power demand satisfied.

Specifically, the AC power flow aims at solving a system of non-linear power balance equations. It accounts for both active and reactive power without neglecting line loses (see Table 3.6). In the AC model, the active and reactive nodal power balance equations

are defined as follows [149]:

$$\begin{aligned} P_k &= \sum_{i}^{N_b} |V_i||V_k|[G_{i,k}cos(\theta_{i,k}) + B_{i,k}sin(\theta_{i,k})] \\ Q_k &= \sum_{i}^{N_b} |V_i||V_k|[G_{i,k}sin(\theta_{i,k}) - B_{i,k}cos(\theta_{i,k})] \end{aligned} \tag{3.6}$$

where $|V_i|$ is the voltage magnitude of node i, $\theta_{i,k} = \theta_i - \theta_k$ is the voltage phase difference between node i and k, P_k and Q_k are the active and reactive power injected in the node k, respectively. The elements G_l and B_l are parameters of the line l named conductance and susceptance, respectively. The AC power flow solves equations (3.6) for each node k in the set of nodes $k \in \mathcal{N}$, obtaining line active and reactive flows. The solution can be obtained using iterative techniques (e.g. Newton-Raphson method) although, it is worth remarking, convergence is not always guaranteed. In the AC formulation the average power flow in a line (f_{ij}) is obtained as the contribution of power flowing from node i to node j and vice-versa, i.e. $f_{ij} = \frac{|P_{ij}|+|P_{j,i}|}{2}$.

The DC power flow is a linear approximation of the AC power flow which accounts for just active power and neglects line losses. It has been widely used to alleviate the computational cost of numerically intensive codes as it is computationally cheap and it always has a feasible solution. The DC approximation is mainly adopted for transmission network analysis [149] as the DC assumptions are more easily met. Nonetheless, it has been used also toe analyse power distribution systems [88]. The DC formulation is based on the following 3 assumptions:

- Flat voltage profile $|V_i| = 1$ per-unit $\forall\ i \in \mathcal{N}$
- Small phases difference between each line nodes, i.e. $sin(\theta_l) \approx \theta_l\ \forall\ l \in \mathcal{L}$;
- Relatively small lines resistances i.e. $R_l \ll X_l\ \ \forall\ l \in \mathcal{L}$;

Thus, the nodal power equations can be rewritten as [149]:

$$P_k = \sum_{i}^{N_b} |V_i||V_k|B_{i,k}sin(\theta_{i,k}) \approx \sum_{i}^{N_b} B_{i,k}\theta_{i,k} = \sum_{i}^{N_b} P_{i,k} \tag{3.7}$$

where the power injected in the node k is linearly related to the lines susceptances and the voltage phase differences between the linked nodes. Because in the DC approximation the links are lossless, the average power flowing in a line becomes $f_{i,k} = |P_{i,k}| = B_{i,k}\theta_{i,k}$. The DC model although useful in reducing the computational cot of the analysis, produces inaccurate results if the underlying assumptions are not met [149]. In order to obtain good quality results, grid voltage profile should be as flat

as possible and the ratio X/R relatively high. This means that the quality of the DC solution are system and operative state dependent.

3.3.2 Optimal Power Flow (OPF)

The goal of an optimal power flow problem is to find the minimum cost of electricity generation that sattisfies a set of constraints, e.g. generation level constraints, line flow constraints, bus voltage constraints. The basic idea is to find the optimal combination of power generated by the controllable generators in the network which, given their power production cost, will minimize the operating cost of the grid. The AC formulation of the problem is defined as follows [164]:

$$
\begin{aligned}
\underset{\Theta,\mathbf{V},\mathbf{P},\mathbf{Q}}{\text{minimize}} \quad & \sum_{i=1}^{N_g}[C_P^i(P_i) + C_Q^i(Q_i)] \\
\text{subject to} \quad & g_P(\Theta, \mathbf{V}, \mathbf{P}) = 0, \\
& g_Q(\Theta, \mathbf{V}, \mathbf{Q}) = 0, \\
& h_f(\Theta, \mathbf{V}) \leqslant 0, \\
& h_t(\Theta, \mathbf{V}) \leqslant 0, \\
& \theta_{ref} \leqslant \theta_i \leqslant \theta_{ref}, \quad i = i_{ref}, i = 1, .., N_b \\
& |V_i|^{min} \leqslant |V_i| \leqslant |V_i|^{max}, \quad i = 1, .., N_b, \\
& p_i^{min} \leqslant p_i \leqslant p_i^{max}, \quad i = 1, .., N_g, \\
& q_i^{min} \leqslant q_i \leqslant q_i^{max}, \quad i = 1, .., N_g.
\end{aligned}
$$

where C_P^i and C_Q^i are the cost functions specifically defined for the active and reactive power production of the i^{th} generator, Θ, $\mathbf{V}$ are vectors of voltage phases and voltage magnitudes at each buss $i = 1, .., N_b$, $\mathbf{P}$, $\mathbf{Q}$ are the active and reactive power injections by each generator $i = 1, .., N_g$, respectively. In the AC definition of the optimal power flow problem, g_P and g_Q are the non-linear nodal power balance equations, i.e. the equality conctraints to be stattisfied for the N_b busses (see equations 3.6). The inequality constraints h_f and h_t consist of two sets of N_l branch flow limits as non-linear functions of the bus voltage angles and magnitudes, one for the 'from-end' and one for the 'to-end' of each lines [164]. Additional inequality constraints include voltage phases constraints and voltage magnitude constraints for the N_b grid nodes; reactive and active power production limits for the N_g generators installed in the grid. For further details on the problem constraints please refer to Table 3.6.

The OPF minimisation problem can be revritten in a compact form as follows [164]:

$$\begin{aligned} \underset{x}{\text{minimize}} \quad & f(x) \\ \text{subject to} \quad & g(x) = 0, \\ & h(x) \leqslant 0, \\ & x_{min} \leqslant x \leqslant x_{max}. \end{aligned}$$

were g and h are sets of equality and inequality constraints on the design variables x whereas x_{min} and x_{max} define the lower and upper bounds on the variables, respectively.

The DC formulation of the OPF problem is similar to the AC OPF definition, the main difference is that, thanks to the DC assumptions, reactive components in the constraints and in the cost function have to be neglected. Furthermore, the voltage magnitudes constraints are also removed as DC assumes unitary voltage magnitudes in each node. The nodal power flow equations are linearised as described by equation 3.7. One of the major advantages of DC-OPF formulation is that it significantly reduces the computational cost needed to solve the optimization problem and it has better convergence proprieties. Nonetheless, DC assumptions have to be used carefully as they might be unrealistic in many practical situations, thus, leading to severe approximation errors (see discussion in the previous Section).

3.3.3 Security Constrained Optimal Power Flow (SCOPF)

The optimal power flow problem aims to find the minimum cost of electricity generation that takes into account generation level constraints, line flow constraint, bus voltage constraint and other relevant constraints (see Table 3.6). However, the OPF model is not necessarily assuring security and safety of the grid operations. Specifically, if does not assure security against equipment failure, i.e. contingencies of the grid components. In the past years, attention has turned to an improved power flow models to take into account security constraints. The so-called Security Constrained Optimal Power Flow (SCOPF) guarantees that the power network can successfully balance power demand and transfer power flows in a variety of contingency situations and not only for the undamaged network topology. In fact, the generating cost of the network is minimised but ensuring that the power balance and other constraints are met even if any contingency in a predefined contingency list occur in the network (e.g. contingency caused by losing segments of the network, such as power transmission lines or power generators). similarly to the OPF, a compact definition of the SCOPF problem reads:

$$
\begin{aligned}
\underset{x}{\text{minimize}} \quad & f(x) \\
\text{subject to} \quad & g(x) = 0, \\
& h(x) \leqslant 0, \\
& s(x) \leqslant 0, \\
& x_{min} \leqslant x \leqslant x_{max}.
\end{aligned}
$$

where $s(x)$ identifies the set of security constrains on the control variables x.
One of the downsides of the SCOPF method is that it typically involve a large dimensionality of the contingency space and convergence is often difficult to reach.

3.3.4 ENS using OPF and virtual generators

The DC optimal power flow problem finds the minimum cost of electricity given a set of constraints and DC assumptions. However, in order to compute the Energy-not-supplied by the system, its formulation has to be slightly modified. One simple way to calculate the ammount of load curtailed (which is directly linked to the energy not provided to the costumers) is to adopt 'virtual generators'. The sum of the power produced by the virtual generators will correspond to the total load curtailed in the power grid. Virtual generators will be included in the optimisation problem by simply rewriting the design variable $\mathbf{x}$, objective function f as follows:

$$
\mathbf{x} = \begin{pmatrix} \mathbf{P} \\ \mathbf{P}_{vg} \\ \Theta \end{pmatrix} \qquad f(\mathbf{x}) = \mathbf{x}^T \begin{pmatrix} \mathbf{C}_P \\ \mathbf{C}_{vg} \\ 0 \end{pmatrix}
$$

where $\mathbf{P}_{vg}$ is the vector of power injections from virtual generators and $\mathbf{C}_{vg}$ is the cost associated with the power produced by the virtual generators. The cost of virtual generators is set to be $\mathbf{C}_{vg} >> \mathbf{C}_P$. This will force the optimizer to activate virtual generators only when a solution for the optimisation problem cannot be guaranteed otherwise (e.g. contingency scenarios preventing electric loads to be served adequately). Figure 3.3 presents a simple power grid system. The girid is used to illustrate more clearly the procedure for the load curtailed calculation. The system is composed of 3 substations (nodes) and 2 transmission/distribution lines having known susceptance B_{12} and B_{23}. The aggregated power demands have to be satisfied in node 2 and node 3, identified by solid black arrows. The only existing generator is allocated in node 1 and has to serve the 2 loads, however, virtual generators are assumed uniformly allocated within all the nodes of the grid (displayed with dashed lines). For the system, see Figure

Table 3.6: A conceptual comparison between power flow methods and constraints.

Acronym	Problem name	minimise cost.?	Voltage angle constraints?	Voltage Magnitude constraints?	Transmission constraints?	Losses?	Reactive power considered?	Generator costs?	Contingency constraints?
AC-OPF	Alternating-Current Optimal Power Flow	y	y	y	y	y	y	y	n
DC-OPF	Direct-Current Optimal Power Flow	y	y	n	y	n	n	y	n
AC-PF	Alternating-Current Power Flow	n	y	y	y	y	y	n	n
DC-PF	Direct-Current Power Flow	n	y	n	y	n	n	n	n
SCOPF	Security Constrained Optimal Power Flow	y	y	y	y	y	y	y	y

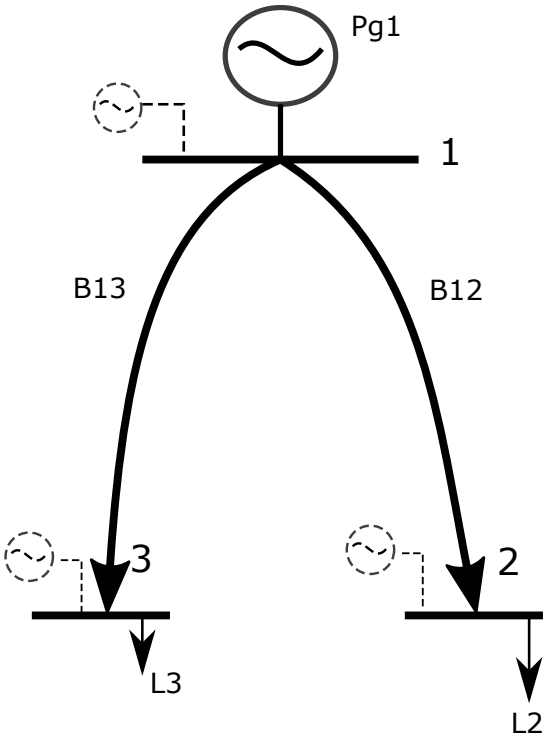

Figure 3.3: A simple 2 lines, 3 nodes power grid allocating 1 generator in node 1 and 2 loads in node 2 and 3. Virtual generators are distributed in dashed line and distributed over the 3 grid nodes to calculate the load curtailment and the ENS.

3.3, the linear DC OPF problem is then defined follows:

$$\underset{\mathbf{P},\mathbf{P}_{vg},\Theta}{\text{minimize}} \quad \begin{pmatrix} P_{g1} & P_{vg1} & P_{vg2} & P_{vg3} & \theta_1-\theta_2 & \theta_1-\theta_3 \end{pmatrix} \begin{pmatrix} C_P \\ C_{vg,1} \\ C_{vg,2} \\ C_{vg,3} \\ 0 \\ 0 \end{pmatrix}$$

and it is subject to power balance constraints

$$\begin{pmatrix} 1 & 1 & 0 & 0 & -B_{1,2} & B_{1,3} \\ 0 & 0 & 1 & 0 & B_{1,2} & 0 \\ 0 & 0 & 0 & 1 & 0 & B_{1,3} \end{pmatrix} \begin{pmatrix} P_{g1} \\ P_{vg1} \\ P_{vg2} \\ P_{vg3} \\ \theta_1-\theta_2 \\ \theta_1-\theta_3 \end{pmatrix} = \begin{pmatrix} 0 \\ L_2 \\ L_3 \end{pmatrix}$$

The power balance constraint defines a power conservation law for each node in the

grid (i.e. sum of in-flows, out-flows, injections and demands should sum up to 0), thus for node 1 it reads:

$$P_{g1} + P_{vg1} + B_{1,2}(\theta_1 - \theta_2) + B_{1,3}(\theta_1 - \theta_3) = 0$$

where $B_{1,2}(\theta_1 - \theta_2) + B_{1,3}(\theta_1 - \theta_3) = f_{1,2} + f_{1,3}$ represent the sum of power flowing from node 1 to node 2 and 3. In addition, voltage phases constraints are defined on each node and relate to the stability of the network:

$$\theta_{ref} \leqslant \theta_1 \leqslant \theta_{ref}$$

$$\theta_{ref} \leqslant \theta_2 \leqslant \theta_{ref}$$

$$\theta_{ref} \leqslant \theta_3 \leqslant \theta_{ref}$$

Power production constraints on each generator are related to technological factors (e.g. capacity and minimum operating power):

$$0 \leqslant P_{vg,1} \leqslant P_{vg,1}^{max}$$

$$0 \leqslant P_{vg,2} \leqslant P_{vg,2}^{max}$$

$$0 \leqslant P_{vg,3} \leqslant P_{vg,3}^{max}$$

$$P_{g1}^{min} \leqslant P_{g1} \leqslant P_{g1}^{max}$$

Line flows constraints on each link of the grid which relate to the cable thermal limit:

$$-P_{i,j}^{max} \leqslant B_{i,j}(\theta_i - \theta_j) \leqslant P_{i,j}^{max}$$

Let consider for this example unitary generator cost $C_P = 1$ £/MW and high cost for the virtual generators $C_{vg,i} = 1e4$ £/MW. Let assume the power demanded in node 2 is $L_2 = 40$ MW and in node 3 $L_3 = 15$ MW, $P_{g1}^{min} = 0$ MW, $P_{g1}^{max} = 40$ MW and $P_{vg,i}^{max} = 1e4$ MW and voltage angles constraints neglected. Finally, consider $B_{i,j} = 1$ for all the lines and $P_{1,2}^{max}$ and $P_{1,3}^{max}$ equal to 20 MW and 30 MW, respectively. For this example the solution of the associated optimization problem returns the design variables and cost for the network:

$$P_{g1} \cdot C_P + \sum_i P_{vg2} \cdot C_{vg,i} = 2.0035e4 \text{ £}$$

$$[P_{g1}, P_{vg1}, P_{vg2}, P_{vg3}, \theta_1 - \theta_2, \theta_1 - \theta_3] = [35, 0, 20, 0, 20, 15]$$

where $\theta_i - \theta_j = P_{i,j}$ due to unitary suceptances. It is clear that this configuration of loads and constraints prevented the network to satisfy the demanded power in node 2

(i.e. the maximum allowed line flow in 1-2 was reached). Thus, the total load curtailed corresponds to the sum of the virtual generators productions, i.e. 20 MW.

Chapter 4

Robust Reliability via Generalised Uncertainty Quantification

4.1 Abstract

In this chapter a generalised probabilistic framework is proposed for reliability assessment and uncertainty quantification under a lack of data. The developed computational tool allows the effect of epistemic uncertainty to be quantified and has been applied to assess the reliability of an electronic circuit and a power transmission network. The strength and weakness of the proposed approach are illustrated by comparison to traditional probabilistic approaches. In the presence of both aleatory and epistemic uncertainty, classic probabilistic approaches may lead to misleading conclusions and a false sense of confidence which may not fully represent the quality of the available information. In contrast, generalised probabilistic approaches are versatile and powerful when linked to a computational tool that permits their applicability to realistic engineering problems.

4.2 Introduction

Nowadays it is generally well accepted that estimating the effect of uncertainty is a necessity, e.g. due to variation in parameters, operational conditions [80] and in the modelling and simulations [122]. In practical applications, situations are common where the analyst has to deal with poor quality data, few available specimens or inconsistent information. A typical example is a situation where very expensive samples have to be collected, such as field proprieties of a deep reservoir [77] or performance of satellites [57]. In these cases, the amount of data will be scarce due to economic and time constraints and in several cases, expert elicitation (i.e. the best estimate of an expert) may be the only viable way of carrying on with the analysis [48].

As a consequence, strong assumptions may be needed to apply classical probabilistic methods given poor information quality, which can lead to erroneous reliability estimations and a false sense of confidence [14]. Generalised approaches, which fit in the framework of imprecise probability [14], are powerful methodologies for dealing with imprecise information and lack of data. These methodologies can be coupled to traditional probabilistic approaches in order to give a different prospective on the results, whilst avoiding the inclusion of unjustified assumptions and enhancing the overall robustness of the analysis. Generalised methods are rarely used in practice and this is probably due to lack of proper guidance, simulation tools, as well as some misconception in the interpretation of the results. Further comparison of different methodologies, both in theoretical aspects and in their applicability to real case studies, are required.

An original throughout analysis of the applicability of different methodologies to deal with different level of imprecision is presented. In addition, this work presents a novel computational framework for generalised probabilistic analysis that can be adopted to deal with low quality data, few available samples and inconsistent information. Efficient and generally applicable computational strategies have been developed and implemented into OpenCossan [41]. The proposed framework is applied to assess the reliability of an electric series RLC circuit (a problem proposed by the NAFEMS Stochastics Working Group [52]) and of a power transmission network, both affected by a lack of data.

Generally speaking, different system performance indicators may be affected very differently by the same (lack of) data. The extent of a lack of information is not a-priori quantifiable and depends on the context of the analysis. The proposed approach is used to assess the information quality by comparison to classical probabilistic results and with respect to system reliability estimates. One of the main contributions of

CASE	R [Ω]	L [mH]	C [μF]
A: Interval	[40,1000]	[1,10]	[1,10]
B: source 1	[40,1000]	[1,10]	[1,10]
B: source 2	[600,1200]	[10,100]	[1,10]
B: source 3	[10,1500]	[4,8]	[0.5,4]
C: Samples	861, 87, 430, 798, 219, 152, 64, 361, 224, 61	4.1, 8.8, 4.0, 7.6, 0.7, 3.9, 7.1, 5.9, 8.2, 5.1	9.0, 5.2, 3.8, 4.9, 2.9, 8.3, 7.7, 5.8, 10, 0.7
D: Interval	[40,R_{U1}]	[1,L_{U1}]	[C_{L1},10]
D: Other info	R_{U1} >650	L_{U1} >6	C_{L1} <7
D: Nominal Val.	650	6	7

Table 4.1: The available information for CASE-A, CASE-B, CASE-C, and CASE-D (data taken from [52]).

this work is a detailed comparison between classical and generalised probabilistic approaches from a straightforward applicative point of view and under different levels of imprecision. This serves as guidance for engineering practitioners to solve problems affected by a lack of data.

The rest of the chapter is structured as follows: The NAFEMS reliability challenge problem is described and solved in Section 4.3. A lack of data problem for power network reliability estimation is solved in Section 4.4. A discussion on the limitations of the different approaches is presented in Section 4.5 and Section 4.6 presents some conclusions on these applications.

4.3 Case Study I: The NAFEMS challenge problem

4.3.1 Problem definition

The challenge problem, prepared by the NAFEMS Stochastics Working Group [52], consists of four uncertainty quantification and information qualification tasks motivated by the need to promote best practices to deal with uncertainty to industry. The analysts are asked to evaluate the reliability of an electronic resistive, inductive, capacitive (RLC) series circuit. Four different cases (A, B, C and D) have been proposed in [52], each one having incomplete, scarce or imprecise information about the system parameters, as shown in Table 4.1. In CASE-A single intervals, i.e. one upper bound and one lower bound for parameter R, L and C are given. In CASE-B, each parameter can lay within multiple intervals, i.e. three upper and lower bounds. In CASE-C, ten sampled points for each parameter are provided. Finally, for CASE-D, imprecise bounds and nominal values is the only available information. The last case is similar to CASE-A, but one bound is not precisely defined. The equations governing the RLC circuit, although very simple, are provided by the challengers and reported here for completeness. The

transfer function of the system is defined as:

$$\frac{V_c(S)}{V} = \frac{\omega^2}{S^2 + \frac{R}{L}S + \omega^2} \tag{4.1}$$

where the voltage at the capacitor V_c is the model output. Depending on the values of R, L and C, the system may be classified as under-damped (Z <1), critically damped (Z =1) or over-damped (Z >1) and having different solutions as detailed below.

$$V_c(t) = \begin{cases} V + (A_1 cos(\omega t) + A_2 sin(\omega t)) \exp^{-\alpha t} & \text{if } Z < 1 \\ V + (A_1 + A_2 t) \exp^{-\alpha t} & \text{if } Z = 1 \\ V + (A_1 \exp^{S_1 t} + A_2 \exp^{S_2 t}) & \text{se } Z > 1 \end{cases} \tag{4.2}$$

Where $\alpha = \frac{R}{2L}$, $\omega = \frac{1}{\sqrt{LC}}$, the damping factor is $Z = \frac{\alpha}{\omega}$ and roots obtained as $S_{1,2} = -\alpha \pm \sqrt{\alpha^2 - \omega^2}$. Coefficients A_1 and A_2 are determined by assuming the initial voltage and voltage derivative equal zero and a unitary step voltage function is considered. In this case study, the main goals consist in qualifying the value of information and evaluating the reliability of the system with respect to three requirements:

$$V_c(t = 10ms) > 0.9\ V \quad , \quad t_r = t(V_c = 0.9V) \leqslant 8\ ms \quad , \quad Z \leqslant 1 \tag{4.3}$$

where t_r is the voltage rise time, i.e. the time required to increase V_c from 0 to 90% of the input voltage, and it has to be less than or equal 8 ms. The first two requirements are on the voltage at the capacitance V_c, the third requirement is on the damping factor, which assures that under-damped system responses are discharged ($Z \leqslant$1). Specifically, V_c(10ms), V_c(8ms) and Z are regarded as performance variable for the system, and if these conditions are not satisfied the system is considered to have failed. Probabilistic and generalised probabilistic approaches are adopted to tackle the four cases and uncertainty characterization and propagation are presented for each case. Depending on the approach selected, CDFs or P-boxes are obtained for the three performance variables, see Eq.(4.3). If V_c(10ms),V_c(8ms) and Z result in crisp CDFs, the probability of failure is computed by estimating the CDF values at 0.9 Volts for the requirements on V_c and voltage rise time t_r as well as the CDF value at Z=1 for the requirement on the damping factor. Similarly, if bounds on the CDFs are obtained (i.e. P-boxes), then bounds on probability of not meeting the requirements are computed as explained in Chapter 2, which are $[\underline{P}_{Vc10}, \overline{P}_{Vc10}]$, $[\underline{P}_{tr}, \overline{P}_{tr}]$, and $[\underline{P}_Z, \overline{P}_Z]$, respectively. This case study was previously tackled by different groups and the author using different approaches. For further reading the reader is reminded to Refs. [52]- [128]. This work presents additional analyses of the NAFEMS challenge problem by adopting novel algorithms in a unified computational framework.

4.3.2 Solution: CASE-A and CASE-B

In CASE-A, a single interval was provided for the parameters while multiple intervals were available in CASE-B (see, Table 4.1). CASE-B degenerates to CASE-A if the probability mass equal one is assigned to the first source of information. This because in CASE-B intervals values for source 1 corresponds to the interval values in CASE-A. Due to the considerations made, the two cases are presented and solved together.

Probabilistic Approach

In the CASE-A the intervals were propagated using a single loop Monte Carlo by assuming a uniform distribution within the bounds on R, L and C, which is an assumption made with respect to the principle of maximum entropy. The reliability is assessed by evaluating if the system requirements are met as shown in Eq. (4.3). For the solutions of CASE-A, failure probabilities have been estimated using 10^7 samples and are P_{Vc10} =0.243, P_{tr} =0.345 and P_Z =0.031. The probability of failure for requirement one is lower than the probability of failure for requirement two.
For the solution of the CASE-B, each interval is considered individually. Hence, three different uniform distributions for each R, L, and C parameter are used, one for each source of information. The reliability analyses have been performed to compute 3 probabilities of failure and results are shown in Table 4.2. The Source 3 has the lowest estimated probability of failure while the Source 1 shows an intermediate failure probability. On the right-hand side of Figure 4.1 the resulting CDFs for the three sources of information and three requirements are displayed.

Table 4.2: The results for CASE-B obtained by Monte Carlo method and 10^7 samples.

CASE-B	Source 1	Source 2	Source 3
P_{Vc10}	0.243	0.549	0.052
P_{tr}	0.340	0.660	0.129
P_Z	0.031	1.25 10^{-5}	0.069

Generalised Probabilistic Approach

Possible values of the parameters (interval) can be represented by means of the generalised probabilistic approach without defining a probability distribution. Parameter uncertainty has been characterised using Dempster-Shafer structures. For CASE-A three Dempster-Shafer structures composed by a single focal element have been defined as $\{([\underline{R_1}, \overline{R_1}], m_1)\}$, $\{([\underline{L_1}, \overline{L_1}], m_1)\}$ and $\{([\underline{C_1}, \overline{C_1}], m_1)\}$, where the probability mass m_1 is equal one. For CASE-B, each DS structure is defined as:

$$\{([\underline{X_1}, \overline{X_1}], m_1), ([\underline{X_2}, \overline{X_2}], m_2), ([\underline{X_3}, \overline{X_3}], m_3)\}$$

Table 4.3: The results of CASE-B obtained adopting generalised probabilistic approach.

CASE-B	Source 1	Source 2	Source 3	All Sources
P_{Vc10}	[0,1]	[0,1]	[0,1]	[0,0.9]
P_{tr}	[0,1]	[0,1]	[0,1]	[0,1]
P_Z	[0,1]	[0,1]	[0,1]	[0,0.7]

where $[\underline{X_i}, \overline{X_i}]$ represents the i^{th} interval source for one of the parameters (R, L or C) and m_i is the associated probability mass. The CASE-B degenerate to the CASE-A if the probability mass m_2 and m_3 are set equal to zero. It was not possible here to establish if some sources of information are better, thus, pieces of information derived from different sources are assumed as equally likely, i.e. $m_1 = m_2 = m_3 = 1/3$. Twenty-seven parameter cells are constructed by the permutation of the intervals. Then, minimizations and maximisations of V_c(8ms), V_c(10ms) and Z were performed to identify the bounds of the system performance. The output Dempster-Shafer structures are used to create probability boxes for the system performances V_c(8ms), V_c(10ms) and Z and the corresponding failure probabilities obtained.

Applying the procedure to the CASE-A, the resulting P-boxes give no valuable information on the failure probability for the three performance requirements. The probability of failure is in fact just bounded in the interval [0,1] for all the requirements. The CASE-B includes all the information available for the CASE-A plus two additional sources of information. The additional intervals contribute to reducing the uncertainty on the system performance as shown on the right-hand side of Figure 4.1. Resulting bounds are also presented in Table 4.3 and it can be noticed that the outputs have high associated uncertainty, but less than that in the CASE-A. P_{tr} lays within the interval [0,0.9], P_{Vc10} within [0,1] and P_Z lays within the interval [0,0.7]. Hence, failure probability for requirement two does not show any reduction in the uncertainty.

The failure probability computed by adopting classical approaches always lays within the bounds obtained using the Dempster-Shafer methodology, as shown in Figure 4.1. The maximum failure probability for the Z requirement is 0.069 (source 3), while the generalised approach bounds the results between 0 and 0.7. This reliability overestimation was due to the assumption made on the parent distribution needed to apply the classical methodology. In fact, by selecting a PDF we explicitly assume a well-defined stochastic behaviour for the parameters. As a matter of fact, no information was given to assume a random behaviour at all, and the imprecise information could be due to different experts advising for different scale ranges to be analysed.

The computational time for CASE-B using classical Monte Carlo simulation was about 6.7 seconds. The generalised solution to CASE-A and CASE-B was relatively

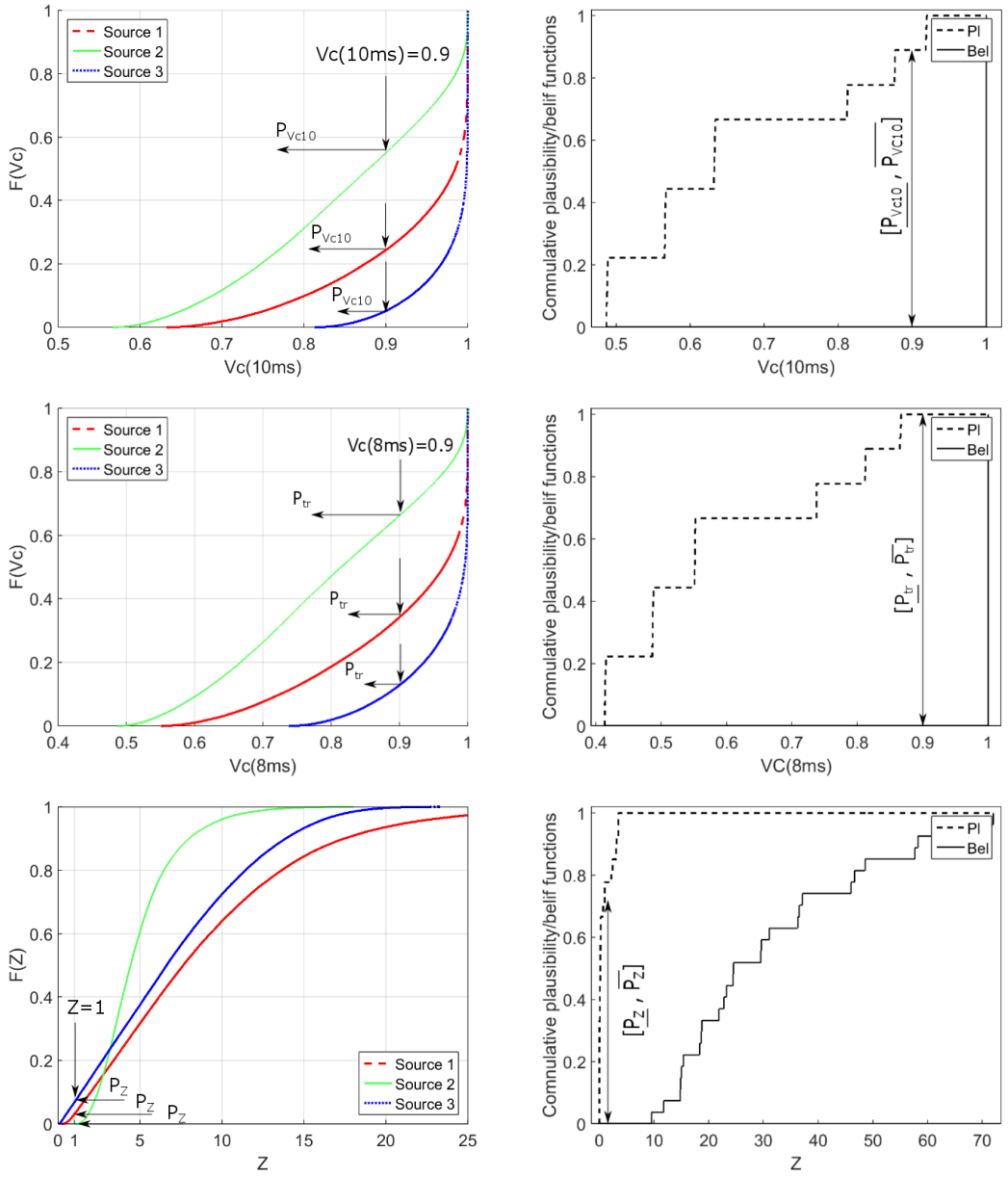

Figure 4.1: Comparison of the $V_c(8ms)$, $V_c(10ms)$ and Z results for CASE-B, respectively. Resulting CDFs obtained using the probabilistic approach (on the left) and P-boxes obtained from the generalised approach (on the right).

computationally inexpensive, taking about 0.07-0.08 seconds for the solution of each min-max problem. Thus, the DS structures propagation for the 3 reliability requirements took just 5-6 seconds for CASE-B on a 4 cores machine with 8.00 Gb ram and a 2.00 GHz Intel Core i5-4590T processor.

4.3.3 CASE-C

Probabilistic Approach

For the solution of CASE-C, two methodologies were adopted. Firstly a uniform distribution approach and secondly a Kernel Density estimation (KDE) approach [115]. The uniform distribution approach allows the values of the parameters to change within the sampled range (but not outside). The bounds are assumed equal to the minimum and maximum values of the samples. Then, 10^5 MC run have been performed obtaining estimated probabilities of failure of P_{Vc10}=0.183, P_{tr}=0.273, P_Z=0.016, respectively. The Kernel Density Estimator is a well-known approach that allows a probability distribution to be constructed based on sample data without assuming its distribution form. Different Kernels can be used and the Gaussian Kernel is a popular choice which has been adopted in this work because it allows the incorporation of measurement error. The optimal bandwidth value was obtained using Silverman's rule of thumb [115]. By adopting KDE the estimated failure probabilities are P_{Vc10}=0.232, P_{tr}=0.292, P_Z=0.121, respectively. These values are slightly larger compared to the one obtained with the uniform distribution approach. Higher values of the probability of failure are due to the tails of the Kernel fitted probability distribution (displayed in Figure 4.2) which allows the value of the parameter to change outside the range of the samples. Plots on the left-hand side in Figure 4.3 show the output CDFs when adopting uniform distributions and KDE to model parameter uncertainty. The CDF of Z has been zoomed around the value Z=1 for graphical reasons. The failure probabilities calculated using sampled values of R, L and C are also lower if compared to the ones obtained in CASE-A and CASE-B. This is due to the smaller upper bound on R in CASE-C (861 Ohm).

Generalised Probabilistic Approach

CASE-C is solved by applying the Kolmogorov-Smirnov (KS) test to characterise the uncertainty of the input parameters as shown in [49], and obtaining bounds on the empirical cumulative probability distribution function (see section 2.6.2 for further details). Maximum and minimum values of the parameters are assumed and the CDF upper and lower bounds are truncated accordingly. Due to the underlying physics governing the system, all the parameters must be positive and this condition allows the lower bounds to be set. Truncating the tails of the distributions, especially in reliability analysis, can lead to erroneous results and safety overconfidence. Thus a relatively high upper bound for the CDF truncation was selected, which was assumed

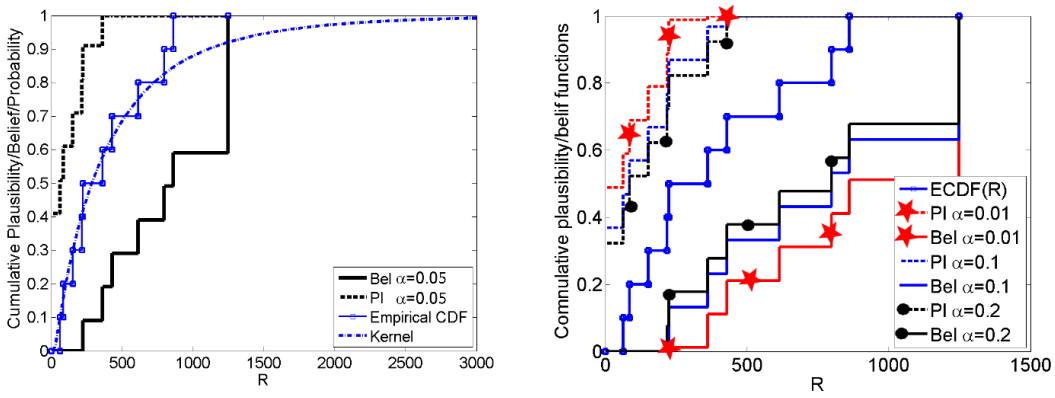

Figure 4.2: The Kernel fitting (on the right panel) and the P-box bounds (on the right panel) of the resistance R for the CASE-C.

equal to the sample mean plus three times the sample's standard deviation. In Figure 4.2 the upper and lower bounds (dashed and solid lines) are shown for the empirical CDF (square marker blue line) and the Kernel density estimator (blue dot-dashed line). Three different confidence levels for the KS test are used for each parameter. The bounds on the left-hand side plots refer to a confidence level α=0.05 and they are compared to the plots on the right-hand side which show the obtained bounds for α=0.01 (dashed and solid star marker lines), α=0.1 (dashed and solid blue lines) and α=0.2 (dashed and solid circle marker lines).

The obtained P-boxes are propagated through the system. On the right plots of Figure 4.3, the voltage at the 10^{th} ms, 8^{th} ms and damping factor P-boxes are presented, red blue and black colour lines with different markers refer to confidence level α=0.01, α=0.1 and α=0.2 respectively. The P-box of the damping factor has been zoomed around the value Z=1 to improve the readability of the plot. The bounds on the probabilities of failure are presented in the Table 4.4. It can be observed that the intervals on the failure probability are quite wide, as already observed for CASE-A and CASE-B. Nevertheless, the failure probability bounds appear to be narrower if compared to CASE-A and CASE-B. This shows that the information provided for CASE-C is of higher quality, which allows less imprecise reliability estimates to be obtained. The results show that the uncertainty in the system reliability was underestimated by using the Monte Carlo method because precise probability distribution functions were assumed despite the small sample size. The failure probabilities estimated by adopting the classical approach lay within the probability interval obtained by adopting generalised approaches.

Using the same machine adopted for solving the previous cases, the classical probabilistic solution of CASE-C required about 0.07 seconds for the fitting and propagation

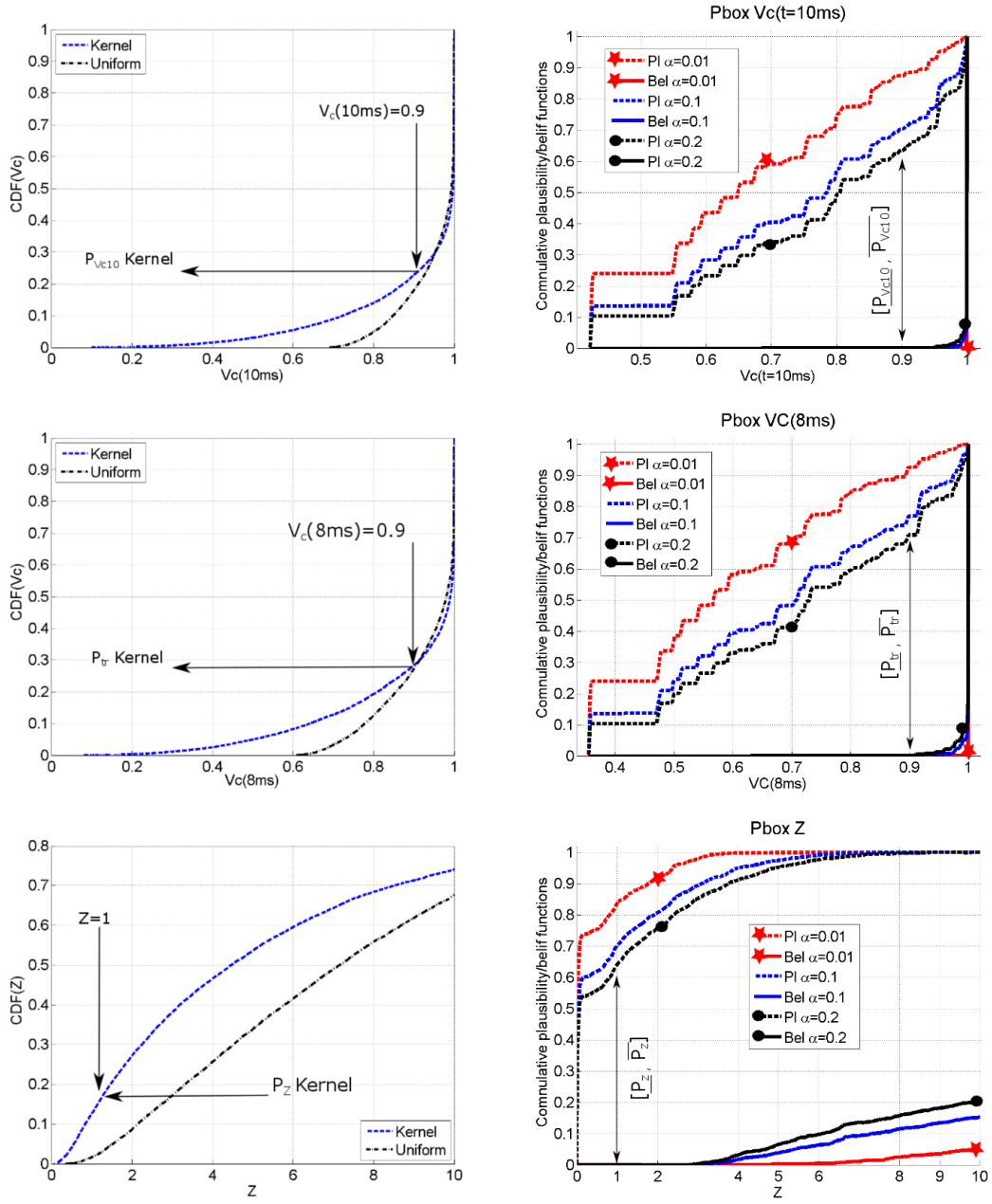

Figure 4.3: CDFs (on the left pannel) and P-boxes (on the right pannel) of V_c(10ms), V_c(8ms) and Z for the CASE-C

Table 4.4: The results for CASE-C, the probability bounds for the three requirements and the three confidence levels.

CASE-C	α=0.01	α=0.1	α=0.2
P_{Vc10}	[0,0.87]	[0,0.7]	[0,0.63]
P_{tr}	[0,0.92]	[0,0.77]	[0,0.7]
P_Z	[0,0.83]	[0,0.7]	[0,0.64]

of the Kernel probability densities and additional 0.05 seconds for the propagation of uniform probability densities. Conversely to the generalised solution to CASE-A and CASE-B, the computational time needed for the propagation of the focal elements is generally higher when compared to its classical probabilistic counterpart. The DS structures propagation took about 461 seconds for each confidence level α (i.e. about 23 minutes for the 3 confidence levels). The higher computational cost is attributable to the larger number of min-max optimisations performed (i.e. 2197 combinations of focal elements).

4.3.4 CASE-D

Similarly to CASE-A, the bounds of the parameters are provided. However, just one bound is precisely defined for each parameter. The upper bounds of R and L and the lower bounds of C are imprecisely defined as shown in the last row of Table 4.1. In addition, the nominal values for the parameter are provided. The problem has been tackled by defining upper bounds of R and L, which were redefined as T times their nominal value while the lower bound of C was redefined as its nominal value divided by T, where T =10. Thus, the maximum truncation bounds are $\overline{R}_n$=6500 Ω, $\overline{L}_n$=60 mH and $\underline{C}_n$=0.7μF. The quantity T is defined as 'truncation level' and n =10 linearly spaced intermediate bounds are also considered.

Probabilistic Approach

Uniform PDFs are assumed within the defined intervals and all combinations of upper and lower bounds are propagated by the Monte Carlo method. Having reduced the semi-definite intervals to a set of defined intervals, it is now possible to estimate the reliability of the systems by adopting the same approach as CASE-B. For the first two requirements, the probability of failure increases from 0.1 up to 0.9. The MC method is not efficient in providing solutions for the lower bounds of the intervals. In fact, the probability of having Z <1 goes from a maximum of 0.2 to a minimum of approximatively 0.0005 (requiring at least 10^5 samples for a rough estimation).

Generalised Probabilistic Approach

The parameters' uncertainty has been characterised using a set of n multiple intervals translated into DS structures. A probability mass function equal to $1/n$ has been assigned to each interval (for normalization reasons) defining Dempster-Shafter structures for the parameters, for instance the structure of R is $\left\{([\underline{R}, \overline{R}_1], \frac{1}{n}), ..., ([\underline{R}, \overline{R}_n], \frac{1}{n})\right\}$. The three probabilities of failure lay within the interval [0,1]. In particular, the imprecision associated with the last requirement indicates a severe misjudgement of the real uncertainty when the only classical probabilistic solution is considered (obtaining a maximum

P_Z =0.2).

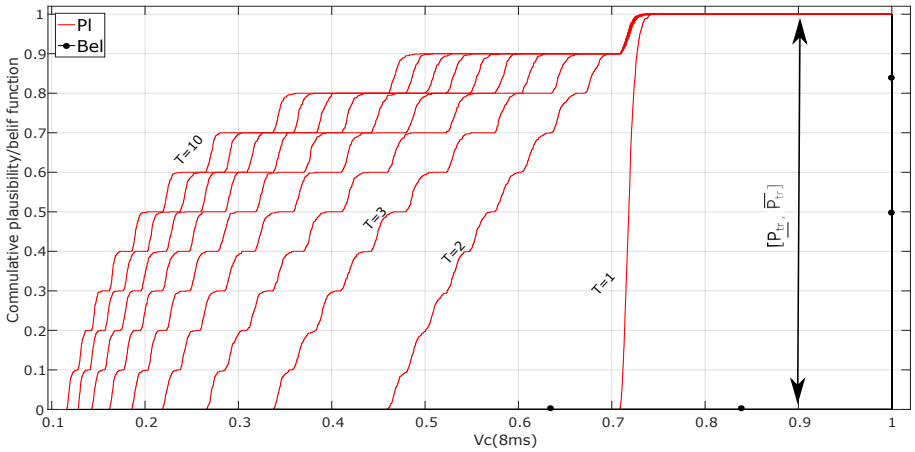

Figure 4.4: Variation in the probability bounds due different values of $\overline{R}_n$. The truncation values are $\overline{R}_n$=650·T Ω with T=1,..,10 and 60 and 0.7 for $\overline{L}_n$ and $\overline{C}_n$, respectively.

In order to investigate the effect of the assumptions on the results, a sensitivity analysis of the values of $\overline{R}_n$, $\overline{L}_n$ and $\underline{C}_n$ is performed. The sensitivity approach adopted is similar to the one-at-a-time method presented in [21]. The selected base-case has truncation level T=10 and truncation bounds $\overline{R}_n$=6500 Ω, $\overline{L}_n$=60 mH and $\underline{C}_n$=0.7μF. A total of 27 sensitivity cases are defined by selecting 9 truncation level to T=9,8,7..,1 for each one of the parameters taken one-at-a-time. Then uncertainty propagation is carried out for the sensitivity cases and results compared to the bounds of the base case. The comparison shows that the shape of the P-boxes is affected most by $\overline{R}_n$. On the other hand, it does not have relevant effects on the bounds of the failure probability. Figure 4.4 displays the sensitivity analysis performed by varying $\overline{R}_n$.

The computational time required to solve CASE-D is about 200 seconds by using the DS structure propagation algorithm whilst the classical approach required 1400 seconds for the solution (selecting 10^5 samples for the Mone Carlo and propagating all the combinations of upper and lower bounds).

4.4 Case Study II: Analysis of a power transmission network

The case study selected for the analysis is a 6-bus and 11-lines power transmission network [155]. Figure 4.5 displays the network topology, nodes indices and load names. The nodes 1-3 represent the generator buses while the nodes 4-6 are the demand buses. To simplify the reliability assessment, loads correlation is neglected and grid stress is

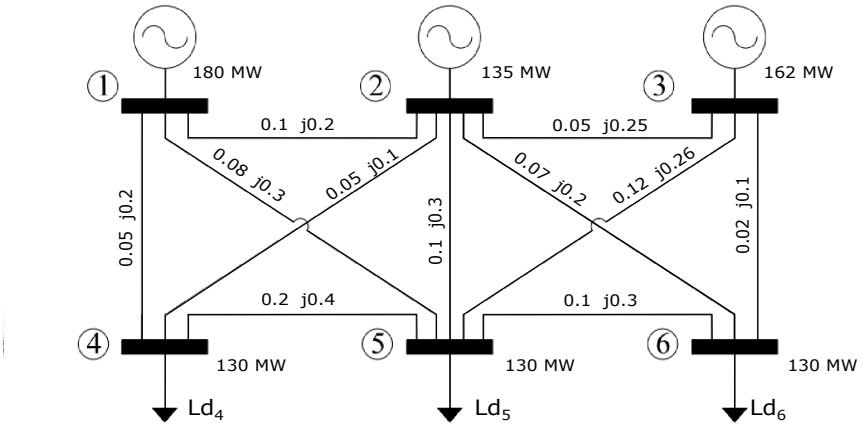

Figure 4.5: The 6-bus power network system.

increased. The reference loads L_{d4}, L_{d5} and L_{d6} and the decreased maximum power capacity of the generators are reported in Figure 4.5.

It is assumed that a lack of data is affecting the failure rate of the transmission lines. This is a common situation for highly reliable components for which at best only a few failures have been observed. A common practice used to estimate the failure rate of transmission lines is to merge the few available failure samples between similar lines. This procedure is named "data pooling" and assumes that the behaviour of similar components can be described by the same probabilistic model. This is often a rational assumption. However, when (similar) components are subjected to different work loads (e.g. close/far from their thermal limits), different conditions (e.g. in a harsh/mild environment) or with different maintenance policies such assumptions are rarely true. Different endogenous and operational-environmental factors will most likely influence the ageing of the components and produce a very different failure behaviour even for identical lines. For more details on the problem, the reader is referred to [94].

The transmission links in the system are assumed to be LGJ-300 and for this specific line, an estimation of the failure rates (λ_l) for each link l is presented in [158]. The available data consists of 40 failure times collected over 10 years for a first line and 5 years of failure times for a second. Over the first 5 years, the estimated λ_l is 0.00027 [failure/h] while for the last 3 years the failure rate increases to 0.00042 [failure/h] (possibly due to a poorly described ageing effect). Similarly to CASE-A in the first case study (Section 4.3), an interval data source is considered for each line failure rate λ_l with $l = 1, .., 11$. The failure rate is imprecisely defined during the ageing of the line (e.g. between 5 years to 8 years from installation) and this might affect the estimation of the power network reliability.

The Energy-not-Supplied is a well-known reliability indicator for power grids and is employed here to assess the network failure probability (for further details refer to Table 3.3). The power network is simulated for a given period of time (e.g. 1 day) and random components' failures are sampled from probability distributions used to model the components' failure times. The probability of failure for a line is assumed to follow a Poison distribution and obtained as explained in Section 3.2.2 and similarly to [122]. During the simulation, the network power flow equations are solved and in the case of occurred failures or unsatisfied constraints (e.g. thermal or generators capacity limits), part of the power load can be curtailed and calculated as explained in subsection 3.3.4. The power grid will fail to meet the performance requirement if the energy not provided to the customers is larger than a predefined threshold level (i.e. $ENS > ENS_{tsh}$). The ENS_{tsh} has been set equal to 0.05 % of the total load demand. Further details on the reliability model are available in Ref. [88]. First, a classical probabilistic approach is used to assess the power grid reliability. The probabilistic model for the grid has to be precisely defined. Hence, a point value for the failure rate of each ageing line has been selected and set equal to the mean failure rate (0.000345 [failure/h]). A plain Monte Carlo is employed to propagate 10^4 independent realisations of the power grid history. In each MC run, failures can randomly occur according to the line failure probability and the ENS is computed for the sampled network state. The resulting CDF of the Energy-Not-Supplied (F_{ENS}) is displayed by the blue circle markers line in Figure 4.6. It can be used to obtain the probability of failure for the network as follows: $P(ENS > ENS_{tsh}) = 1 - F_{ENS}(ENS_{tsh})$.

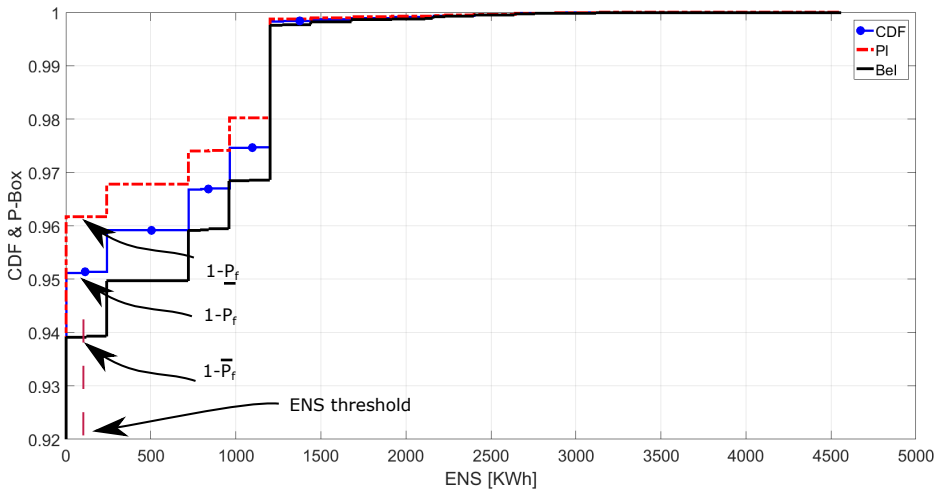

Figure 4.6: The CDF, Cumulative belief and Cumulative plausibility functions for the ENS in [MWh]. The plot is zoomed in to better display the reliability results and ENS_{tsh}.

The imprecise information available for the failure rate has been propagated using a double loop Monte Carlo approach as previously presented. In the outer loop, 50 values of the failure rates are sampled from the interval [0.00027,0.00042] failure/h and forwarded to the inner loop. In the inner loop, analogously to the classical probabilistic analysis, a Monte Carlo simulation is used to obtain independent histories for the power network, sampling failed components and obtaining the ENS. The results are cumulative belief (black solid line) and plausibility (dot-dashed red line), displayed in Figure 4.6. The threshold ENS_{tsh} is also presented with a dashed line. The resulting reliability interval is $[3.89,\ 6.09]\cdot 10^{-2}$ which includes the single-valued reliability estimator obtained by the classical probabilistic approach, $4.99\cdot 10^{-2}$.

The analysis has been extended by accounting for imprecision in the power loads L_{d4}, L_{d5} and L_{d6}. Generally speaking, electric loads in power networks are inherently variable and changing their magnitude significantly during the day (e.g. night loads vs daytime loads) and during the year (e.g. cooling/heating winter/summer loads vs spring/autumn loads). Hence, power grid loads are often characterized as aleatory uncertain quantities variables (e.g. using stochastic processes, PDFs, CDFs). These mathematical tools are generally fitted using historical time series, possibly pooling a lot of data gathered from several years of operations. Although the amount of information and data available to fit load distribution is generally quite high, the author believes that loads are also affected by a significant amount of epistemic uncertainty. This is mainly due to newly installed technologies (e.g. distributed generators, micro grids), new sources of electric power demand (e.g. electric vehicles, new load nodes and new customers) which can change substantially the overall demand behavior from year to year. An accurate uncertainty model for the loads, considering both the effect of inherent day/night winter/summer variability and epistemic uncertainty can be accounted for. However, for sake of simplicity and to test the framework, this work considers a characterization of the load demand as a purely epistemic uncertain quantity (similarly to Ref. [11] where power demand is affected by imprecision and modelled using two interval cases). Specifically, 4 imprecision levels on the power demanded (from 5% to 20% of the design load) are considered, due, for instance, to measurement errors, forecast incertitude and newly installed load-affecting devices (e.g. storage, electric vehicles, renewable generators). Table 4.5 summarises the result for increasing imprecision on the load value and Figure 4.7 displays the output cumulative Pl and Bel. The reliability bound gets wider the larger the imprecision surrounding the system loads is. It is worth noticing that when the load interval is increased from 15 to 20 % the upper failure probability increases drastically, from $9.64\cdot 10^{-2}$ to 1 (dashed marked lines in Figure 4.7). This because within the parameter cell $\omega : \left\{\underline{L}_{di} \leqslant L_{di} \leqslant \overline{L}_{di}\ \forall\ i = 4,5,6\right\}$ exists at least one combinations of loads (L_{d4}, L_{d5}, L_{d6}) for which the power flow can not satisfy the given constraints

Table 4.5: The probability bounds resulting from the generalised approach accounting for 4 levels of imprecision for the nodal load demand, L_{di}.

Imprecision on L_{di}	5%	10%	15%	20%
$\overline{P}_f$	0.0874	0.0964	0.0964	1
$\underline{P}_f$	0.0389	0.0387	0.0384	0.032

(i.e. power balance, thermal limit and generators capacity constraints). As consequence, the power flow solver curtails a significant amount of load even for undamaged grid conditions and for each realisation within the inner loop the ENS exceeds ENS_{tsh}.

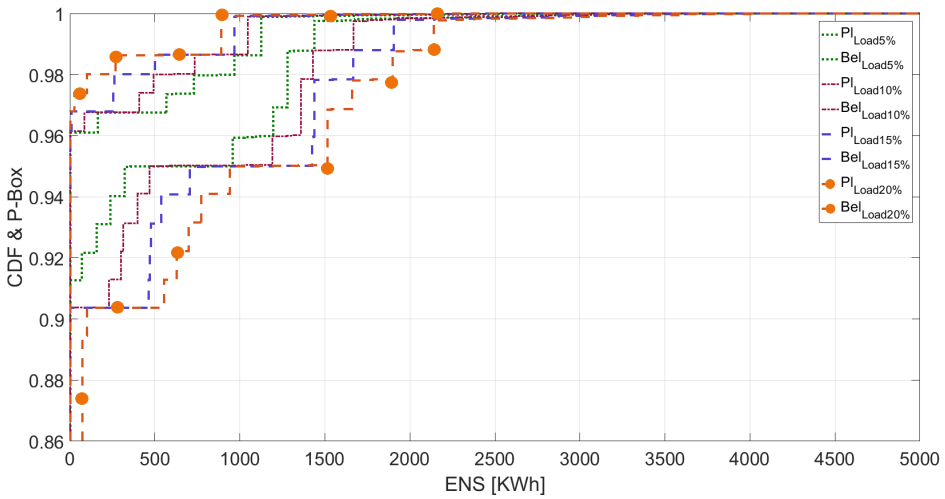

Figure 4.7: The Cumulative belief and plausibility functions for different levels of imprecision on the loads. The plot is zoomed in to improve the graphical output.

In this final application, the developed framework has been tested using a more complex engineering application. Comparing the results obtained using the classical and generalised probabilistic approaches helped to understand the quality of the information on λ_l and loads and their impact on the network reliability. In the first case, the information quality was good and the imprecise data resulted in a moderate (but definitely observable) effect on the network reliability. In the second analysis, an increasing level of imprecision affecting the power demand is considered. The results showed that more imprecision in the input load increases the imprecision in the reliability estimate. Moreover, the generalised approach pointed out that increasing the imprecision in the load up to 20%, drastically stretched the reliability bounds (about [0,1]). This is indeed an indicator of a severe lack of the available information quality, which has been successfully pointed out by the generalised approach. The computational time for the solution was about 98 seconds using classical approaches (MC with 10^4 samples) and about 4900 seconds for the generalised approach (50 outer loop samples and 10^4 inner

loop samples).

4.5 Limitation faced and discussions

Classical probabilistic approaches require the estimation of (or assuming) PDFs to describe parameters. Uncertainty and uniform distributions and Kernel density estimators have been used to characterise parameter uncertainty. In both cases, it has been explicitly assumed that the analysed parameters have some sort of stochastic nature, which in reality might not be true. One of the strongest limitations of classical probabilistic approaches is the need to represent the epistemic uncertainty as aleatory and then mix these two types of uncertainty. The analysed NAFEMS reliability problem has confirmed that artificial model assumptions might lead to an underestimation of the uncertainty. Hence the reliability analysis might not represent precisely the real quality of the available data. For extreme cases, a severe lack of data can lead to non-informative bounds [0,1]. The large epistemic uncertainty about the system parameters may suggest considering an investment in collecting more empirical data rather than refining the model for the reliability assessment. The overall outcomes of the study highlighted some of the positive and negative aspects of employ a generalised approach with respect to classical uncertainty quantification methodologies.

The reliability assessments were affected by severe uncertainty when, if tackled using classical probabilistic approaches, the analyst is forced to make unjustified assumptions leading to a strong underestimation the true output uncertainty. A case affected by a severe lack of data was the NAFEMS reliability problem for which the epistemic component appeared to be a dominant part of the outcomes' uncertainty. On the other hand, a reliability problem affected by a mild lack of data would have had results less sensitive to the epistemic uncertainty. This might be well-represented by the power grid reliability problem for which the failure rate imprecision influenced moderately (but visibly) the precision of reliability estimate. Similar results have been obtained for imprecision on the load demand up to 15 %. On the other hand, higher imprecision on the load (20%) drastically widened the reliability bounds. This has been pointed out thanks to the proposed comparison framework for classical and generalised probabilistic approaches.

4.6 Conclusions and future direction

In order to define a precise and 'exact' probabilistic model, a very high amount of data (possibly infinite) would be necessary. Unfortunately, a lack of information always affects engineering analysis and its extent cannot be quantified a priori. In general, the quality of the available information is context and scope-dependent, e.g. different

systems performance indicators may react very differently to the same lack of data. The proposed framework provides a simple but effective way to assess a data deficiency by comparing the system reliability bounds (obtained through generalised probabilistic approaches) against single-valued probability indicators (obtained adopting classical probabilistic methods). If the lack of knowledge is not too large, the system reliability will result in relatively narrow bounds and always include the point reliability estimator. In this case, classical approaches will be well-suited to tackle the problem. Conversely, if the lack of data is severe, the reliability bounds will result very wide or, for extreme cases, even non-informative ([0,1]). Combination of pure probabilistic approaches (e.g. Monte Carlo Simulation) and generalised uncertainty quantification approaches (e.g. based on Dempster-Shafer structures and probability boxes), implemented in a common computational framework, are unavoidable tools for the industry which may rely on multiple accurate information qualification approaches. This will aid understanding if the data is of high quality or poor quality, with the aim of designing safer and more reliable systems and components. The NAFEMS uncertainty quantification challenge problem and a small-scale power system reliability assessment have been selected as representative test cases and have been solved using the proposed computational tool. Essential information has been provided and the quality of the available data assessed.

In order to deal with low-probability failures, characterised by a low occurrence probability, becomes particularly challenging using sample-based approaches. In order to provide a different perspective to the analysis, vulnerability assessment methods were developed, which can be used to perform structural robustness evaluations of power grids given that large size failures occurred (e.g. due to malicious targeted attacks). Vulnerability methods generally neglect occurrence probabilities of those contingencies and focus on (generally severe) consequences of those events, trying to assess the innate ability of the system to absorb or minimize these consequences from a structural/topological point of view. Although occurrence probability is often neglected, several uncertain factors are affecting the assessment (such as model imprecision and variable electrical setting of the system). In the next Chapter, we compare spectral vulnerability metrics for the ranking of relevant contingencies. The generalised uncertainty quantification framework is adapted to propagate both aleatory and epistemic uncertainty. Effect of model imprecision and inherent variability in the system operative setting are quantified in the vulnerability output and in the contingency ranking.

Acknowledgement

A journal paper version of this chapter has been published as:

1. Roberto Rocchetta, Matteo Broggi, and Edoardo Patelli. Do we have enough data? robust reliability via uncertainty quantification. *Applied Mathematical Modelling*, 54(Supplement C):710 – 721, 2018

Chapter 5

Assessment of Power Grid Vulnerabilities

5.1 Abstract

Vulnerability and robustness are major concerns for future power grids. Malicious attacks and extreme weather conditions have the potential to trigger multiple components outages, cascading failures and large blackouts. Robust contingency identification procedures are necessary to improve power grids resilience and identify critical scenarios. This work proposes a framework for advanced uncertainty quantification and vulnerability assessment of power grids. The framework allows critical failure scenarios to be identified and overcomes the limitations of current approaches by explicitly considering aleatory and epistemic sources of uncertainty modelled using probability boxes. The different effects of stochastic fluctuation of the power demand, imprecision in power grid parameters and uncertainty in the selection of the vulnerability model have been quantified. Spectral graph metrics for vulnerability are computed using different weights and are compared to power-flow-based cascading indices in ranking $N-1$ line failures and random $N-k$ lines attacks. A rank correlation test is proposed for further comparison of the vulnerability metrics. The IEEE 24 nodes reliability test power network is selected as a representative case study and a detailed discussion of the results and findings is presented.

5.2 Introduction

The Power Grid is the world's largest, man-made interconnected structure and plays a critical role in the well-being of society. The working productivity, comfort and safety of local citizens relies on on power grids integrity and even modest power outages can seriously compromise their welfare. Severe blackouts may have a huge social and economic impact and is therefore necessary to develop resilient future power grids, capable of withstanding their occurrences. This requires vulnerability assessments of the electric power supply, the identification of critical scenarios, contingency plans and a high degree of confidence in the results. It is also necessary to better understand the relationship between power grids operational risks and those associated with a vulnerable topological structure. This will help mitigate the effects of unexpected and hazardous failures, and enhance the overall network robustness and resilience.

The structure and operations of power grids are changing radically [167]- [51]: The growing share of intermittent and uncertain renewable power sources is making grid behaviour less predictable; climate change is predicted to increase the intensity and frequency of extreme weather events with the potential to deeply compromise grid integrity [122]; and as highly meshed (non-radial) distribution grid topology is expected to become more common in the future [101], it is likely to see an increasing structural complexity and interconnection between the power grid components. Due to this scenario of increasing complexity and uncertainty, it is important to assess both the inherent variability in the system and imprecision affecting the network parameters. Topological and operational weaknesses have to be better understood in order to provide superior network designs capable of promptly react to unexpected hazardous situations. One potential method of achieving higher grid resilience is by enhancing existing frameworks for power grid vulnerability assessment and by adopting sophisticated uncertainty quantification techniques.

The robustness of power networks is defined as the degree to which the grid is able to withstand unexpected events without degradation in performance [64]. A closely related concept is the vulnerability, which is generally regarded as the lack of robustness. Vulnerability metrics can be obtained in several ways and, in the literature, overload cascading indices based on power-flow evaluations have been proposed to assess the effect of cascading failure events [157]- [18]. This approach has proven adequate in cases where the cascades are mainly driven by overload line trippings [18]. Alternative approaches have focused on the grid topology by using graph theory to analyse its structure [64]- [65]- [31]- [20]- [35]- [56]- [69]- [125]. The so-called pure topological analysis use unweighted adjacency matrices to calculate vulnerability whilst extended topological approaches enrich the analysis by incorporating electrical

engineering information in the weights of the graph. The extended metrics have been introduced based on the idea that pure topological approach may fail in exhaustive captivation of the electric network complexity. Whether or not pure topological approaches and their extended version are capable of fully capture vulnerabilities of power grids is still an open debate [34].

Imprecision is a common problem for power grid models and their parameters, appearing in the calculations due to a number of factors such as, tolerance errors, scarcity of data, inconsistent information, and experts' judgement. This type of uncertainty is generally referred as epistemic or subjective. For example, earlier works dealt with this type of uncertainty using fuzzy power flow analysis [83] or stochastic frameworks for reliability analysis [135]. To the authors' knowledge, topological approaches are generally applied by assuming an exact knowledge of the network parameters and do not account for uncertainty in the calculations. Authors of Ref. [31] analysed the correlation between vulnerability metrics and power flow models. E. Bompard et al. [20] compared two enhanced metrics (i.e. the extended betweenness and net-ability) by ranking components with respect to the system vulnerability. Recently, Lucas Cuadra et al. [34] reviewed power grid robustness metrics which were computed by adopting complex network theory approaches. G. J. Correa et al. [31]- [32] investigated power network structural vulnerability to single and multiple failures and compared graph-theory approaches against power flow approaches. S. Cvijić and M. Ilić [35] discussed the applicability of graph-theory methods (generally applicable in transportation networks) to power grids. It was showed that some of the physical laws applied to power systems are limiting factors but, when graph-theory methods are applied, the computational cost of analysis is greatly reduced. P. Hines et al. [56] discussed the use of topological measures for power grid vulnerability analysis. Through the analysis of random failures it was argued that topological measures can be useful as general trend indicators of vulnerability, although physical-based models (e.g. power flow models) are believed to be more realistic. S. LaRocca et al. [69] investigated different measures for power grids vulnerability and risk assessment by randomly removing grid components. Similarly, R. Rocchetta and E. Patelli [125] compared graph-theoretic spectral vulnerability metrics to power flow based vulnerability metrics in ranking power grid most critical lines. They showed that load demand uncertainty and tolerance imprecision affect the results of the contingency ranking.

To the authors knowledge, none of the reviewed works analysed the effects of both aleatory and epistemic uncertainty on the computation of graph-theoretic spectral vulnerability metrics. However, it is known that sources of uncertainty will inevitably affect power grids robustness. There are several representative examples which consider these effects in the power grid reliability assessment literature. Few notable approaches

include reliability assessments of power grids allocating renewable energy sources [88], increasing interdependency between different networks (e.g. telecommunication network transportation network, etc.) and the inherent variability of the (changing) external environmental conditions [122]. Accounting for relevant sources of uncertainty affecting power grid robustness and vulnerability may help to improve the overall confidence in the results and better identify critical scenarios. Being able to distinguish between the (inherently variable) aleatory component of the uncertainty and the (in principle) reducible epistemic uncertainty can be beneficial for the analysis and for improve confidence in the results. Furthermore, many vulnerability metrics have been proposed in the literature and the results will be inevitably affected by a specific metric selection. It is therefore necessary to assess the level of uncertainty associated to power grid robustness when different metrics are employed for vulnerability analysis.

In this work, drops in performance due to single and multiple line failures are analysed by employing algorithms developed by the authors. A novel weighting factor based on the line percentage of rating is also introduced and compared to weights applied in the literature. Load demand is inherently variable and the increasing allocation of non programmable renewable energy sources are making its behaviour even more uncertain. Thus, the aleatory and the epistemic uncertainty affecting load demands and network parameters are accounted for and propagated to the vulnerability metrics and respective contributions highlighted. The proposed framework is flexible and can account for renewable energy sources uncertainty. This can be done by proposing a different characterisation of the uncertainty in the load. One of the main contributions of this work is a systematic comparison of the vulnerability based on operational flow-based models and topological approaches (pure and extended). Furthermore, none of the reviewed works compared spectral vulnerability metrics for contingency ranking purposes embedding the methods within advanced uncertainty quantification framework. Thus, similarities and differences of the different metrics are discussed for increasing damage size and accounting for uncertainties due to stochastic loads and line parameters imprecision.

The chapter is structured as follows: A concise review on power grid modelling and spectral graph analysis is proposed in Section 5.3. In Section 5.4, vulnerability metrics are defined. The uncertainty modelling and contingency analysis are described in Section 5.5. The developed algorithms and framework are summarised within Section 5.6. In Section 5.7 presents the analysis of the IEEE reliability test system. The limitation faced are discussed in Section 5.8 and in Section 8.8 conclusions are drawn.

5.3 Background and Power Grid Modelling

A power network structure can be modelled using weighted or unweighted undirected graphs $\mathcal{G} = \{\mathcal{N}, \mathcal{L}, \mathbf{w}\}$, where $\mathcal{N}$ is the set of network buses (or nodes set), $\mathcal{L}$ is the set of lines connecting the nodes (i.e. links set) and $\mathbf{w}$ is the set of weights associated to the lines [20]- [73]- [47]- [38]. Generally when graph-theory approaches are used, a conservative (pessimistic) hypotesis is made on the network structure, to ease the calculations. Self-loops such as parallel lines are removed from the graph $\mathcal{G}$ and replaced by the equivalent single line model. Different weights define different graph models of the power network, for instance, if $\mathbf{w}$ =1 the model and following analysis will be named purely topological [34], since no electrical quantities are employed. Alternatively, weights can be used to represent specific electrical engineering information. Quantities such as the line susceptance (B_{ij}) or power flow (f_{ij}) have been previously adopted as line weights, see e.g. [65]- [145], where i and j represent the generic nodes. The number of buses and the number of branches in the power network is represented by the cardinality of the node set $N_b = |\mathcal{N}|$ and the cardinality of the line set $N_L = |\mathcal{L}|$, respectively. To simplify the notations the line subscript $(ij) \in \mathcal{L}$ can be replaced with the subscript l representing the line index.

5.3.1 Overflow Cascading Vulnerability

A 'cascade' is a sequential succession of dependent events [157]. In power systems cascading analysis a failure sequence (lines tripping) can be defined as load-driven when the thermal expansion results in the line dropping beneath its safety clearance, or load-independent such as in case of a mechanical failure. The metric adopted in this work focuses on load-driven failures and is used to assess the network vulnerability to overload cascading events. We recall the definition of cascading index (CEI), which is is obtained computing the 'immediate' post-contingency power-flow operative state and it is defined as follows [157]:

$$CEI(C_{N-k}) = \sum_{l \in \mathcal{L}} \mathcal{P}(C_l | C_{N-k}) \cdot S_l(C_{N-k}) \tag{5.1}$$

where $\mathcal{P}(C_l|C_{N-k})$ is the probability of a secondary (post-contingency) trip of the line (l) after the contingency denoted as C_{N-k} occurred. The severity $S_l(C_{N-k})$ is a overload severity function for the line l due to the occurrence of a single trip ($k = 1$) or multiple failures ($k > 1$).

Severity functions can be used to quantify the operational risk due to components failures [122]. The continuous severity function for overload is specifically defined for each circuit (lines and transformers). It measures the extent (severity) of failures in terms of line percentage of rating $PR_l = \frac{f_l}{f_{emerg,l}}$. The quantity $f_{emerg,l}$ is the emergency rating of the line $l \in \mathcal{L}$ and is related to its thermal limit and f_l is the power flow in

the line. The expression for the continuous severity due to overload (S_l) of a line l is defined as follows [122]:

$$S_l(C_{N-k}) = d * PR_l(C_{N-k}) + c \quad for \quad PR_l \geqslant PR_l^{min} \tag{5.2}$$

where S_l is zero for values of the flow rating less than a safety limit PR_l^{min}=0.9. The deterministic limit for the violation of line l is PR_l=1, the near violation region is 0.9$\leqslant PR_l <$1, and the value PR_l under 0.9 is regarded as safe, parameters of the severity model are d=10 and c=-9. Continuous severity functions provides non zero values for scenarios close to the performance limits, which reflects the realistic sense that close to failure scenarios have non-zero risk (but deterministically safe). The probability of cascading trip of line l after an initiating contingency C_{N-k} occurs can be expressed as follows [157]:

$$\mathcal{P}(C_l|C_{N-k}) = \frac{f_l(C_{N-k}) - f_{0,l}}{f_{trip,l} - f_{0,l}} \tag{5.3}$$

where $f_l(C_{N-k})$ is the flow on the line l after the contingency C_{N-k} occurred, $f_{trip,l}$ is the flow leading to a certain trip of the line l (assumed to be 1.25 times its thermal limit [157]) and $f_{0,l}$ is the flow in the line l before contingency C_{N-k}. The rationale underpinning Eq.5.3 is that higher load levels and larger transients increase the likelihood of the secondary contingency (i.e. cascading) on the line l after an initiating event C_{N-k}. The probability $\mathcal{P}(C_l|C_{N-k})$ is set equal 1 for each $f_l(C_{N-k}) \geqslant f_{trip,l}$.

The cascading index has indeed some limitations (i.e. the criteria for post-trip probability calculation is based on expert judgement and pre-contingency trip probabilities are neglected). Nevertheless, the computational time needed for its calculation is very small (i.e. that of a single power flow calculation) and this makes it suitable for advanced frameworks for uncertainty quantification, which are generally computationally very demanding.

5.3.2 Spectral Graph Analysis for Power Grids

The topology of the graph $\mathcal{G}$ can be fully characterised by its adjacency matrix W. An adjacency matrix is a $N \times N$ symmetric matrix in which the non-null elements represent weights of existing lines connecting different nodes. In general, the weight are associated to some measure of interest or set equal to 1 (i.e. unweighted adjacency matrix). The matrix D is the diagonal matrix which contains information about the degrees of each node and its diagonal elements (d_i) are equal the sum of the weights of the lines connected to the node i. The Laplacian L of the matrix W is simply $L = D - W$

and the elements can computed as follows [145]:

$$[L]_{ij} = \begin{cases} \sum_{j}^{N} w_{ij} & \text{if } i = j \\ w_{ij}, & \text{if } i \neq j, (ij) \in \mathcal{L} \\ 0, & \text{otherwise} \end{cases} \tag{5.4}$$

where the term $\sum_{j}^{N} w_{ij}$ is the degree (d_i) of the node i.

Spectral graph analysis has been recently used to assess power grids robustness [65] and to tackle islanding problems [145]- [46]. The eigen-proprieties of the adjacency matrix are obtained as follows:

$$\begin{aligned} W &= \Phi_W \Lambda \Phi_W^T \\ \Lambda &= [\lambda_1, .., \lambda_N] \end{aligned} \tag{5.5}$$

Analogously, the spectrum of the network Laplacian is obtained as follows:

$$\begin{aligned} L &= \Phi_L \Psi \Phi_L^T \\ \Psi &= [\mu_1, .., \mu_N] \end{aligned} \tag{5.6}$$

where $\Phi = [\Phi_1, .., \Phi_N]$ is the set of eigenvectors, Λ is the set of eigenvalues of the adjacency matrix and Ψ is the set of eigenvalues of the Laplacian, such that $0 = \mu_1 \leqslant \mu_2 \leqslant ... \leqslant \mu_N$. The eigenvalues of L are non-negative and the smallest (μ_1) is equal to 0. The multiplicity of μ_1 is equal to the number of connected components. If the graph is disconnected, $\mu_2 = 0$ and at least two separate grids exist. Further details are going to be discussed in Section 5.4.

5.4 Vulnerability Metrics and Spectral Analysis for Power Networks

An $N - k$ contingency is defined as the unexpected simultaneous loss of k components in the network [27] (e.g. lines, generators, transformers). Vulnerability indices can be used to quantify the reliability of power networks by assessing relative changes in performance metrics. The network vulnerability $\mathcal{V}(C_{N-k})$ associated to the contingency (C_{N-k}) can be generally quantified as follows [34]:

$$\mathcal{V}(C_{N-k}) = \frac{|\mathcal{M} - \mathcal{M}(C_{N-k})|}{\mathcal{M}} \tag{5.7}$$

where $\mathcal{M}(C_{N-k})$ is a vulnerability metric after contingency C_{N-k} and $\mathcal{M}$ is the metric value for the undamaged network.

5.4.1 Pure and Extended Spectral Vulnerability Metrics

Power network structural vulnerability can be assessed by using pure or extended topological models of the grid. The first uses the unweighted adjacency matrix and lines are regarded as identical [34] whilst the second extends the approach by including electrical parameters to weight to the adjacency matrix. Extended topological approaches often made use of the DC approximation, conveniently used to build the adjacency matrix using the grid susceptance matrix [65]. Active power flows have also been used as an alternative weighting factor [34].

In this work, a new weighting factor based on the line percentage of rating is introduced. The weight is compared to existing weights taken from the literature. Thus, the adjacency matrices will built using 4 different weights for each line l (i.e. 1, B_l, f_l and PR_l). The first 3 weights are selected based on earlier works while the percentage of rating is selected on the idea that by weighting lines using f_l relevant information might be missing. For instance, a line that has a very small f_l (e.g. few MW flowing into the lines), can be nonetheless very close to failure (e.g. high PR_l). It is worth remarking that analysis performed using unweighted adjacency matrix or weighted using susceptances have to be regarded as a static analysis (because weights do not change over time). Conversely, using $w_l = f_l$ or $w_l = PR_l$ the analysis has to be regarded as dynamic because weights change over time [145].

Recently, vulnerability metrics obtained from spectral decomposition of W and L have been used to extract indicators of the grid robustness [122]. The metrics considered are: the spectral radius ($\rho_{\mathcal{G}}$) [148], the algebraic connectivity (μ_2) [65]- [122], the natural connectivity $\overline{\lambda}_{\mathcal{G}}$ [112] and effective graph resistance $R_{\mathcal{G}}$ [65]. The Spectral radius is the largest eigenvalue of W whilst μ_2 is the second smallest eigenvalue of L. The natural connectivity and the effective graph resistance can be computed as follow:

$$\overline{\lambda}_{\mathcal{G}} = \ln\left(\frac{1}{N}\cdot\sum_{1=1}^{N} e^{\lambda_i}\right) \tag{5.8}$$

$$R_{\mathcal{G}} = N\cdot\sum_{i}^{N}\frac{1}{\mu_i} \tag{5.9}$$

where λ_i is the i^{th} eigenvalue of W and μ_i is the i^{th} eigenvalue of the L and the sum is such that null μ_i are neglected. The measure $\rho_{\mathcal{G}}$ can be regarded as an indicator of robustness of networks against dynamic processes (e.g. virus spreading, synchronization processes and phase transition behaviours), high μ_2 indicates a highly connected network (difficult to be partitioned into independent components). The natural connectivity quantifies the redundancy of alternative paths by quantifying the weighted

Spectral Graph-Theoretic Metrics:	$\overline{\lambda}_{\mathcal{G}}$	$R_{\mathcal{G}}$	$\rho_{\mathcal{G}}$	μ_2
Type:	Static		Dynamic	
Weights:	$w_{ij}=1$	$w_{ij}=B_{ij}$	$w_{ij}=f_{ij}$	$w_{ij}=PR_{ij}$
Approach:	Topological	Extended topological		

Table 5.1: The spectral graph metrics considered in this work and the weighting factors. Each weight can be associated to different type of approaches (i.e. extended topological, topological, dynamic and static).

number of closed walks of all lengths. The physical meaning is related to the Helmholtz free energy of a network [45]. Finally, $R_{\mathcal{G}}$ computed using susceptances is the sum of effective resistances R_l between all l, the lower it is the higher the network robustness is. The graph spectral radius, the natural connectivity, the algebraic connectivity and the effective graph resistance are computed using the 4 lines weights and used to assess drops in power grids robustness as summarised within Table 5.1. The overload cascading index presented in Section 5.3.1 will be for additional comparison between the metrics.

5.5 Treatment of Uncertainty

5.5.1 Uncertainty Characterisation

In this work, the sources of uncertainty investigated are:

1) The aleatory uncertainty associated to load demand variability. The aggregated load connected to a node i ($P_{L,i}$) can be described by a Normal distribution [122] $f(P_{L,i}) = \frac{1}{\sqrt{2\pi}\sigma_i} e^{-\frac{(P_{L,i}-\mu_i)^2}{2\sigma_i^2}}$, where $P_{L,i}$ is the load demand at node i, μ_i is the load mean value and σ_i is the standard deviation at node $i \in \mathcal{N}$. The parameter of the distribution can be estimated from historical records of load demand per node.

2) Imprecision in the lines parameters (B_l), attributable to design tolerance modelled as intervals (i.e. epistemic uncertain).

3) Uncertainty in the selection of the vulnerability model. Different vulnerability metrics computed using different models (e.g. power-flow model, pure or extended topological models) will be compared and discussed.

Once uncertain inputs are propagated through the computational model, the vulnerability outputs will be characterised by a mixture of aleatory and epistemic uncertainty and described using P-boxes.

5.5.2 Uncertainty Propagation

The double loop Monte Carlo methods (see Figure 2.8) is used in this work to propagate aleatory and epistemic uncertainty without mixing them. First,the epistemic uncertainty space Θ is obtained by Cartesian product of the imprecisely defined interval parameters of the lines $\Theta = [\underline{B}_1\overline{B}_1] \times ... \times [\underline{B}_l\overline{B}_l] \times ... \times [\underline{B}_{N_L}\overline{B}_{N_L}]$. Then, the outer loop starts by sampling random realization of the imprecise parameters, i.e. sampling uniformly within the n-orthotope Θ a parameters vector realisation $\theta_j = \mathbf{B}$. Each epistemic space realisation correspond a traditional probabilistic uncertainty quantification problem (i.e. inputs CDFs for the loads and a crisp values for each interval) for which only aleatory type of uncertainty has to be accounted. Then, a traditional MC simulation can be used (inner loop) to propagate aleatory uncertainty in the loads. The output will be an envelope of cumulative distribution $F_{\mathcal{V}|\theta_j}(\mathcal{V})$. The CDFs results of the inner loop are not to be averaged over the outer loop but only collected. Then the minimum and maximum can be selected to obtain bounds on the quantity of interest to assess the effect of lines tolerance imprecision on the output vulnerability.

5.5.3 Contingencies and Combinatorial Problem

In some power flow applications, contingency analysis is performed to constrain the network to safe operational states, for instance, by means of Security Constrained Optimal Power Flows. Those states are safe (e.g. thermal constraints are met and no cascading sequence occur) even if one of the contingencies listed is faced by the grid. In general, even if the network has modest size (e.g. small distribution grid), analyse a complete list of all possible failures is infeasible. A comprehensive contingency list will include $\sum_{k=1}^{N} N!/k!(N-k)!$ failures, where k is the number of failed components and N the number of network components. Consider, as example, a very small network of just $N = 50$ components, exhaustive contingency list includes 50 single component failures (i.e. $N-1$ contingencies), 4900 $N-2$, 705600 $N-3$, more than $1.32 \cdot 10^8$ $N-4$ contingencies and so on. In order to proceed with the calculations, a subset of failures is generally selected from the full set of combinations, the one considered more likely and with higher consequences. Higher order contingencies are often forsaken by assuming a negligible probability of facing those events, too low to be relevant. Nevertheless, targeted malicious attacks, extreme weather induced failures and other common cause failure mechanisms have the potential to increase the likelihood of face severe $N-k$ contingencies [29] and have generally higher consequences for the system. In this work, the complete set of $N-1$ single line failure are analysed and the most severe are identified using different vulnerability metrics. Random number N_c of $N-k$ contingencies are also analysed and for increasing damage size k. The most threatening events will be ranked and the average network vulnerability for increasing k discussed.

Relevant sources of uncertainty have been accounted in all the phases of the calculation.

5.6 The Proposed Framework

Algorithms (designed by the authors) are presented here and will be used to analyse the power grid under $N-1$ and $N-k$ line contingency scenarios. These will be later coupled to advanced, non-intrusive, uncertainty quantification approaches. Algorithm 1 is used for the $N-1$ contingency analysis. First, a power grid case study is loaded (e.g. a MATPOWER '*Case*' [165]) and additional input provided. A pre-contingency power flow (AC or DC) is solved and lines flows f_l and rating PR_l are obtained for the undamaged network. The weights w_l are selected, the undamaged adjacency and Laplacian matrices (W_{und} and L_{und}) obtained and used to compute vulnerability as explained in Sections 5.3.2 and 5.4. Single-line failures are evaluated one-at-a-time, either using '*Power-Flow Analysis*' and '*Topological Analysis*' methods.
The '*Power-Flow Analysis*' method works as follows:

1) Removed the line l from the undamaged network structure.

2) Compute post-failure f_l and PR_l using the post-contingency power flow presented in Algorithm 2 which is summarised by steps (3-5).

3) Run the depth-first-search algorithm to find the connected components (cc) in the damaged grid.

4) If the network is fully connected (i.e. $cc = 1$), the power flow is solved, line post-contingency flows obtained and percentage of rating computed.

5) If the network is not fully connected (i.e. $cc > 1$), the islands G_{is} with a single node are removed (the islanding is assumed unsustainable). For the remaining islands G_{is}, a slack bus is selected among the P-V nodes generator nodes) and the post-contingency $f_j(C_l)$ and $PR_j(C_l)$ obtained. If the grid island has no generators, the partition is set as isolated (outage).

6) Compute the overload severity and the cascading probability for all survived lines j and the cascading index $CEI(C_l)$ for the failed line l (i.e. the one removed in step 1).

7) The algorithm steps from 1) to 6) are repeated until all $N-1$ line failures are analysed.

Similarly, the '*Topological Analysis*' method proceeds as follows:

1) Remove the line l from W_{und} and compute the damaged network L.

2) Compute eigen-proprieties ($\Phi_{W_{und}}$, $\Phi_{L_{und}}$, Ψ, Λ).

3) Compute the effective graph resistance, the natural connectivity, the spectral radius and the algebraic connectivity as explained in Section 5.4.1.

4) Evaluate vulnerability to the analysed contingency $\mathcal{V}(C_l)$ as in Equations 5.7.

5) Repeat the Algorithm steps 1) to 4) until all the single line failures are analysed.

Algorithm 1 Vulnerability to $N-1$ Line Contingencies

procedure $N-1$ *Line Contingency*
    Load Power Grid '*Case*'
    Input: Load power demand and line parameters
    Run: pre-contingency AC (or DC) power flow
    Select $w_l \in \{1, B_l, f_l, PR_l\}$ and build W_{und} and L_{und}
    Compute & Save $\Phi_{W_{und}}, \Phi_{L_{und}}, \Psi$, Λ and $\mathcal{M} = \{\rho_{\mathcal{G}}, \mu_2, \overline{\lambda}, R_{\mathcal{G}}\}$

    Power-Flow Analysis
    for each line $l \in \mathcal{L}$ **do**
        Reset undamaged state and remove line l
        Run: Post-Contingency Algorithm 2
        Compute $S_j(C_l)$ and $\mathcal{P}(C_j|C_l)$ for each line in service j.
        Compute $CEI(C_l)$
    end for

    Topological Analysis
    for each line $l \in \mathcal{L}$ **do**
        Set $W = W_{und}$ and $w_l = 0$, build L
        Obtain Φ_W, Φ_L, Ψ and Λ and $\mathcal{M}(C_l) = \{\rho_{\mathcal{G}}, \mu_2, \overline{\lambda}, R_{\mathcal{G}}\}$
        Compute $\mathcal{V}(C_l)$ for each metric
    end for
end procedure

Algorithm 2 Post-Contingency Power Flow

procedure *Post-Contingency Power Flow*
    Search for connected components (cc) (depth-first-search)
    if $cc > 1$ **then**
        Check and remove isolated node
        $\forall$ island:
        Select one slack among the P-V nodes
        Run: AC (or DC) power flows
    end if
    if $cc = 1$ **then**
        Run: AC (or DC) power flows
    end if
end procedure

The method used for the $N-k$ line contingency analysis is summarised in the Algorithm 3. First the network data, the size of the contingency k and the number of contingency scenarios to be analysed N_C are selected. Then, k lines are randomly

removed from the undamaged network and the consequence are evaluated using both Algorithm 2 and spectral analysis of the damaged adjacency matrix W. The procedure is repeated until N_C scenarios are analysed and the results are statistical description of the vulnerability of each line (e.g. expectations and CDFs). For instance, the expectation of the vulnerability is computed as $E\left[\mathcal{V}(C_{N-k})\right] = \frac{\sum_{i=1}^{N_C} \mathcal{V}_i(C_{N-k})}{N_C}$.

Algorithm 3 Vulnerability to the $N-k$ Line Contingencies

procedure *Vulnerability to an $N-k$ Line Contingency*
  Input: Load Power Grid '*Case*', set k and N_C
  Run: Pre-contingency AC (or DC) power flow
  Select one $w_l \in \{1, B_l, f_l, PR_l\}$ and build W_{und} and L_{und}
  Compute $\Phi_{W_{und}}$, $\Phi_{L_{und}}$, Ψ, Λ and obtain $\mathcal{M} = \{\rho_{\mathcal{G}}, \mu_2, \overline{\lambda}, R_{\mathcal{G}}\}$
  for $i = 1$ to N_C **do**
    Remove k lines randomly and compute L
    Obtain Φ_W, Φ_L, Ψ, Λ and $\mathcal{M}(C_{N-k}) = \{\rho_{\mathcal{G}}, \mu_2, \overline{\lambda}, R_{\mathcal{G}}\}$
    Compute $\mathcal{V}_i(C_{N-k})$ for each metric
    Run: Post-Contingency Algorithm 2
    Compute $S_l(C_{N-k})$ and $\mathcal{P}(C_l|C_{N-k})$ for each line in service k.
    Compute $CEI_i(C_{N-k})$ and restore undamaged topology
  end for
  Compute CDFs and expectations:
  $F_{CEI_i(C_{N-k})}$, $F_{\mathcal{V}(C_{N-k})}$, $E\left[\mathcal{V}(C_{N-k})\right]$, $E\left[CEI_i(C_{N-k})\right]$
end procedure

Main difference between Algorithm 1 and 3 is that the first analyses all the possible single line failures while the second considers random line failures of order k. The main drawback is that it can result time consuming for large size network. Different networks and weights can be easily selected and compared and both topology-based and flow-based analysis performed in a common flexible computational framework. The Algorithms for $N-1$ contingency analysis is used in combination with non-intrusive uncertainty propagation methods. The effect of aleatory uncertainty (stochastic load demand) and epistemic uncertainty (parameters tolerances) on the vulnerability output of Algorithm 1 are propagated using classical MC and double loop MC methods.

In this work the number of scenarios N_c has been selected based on experience. However, for future analysis it would be interesting to determine a sufficiently high number N_c of $N-k$ contingency scenarios in order to ensure a good statistical description of the vulnerability of each line. For instance N_c can be selected such that at least $N_{c,l}$ failures are extracted for each line l, i.e. select N_c so that the moments of the vulnerability distribution converge.

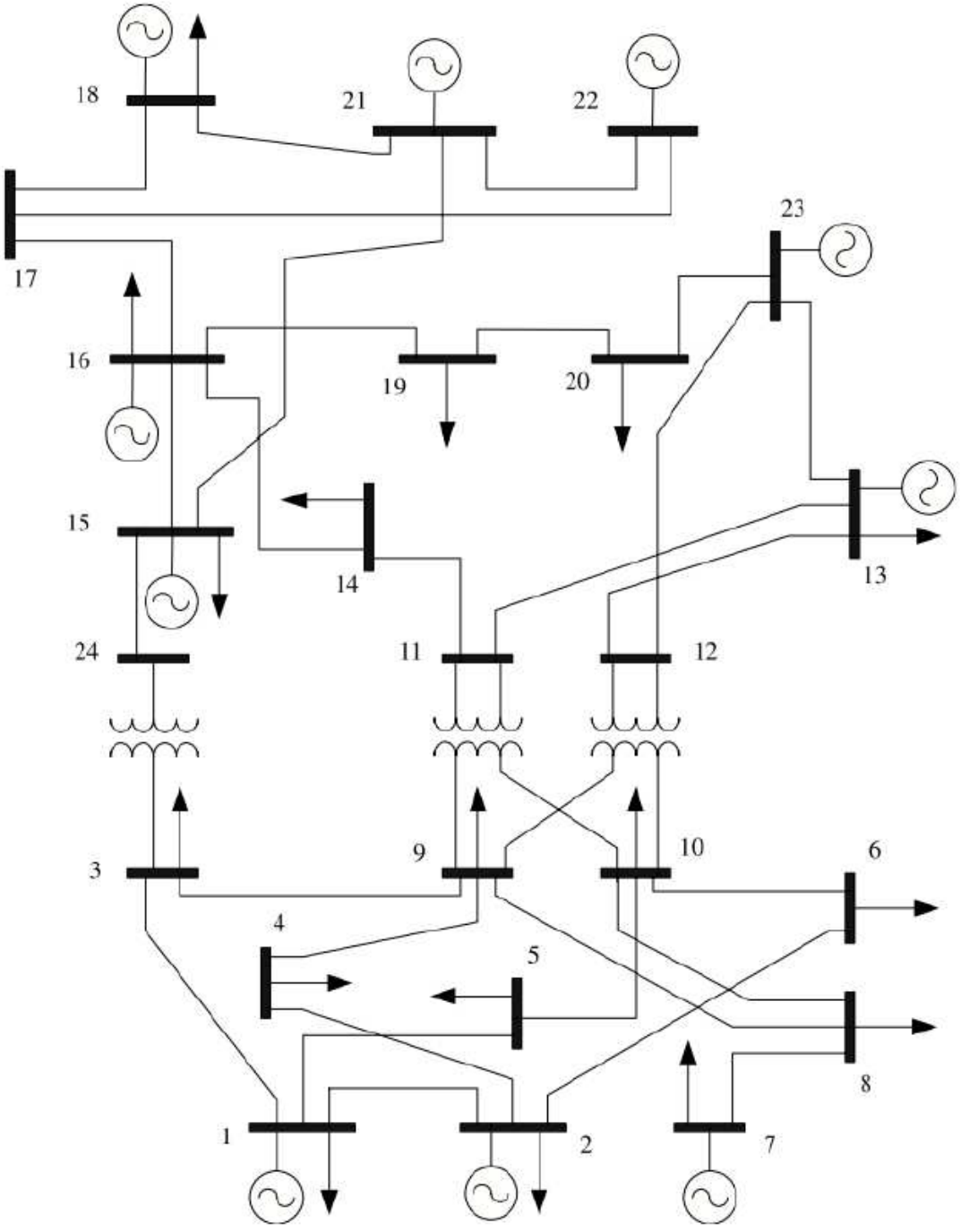

Figure 5.1: The modified IEEE-RTS 24 nodes layout.

5.7 A Case Study: IEEE 24 node reliability test system

The selected case study is a modified version of the IEEE 24 nodes reliability test system [154]. The grid is realistic, fairly complex and suitable to test the proposed framework. The modified network counts 24 nodes, 17 loads, 34 lines and 33 generators distributed over 11 nodes. Within the grid, there are 11 P-V nodes (i.e. generator nodes) and 13 P-Q nodes (i.e. load nodes). The original network topology has been modified to substitute parallel lines with equivalent single lines (i.e. the lines l_{19-20}, l_{15-21}, l_{18-21} and l_{20-23}). The modified structure is presented in Fig.5.1 whilst the design data can be found in Refs. [165]- [154].

5.7.1 Results: N-1 line failures

The $N-1$ line failures are analysed using the Algorithm 1 and using '*Power-Flow Analysis*' and '*Topological Analysis*' methods as presented in Section 5.6. The vulnerability results obtained using '*Topological Analysis*' method are displayed in Fig.5.2. The Y-axis display relative changes in spectral vulnerability metrics due to failure of the line l, i.e. $\mathcal{V}(C_l)$. Each line is identified by an identification number (ID) and displayed on the X-axis. On the right hand side of Fig.5.2 are presented vulnerability results obtained using μ_2 (the top plot) and $R_{\mathcal{G}}$ (the bottom plot). The relative drops in $\rho_{\mathcal{G}}$ and $\overline{\lambda}$ are presented on the left-hand-side in the bottom and top panels, respectively. Red solid lines are obtained using pure topological analysis ($w_l = 1$), the bars are obtained weighting adjacency with susceptances ($w_l = B_l$), the black dashed lines using the line active flows ($w_l = f_l$) and the green marked lines using percentage of rating ($w_l = PR_l$).

The analysis is performed very efficiently and the 5 most vulnerable lines are ranked in approximatively 0.15 seconds (which is the overall time for all the metrics and weights). The ranking results are presented in Table 5.2 and pure topological rankings are reported in the first column on the left. The results show similarities and differences in ranks. For instance when algebraic connectivity is employed, the lines l_{7-8} and l_{11-14} are identified as vulnerable, independently from the choice of the lines weights.

The AC power flow and the DC linearised version are used to solve the network and by running the method '*Power-Flow Analysis*' the cascading indices CEI are obtained and line failures ranked. The ranking results for the 5 most vulnerable lines are presented in Table 5.3. The DC results are quite similar the AC results, although the DC approximation overestimates slightly some of the line flows. This is probably due to the errors introduced by the DC approximation when the network is in contingency state (e.g. for higher system stress, possibly higher losses and larger voltage angles [149]). Furthermore for the selected MATPOWER case, the PV nodes have voltage magnitudes greater than 1 per-unit, whilst the DC formulation assumes flat voltage profile

	$w_{ij}=1$	$w_{ij}=B_{ij}$	$w_{ij}=f_{ij}$	$w_{ij}=PR_{ij}$
Rank	Algebraic Connectivity μ_2			
1	l_{7-8}	l_{7-8}	l_{7-8}	l_{7-8}
2	l_{3-24}	l_{16-17}	l_{15-24}	l_{11-14}
3	l_{15-24}	l_{11-14}	l_{3-24}	l_{14-16}
4	l_{11-14}	l_{14-16}	l_{5-10}	l_{15-24}
5	l_{16-17}	l_{3-24}	l_{11-14}	l_{16-19}
Rank	Natural Connectivity $\overline{\lambda}_{\mathcal{G}}$			
1	l_{12-13}	l_{16-17}	l_{16-17}	l_{16-17}
2	l_{9-12}	l_{15-16}	l_{14-16}	l_{14-16}
3	l_{10-12}	l_{17-18}	l_{17-18}	l_{7-8}
4	l_{9-11}	l_{16-19}	l_{17-22}	l_{17-18}
5	l_{10-11}	l_{14-16}	l_{16-19}	l_{12-23}
Rank	Spectral Radius $\rho_{\mathcal{G}}$			
1	l_{9-12}	l_{16-17}	l_{16-17}	l_{16-17}
2	l_{10-12}	l_{15-16}	l_{14-16}	l_{14-16}
3	l_{9-11}	l_{17-18}	l_{17-18}	l_{17-18}
4	l_{10-11}	l_{16-19}	l_{17-22}	l_{17-22}
5	l_{12-13}	l_{14-16}	l_{16-19}	l_{16-19}
Rank	Effective Resistance $R_{\mathcal{G}}$			
1	l_{3-24}	l_{16-17}	l_{15-24}	l_{11-14}
2	l_{15-24}	l_{11-14}	l_{3-24}	l_{14-16}
3	l_{16-19}	l_{14-16}	l_{5-10}	l_{15-24}
4	l_{16-17}	l_{16-19}	l_{11-14}	l_{16-19}
5	l_{20-23}	l_{15-24}	l_{14-16}	l_{20-23}

Table 5.2: The most vulnerable lines for the IEEE 24 nodes reliability test system. The top 5 most vulnerable lines are compared with respect to the 4 spectral metrics obtained using 4 different weighs for the adjacency matrix.

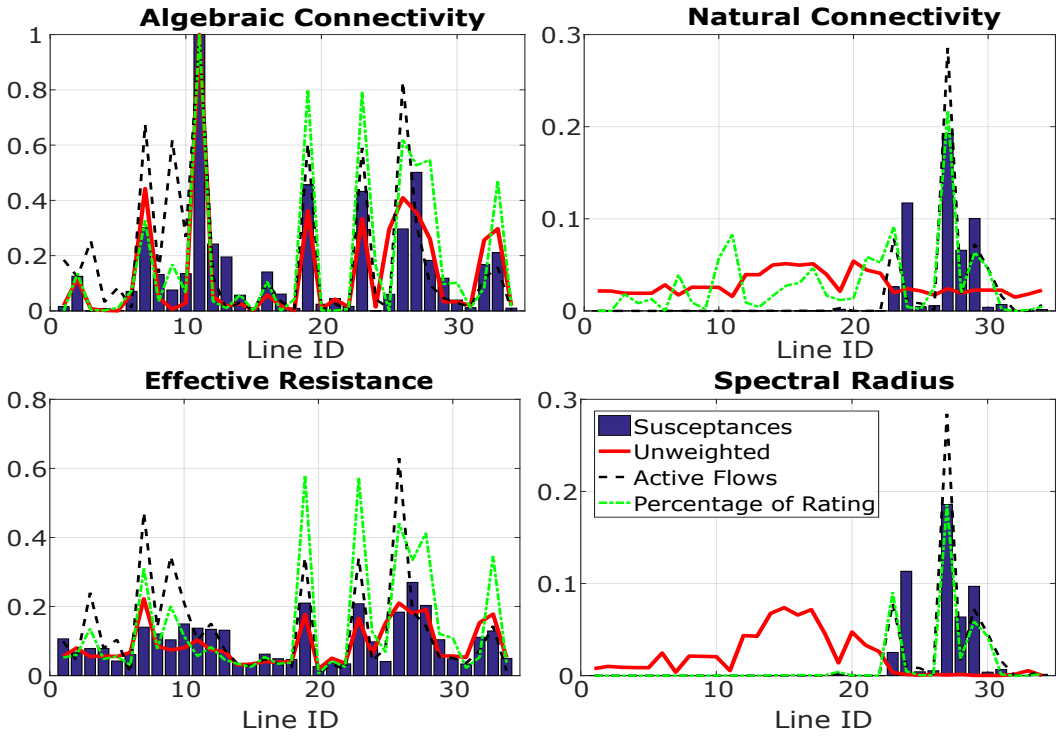

Figure 5.2: The grid vulnerability to the $N-1$ line failures obtained as relative changes in performance metrics. Comparison between four spectral metrics ($\mu_2, \rho_{\mathcal{G}}, \overline{\lambda}_{\mathcal{G}}, R_{\mathcal{G}}$) and different adjacency matrix weights ($w_l \in \{1, B_l, f_l, PR_l\}$).

(i.e. voltage magnitudes set to 1 per-unit). This is likely to affect the calculation and lead to a relevant differences between the DC and AC solutions. Nonetheless, a very good agreement exists between AC and DC rankings (failure of lines l_{15-21}, l_{15-24}, l_{21-22} and l_{3-24} were identified in both lists). It can be concluded that for the analysed network the DC method approximates the AC solutions fairly well also for the aim of contingency ranking. The computational time for the solution for both AC and DC $N-1$ contingency is about 0.9 seconds on a typical desktop PC (8.00 Gb RAM and 2.00 GHz processor). The line l_{15-24} is identified among the 5 most vulnerable by both μ_2 and $R_{\mathcal{G}}$. None of the topological metrics (pure or extended) were able to identify the vulnerability of line l_{15-21}, which scored highest from the overloading cascading perspective. This can be interpreted as a limitation of the topological approaches, which are unable to capture important features in the network operations.

5.7.1.1 Correlation analysis

An analysis of rank correlations is proposed to assess similarities and differences between the vulnerability metrics. The Spearman's correlation coefficient is a non-parametric measure of rank correlation and it can be used to measure the statistical dependence between metrics. It is sometimes defined as the Pearson correlation coefficient between

Rank	CEI_{AC}		CEI_{DC}	
1	l_{15-21}	1.00	l_{15-21}	1.33
2	l_{21-22}	0.17	l_{15-24}	0.64
3	l_{15-24}	0.07	l_{3-24}	0.64
4	l_{3-24}	0.07	l_{16-19}	0.22
5	l_{20-23}	0.02	l_{21-22}	0.21

Table 5.3: The 5 most vulnerable lines from an operational prospective. Comparison between AC and DC results.

ranked variables [113]. The matrix of Spearman's rank correlation coefficients is calculated for 2 CEI indices (computed using the AC and DC methods) and for 16 spectral graph metrics (the 4 metrics and 4 weights for each metric). Table 5.4 presents the correlation results calculated from the ranking of the 10 most vulnerable lines. Figure 5.3 displays graphically the correlation matrix. It can be observed, as expected, a very high positive correlation between the AC and DC cascading indices (close to 0.8). It can be also observed high/moderate correlations (from 0.6 to 0.9) between the same spectral vulnerability metric but computed with different weights. Algebraic connectivity and effective resistance are also highly correlated, which can be explained as both are computed using the eigenvalues of the Laplacian matrix. Many pairs of vulnerability metrics are weakly correlated (i.e. coefficients <0.3). However, other metrics display a high degree of correlation (i.e. coefficients between 0.6 and 0.9) or a moderate degree of correlation (i.e. coefficients between 0.3 and 0.6).

5.7.1.2 Uncertainty Quantification

The aleatory uncertainty in the power demand is propagated to the cascading index and to the extended topological metrics using the MC method. For each MC run, a random realisation of the load profile is obtained (i.e. a vector containing 17 random loads $P_{L,i}$) and forwarded to the $N-1$ solver (Algorithm 1). The network vulnerability is then evaluated using cascading indices computed with the AC and DC power flow methods. Spectral metrics are computed using 2 different weights for the line (f_{ij} and PR_{ij}). The results for the remaining weights ($w_{ij} = 1$ and $w_{ij} = B_{ij}$) are not affect by load variability and thus neglected here. The Monte Carlo method stops when a predefined number of realisations is reached (set to 500).

Figs. 5.4-5.6 display the uncertainty quantification results for CEI and the spectral vulnerability metrics, respectively. The red solid lines display the expected vulnerability whilst the blue dashed lines show the expectation plus or minus 2 times the sample standard deviation ($\mathbb{E}[\mathcal{V}(l)] \pm 2\sqrt[2]{\mathbb{V}ar[\mathcal{V}(l)]}$). The red markers are the vulnerability realisations of the MC method (i.e. CEI and $\mathcal{V}$ for each line and for each load demand

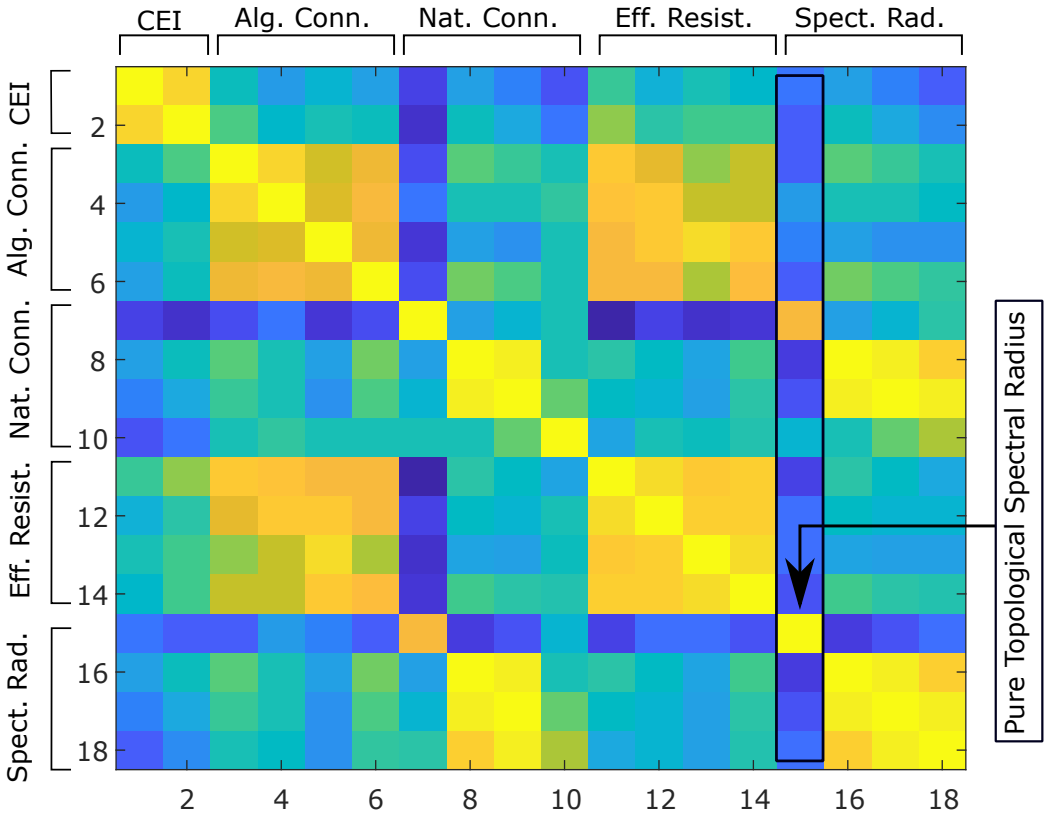

Figure 5.3: The matrix of Spearman's rank correlation coefficients. It can be observed high correlation between the two CEI indices and between the same topological metric computed using different weights.

CEI		μ_2				$\overline{\lambda}_{\mathcal{G}}$				$R_{\mathcal{G}}$				$\rho_{\mathcal{G}}$			
AC	**DC**	**1**	**B**	**f**	**PR**	**1**	**B**	**f**	**PR**	**1**	**B**	**f**	**PR**	**1**	**B**	**f**	**PR**
1.0	0.8	0.1	-0.1	0.1	-0.1	-0.5	-0.1	-0.2	-0.4	0.3	0.0	0.2	0.1	-0.3	-0.1	-0.2	-0.4
0.8	1.0	0.3	0.1	0.2	0.2	-0.6	0.1	0.0	-0.3	0.5	0.2	0.3	0.3	-0.4	0.1	0.0	-0.2
0.1	0.3	1.0	0.8	0.6	0.7	-0.5	0.4	0.3	0.2	0.8	0.6	0.5	0.6	-0.4	0.4	0.3	0.2
-0.1	0.1	0.8	1.0	0.6	0.7	-0.3	0.2	0.2	0.2	0.7	0.8	0.6	0.6	-0.1	0.2	0.2	0.1
0.1	0.2	0.6	0.6	1.0	0.7	-0.6	-0.1	-0.2	0.2	0.7	0.8	0.9	0.8	-0.2	-0.1	-0.2	-0.2
-0.1	0.2	0.7	0.7	0.7	1.0	-0.5	0.4	0.3	0.2	0.7	0.7	0.5	0.7	-0.4	0.4	0.3	0.3
-0.5	-0.6	-0.5	-0.3	-0.6	-0.5	1.0	-0.1	0.1	0.2	-0.7	-0.5	-0.6	-0.6	0.7	-0.1	0.1	0.2
-0.1	0.1	0.4	0.2	-0.1	0.4	-0.1	1.0	0.9	0.2	0.2	0.1	0.0	0.3	-0.5	1.0	0.9	0.8
-0.2	0.0	0.3	0.2	-0.2	0.3	0.1	0.9	1.0	0.4	0.1	0.1	-0.1	0.2	-0.4	0.9	1.0	0.9
-0.4	-0.3	0.2	0.2	0.2	0.2	0.2	0.2	0.4	1.0	0.0	0.2	0.1	0.2	0.1	0.2	0.4	0.5
0.3	0.5	0.8	0.7	0.7	0.7	-0.7	0.2	0.1	0.0	1.0	0.8	0.8	0.8	-0.5	0.2	0.1	0.0
0.0	0.2	0.6	0.8	0.8	0.7	-0.5	0.1	0.1	0.2	0.8	1.0	0.8	0.8	-0.3	0.1	0.1	0.1
0.2	0.3	0.5	0.6	0.9	0.5	-0.6	0.0	-0.1	0.1	0.8	0.8	1.0	0.9	-0.3	0.0	-0.1	-0.1
0.1	0.3	0.6	0.6	0.8	0.7	-0.6	0.3	0.2	0.2	0.8	0.8	0.9	1.0	-0.4	0.3	0.2	0.2
-0.3	-0.4	-0.4	-0.1	-0.2	-0.4	0.7	-0.5	-0.4	0.1	-0.5	-0.3	-0.3	-0.4	1.0	-0.5	-0.4	-0.3
-0.1	0.1	0.4	0.2	-0.1	0.4	-0.1	1.0	0.9	0.2	0.2	0.1	0.0	0.3	-0.5	1.0	0.9	0.8
-0.2	0.0	0.3	0.2	-0.2	0.3	0.1	0.9	1.0	0.4	0.1	0.1	-0.1	0.2	-0.4	0.9	1.0	0.9
-0.4	-0.2	0.2	0.1	-0.2	0.3	0.2	0.8	0.9	0.5	0.0	0.1	-0.1	0.2	-0.3	0.8	0.9	1.0

Table 5.4: The matrix of the Spearman's rank correlation coefficients. Comparison between the top 10 most vulnerable lines accordingly to the *CEI* indices (AC and DC) and to the 16 spectral graph metrics (4 metrics and 4 weights for each metric).

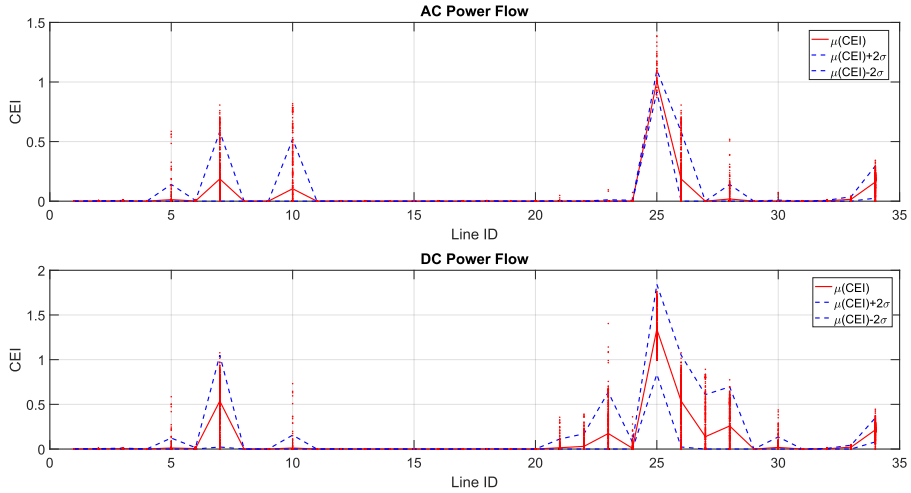

Figure 5.4: Comparison between AC and DC solver with respect to the variability in the flow-based vulnerability metric. The analysis is performed for the cascading index due to single line failure and random load profiles.

sample). A 2-sigma rule has been used to robustly rank the 5 most vulnerable lines under uncertainty the results are compared to the deterministic case. Using of a 2-sigma rule means that the rank is based on the upper tail of the vulnerability distribution (i.e. the value selected for the ranking includes 97.73% of the vulnerability realisations if assumed normally distributed). The result significantly changes if compared to the deterministic results presented in Table 5.3. Table 5.6 shows the results for the uncertainty quantification on the cascading index applying the AC and the DC solvers. Accordingly to the AC results, the 5 most vulnerable lines are l_{15-21}, l_{15-24}, l_{3-24}, l_{6-10} and l_{21-22}, whilst for the DC result the most vulnerable lines are l_{15-21}, l_{15-24}, l_{3-24}, l_{16-19} and l_{14-16}. The overall computational time needed for the power flow analysis was about 7-8 minutes. On the other hand, the time needed to perform the *Topological Analysis* method was significantly lower, just 68 seconds were needed (i.e. about 17 seconds for each line weight).

The effect of parameter imprecision on the vulnerability result is also assessed. Sources epistemic uncertainty considered are: 10 % imprecision intervals on the 34 lines susceptances, which are attributable to design tolerances. Both the imprecision on B_l and the aleatory uncertainty in the load profile are propagated using a double loop MC approach and without mixing aleatory and epistemic components. Previous analysis suggested that the metrics adopted to assess the vulnerability of the power grid $\mathcal{G}$ vary monotonically with respect the imprecise parameters B_l. Thus, the upper and lower bounds on the CDFs can be efficiently approximated by random search within the vertex boundaries of the hyper-rectangle $\mathcal{I}_X = [0.95B_1, 1.05B_1] \times ... \times [0.95B_{34}, 1.05B_{34}]$. Five-hundred random realisations of B_l from the epistemic space are generated in the outer loop and forwarded to the inner loop where a classical MC samples 500 load

	$w_{ij} = f_{ij}$	$w_{ij} = PR_{ij}$	$w_{ij} = f_{ij}$	$w_{ij} = PR_{ij}$
Rank	Expected μ_2 $+2\sigma$		Expected $\overline{\lambda}_{\mathcal{G}}$ $+2\sigma$	
1	l_{7-8}	l_{7-8}	l_{16-17}	l_{16-17}
2	l_{15-24}	l_{11-14}	l_{17-18}	l_{14-16}
3	l_{5-10}	l_{14-16}	l_{14-16}	l_{7-8}
4	l_{1-5}	l_{16-19}	l_{17-22}	l_{17-18}
5	l_{3-24}	l_{20-23}	l_{15-16}	l_{6-10}
Rank	Expected $R_{\mathcal{G}}$ $+2\sigma$		Expected $\rho_{\mathcal{G}}$ $+2\sigma$	
1	l_{15-24}	l_{11-14}	l_{16-17}	l_{16-17}
2	l_{1-5}	l_{14-16}	l_{17-18}	l_{14-16}
3	l_{3-24}	l_{16-19}	l_{14-16}	l_{17-18}
4	l_{5-10}	l_{1-5}	l_{17-22}	l_{17-22}
5	l_{1-3}	l_{20-23}	l_{15-16}	l_{16-19}

	$w_{ij} = f_{ij}$	$w_{ij} = PR_{ij}$	$w_{ij} = f_{ij}$	$w_{ij} = PR_{ij}$
Rank	Expected μ_2 $+2\sigma$		Expected $\overline{\lambda}_{\mathcal{G}}$ $+2\sigma$	
1	1	1	0.36	0.25
2	0.84	0.82	0.10	0.10
3	0.77	0.81	0.09	0.09
4	0.72	0.77	0.06	0.09
5	0.71	0.72	0.03	0.08
Rank	Expected $R_{\mathcal{G}}$ $+2\sigma$		Expected $\rho_{\mathcal{G}}$ $+2\sigma$	
1	0.57	0.53	0.35	0.26
2	0.56	0.51	0.09	0.12
3	0.43	0.49	0.08	0.09
4	0.4	0.45	0.05	0.05
5	0.39	0.44	0.03	0.03

Table 5.5: The most vulnerable lines for the IEEE 24 nodes reliability test system accordingly to the expectations plus 2σ of topological vulnerability measures.

Rank	Expected CEI_{AC}+2σ		Expected CEI_{DC}+2σ	
1	l_{15-21}	1.05	l_{15-21}	1.84
2	l_{15-24}	0.59	l_{15-24}	1.07
3	l_{3-24}	0.57	l_{3-24}	1.02
4	l_{6-10}	0.51	l_{16-19}	0.69
5	l_{21-22}	0.29	l_{14-16}	0.62

Table 5.6: The 5 most vulnerable lines accordingly to the CEI expectations plus 2σ. Comparison between AC and DC results.

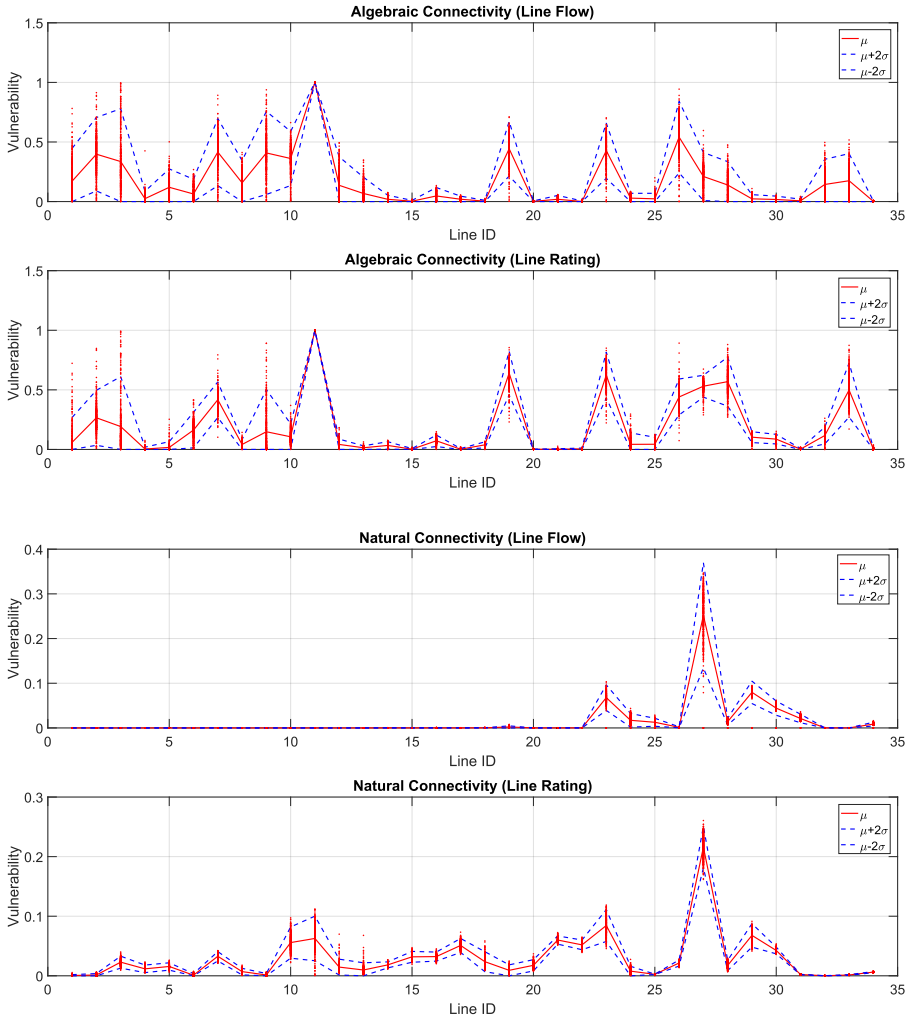

Figure 5.5: Quantification of the variability of spectral vulnerability metrics due to $N-1$ line failures and random load profiles.

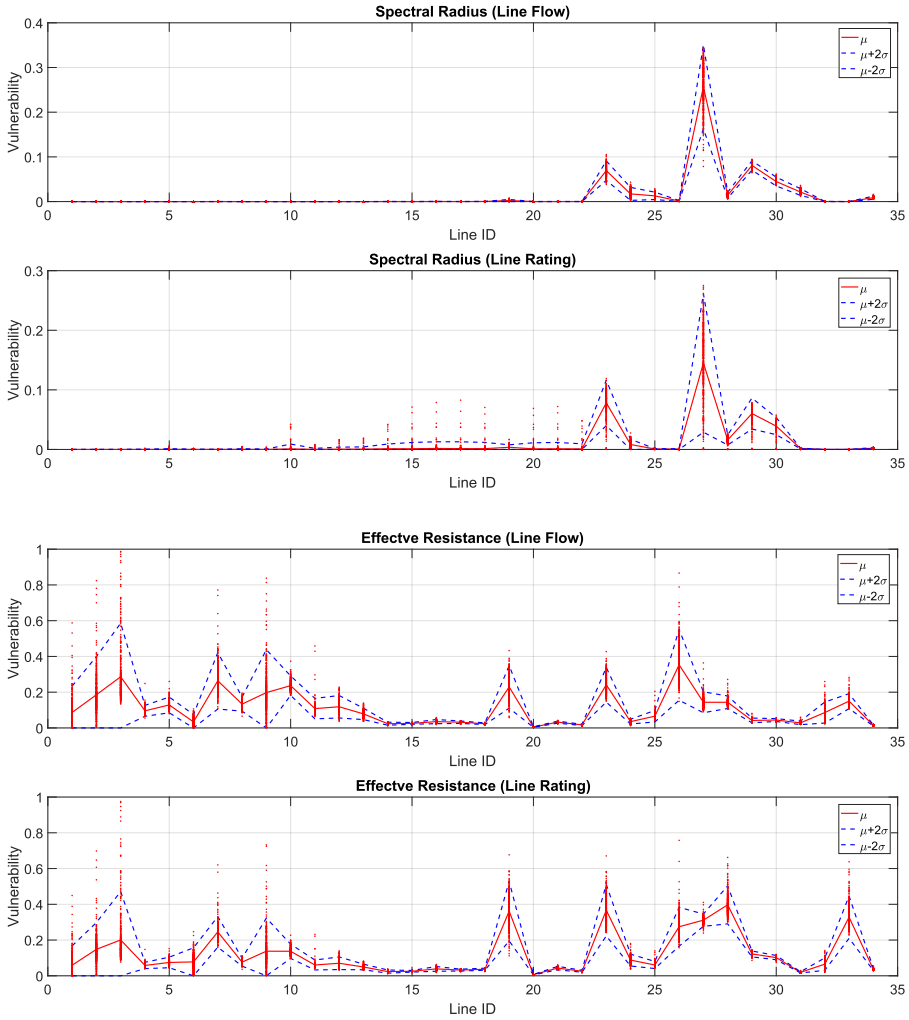

Figure 5.6: Quantification of the variability of spectral vulnerability metrics due to $N-1$ line failures and random load profiles.

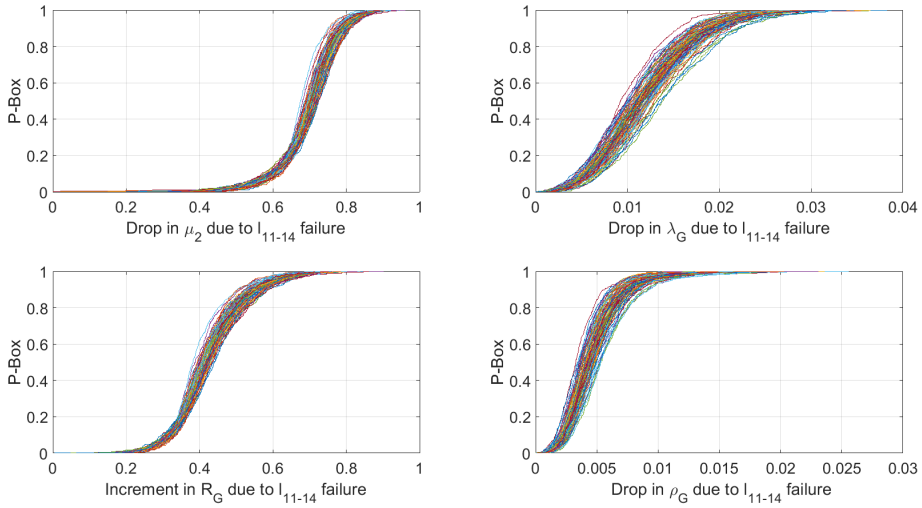

Figure 5.7: An example of output P-boxes obtained using advanced UQ methods. The vulnerability is greatly affected by aleatory uncertainty, but also epistemic uncertainty plays a role (metrics computed for $w_{ij} = PR_{ij}$).

realisations. The vulnerability is obtained as a P-box and an example is depicted in Fig.5.7 which presents 4 CDF envelopes (i.e. P-boxes) for the 4 considered metrics and weight $w_{ij} = PR_{ij}$. For sake of synthesis, only vulnerability scores due to failure of l_{11-14} are plotted (other lines produces analogous results). In can be noticed that the aleatory component is dominating the uncertainty associated to the spectral vulnerability metrics. The effect of parameters imprecision has been quantified and it resulted small but observable. Same uncertainty sources have been propagated on the cascading index CEI solving the network using the DC power flow method. The P-boxes of CEI and for two of the most vulnerable lines have been reported in Fig.5.8. Especially for the failure of the line connecting node 15 to node 21 the CEI precision results highly affected by parameter tolerances. This is an interesting result showing that some failure scenarios are more sensitive to a data deficiency, tolerance imprecision and epistemic uncertainty.

5.7.2 Results: N-k line failures

Higher order $N - k$ contingencies are analysed using the Algorithm 3 presented in Section 5.6. The contingency analysis is carried out by increasing damage sizes, i.e. $k = 1, .., 8$. The random number of failures N_C is set equal to 1000 for each damage size k. Fig.5.9 shows that the average topological vulnerabilities computed weighting adjacency elements by susceptances, which result increasing for increasing k. It is interesting to notice that average drops in spectral radius and the natural connectivity result very similar and that have the lower gradient with respect to the contingency size. Conversely, the mean drop in algebraic connectivity has the higher gradient and

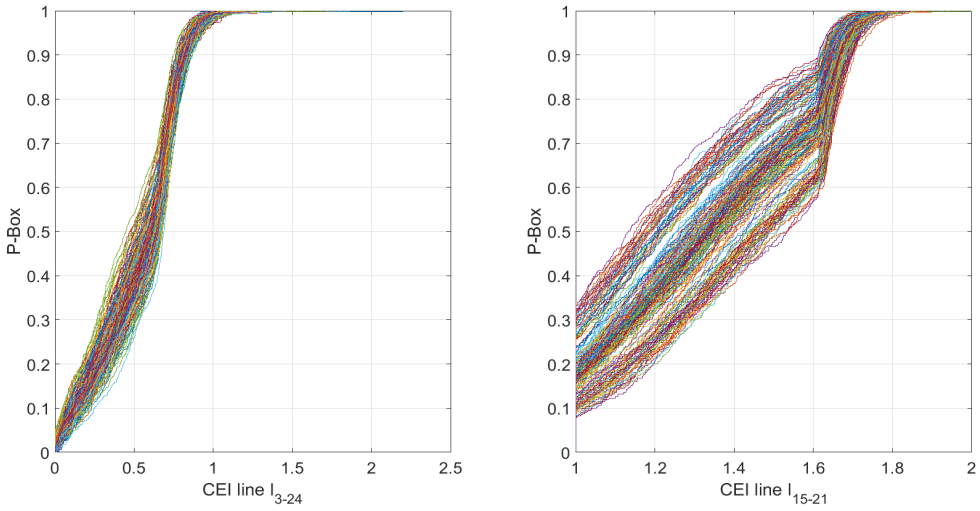

Figure 5.8: An example of output P-boxes for the CEI indices associated to two vulnerable lines in the system. The index associated to line l_{15-21} is greatly affected by both epistemic and aleatory uncertainty.

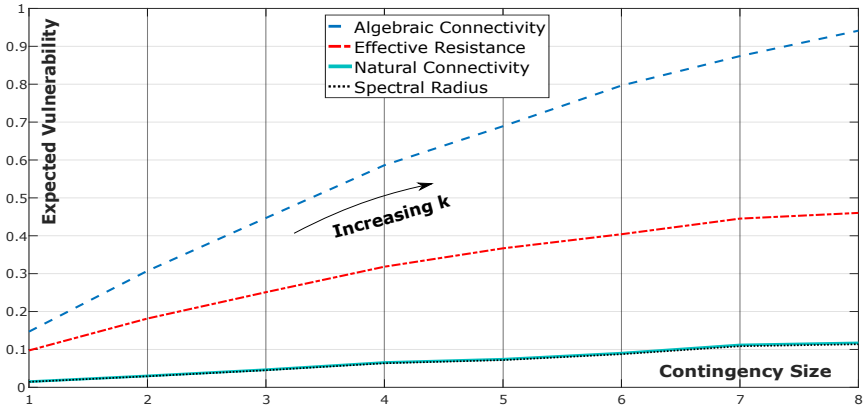

Figure 5.9: Comparison between the expected vulnerability when facing an $N-k$ contingencies using different spectral metrics. Adjacency built using B_{ij} as weights.

for a contingency of type $N-8$, it results close to 1. This indicates that it is highly unlikely to face an $N-8$ failure which keeps the power grid fully connected (i.e. $\mu_2 \neq 0$ for the damaged network). Furthermore, the relative drop in algebraic connectivity will be of little use to analyse higher order contingencies (i.e. the vulnerability result will be likely equal to 1).

5.8 Discussion

The vulnerability of the IEEE 24 nodes reliability test system has been analysed. Different metrics have been compared in ranking contingencies and the uncertainty

due to load demands variability and line parameters imprecision has been quantified.

The comparison between pure topological and extended topological approaches shows significant correlation (similarities) between the ranking results. Spectral analysis of the network requires a moderate computational cost for obtaining a full spectrum of eigenvalues and eigenvectors for each contingency; significantly less than the cascading indices. The higher computational complexity is attributable to the (at least two) power flow solutions which have to be computed to obtain the cascading indices. Of course, the larger the network size the higher will be the computational cost for the analysis. Nevertheless, adjacency matrices for real world power network are often sparse matrix and, therefore, dedicated approaches can be used to speed up the procedure when just few eigenvalues are needed, e.g. spectral radius and algebraic connectivity. In this case, the on-line applicability of the spectral vulnerability metric for contingency ranking also accounting uncertainties might be feasible.

However, the spectral vulnerability metrics, even if enhanced by electrical engineering concepts, seem unable to fully capture the complexity of the network operation, i.e. major difference has been observed between cascading index results and results using extended topological approaches. Nevertheless, many of the lines which have been ranked using cascading indices resulted in a null contribution to the vulnerability (due to null post-failure overload severity). This might be regarded as a limitation of the CEI metric which has not been able to fully capture all the relevant consequences of certain line failures.

The uncertainty in vulnerability metrics, due to the load demands variability and lines parameters imprecision (tolerances) has been quantified. This provides a more robust identification of the critical components. The line ranking results under uncertainty differ from the deterministic results, although some of the most critical line contingencies have been similarly identified. Analysing the output P-boxes, it has been observed that the vulnerability computed using spectral vulnerability metrics and power flow as the weighting factor is greatly affected by the stochastic load profile. Also tolerance imprecision (epistemic uncertainty) has a non-negligible effect, although its contribution to the uncertainty seems less significant on spectral vulnerability metrics. Conversely, some of cascading indices show high sensitivity to parameters imprecision.

As expected, the uncertainty propagation using advanced uncertainty quantification techniques was very demanding, especially for the power-flow methods. This is a clear limitation of the advanced UQ approach which makes it difficult to apply to on-line analysis. Nevertheless, the method is powerful and versatile and can be effectively used to point out how much of the output uncertainty is reducible by further data collection

(i.e. due to lack of information). This can be useful in may ways. For instance, a decision makers can use the method to to determine if a power grid is robust, if it is vulnerable, or if the available information is not sufficient to provide a clear answer to questions relating to the network ability to withstand targeted or random contingencies.

To summarise, select good vulnerability metrics for the identification of relevant contingencies is not an easy task. Among the different metrics considered in this work, pure topological metrics present two relevant features: 1) less information is generally required (only the structure of the grid was needed); 2) uncertainty associated to operative variables (e.g. load demand) and imprecision associated with power grid parameters are not affecting the metrics. These may be regarded as positive features, nonetheless, it might be argued that the pure topological metrics (being less sensitive to variability) are less effective in capturing complex behaviours which are typical of varying operative states in power grids. Although a correlation analysis pointed out some similarity between topological metrics and the cascading indices, their capabilities for contingency ranking prospects are still questionable. Further comparisons between graph-theory methods and traditional approaches are necessary.

5.9 Conclusions

In this work, a novel framework for assessing power grids vulnerability has been presented. The vulnerability assessment framework is embedded to advanced uncertainty quantification methods used to quantify the level of epistemic and aleatory uncertainty on the results. Single line and multiple line contingencies have been analysed and their vulnerability ranked with respect to topology-based metrics, flow-based metrics and accounting for model imprecision and stochastic loads. Four spectral vulnerability metrics have been computed using four different weighting factors (taken from literature and newly defined) and used to assess the robustness of a modified version of the IEEE 24 nodes RTS. Different effects of epistemic and aleatory uncertainty on network operational weaknesses (i.e. AC and DC overflow cascading models) and structural vulnerabilities have been discussed and relevant differences in the contingency ranking have been pointed out. Major differences in ranking results are attributable to the different vulnerability metrics rather than to different line weights. In case that only one vulnerability metric is selected, the choice of metric must be done with a high degree of care and done so whilst accounting for all the relevant sources of uncertainty which may generate misleading results.

Acknowledgement

A journal paper version of this chapter has been published as:

1. Roberto Rocchetta and Edoardo Patelli. Assessment of power grid vulnerabilities accounting for stochastic loads and model imprecision. *International Journal of Electrical Power & Energy Systems*, 98:219 – 232, 2018

Chapter 6

Power Grid Resilience: Weather-Induced Effects, Data Deficiency and a Power-Flow Emulator

6.1 Abstract

A generalised uncertainty quantification framework for resilience assessment of weather-coupled, repairable power grids is presented. The framework can be used to efficiently quantify both epistemic and aleatory uncertainty affecting grid-related and weather-related factors. The power grid simulator has been specifically designed to model interactions between severe weather conditions and grid dynamic states and behaviours, such as weather-induced failures or delays in components replacements. A resilience index is computed by adopting a novel algorithm which exploits a vectorised emulator of the power-flow solver to reduce the computational efforts. The resilience stochastic modelling framework is embedded into a non-intrusive generalised stochastic framework, which enables the analyst to quantify the effect of parameters imprecision. A modified version of the IEEE 24 nodes reliability test system has been used as representative case study. The surrogate-based model and the power-flow-based model are compared, and the results show similar accuracy but enhanced efficiency of the former. Global sensitivity of the resilience index to increasing imprecision in parameters of the probabilistic model has been analysed. The relevance of specific weather/grid uncertain factors is highlighted by global sensitivity analysis and the importance of dealing with imprecision in the information clearly emerges.

The power grid is the largest man-made critical infrastructure and is extremely complex in both its operations and structure. The weather conditions drifting towards extremes and the increasing use of renewable energy sources are tightening the interactions between power network states and the external environment. Reliability/availability analysis frameworks have, then, to incorporate weather models and consider interactions between grid states and environmental states, accounting for relevant sources of randomness (i.e. aleatory uncertainty) but also for parameters values imprecision (i.e. epistemic uncertainty).

Power network reliability is a well-defined mathematical concept [67]. Many frameworks for reliability assessment have been proposed in the past, which generally focus on known threats such as $N-1$ or $N-2$ failures paradigms [160] or on a predefined contingency set [1]- [98]. System resilience broadens the reliability concept by accounting for low-probability-high-consequence events (such as severe weather conditions [102]) and recovery process of the system. A generally accepted definition of resilience still has to be formulated, an example being '*the network ability to withstand high impact low probability events, rapidly recovering and improving operations and structures to mitigate the impact of similar events in the future*' [104]- [103]. It can be argued that a main difference between a reliable power grid and a resilient power grid is that, in the latter, low-probability-high-consequence events (e.g. extreme weather events) are specifically considered and handled, with the ability to learn from past occurrences. To achieve this, a comprehensive analysis of the relevant sources of uncertainty should be performed. In particular, lack of data is generally affecting low probability events. To improve overall robustness of the analysis, it is uttermost important to develop and improve frameworks capable of tackling (effectively and efficiently) data deficiency issues. A rigorous quantification of the lack of data affecting extreme low-probability-high-consequence events is necessary.

In the last years, many studies have focused on analysing the effect of extreme weather events on the power grid risk and reliability. Some research was carried out with the support of international organizations [82]; other focused on different extreme events such as floods, ice storms, strong wind gusts and more [104]- [82]- [23]- [75]- [122]- [4]- [152]. More recently, Cadini, Zio and Agliardi [23] proposed a probabilistic reliability/availability assessment framework extended from Ref. [4]. The framework incorporates a sampler of severe weather conditions and models weather-induced effects on the grid's components failures and replacements. One of the challenges for the application of the framework is the high computational cost. This is mainly attributable to the number of calls to the cascading failure model (i.e. the power-flow solver): *'...analysis of a more realistic grid is probably still feasible, although more complex analyses, e.g. including uncertainty and sensitivity analyses or optimizations,*

would require either to resort to processor clusters, or to identify strategies for accelerating the computations, possibly based on the use of surrogate, approximating models' [23].

In general, the time needed to compute the load curtailed can be quite small (e.g. that of a single optimal power flow evaluation); this is especially true if the power network size is modest. Unfortunately, optimisation problems cannot be vectorised and power flows have to be solved one-at-a-time. Consequently, any analysis for which a large number of power flow evaluations are needed may result computationally untreatable. Examples of such costly analysis are global sensitivity analysis [134], cascading failures analysis [23], or imprecise (generalised) uncertainty quantification analysis [36]. To perform such computationally demanding analysis, a significant reduction in the computational complexity (while reducing marginal accuracy) is needed and emulators can be adequate for this aim. A surrogate model, also known as emulator or meta-model, is a numerically cheap mathematical approximation of a computationally expensive realistic model [12]. Some examples of popular meta-models are Artificial Neural Networks [86]- [6], Poly-Harmonic Splines [78] and Kriging models [33]. Surrogates have been extensively applied to reduce time expenses of numerically burdensome models and few works have attempted to use meta-models to analyse power grids, see for instance [7]- [10]- [5]- [137]- [26]- [162]. N. Amjady et al. [5] proposed an emulator to assess the power system reliability providing as input forced outage rates. Silva et al. employed artificial neural networks to monitor voltage magnitudes [137]. Chen et al. [26] adopted a surrogate-based strategy for optimal power flow inequality constraints aggregation. To the Authors knowledge, none of the reviewed papers attempted to mimic the relationship between the grid components state vector, load profile and power load curtailed within a resiliency assessment framework.

Probabilistic reliability assessments of power grids are traditionally carried out with reference to a well-defined probabilistic characterisation of the uncertain output, whose calculation generally requires a large body of empirical information. A sufficient amount of samples are necessary to properly estimate the underlying probability distributions parameters and often, due to technological limits or time/cost constraints, the available data is not sufficient for accurately estimating all relevant parameters [94]. In those situations, expert assumptions are made on the probabilistic model, which can lead to erroneous conclusions, overestimation of the system performance and a false sense of confidence [14]. Data scarcity often affects the analysis of power grid resilience and safety [2]. In fact, consider the highly reliable components (e.g. transformers, underground cables, etc.) of which power grids are made. Those components will likely fail only a few times during their life span (or possibly even never). The lack of statistical failure data makes it difficult to characterise the failure behaviour

of these components with confidence. In this situation, a common practice is to estimate the failure rates of the components by considering the few available failure occurrences in similar components. This procedure, so-called "data pooling" [94], assumes similar elements behave as described by the same probabilistic model. This is a rational assumption, but when (similar) components operate differently (e.g. close/far from their thermal limits or in harsh/mild environments) or undergo different maintenance/repairing policies, such assumption is rarely true. In practice, different factors influence the components, leading to different failure behaviours even for identical components. In those situations, it is advisable to relax the assumption of a precise probabilistic model, for instance, by accounting for imprecision in the distribution parameters (e.g. in the estimation of components failure rates and events occurrence rates) [14]- [124]. Generally speaking, a set of plausible distribution families can be considered for describing imprecision (for instance, an envelope of Weibull, Exponential, Normal, etc. CDFs modelled using a non-parametric P-box). However, dealing with several distribution families was not the aim of this work. In this research, the parameters of the probability distribution families (e.g. used to sample the high wind event duration and intensity) and of the components of the grid-weather model are assumed affected by an increasing level of imprecision.

In this chapter, a generalised framework is proposed for (imprecise) probabilistic resilience assessment of power networks. The framework has been designed to capture complex coupling between weather conditions and power grid operations, by incorporating weather-influenced failures and repairs of the grid's components. An Artificial Neural Network (ANN) is trained to emulate the total load curtailed given specific lines failures and the load profile, and has been embedded within the framework to increase computational efficiency. Comparison between the novel surrogate-based framework and the original solver shows significant improvement in efficiency at the expense of a small reduction in accuracy. Aleatory uncertainty is accounted for and epistemic uncertainty is associated with imprecision and lack of knowledge. Both types of uncertainty are propagated by generalised probabilistic methods based on Credal sets and Fuzzy sets. The sensitivity of the resilience index to parameters imprecision is quantified. Aleatory uncertainty propagation and generalised uncertainty propagation (i.e. accounting also for imprecision) are performed and the ANN capabilities tested against the full power-flow. The results again show that the use of the ANN meta-model allows advanced sensitivity analysis to be performed on the parameters of the probabilistic model at the expense of a small reduction in accuracy but with a significant gain in computational time.

The rest of the chapter is organised as follows. Section 6.2 introduces the probabilistic model for coupling weather conditions and grid states. The emulator is presented in

Section 6.3. Section 6.4 presents the overall modelling and computational framework. In Section 6.5 the generalised probabilistic framework based on Credal sets is described. The case study and results are presented in Section 6.6. Section 6.7 presents a discussion of the findings from an applicative perspective and Section 6.8 closes the chapter.

6.2 A Probabilistic Model for Weather-Grid Coupling

A power grid topology can be represented by a graph $\mathcal{G}(\mathcal{N}, \mathcal{E})$, where i denotes a node within the node set $\mathcal{N}$ and (i, j) the link between node i and j in the line set $\mathcal{E}$ [73]- [66]- [163]- [74]. Denote with N_L the number of loads, with N_l the number of lines and with N_g the number of generators in $\mathcal{G}$.
Optimal-Power-Flow (OPF) methods can used to solve the network power dispatch problem [89]- [71]. In the adopted formulation, loads can be curtailed if necessary. This has indeed very high cost for the grid and will occur only if the cost minimization problem can not be solved otherwise, for instance, if load demand exceeds power capacity or to avoid line overloads. Mathematically, the problem is defined as follows:

$$\min_{P_g, L_{cut}} \quad f(P_g, L_{cut}) \tag{6.1}$$

where the cost function depends on the power generated and the load curtailed (L_{cut}).

6.2.1 Power Grid Resilience Index

The Expectation of Energy-not-Supplied ($\mathbb{E}[ENS]$), has been commonly used as a reliability index in a number of studies as well is previous chapter of this thesis. Although initially conceived as a reliability indicator, it has been claimed it is also suitable to the resilience concept [44]. Indeed, it is worth recalling that $\mathbb{E}[ENS]$ is not full capable of capture relevant resilience features, such as how fast the performance of different hazards in potential future scenarios and lack an economic dimension. The design of comprehensive resilience measures capable of capturing all relevant features is a challenging research topic itself and is further discussed in the concluding session of this thesis. For the aim of this framework, the $\mathbb{E}[ENS]$ is a sophisticated enough indicator of resilience and can be obtained by averaging contributions of N_s independent simulations:

$$\mathbb{E}[ENS] = \frac{\sum_{i=1}^{N_s} ENS_i}{N_s} \tag{6.2}$$

where the Energy-not-Supplied, ENS, for a given simulation period T_{sim}, here considered to be 1 year, is obtained as follows:

$$ENS = \sum_{t=1}^{T_{sim}} \sum_{i \in \mathcal{N}} L_{cut,i,t} \cdot t \tag{6.3}$$

where $L_{cut,i,t}$ is the load curtailed at each time t and each node i, obtained solving the minimisation problem in Eq. (6.1). The ENS due to a failure event f can be obtained as $\sum_{t=1}^{T_f} \sum_{i \in \mathcal{N}} L_{cut,i,t} \cdot t$, where T_f is the duration of the failure event.

6.2.2 Weather-Dependent Failures

In this work, weather events can trigger failures in the network. The network state is therefore identified by the combination of a 'normal weather' failure mode and the 'severe weather' failure mode. A normal weather model represents weather-independent effects such as ageing, malicious attacks or manufacturing errors in general. A severe weather model describes failures which are triggered by extreme weather conditions, for instance, lightning-induced dielectric breakdowns or wind-driven structural failures. High winds storms and lightning storms are here considered and, for simplicity but without loss of generality, the entire network is assumed facing the same weather conditions. The random occurrence of failures in 'normal' weather conditions is modelled as a Homogeneous Poisson process (HPP) [4]:

$$P(N_f(t) = k) = \frac{[\lambda_n \cdot t]^k}{k!} e^{-\lambda_n \cdot t} \; k = 0, 1, .., N \tag{6.4}$$

where λ_n $[\frac{occ}{h \cdot km}]$ represents the line failure rate in normal weather conditions, $P(N_f(t) = k)$ is the probability that k failures occur in the network in the period $(0, t]$ and $N_f(t)$ is the number of failures per km of grid line occurring in the period $(0, t]$ and measured in $[\frac{occ}{km}]$.

The severe weather events (e.g. high wind and lightning storms) are affected by uncertainty due to climate changes and inherent variability. In general, events are more likely to occur during specific periods of the year. The occurrence of severe weather events is modelled by a Non-Homogeneous Poisson Process (NHPP) [4]:

$$P(N_e(t) = k) = \frac{[V_e(t)]^k}{k!} e^{-V_e(t)} \; k = 0, 1, .., N \tag{6.5}$$

where $V_e(t)$ represents the time dependent occurrence rate of the severe weather event e, $P(N_e(t) = k)$ is the probability that k events occur in the period $(0, t]$ and $N_e(t)$ is the number of events of type e occurring in the period $(0, t]$. The quantity $V_e(t)$ can be

obtained as:

$$V_e(t) = \int_0^t v_e(t')\,dt' \tag{6.6}$$

where $v_e(t')$ is the time-varying occurrence rate of the event e. In this model, lightning storms and high wind speeds are considered as threatening environmental conditions $e \in \{lg, w\}$. In Ref. [4], the ratios $v_w(t)$ and $v_{lg}(t)$ of occurrence of these conditions are evaluated on a monthly basis and assumed to be stepwise constants, as depicted in Fig. 6.1.

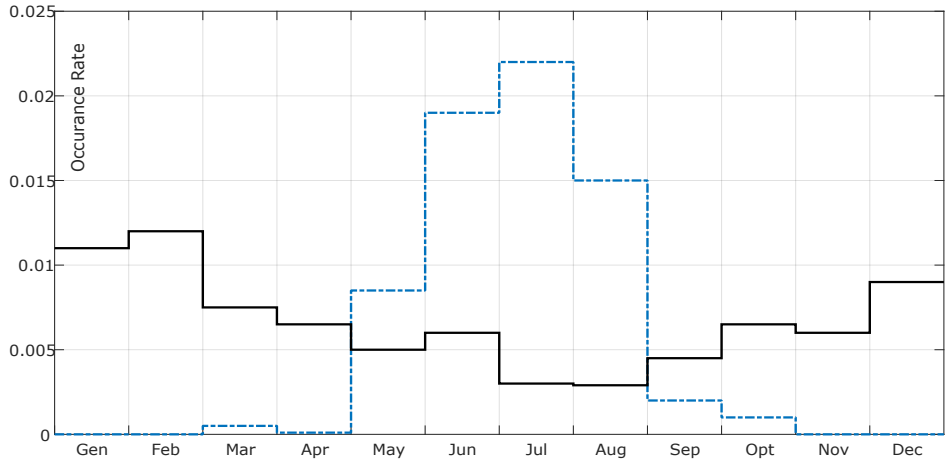

Figure 6.1: The variable occurrence rate of wind storm events, solid line, and lightning events, dashed line (data taken from [4]).

Once a severe weather scenario occurs (i.e high wind and/or lightning storm), its intensity and duration are described by characteristic historically fitted, probability distribution functions. Specifically, the wind storm intensity is obtained as follows [4]:

$$W_w(t) = W_{crt} + \Delta_w(t) \tag{6.7}$$

where $W_w(t)$ is the wind speed intensity at time t for the wind event w, W_{crt} is the 'critical' wind speed assumed to be 8 $[\frac{m}{s}]$ and Δ_w is a random surplus of the critical wind speed threshold. The intensity of a lightning storm is quantified by its lightning ground strike density $N_g(t)$, measured as the number of ground-flashes (or ground-strikes) per unit of time and area $[\frac{occ}{h \cdot km^2}]$. The variability of the ground flash density is assumed log-normally distributed, with parameters fitted based on historical records. The probabilistic model for wind storm duration (Dw), lightning storm duration (Dlg) and the respective intensities are summarised in Table 6.1.

High wind speeds can directly or indirectly damage the line structure, e.g. by friction-induced fatiguing of structure's joints or by moving/breaking trees branches in

	Distribution	Scale(a)	Shape(b)
Dw	Weibull	9.89	1.17
Dlg	Weibull	0.96	0.85
$\Delta_w(t)$	Weibull	1.23	1.05
		Mean(μ_{N_g})	Standard Deviation(σ_{N_g})
$N_g(t)$	log-Normal	-5.34	1.07

Table 6.1: Probability distributions for intensity and duration of severe weather events [4].

the proximity of the line. Lightning strikes can damage lines, for instance triggering insulator dielectric breakdown. By considering an overhead line as made of subcomponents in series (the insulation and the mechanical structure) and assuming that the individual subcomponent failure depends on different physical phenomena, the total failure rate can be obtained as follows [4]:

$$\lambda(t) = \lambda_n + \lambda_w(W_w(t)) + \lambda_{lg}(N_g(t)) \tag{6.8}$$

were λ_w is the contribution to the total line failure rate per km due to high wind speed at time t and λ_{lg} the lightning storms contribution. Note that it is possible, although very unlikely, to face the simultaneous occurrence of a lightning storm and a high wind event.
The contribution to the line failure rate due to high wind is expressed as follows [4]:

$$\lambda_w(W_w(t)) = \lambda_n \left(\frac{W_w(t)^2}{W_{crt}^2} - 1 \right) \alpha_w \tag{6.9}$$

were α_w is a regression parameter obtained from failure data. The failure rate due to a wind event has a strong relation with the wind intensity, following a quadratic law. It can be observed that for wind speed less or equal to the critical wind speed ($W_w(t) \leqslant W_{crt}$) the wind contribution to the failure rate is null.
The contribution to the line failure rate due to lightning is obtained as follows [4]:

$$\lambda_{lg}(N_g(t)) = \lambda_n \beta_{lg} N_g(t) \tag{6.10}$$

β_{lg} is a regression coefficient fitted on historical data and the line failure rate is linearly related to the lightning event intensity. According to [23], the failure rate of the generic line $\lambda_i(t)$ expressed in $[\frac{occ}{h}]$ can be obtained from the total failure rate by multiplying it by the line length (l_i).

6.2.3 Weather-Dependent Repairs

Delays in the repair of power grid components can be caused by, for instance, ineffective communication between all of the parties involved (e.g. non-cooperative landowner) or harsh weather which slows down the identification of the trouble location (e.g. heli-

copters can not be sent to find the fault location and report back). Recently a weather-dependent repair model has been proposed, reflecting the realistic sense that the efficiency of repairing crews is strongly affected by the external weather conditions [23]. The model assumes that: (1) a crew of repairmen is dispatched with no delay as soon as a failure in one line occurs, (2) the network becomes fully functional as soon as failed lines are replaced, (3) the time of the failure transient is negligible with respect to the time to repair. It is clear that the time needed to fully replace an overhead line increases if the crew operates in harsh weather conditions. In particular if wind and/or lightning events occur, the normal average repair speed (ν_{norm}) is assumed to decrease accordingly to the intensity of the severe weather condition. The repair speed can be defined as follows [23]:

$$\nu_{repair} = \begin{cases} \frac{\nu_{norm}}{1+\eta\cdot(W_w(t)-W_{crt})}, & if\, W_w(t) \geqslant W_{crt}\ \&\ N_g = 0 \\ \frac{\nu_{norm}}{1+\psi\cdot N_g}, & if\, W_w(t) < W_{crt}\ \&\ N_g > 0 \\ \frac{\nu_{norm}}{[1+\eta\cdot(W_w(t)-W_{crt})]+[1+\psi\cdot N_g]}, & if\, W_w(t) \geqslant W_{crt}\ \&\ N_g > 0 \end{cases} \tag{6.11}$$

where ψ and η are positive parameters. The normal speed ν_{norm} is set equal to 20 $[\frac{\%}{h}]$ (i.e. 5 [h] are needed to replace a line in normal weather conditions), whilst ψ and η are set to 40 and 0.4 following engineering judgement [23]. Also in this work, a line under repair is not subject to further failures (i.e. its time-to-replacement monotonically decreases) whilst repaired/working lines are subject to failures.

6.2.4 Probabilistic Load Demand

Load demands generally display time and space correlations, i.e. the variability of the different power demands depends on the time of the day and their relative position within the network. Stochastic models for load demand have been designed to account for time correlation, e.g. [87]. The model employed here considers daily variability of the average load demand and neglects seasonal and holiday effects. The aggregated load connected to a node i at a time t ($L_i(t)$) can be described by a Normal distribution with parameters fitted on historical data [122]:

$$f(L_i(t)) = \frac{1}{\sqrt{(2\pi)\sigma_{L_i}(t)}} e^{-\frac{L_i(t)-\mu_{L_i}(t)}{2\sigma_{L_i}(t)^2}} \tag{6.12}$$

where $L_i(t)$ is the load demand at node i at hour of the day t, $\mu_{L_i}(t)$ is the load mean value and $\sigma_{L_i}(t)$ is the standard deviation at node $i\ \in \mathcal{N}$ and time t.

6.3 Artificial Neural Networks: OPF Load Curtailed Emulator

A reliable estimation of the Energy-Not-Supplied requires a high number of simulations to be performed, i.e. many ENS have to be computed over the simulation time T_{sim} and even more OPF solved (one for each failure). In general, the time needed to solve a OPF is not too large, which is especially true if the size of the network is modest. If necessary, the solution can be fastened by employing parallel computing strategies, i.e. distributing the OPF to several cores in a computer cluster. Unfortunately, the optimisation problem cannot be vectorised and the OPF has to be solved one-at-a-time. This can be computationally time-costly if a large number of model evaluations are necessary.

To address the computational challenge, an Artificial Neural Network (ANN) is trained to emulate the power flow solution. The j^{th} ANN input vector assembles the loads demanded in the nodes and the state vector of the lines connecting the nodes $\mathbf{I}_j = [\mathbf{L}, \mathbf{X}]_j$. The load vector for the failure state f is $\mathbf{L}_f = [L_1, ..., L_{N_L}]_f$, whilst the lines states vector is $\mathbf{X}_f = [X_1, ..X_{|\mathcal{E}|}]_f$, where $L_1 \in \mathbb{R}^+$ and $X_i \in \{0, 1\}$ and the cardinality of the link set is the number of lines in the grid $N_l = |\mathcal{E}|$. The j^{th} input vector $\mathbf{I}_j$ is associated to a positive real valued output, the total load curtailed $Y_j = \sum_{i \in \mathcal{N}} L_{cut,i,j}$, obtained solving the minimisation problem in Equation 6.1 (i.e. solving optimal power flow as described in Section 3.3).

6.4 The Proposed Efficient Framework

Fig. 6.2 presents the flow chart of the proposed framework, where the Artificial Neural Network is employed to speed up the calculations. The algorithm starts by inputting parameters of the stochastic model (e.g. shape and scale parameters, critical wind speed, failure rates, etc.) and two main blocks can be seen. The first block is, in essence, an event sampler whilst the second uses the emulator to calculate the load curtailed for each sampled failure event f. Then, the ENS is obtained by Eq. 6.3.

First, 'normal' time to failures and occurrence time of severe weather events are sampled using HPP and NHPP, respectively. Then, a vector of Times-to-Events (TTEs) is obtained by sorting the occurrence times and recording the type of event (i.e. normal failure, lighting and/or strong wind). Then, a sequential Monte Carlo (S-MC) starts, see as example Refs. [23]- [143]. This iterative procedure terminates if the maximum simulation time is reached ($t > 8760$ [h]) or all the sampled events (normal failure and severe weather) have been analysed. The S-MC procedure is summarised as follows:

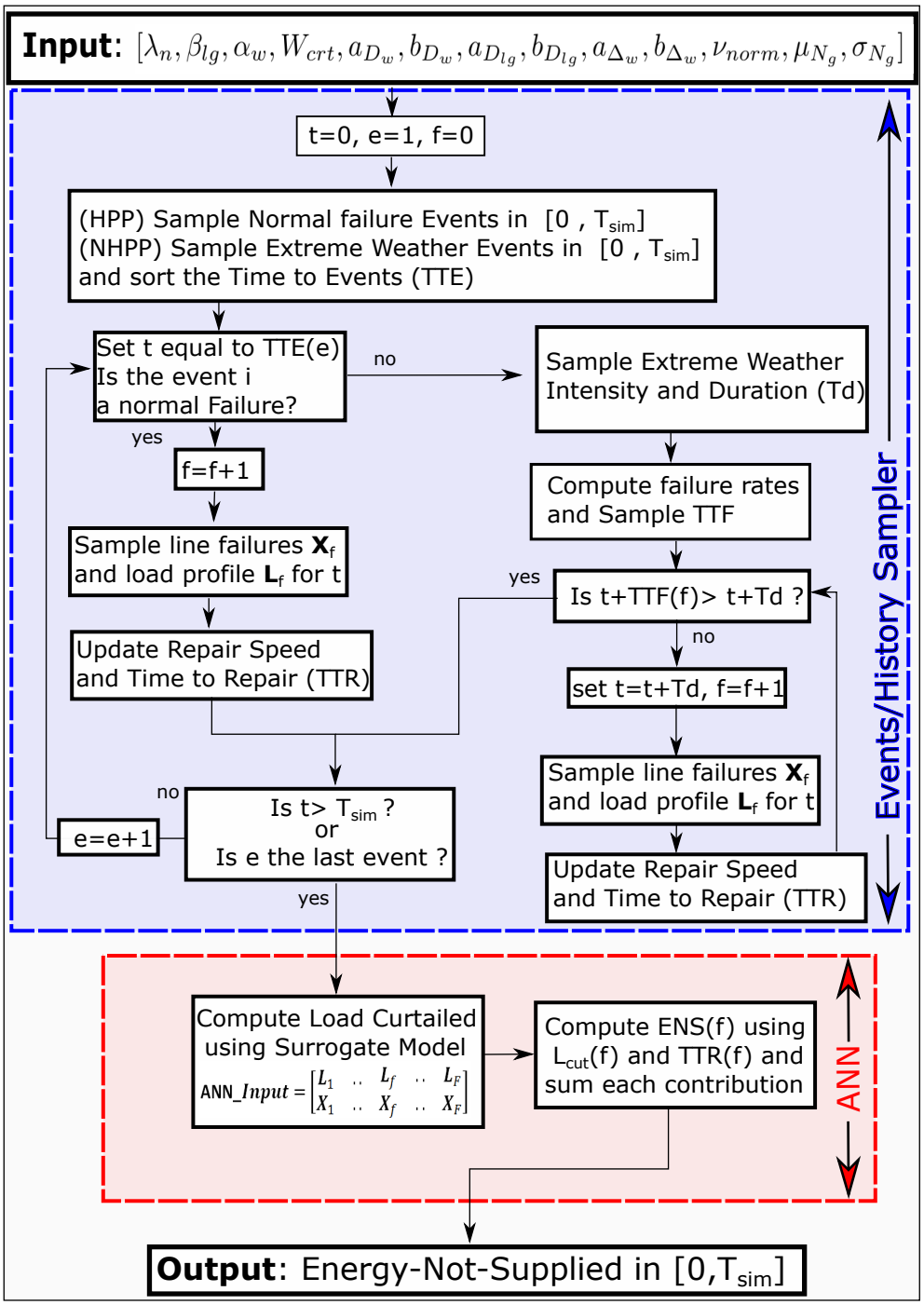

Figure 6.2: A simplified flow-chart for the resilience analysis by sequential Monte Carlo simulation. The probabilistic model is used to sample failures and repairs whilst the Artificial Neural Network is used to compute load curtailments.

1 Set t equal to the occurrence time of first event, TTE($e = 1$) and failure index $f = 0$. If e is a 'normal' failure, go to point 2 otherwise go to point 3.

2 Set $f = f + 1$ and sample a line i from the probability mass distribution with values $\frac{\lambda_n \cdot l_i \cdot X_{f,i}}{\sum_{l=1}^{N_l} \lambda_n \cdot l_i \cdot X_{f,i}}$ and $l = 1, .., N_l$. Set $X_{f,i} = 0$, sample a load profile ($\mathbf{L}_f$) accordingly to t. Set the failed line replacement to 100 % and save $\mathbf{X}_f$ and $\mathbf{L}_f$ for f. Update % from full replacement using TTE($e + 1$)-TTE(e) and normal replacement speed. Then, go to point 5.

3 Sample the severe weather duration (T_e) and intensity (Ng, Δ_w), compute the increased total failure rate $\lambda(t)$ using Eq.6.8. Sample time-to-failure using the HPP, and by inputting $\lambda(t)$ and the interval $[t \; t + T_e]$. If at least one failure event is sampled, set t equal to the next failure occurrence and proceed to step 4, otherwise go to step 5.

4 Set $f = f + 1$, sample one failed line using the probability mass function $\frac{\lambda(t) \cdot l_i \cdot X_{f,i}}{\sum_{l=1}^{N_l} \lambda(t) \cdot l_i \cdot X_{f,i}}$ and $l = 1, .., N_l$. Sample a load profile ($\mathbf{L}_f$) accordingly to t. Set the failed line replacement to 100 % and save the lines states vector $\mathbf{X}_f$ and load profile $\mathbf{L}_f$ for failure f. Update lines % from full replacement, using the reduced repairing speed computed as in Eq. 6.11. If the severe weather failures are all evaluated go to step 5, otherwise set t equal to the occurrence time of the next failure and repeat point 4.

5 If $t > T_{sim}$ or e is the last event in the TTE list, stop simulation. Otherwise, set $e = e + 1$ and $t = TTE(e)$. If it is a 'normal' failure, go to point 2 otherwise go to point 3.

The first unit is used to produce a set of $\mathbf{X}_f$ and $\mathbf{L}_f$ to be used as vectorised input to a previously trained ANN. The ANN input is an $(N_l + N_L) \times F$ matrix of load profiles and state vectors, where F is the total number of failures faced by the grid in 1 year. A total of N_s independent histories (N_s S-MC) are simulated until convergence of the $\mathbb{E}[ENS]$ is obtained.

Fig.6.3 displays a simplified version of the methods used within the framework. The procedure used to simulate N_s independent grid years is displayed in the top panel on the left-hand side. The method run by first selecting the OPF solver or the efficient method based on the ANN emulator (i.e. presented in Fig.6.2). If the (time costly) S-MC optimal power flow solver is selected, the procedure displayed in the top panel on the right-hand side run N_s times (the diagram has been adapted from [23]). If the efficient method is selected, the procedure displayed in Fig.6.2 run N_s times.
The bottom panel in Fig.6.3 summarises the overall work flow for the analysis. This is used to present, from an intuitive point of view, how the efficient resilience assessment

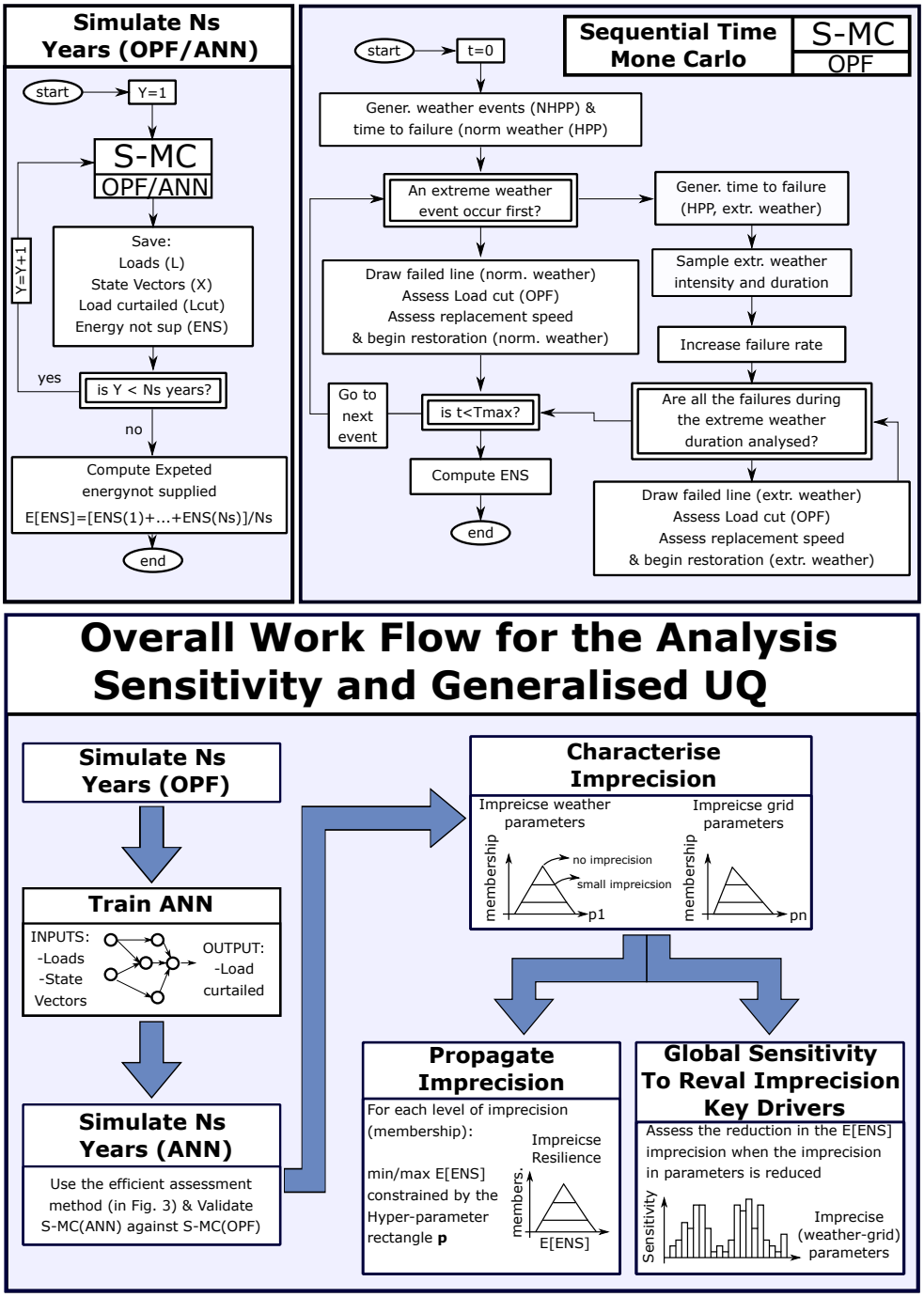

Figure 6.3: A diagram for the overall work flow of the analysis (in the bottom panel). The procedure to compute the $\mathbb{E}[ENS]$ using the S-MC (in top panel on the left-hand side) and the (computationally demanding) algorithm adapted from [23] (in the top panel on the right-hand side).

method is embedded within an advanced uncertainty quantification framework to assess effects of imprecision (i.e. introduced in Section 6.5). The analysis starts by simulating N_s grid years using the S-MC OPF solver. Then, the ANN is trained as explained in Section 6.3 and its results are validated against the original model (S-M OPF). Once the emulator is validated, the imprecision affecting the poorly known parameters of the grid and weather models is characterised using Credal sets. To conclude, the effect of imprecision on the grid resilience is quantified using advanced uncertainty propagation methods and global sensitivity analysis.

6.5 A Generalised Framework for Uncertainty Quantification

The assessment of power grid reliability indices is traditionally based on well-defined probabilistic models. The definition of these models may require a large body of empirical information to estimate the parameters of the underlying probability distributions. This is not always available in practice and imprecision in the parameters of the deterministic and probabilistic models must be accounted for [14]. Bayesian methods and set-theoretical methods are two of the most widely applied paradigms to deal with epistemic uncertainty. The formers are entirely based on probability theory and use probability distributions to describe lack of knowledge (e.g. uniform probability distributions). The set-theoretical models [91] use set-valued descriptors (e.g. intervals) to model epistemic uncertainty, e.g. intervals [93], random sets [146] or fuzzy sets [92]. Intervals are used when variables are only known to be bounded within lower and upper limits whereas Fuzzy Sets can be used to simultaneously analyse different bounded sets. This is particularly helpful if the bounds are not precisely known [124]- [36]. Credal sets theory [63] provides strong mathematical foundation to express sets of probability distributions and is for this reason employed in this work to explore different levels of imprecision, which can affect the parameters of the probabilistic model.

In this work, the parameters of the coupled grid-weather model are considered affected by imprecision and the $\mathbb{E}[ENS]$ bounds are approximated by searching its minimum and maximum values within the hyper-parameter space. Credal sets ($\mathfrak{C}$) are defined for the imprecisely defined model parameters to express sets of probability distribution functions. Given the imprecision affecting the problem, the expectation of the Energy-not-Supplied becomes imprecise and can be obtained as follows:

$$\begin{bmatrix} \overline{\mathbb{E}}[ENS] \\ \underline{\mathbb{E}}[ENS] \end{bmatrix} = \begin{bmatrix} \sup\limits_{\underline{\mathbf{p}}<\mathbf{p}<\overline{\mathbf{p}}} \\ \inf\limits_{\underline{\mathbf{p}}<\mathbf{p}<\overline{\mathbf{p}}} \end{bmatrix} \int_{\Theta(\mathbf{p})} F_X(x;\mathbf{p})dx \tag{6.13}$$

.

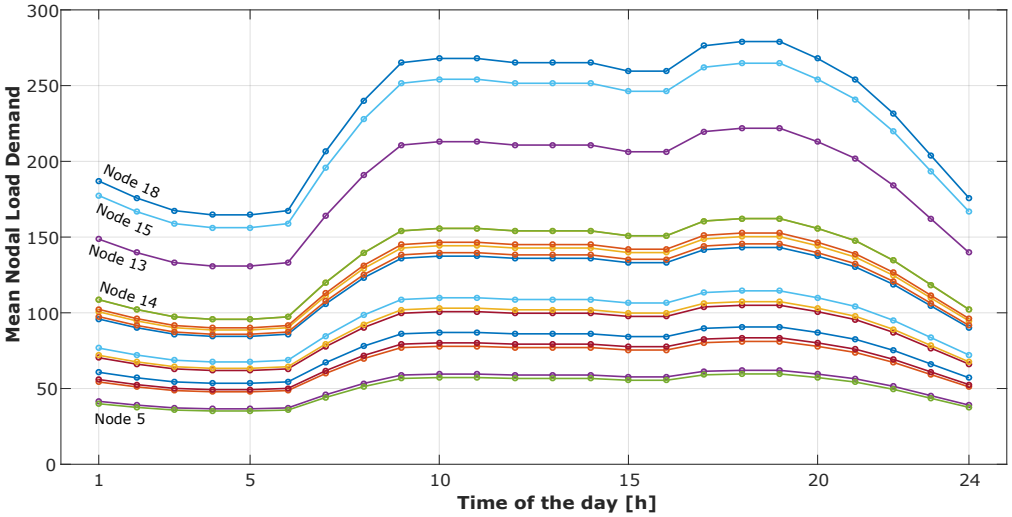

Figure 6.4: The mean of the load value per node and hour of the day, $\mu_{L_i}(t)$, for the modified IEEE-RTS [140].

6.6 A Case Study

The framework has been applied on a modified version of the IEEE-RTS 24 nodes power grid [140], which counts 24 nodes, 17 loads, 32 generating units, 33 transmission lines, 5 transformer links and a total installed capacity of 3.405 GW. The adopted line failure rates in normal weather conditions and lengths are presented in Tab. 6.2, the transformers branches have been assumed fully reliable, i.e. $\lambda_{n,l} = 0$ where lines l are 10-11, 10-12, 9-11, 9-12 and 3-24. The mean load per hour of the day and node is presented in Fig. 6.4, the standard deviation $\sigma_{L_i}(t)$ is assumed to be 10 % of the mean for each t and node.

6.6.1 Results: OPF Sequential Monte Carlo

Depending on the number of failures sampled within each simulated year, sequential Monte Carlo analysis requires between 4 seconds and 10 seconds on a standard desktop machine (8.0 GB RAM and 2 GHz processors) using the full OPF model. Fig.6.5 shows 9 failure events randomly occurred between hours 27 and 293. The first 3 lines failures (displayed by thicker lines) occur independently and in either normal or severe weather conditions. The time needed to replace the line increases due to high wind, 5.3 [h] for the first event and 6.2 [h] for the second, without additional failures. Conversely, the failures of lines 15-24, 12-13, 8-9 and 15-16 are driven by a common generating event (high wind), which occurs at hour 177 and with random duration of 3 hours. It can be observed that the repair crew is unable to restore the lines in such a small time window.

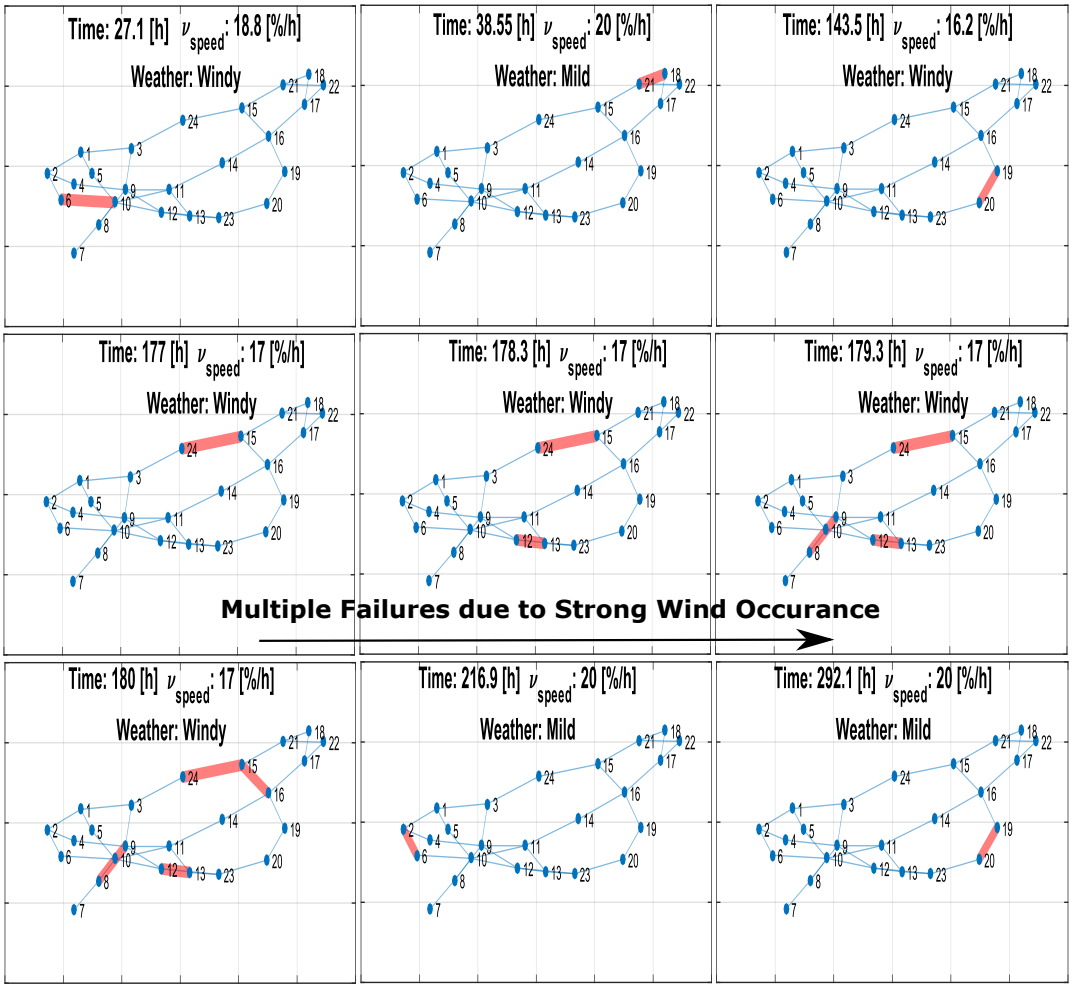

Figure 6.5: An example of 9 sequential failure events extracted from a simulated year for the grid. Strong Wind occurrence (from hour 177 to hour 180) increase line failure rates and decrease the repair speed, hence, leading to 4 common cause outages.

Line i	l_i [km]	$\lambda_{n,i}$ $[\frac{occ}{km \cdot year}]$	Line i	l_i [km]	$\lambda_{n,i}$ $[\frac{occ}{km \cdot year}]$
1- 2	4.8	$1.24 \cdot 10^{-3}$	11-13	53.1	$0.19 \cdot 10^{-2}$
1- 3	88.5	$0.144 \cdot 10^{-2}$	11-14	53.1	$0.19 \cdot 10^{-3}$
1- 5	35.4	$0.233 \cdot 10^{-3}$	12-13	53.1	$0.19 \cdot 10^{-3}$
2- 4	53.1	$0.184 \cdot 10^{-3}$	12-23	107.8	$0.121 \cdot 10^{-3}$
2- 6	80.4	$0.149 \cdot 10^{-3}$	13-23	96.5	$0.126 \cdot 10^{-3}$
3- 9	49.8	$0.19 \cdot 10^{-3}$	14-16	43.4	$0.218 \cdot 10^{-3}$
4- 9	43.4	$0.2 \cdot 10^{-3}$	15-16	19.3	$0.42 \cdot 10^{-3}$
5-10	37.0	$0.23 \cdot 10^{-3}$	15-21	54.7	$0.19 \cdot 10^{-3}$
6-10	25.7	$0.32 \cdot 10^{-3}$	15-21	54.7	$0.19 \cdot 10^{-3}$
7- 8	25.7	$0.29 \cdot 10^{-3}$	15-24	57.9	$0.177 \cdot 10^{-3}$
8- 9	69.2	$0.16 \cdot 10^{-3}$	16-17	28.9	$0.3 \cdot 10^{-3}$
8-10	69.2	$0.16 \cdot 10^{-3}$	16-19	25.7	$0.33 \cdot 10^{-3}$
21-22	75.6	$0.15 \cdot 10^{-3}$	17-18	16.0	$0.5 \cdot 10^{-3}$
20-23	24.1	$0.35 \cdot 10^{-3}$	17-22	117.4	$0.115 \cdot 10^{-3}$
20-23	24.1	$0.35 \cdot 10^{-3}$	18-21	28.9	$0.3 \cdot 10^{-3}$
19-20	44.2	$0.215 \cdot 10^{-3}$	18-21	28.9	$0.3 \cdot 10^{-3}$
19-20	44.2	$0.215 \cdot 10^{-3}$			

Table 6.2: The line failure rates in normal weather conditions and line lengths. The transformers links are assumed perfectly reliable and not reported within the Table.

6.6.2 Results: Traditional UQ and Artificial Neural Network Performance

A parallel computing strategy has been used to solve 15000 independent years; the computational time required for its completion is about 1 hour and 15 minutes on a 20 cores machine cluster with 8.00 Gb ram and a 2.00 GHz Intel Core i5-4590T processor. The average number of failure events per each $T_{sim} = 8760$ [h] (1 year) is estimated to be 311, of which 73 normal failures 223 wind-induced failures and 15 lightning-induced failures. The $\mathbb{E}[ENS]$ is 147.5 [MWh/yr] with coefficient of variation (CoV) 0.175, and slowly converges after about 2000 simulations.

A total of 100 years worth of failures (about 31000 events) are randomly selected. For each failure event f, the lines state vector ($\mathbf{X}_f$) and load samples ($L_{i,f}(t)$) are assembled and 70 % are used as training set for an ANN. The remaining samples are used for validation (15 %) and testing (15 %). The network architecture consist of 1 input layer counting 50 nodes, 2 hidden layers (45 and 35 nodes) and 1 single node output layer. The architectural selection was done by trial and error of hidden layers and number of neurons per layer. The topology with lowest mean squared error between the emulator output and the original model target was selected. The regression plot is presented in the top panel of Fig. 6.6 and the regression coefficient is about 0.98-0.99. This is considered a satisfactory result and no further optimization of the ANN architecture was performed. In the bottom panel of Fig.6.6, a comparison

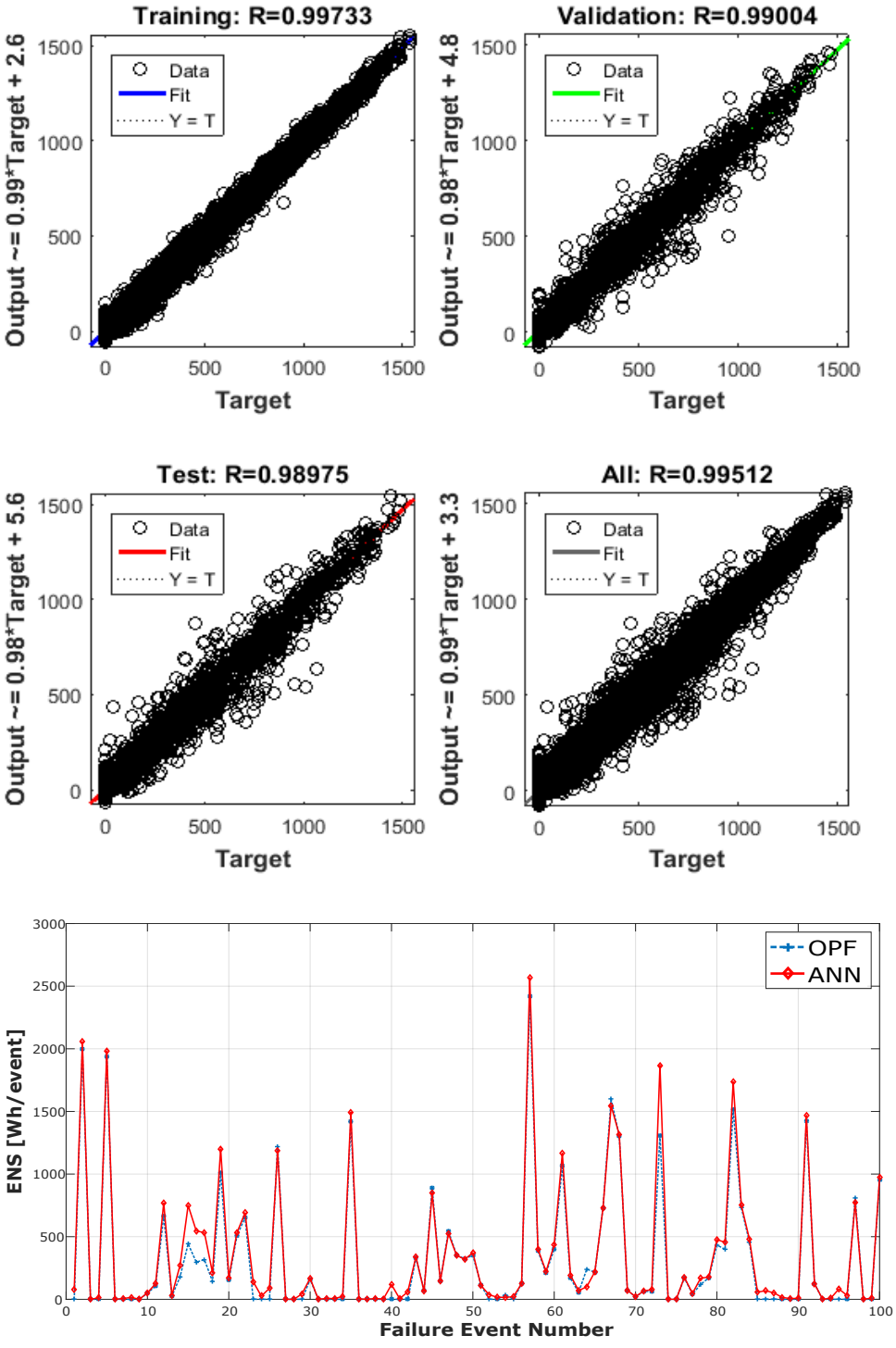

Figure 6.6: The regression plots for the ANN (top panels) and an example of load curtailed computed using the OPF compared to the ANN result (bottom panel).

between the total load curtailed $\sum_{i\in\mathcal{N}} L_{cut,i,t}$ computed using the OPF and the ANN (diamonds marked line) is reported.

The algorithm displayed by Fig.6.2 has been run 15000 times (i.e. 15000 simulated years). The ANN has been used to calculate the load curtailed for each failure event and the ENS is obtained. In Fig. 6.7, the $\mathbb{E}[ENS]$ computed is displayed by the dotted line and converges to 145.5 [MWh/yr] with CoV 0.185. Compared to the OPF result (solid line) the error of the ANN is just 0.5 % but the reduction in computational time is remarkable 98.8%: in fact, just 58.4 seconds were needed to solve the 15000 independent S-MC histories (on the 20 workers cluster).

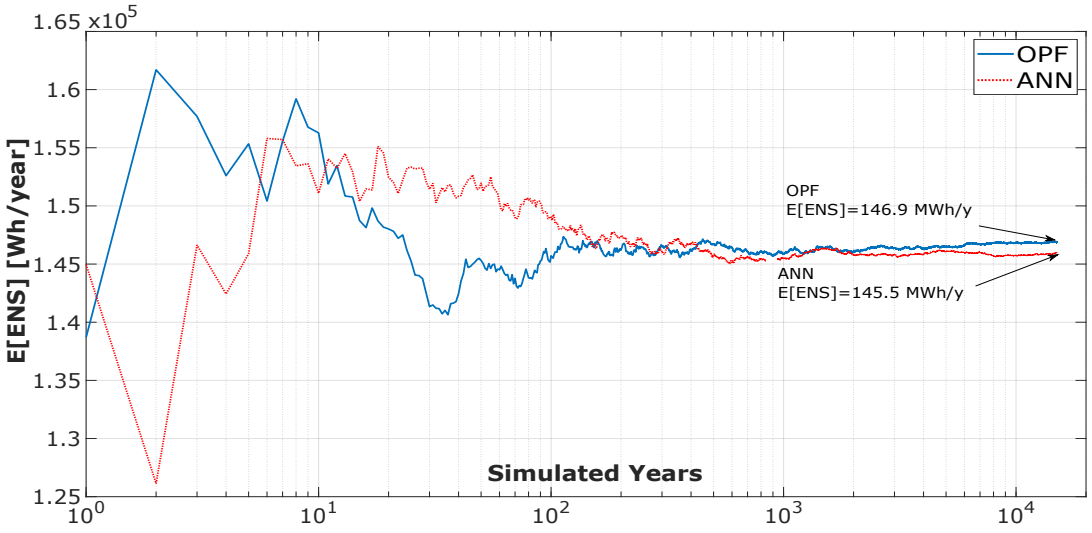

Figure 6.7: Comparison between $\mathbb{E}[ENS]$ computed using ANN and the OPF solver.

6.6.3 Results of the Generalised Uncertainty Quantification

The probabilistic model describing the uncertainty affecting the grid and weather is extended to include the Credal set

$$\mathfrak{C} = \{F_X(\mathbf{x};\mathbf{p}) | \mathbf{p} \in \mathbb{R}^{45}\ \underline{\mathbf{p}} < \mathbf{p} < \overline{\mathbf{p}}\} \tag{6.14}$$

The imprecise parameters $\mathbf{p}$ accounted in the analysis are:

$$\mathbf{p} = [\beta_{lg}, \alpha_w, W_{crt}, a_{D_w}, b_{D_w}, a_{D_{lg}}, b_{D_{lg}}, a_{\Delta_w}, b_{\Delta_w}, \nu_{norm}, \mu_{N_g}, \sigma_{N_g}, \lambda_{n,i}]$$

The parameters uncertainty (intervals) are characterised using the quantity ι which quantifies the extent of the imprecision. Defining the estimated values of the parameters as $\mathbf{p}_{est}$, lower and upper bounds are defined as $\underline{\mathbf{p}} = \mathbf{p}_{est}(1-\iota)$ and $\overline{\mathbf{p}} = \mathbf{p}_{est}(1+\iota)$, respectively. The levels of imprecision considered in this analysis

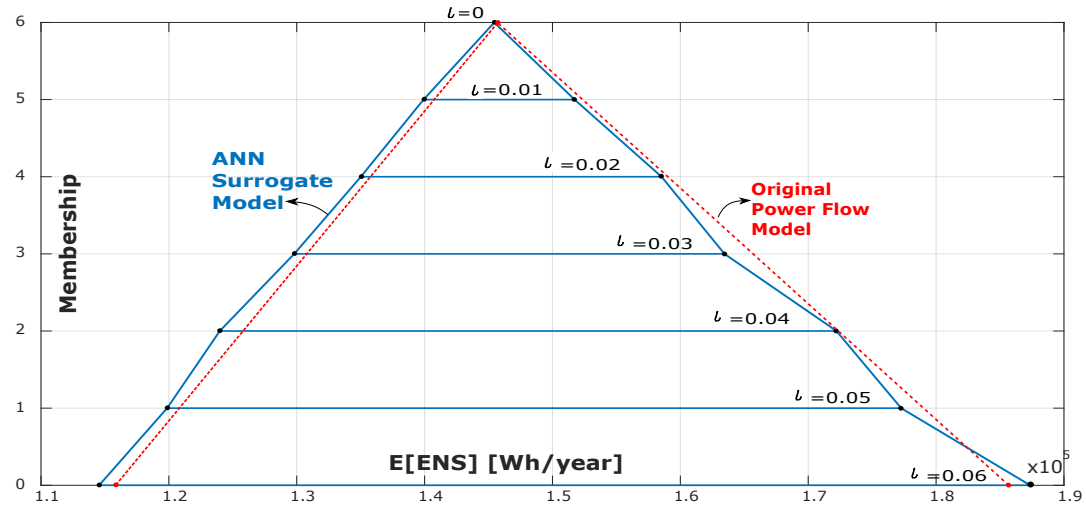

Figure 6.8: Comparison between Fuzzy $\mathbb{E}[ENS]$ computed using the original OPF model and the ANN surrogate.

are $\iota = \{0, 0.01, 0.02, 0.03, 0.04, 0.05, 0.06\}$. A value of ι=0 means that the probabilistic analysis is performed assuming a perfect estimation of the parameters and equal to $\mathbf{p}_m$. If ι=0.06, the true value of the parameters is ± 6 % imprecise. Based on previous analysis, the number of samples used to compute $\mathbb{E}[ENS]$ is set equal to 5000 and each Credal set is propagated by minimising (inf) and maximising (sup) the $\mathbb{E}[ENS]$ expectation within the bounds $\mathbf{p} \in [\underline{\mathbf{p}}, \overline{\mathbf{p}}]$. In this work, $\inf \mathbb{E}[ENS]$ and $\sup \mathbb{E}[ENS]$ are obtained using a derivative-free stochastic optimiser, which constrains $\mathbf{p}$ within the hypercube $[\underline{\mathbf{p}}, \overline{\mathbf{p}}]$ [110]- [36]. Fig.6.8 shows the nested bounds for the $\mathbb{E}[ENS]$ displayed as a Fuzzy set. The model based on power-flow (dashed line) and the surrogate model (solid line) are compared. The ANN was effective in capturing the imprecision trend expected from the original model. It is clear that the larger is the imprecision in the parameters, the wider the bounds of the resilience index are. The analysis performed using the original OPF model were very time consuming, thus, for comparison purposes just two $\iota = \{0, 0.06\}$ were considered. It is also interesting to notice that, although the level of imprecision for each input was relatively modest (maximum of 6 %), it produces a severe imprecision on the model expectation (21-29 %). This is partially confirming earlier results in the structural reliability analysis context [36], where sensitivity of the system reliability to the imprecision in the probabilistic model parameters has been pointed out. This issue has proven to be particularly relevant if many imprecise variables are involved. In those cases, a solution based on double loop Monte Carlo would have been infeasible, or extremely time consuming. The proposed approach and obtained results are indeed useful from a decision maker perspective, for instance, to identify the maximum level of input imprecision (e.g. tolerances) in order to assure a minimum power grid resilience standard (i.e. $\overline{\mathbb{E}}[ENS]$ less than a predefined

Input	OPF		ANN		Output (ANN)	
ι [%]	$\underline{\mathbb{E}}[ENS]$	$\overline{\mathbb{E}}[ENS]$	$\underline{\mathbb{E}}[ENS]$	$\overline{\mathbb{E}}[ENS]$	ι [%] $\underline{\mathbb{E}}$	ι [%] $\overline{\mathbb{E}}$
0	146.9	146.9	145.5	145.5	0	0
1	n.a.	n.a.	139.9	151.7	3.8	4.3
2	n.a.	n.a.	135.0	158.5	7.2	8.9
3	n.a.	n.a.	129.8	163.4	10.7	12.4
4	n.a.	n.a.	123.9	172.3	14.8	18.4
5	n.a.	n.a.	119.8	177.2	17.6	21.8
6	116.7	185.3	114.5	187.3	21.3	28.8

Table 6.3: Comparison between upper and lower $\mathbb{E}[ENS]$ bounds obtained using the ANN (6 Credal sets) and the OPF (2 Credal sets). The levels of imprecision in the input model parameters and corresponding imprecision in the expectation upper and lower bounds is also presented.

threshold level). Considering for example a minimum allowed resilience level, set to be $E[ENS] \leqslant 1.6\ 10^5\ [\frac{Wh}{year}]$, then, the maximum level of tolerance imprecision for the considered parameters has to be limited to just 2%.

6.6.4 Variance-Based Global Sensitivity

Variance-based sensitivity aims at quantifying the importance of a model input by assessing the expected reduction in model output variance induced by a reduction in input variances (e.g. knowing the value of the model input with certainty). The total effect sensitivity index, i.e. the first order (additive) and higher order (interactions) effects of factor i, can be expressed as $1 - \frac{Var[E[Y|X_i=x_i]]}{Var[Y]}$, where the variance of the expectation of the output Y when fixing the input X_i to the value x_i is divided by the total variance of the output. Similarly, the first order sensitivity index can be obtained as $\frac{Var[E[Y|X_i=x_i]]}{Var[Y]}$ and it quantifies the additive effects in the model [134].

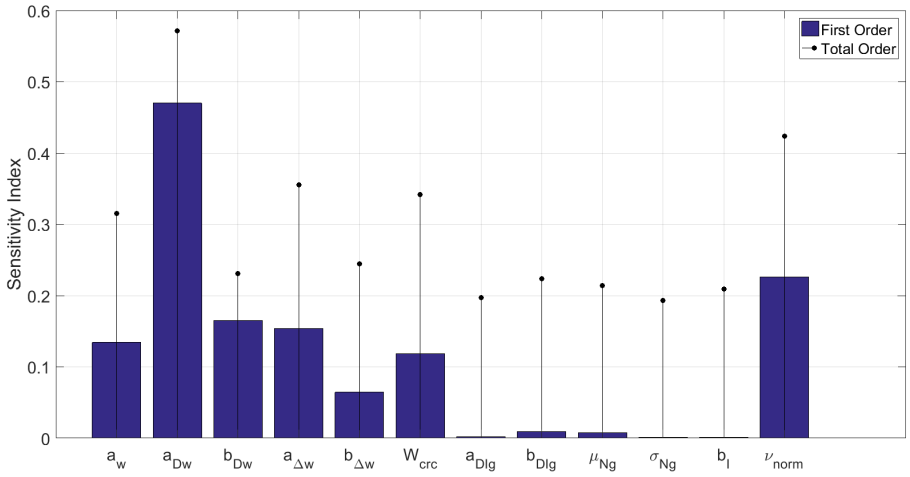

Figure 6.9: Total sensitivity indices.

Global sensitivity analysis has been performed using $Y = \mathbb{E}[ENS]$ and assuming uniform distributions for the imprecise parameters in the range $[\mathbf{p}_{est}(1-0.1), \mathbf{p}_{est}(1+0.1)]$. For simplicity, the normal failure rates of the lines are set constant to the nominal value parameters. The analysis is performed using the method proposed in Ref. [134] and employing the surrogate-based Sequential Monte Carlo (see flow chart in Fig. 6.2). The results are presented in Fig. 6.9. It can be observed that the model is more sensitive to changes in the replacement speed in normal weather conditions and to changes in the wind duration scale parameter (a_{D_w}), and to wind events over lightnings events in general.

6.7 Discussion on the use of the framework in a practical context

In real situations, power grid analysts have to complete the needed assessments quickly, with a limited amount of time. Unavoidably, the information available for the assessment will be limited and in some cases, when the data does not suffice, expert judgment elicitation is the only viable way for carrying out the assessment.
Both problems of computational efficiency and limited data availability have been discussed and tackled in this work. To overcome lack of data issues, a generalised uncertainty quantification framework has been adopted. Computational efficiency has been greatly improved by using a novel emulator of the optimal power flow and a simulation tool allows the impact of extreme weather on the power grid to be assessed.

When the information is poor, inconsistent or limited, it is common in practice to proceed with some (strong or weak) assumptions based on expert judgement. In the power grid reliability assessment context, a typical situation is to have just a few available failure samples for a given (reliable) component type. Similarly, in a weather modelling context, few samples of a (rare) weather event will be available and it will be difficult to assess with confidence its occurrence rates. In those cases, the lack of data is probably a most relevant source of uncertainty. Nevertheless, it is common to assume a well-defined probability model to describe the component failure behaviour (e.g. precise point-valued failure rates) or the weather occurrence (e.g. precise events occurrence rates). These assumptions will likely lead to an underestimation of the effect of the uncertainty. To improve the overall robustness of the analysis, it is necessary to rigorously assess the effect of lack of data on the results. Within an imprecise-information scenario (e.g. few samples, probability distribution not specified or unknown, or known but with vague parameters, conflicting and limited knowledge, linguistic incomprehension, single or multiple intervals, etc.), generalised (imprecise) probabilistic approaches can be employed to model lack of information with fewer

constraining assumptions. Once the uncertainty is propagated through the model, the result will discriminate between the non-reducible uncertainty (aleatory components, randomness, variability) and reducible uncertainty (epistemic component, lack of information). This can trigger a discussion on whether it is necessary to collect more data (which can be costly) to guarantee a probabilistic standard, for instance, the 1-day-in-10-years loss of load probability standard or an expected energy not supplied less than a predefined threshold level.

The proposed framework can be used to tackle those types of issues and within reasonable time thanks to the improvement in computational efficiency by the emulator. As an additional example, consider the sensitivity results. The results show that the lack of data on the repairing crew speed in normal weather conditions and for the probabilistic model of the wind is affecting the most the grid resilience precision. Consequently, a decision-maker which recommends an imprecision reduction strategy (i.e. reduce the tolerance intervals on the parameters) would suggest starting the data collection to refine the wind model and the repairing crews model first. In this way, the assessment would profit the most in term of resilience index imprecision reduction and, if the score is not satisfactorily low, a strategy to enhance the network resilience can be discussed (e.g. by reducing the average repairing crew intervention time).

6.8 Conclusion

A generalised uncertainty quantification framework for power grid resilience assessment has been presented. A power grid stochastic model accounts for interactions between severe weather conditions, transmission line failures and repairing crew working efficiency. The stochastic model needs accurate estimation of its parameters and data is often insufficient or limited. Thus, the framework has been extended adopting a generalised, non-intrusive uncertainty quantification method. An efficient solution has been proposed employing a vectorisable Artificial Neural Network to emulate the relation between load curtailments, lines states vectors and load profiles. The proposed surrogate reduces the computational time of about 99 % although a small error is inevitably introduced in the results. The surrogate accuracy was tested against the original model based on OPF; both classical and generalised stochastic framework were tested and pointed out the goodness of the emulator. The effect of imprecision was tested by propagating nested Credal sets to the Expected-Energy-Not-Supplied. Results pointed out that the precision of the estimator decreases rapidly for increasing imprecision in the model parameters. To conclude, a global sensitivity analysis pointed out which among the wind, lightning and replacement related parameters are key drivers for the uncertainty in the proposed power grid resilience index.
The main contributions of this work can be summarised as follow:

1 A novel simulation method based on a computationally cheap emulator of the optimal power flow is presented and used to speed up the computation of the expected energy not supplied by the network;

2 The method greatly reduces the computational cost of the time-demanding analysis (up to a 99% reduction);

3 Problems of lack of data are discussed and the efficient simulator, embedded within a generalised uncertainty quantification framework, allows the effect of lack of data to be quantified;

4 Sensitivity analysis has allowed to point out which among the imprecise parameters have to be prioritised if further data were collected (for highest reduction of the imprecision in the resilience index);

Acknowledgement

A journal paper version of this chapter has been published as:

1. Roberto Rocchetta, Enrico Zio, and Edoardo Patelli. A power-flow emulator approach for resilience assessment of repairable power grids subject to weather-induced failures and data deficiency. *Applied Energy*, 210:339 – 350, 2018

Chapter 7

Effect of Load-Generation Variability on Power Grid Cascading Failures

7.1 Abstract

Cascading failures events are major concerns for future power grids and are generally not treatable analytically. For realistic analysis of the cascading sequence, dedicated models for the numerical simulation are often required. These are generally computationally costly and involve many parameters and variables. Due to uncertainty associated with the cascading failures and limited or unavailable historical data on large size cascading events, several factors turn out to be poorly estimated or subjectively defined. In order to improve confidence in the model, sensitivity analysis is applied to reveal which among the uncertain factors have the highest influence on a realistic DC overload cascading model. The 95^{th} percentile of the demand not served, the estimated mean number of line failures and the frequency of line failure are the considered outputs. Those are obtained by evaluating random contingency and load scenarios for the network. The approach allows to reduce the dimensionality of the model input space and to identifying inputs interactions which are affecting the most statistical indicators of the demand not supplied.

7.2 Introduction

Assure high-reliability of electric power supply is a major concern for next-generation power grid. Power grid should have the ability to withstand know threats, such as N-1 and N-2 contingencies, but also poorly understood low-probability-high-consequence events such as N-k contingencies leading to cascading sequences. Due to the inherent complexity of cascading failure events, associated mathematical models are, generally, analytically not solvable. This is mainly due to the high dimensionality of the problem and to the complex, non-linear and dynamic behaviour characterizing domino failures.

Computational models for the simulation of the cascading sequences are used to provide a solution to the cascade problem. A wide variety of models have been proposed in the past, aiming at analysing different system behaviours and with several different objectives. For instance, models employing the AC power flow (PF) equations, such as the Manchester model [96] or the linearized AC PF model [70], the ORNL-PSerc-Alaska (OPA) model [39] and DC PF-based models have been developed to simulate realistically cascading failures sequences.

Numerical models for cascading simulation have to be adequately designed, calibrated and validated [18]. Calibration and validation should use available historical cascading data, which is (in particular for large size cascade events) quite limited [133] or affected by imprecision [131]. Consequently, the resulting model verification and calibration is very challenging and affected by high level of uncertainty. Uncertainty will result particularly prominent when the model is used to simulate rare events leading to very severe consequences.
To increase confidence in the cascading model results and better understand the relation between its inputs and outputs, all the relevant sources of uncertainty affecting the analysis should be quantified. Dimensionality and complexity issues are often involved in cascades analysis problems and the numerical simulators generally reflect these problems. In fact, the simulators often are time costly and involve a large number of uncertain variable and parameters.

Sensitivity analysis methods are useful to deal with both dimensionality and uncertainty issues. These methods can be used to reveal which sources of uncertainty are affecting the most the model output and can be used to reduce the dimensionality of the aleatory space by prioritizing only the most important factors. This is indeed a useful information, necessary to better comprehend inputs-outputs relations otherwise hidden within the complexity of the model.
Global sensitivity analysis methods are often employed by uncertainty analysts to sharpen the view of the problem. Sensitivity analysis is sometimes regarded as a

fundamental part of works that involves the assessment and propagation of uncertainty. Applying global sensitivity analysis methods, insights can be gained regarding the input-output mapping and the key drivers of uncertainty can be clearly revealed.

In this chapter, an integrated framework for sensitivity analysis and power grids cascading analysis is proposed. The framework can be used to identify and prioritize the most relevant uncertain input factors by revealing their effect on different cascading failures indicators. Both system-level indicators, describing the overall impact of cascading failures, and component-level indicator, focusing on a single component performance, are considered. One of the aims of this work is to provide some guidance for the application of given data sensitivity analysis and screening methods to engineering practitioners, promoting their potential.

The framework is tested on a modified version of the RTS96 IEEE system. Two uncertainty cases are analysed, first accounting for only the uncertainty in the load demand. Then, a more complex and realistic case has been considered by accounting for randomness in the generators costs, thus inflating the dimensionality of the input space, i.e. more flexibility for the generators outputs. The analysis allows to point out which among loads and generator costs uncertainties is affecting the most the outputs of cascading failures model and for a modest computational effort.

The rest of the chapter is organized as follows: In Section 7.3 the algorithm for cascading failure simulation and the performance indicators are introduced. A benchmark case study, the RTS96 system, tests the framework in Section 7.4, 2 uncertainty cases are analysed. Section 7.5 closes the analysis with a discussion on the results and conclusions.

7.3 The cascading model

A model for the simulation of steady-state operations of electric networks has been developed and calibrated in [19]. It can be used to simulate the initial contingencies that trigger the cascading events and estimate the post-contingency system states. The initial generation dispatch for each load demand is computed with a Security Constrained Optimal Power Flow, which takes into account the generators constraints, line flow constraints, voltage angles constraints and, optionally, the N-1 security constraints. After line tripping, DC power flow is used to evaluate the post-contingency power flow. The failures propagate in the grid through line over loading. Frequency control and protections, voltage protections and a variety of other automatic and realistic regulations and remedial actions are also included in the model.

A simplified flow chart of the cascading failures analysis is presented in Figure 7.1 which have been adapted from Ref [19]. The algorithm starts by loading power grid data, selecting the steady-state solver (e.g. DC-SCOPF) and a list of N-k contingencies. Then, for each contingency N-k, islands are identified, frequency deviation assessed and under frequency load shedding performed if necessary. Once power balance is restored, line flows are evaluated using the power flow solver and the lines exceeding their flow limit are removed from the grid topology. This process is repeated until grid stability is reached. The considered outputs are the total Demand-Not-Served (DNS) due to contingency N-k and lines failure indicator functions indicating if a line tripped during the simulation of the N-k contingency.

For simplicity, the contingency list has been obtained by random sampling N-1, N-2 and N-k line contingencies. To better identify and select critical failure scenarios, methods such as the N-2 contingency screening, eg. the method presented in [62], could have been employed. However, a smart exploration of the contingency space was not the main aim of this work. Once the list is obtained, repeated N-k contingency analysis are performed as presented in Algorithm [19].

7.3.1 System and components performance indicators

Several output measures can be obtained from the cascades model. In this work, we focus on 2 system-level indicators, which provide insights on the grid performance as a whole, and on N_l components performance indicators, one for each line in the system.

The indicators are the 95^{th} percentile of the DNS cumulative distribution function $p_{95}(DNS)$, the average total number of lines tripped $\mu(N_f)$ and the line outage frequency $P_{f,l}$, defined as follows:

$$\mu(N_f) = \frac{\sum_{c=1}^{N_c} \sum_{l=1}^{N_l} I_{l,c}}{N_c}; \quad P_{f,l} = \sum_{c=1}^{N_c} \frac{I_{l,c}}{N_c};$$

where N_c is the total number of contingencies listed, N_l is the total number of lines in the system and $I_{l,c}$ is the indicator function for line l and contingency c. The indicator function will result 0 if the line survived the cascading propagation initiate by contingency c or 1 if the line failed, e.g. due to flows redistribution leading to an overload.

7.4 A case study

The IEEE RTS96 power grid is used to test the methods and the cascading model and Figure 7.2 displays the grid layout. The power grid data can be found in [53]

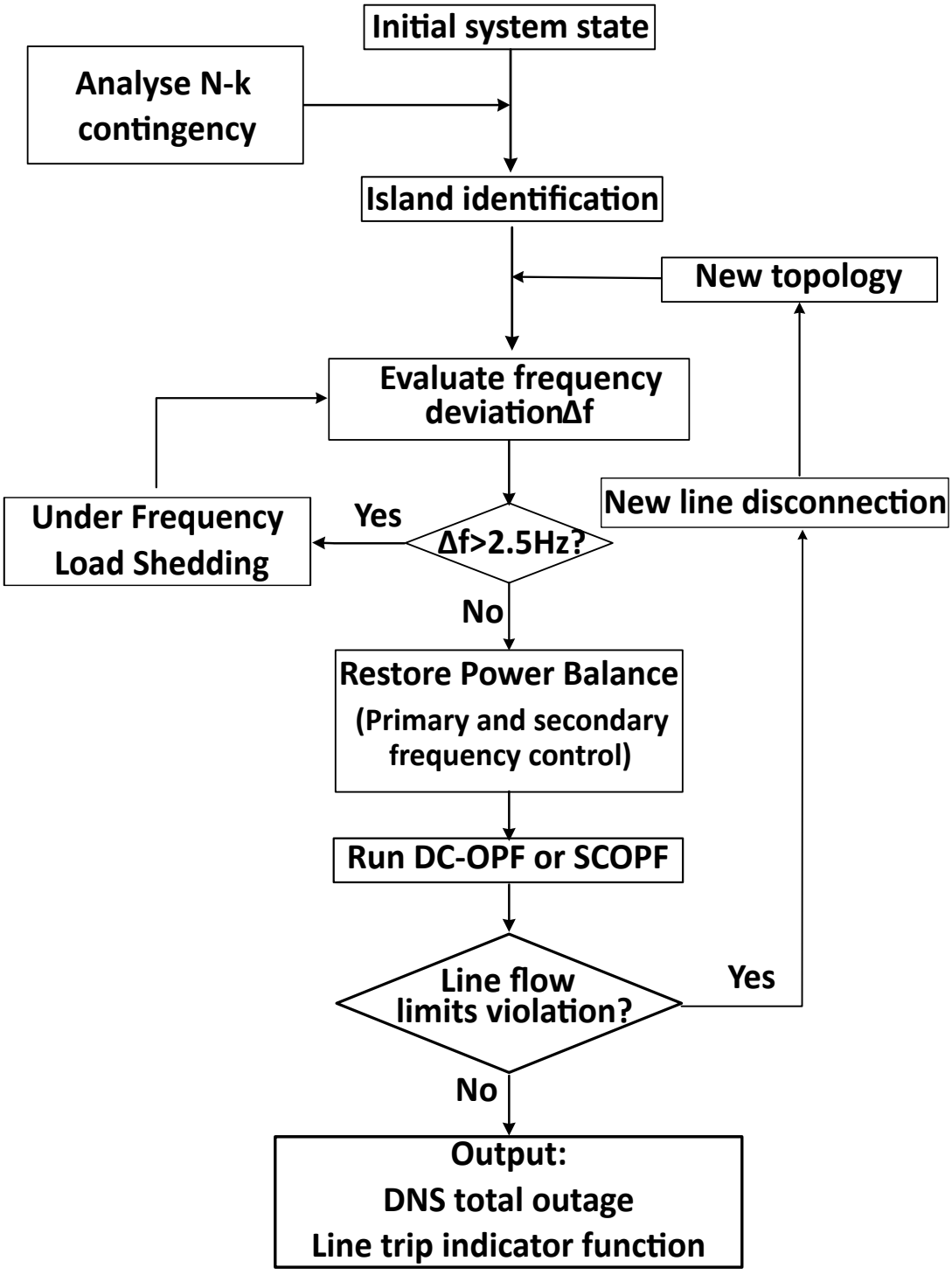

Figure 7.1: The flow chart of the algorithm for cascading failures analysis developed in Zurich ETH by Li Bing and Giovanni Sansavini [19].

and are not reported here for sake of synthesis. In this analysis, two representative uncertainty cases, named Case A and B, are considered. In Case A, the uncertainty associated with the load demand is explicitly modelled. In the second case, CASE B, also random generation costs are accounted for, thus introducing uncertainty in the power dispatch and increasing the dimensionality of the random input space. The DC cascading model presented in section 7.3, is employed for the solution of the cascading problem. A predefined contingency list is selected and includes 2444 line contingencies. The list counts the full set of N-1 and N-2 line failures and a set of 1000 random N-3 line failures. To simplify comparison between uncertainty cases and the different sensitivity analysis methods, the contingency list has been kept the same throughout all the analysis (i.e. the random set of N-3 contingencies has been sampled just once).

7.4.1 CASE A: Random loads

The first uncertainty case A assumes that uncertainty affects the 17 loads in the system due to inherent variability. The analysts lack better information regarding the variability affecting the load at each node, thus, the uncertainty in L_i is simply modelled by assuming uniform distributions. The distribution parameters have been selected to cover a range of values around the design loads and based on experts opinion:

$$L_i \sim U(0.5L_{d,i}, 1.2L_{d,i}) \quad i = 1, .., N_l$$

where $L_{d,i}$ is the design load of node i as presented in [53] and the number of lines is $N_l = 17$.

Once the uncertainty sources are characterized, a preliminary uncertainty analysis is performed. Monte Carlo method is used to propagate 5e4 samples of the load profile. For each load sample, the cascading failure model is solved 2444 times, one for each contingency listed. The percentile of the demand not served, the average number of failed lines and the line outage frequencies are computed for each load sample as described in Section 7.3.1. The $p_{95}(DNS)$ results are summarised in Figure 7.3. This figure presents a so-called cobweb plot, also known as parallel coordinates plot. It is a simple and effective way of visualising random input and output spaces in high dimensions. The X-axis reports the inputs loads and the percentile of the DNS (on the far right). The Y-axis reports the normalized inputs and output realisations of the Monte Carlo method. Each one of the dark dashed line in the background corresponds to one load profile realisation and corresponding $p_{95}(DNS)$ obtained through N_c model evaluations. Red solid lines are conditional samples, which highlight only the load combinations leading to the highest $p_{95}(DNS)$. It can be observed, later confirmed by Morris' and Sobols' analysis, that there is a strong influence of some of the loads (e.g. in nodes 15 and 18) on the extremes of the DNS. In particular, when the power

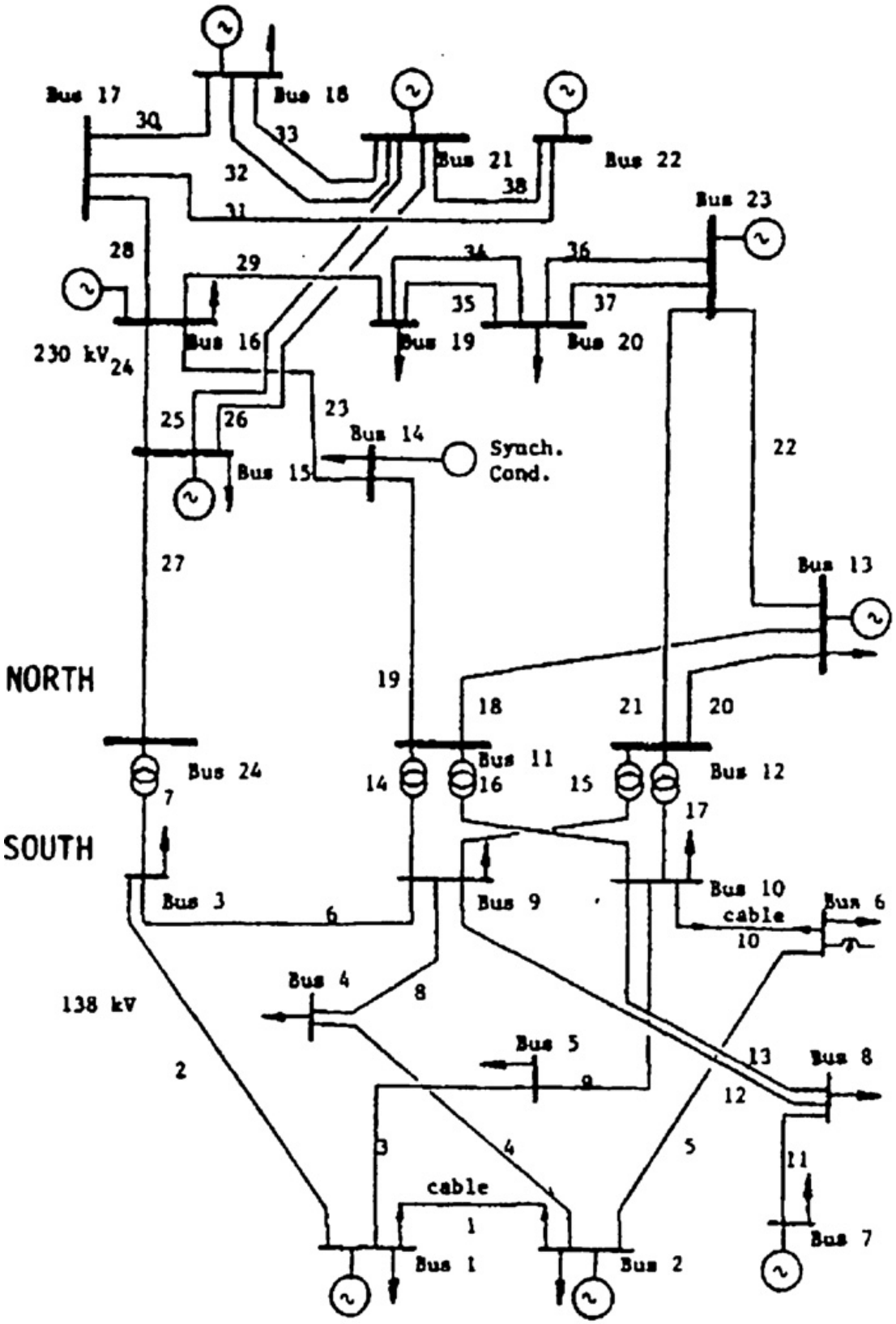

Figure 7.2: The IEEE RTS96 system, the connections between the 24 nodes, the lumped generators (32 generators) and the location of the aggregated loads (17 arrows).

demanded in nodes 15 and 18 is small, the risk of facing severe DNS scenarios increases.

Morris and Sobol's indices have been computed aiming at better investigating which among the uncertain factors are key drivers for the output uncertainty. The Morris indices are obtained by selecting 250 random input vector realisations (saved from the MC) and computing incremental ratios δ as described in section 2.8.1. The Sobol's first order coefficents are obtained using given data sensitivity approaches, see ref. [114] for further details. This is a very convenient approach as for calculations, as the data from the MC run can be used for this and with essentially no-extra computational cost. On the other hand, total Sobol's indices require higher computational cost and in this work the Liu and Owen method [117] is used for their computation.

The result relative to the DNS percentile and the average total number of line failed are presented and compared in Table 7.1. The Morris statistics and Sobol's main and total effect indices are also graphically presented in the $\mu - \sigma$ plot in Figure 7.4 and in Figure 7.5, respectively. Both methods identify L_{18} and L_{15} as the most influencing factors for the DNS and average number of line failures. Less relevant but, not to be neglected, is the effect of loads in nodes 8, 19 and 16. Morris analysis has the advantage of revealing an inverse relation between L_{18}, L_{15}, L_{19} and the outputs (see figure 7.4) which could not be revealed only using Sobol's indices. On the other hand, an increment in load 8 lead to higher risk of extreme DNS.

This result can be explained looking at the generators production profile, which is obtained solving the pre-contingency DC-SCOPF with objective of minimizing generation costs. The generators in nodes 18, 22 are associated with lower generation costs. This lead to the maximum exploitation of their production capacity, independently from the load profile realisation. Consequently, when electrical power is consumed in loco (e.g. the loads close to these generators as in 15 and 18), less power will be flowing from the 'northern' area to the 'southern' area of the network. On the other hand, if less power is demanded in, for instance, nodes 18 and 15 (or more power in 8), this increases the risk of higher loads on line such as 24, 25 and 26 which connecting the upper part of the grid with the lower part, and with it the risk of facing more severe post-contingency scenarios.

7.4.2 CASE B: Random loads and generator costs

The second uncertainty case B extends case A by accounting for generators costs uncertainties. The generation cost variability is characterised by uniform probability distributions as follows:

$$C_{g,i} \sim U(0.9, 1.1) \quad i = 1, .., N_g$$

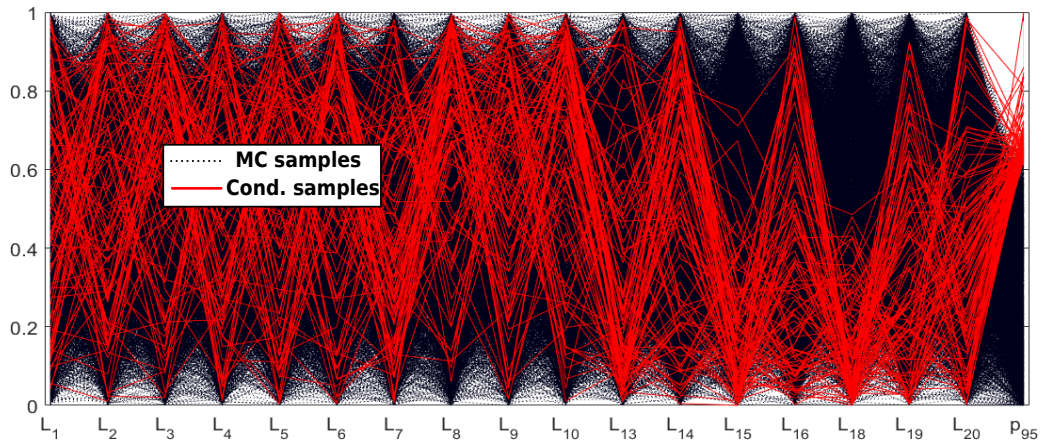

Figure 7.3: The parallel plot of the Monte Carlo loads and $p_{95}(DNS)$ realizations. In red solid line the conditional samples which lead to the highest p_{95} and in the background (black dashed lines) all the MC realisations.

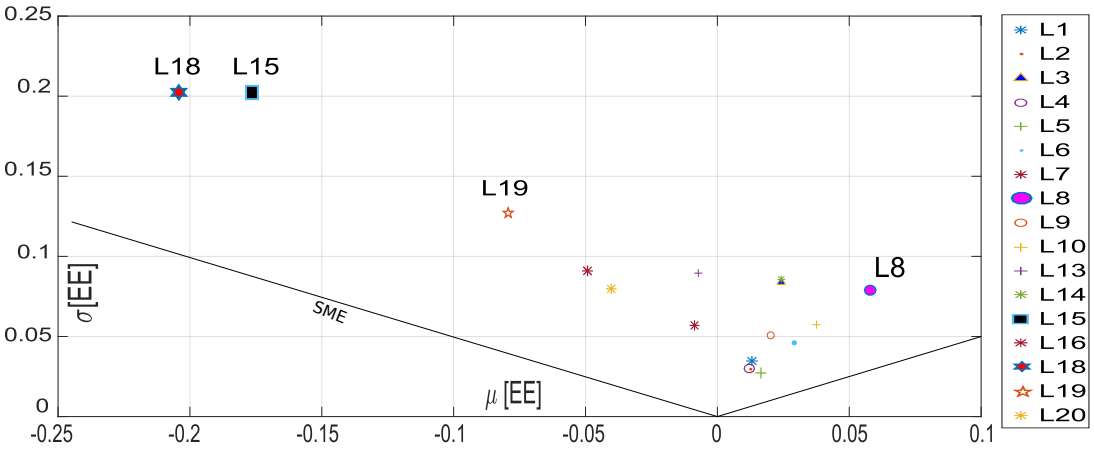

Figure 7.4: The Morris diagram for uncertainty case A and for the DNS percentile output. The mean and standard deviation of the EEs are reported on the X and Y axis, respectively.

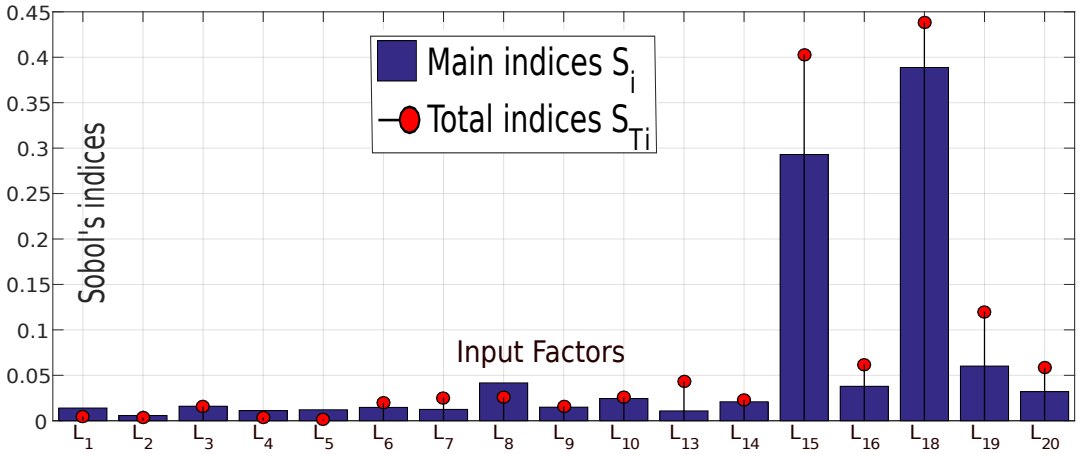

Figure 7.5: The Sobol s main and total effects obtained for the uncertainty case A and for the DNS percentile output.

Table 7.1: Sobol's main and total effect mean and standard deviation for the elementary effects for the uncertainty case A for the DNS percentile and average total failed lines outputs.

	$p_{95}(DNS)$				$\mu(N_f)$			
	Sobol		Morris		Sobol		Morris	
	S_i	S_{Ti}	$\mu(\delta_i)$	$\sigma(\delta_i)$	S_i	S_{Ti}	$\mu(\delta_i)$	$\sigma(\delta_i)$
L_1	0.01	0.00	0.01	0.03	0.01	0.00	-0.1	0.4
L_2	0.01	0.00	0.01	0.03	0.00	0.00	-0.1	0.4
L_3	0.02	0.02	0.02	0.08	0.02	0.01	-0.5	0.7
L_4	0.01	0.00	0.01	0.03	0.01	0.00	-0.1	0.3
L_5	0.01	0.00	0.02	0.03	0.01	0.00	0.0	0.3
L_6	0.01	0.02	0.03	0.05	0.01	0.00	0.0	0.4
L_7	0.01	0.03	-0.01	0.06	0.01	0.01	0.0	0.7
L_8	0.04	0.03	0.06	0.08	0.03	0.05	0.4	0.7
L_9	0.01	0.02	0.02	0.05	0.01	0.01	-0.2	0.7
L_{10}	0.02	0.03	0.04	0.06	0.01	0.01	0.0	0.5
L_{13}	0.01	0.04	-0.01	0.09	0.01	0.03	-0.4	0.9
L_{14}	0.02	0.02	0.02	0.09	0.01	0.01	0.0	0.7
L_{15}	0.29	0.40	-0.18	0.20	0.33	0.33	-2.1	1.7
L_{16}	0.04	0.06	-0.05	0.09	0.03	0.02	-0.5	0.6
L_{18}	0.39	0.44	-0.20	0.20	0.47	0.54	-2.7	1.9
L_{19}	0.06	0.12	-0.08	0.13	0.03	0.05	-0.6	0.8
L_{20}	0.03	0.06	-0.04	0.08	0.02	0.02	-0.5	0.7

Table 7.2: Comparison between the top 5 most influencing factors according to the Sobol's main index and Morris mean and standard deviation. The output considered is the DNS percentile.

rank	S_i	$\lvert\mu(\delta)\rvert$	$\sigma(\delta)$
1	L_8	L_8	$G_{18}(1)$
2	L_3	$G_{18}(1)$	$G_{13}(2)$
3	$G_{18}(1)$	L_3	L_8
4	$G_{21}(1)$	L_6	$G_7(1)$
5	L_{18}	L_{18}	L_7

where $C_{g,i}$ is the cost of the generating unit i and the number of generators N_g is equal to 32. By assuming costs $C_{g,i}$ distributed uniformly between 0.9 and 1.1, the economic viability of the generators drastically changes if compared to case A. This lead to a higher variability in the economic dispatch, i.e. generators in nodes from 18 to 22 will sometime produce less than their maximum capacity. This case study shows the applicability of the method to larger input spaces and larger power grids. Furthermore it shows the impact of different generation profiles, in combination with load demands, on the cascading failures.

Similarly to the uncertainty case A, a Monte Carlo uncertainty propagation is performed and the Sobol's S_i indices and Morris $\mu(\delta)$ and $\sigma(\delta)$ have been calculated. The 5 most influencing factors (among the 17 loads and 32 generator costs) affecting the 95^{th} percentile of the DNS are reported in Table 7.2. Multiple generators can be found in the same bus and to simplify the notation, the relevant costs are presented using the symbol $G_k(j)$, where j is the machine reference number within the bus k where the generator is installed. Differently from case A, load in node 8 emerged as the most relevant factor for the DNS percentile.

Figure 7.7 presents the mean of the EEs for the 17 loads and the 32 generators costs. Similarly to case A, a reduction in loads 18 and 15 increase the risk of extreme DNS. Conversely, a reduction of power demanded in nodes 3, 6 and 8 reduces the risk of high DNS. Generators costs sensitivities result in similar trends. Specifically, an increment in the costs of the generators in the lower part of the system increases the risk of facing high DNS, this is primarily attributable to a penalisation of the power production due to higher costs of e.g. nodes 16 and 21.

Uncertainty in the loads and generator costs has been propagated to the line outage frequency indicator $P_{f,l}$. The resulting MC realisations are displayed using a box plot in Figure 7.6. The X-axes shows the lines identification number and the Y-axes presents the $P_{f,l}$ values (red markers). Each box indicates the median (the central mark) and the

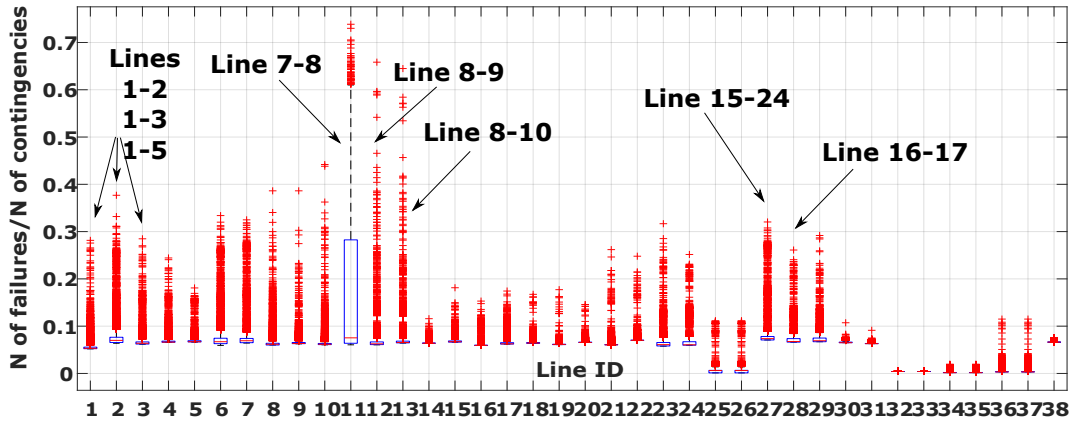

Figure 7.6: The box plot of the $P_{f,l}$ realisations corresponding to different load and generation cost samples.

bottom and top edges of the box indicate the 25th and 75th percentiles, respectively. It can be observed that the line connecting node 7 to node 8 results in the higher failure frequency and that lines in the lower voltage area of the grid (ID from 1 to 13) are more prone to failure. This result is probably due to the lower thermal limit (175 MW) and to the specific combination of grid topology, design load demanded in node 7 and 8 (125 and 171 MW, respectively) and generators in node 7 maximum lumped capacity (300 MW). Thanks to the sensitivity analysis, it has been possible to clarify which are the factors responsible for this peculiar behaviour, i.e. better understanding which are the variables which are contributing the most to $P_{f,7-8}$.
Main effect sensitivity indices have been computed for each line $P_{f,l}$ to reveal which of the input factors is affecting the most their variability. Results are presented graphically with a bar plot in Figure 7.8 and reported in Table 7.3. Table 7.3 presents only the factors leading to relatively high S_i, i.e. greater than 0.08, and the corresponding components. It can be observed that the variability in the line 7-8 outage frequency is mainly affected by uncertainty in node 7 (generators and load). On the other hand, uncertainty in L_8 is not affecting much the variance of $P_{f,7-8}$ but it is the most relevant factor for $P_{f,8-9}$, $P_{f,8-10}$.

7.5 Discussion

In this chapter, the sensitivity of a cascading failures model for power grids has been analysed. Variance-based global sensitivity analysis indices, i.e. Sobol's indices, have been computed to reveal which among the uncertainty sources is affecting the most the variances of the cascading failure model output. The Morris screening indices are also obtained and compared to variance based indices to improve confidence in the results

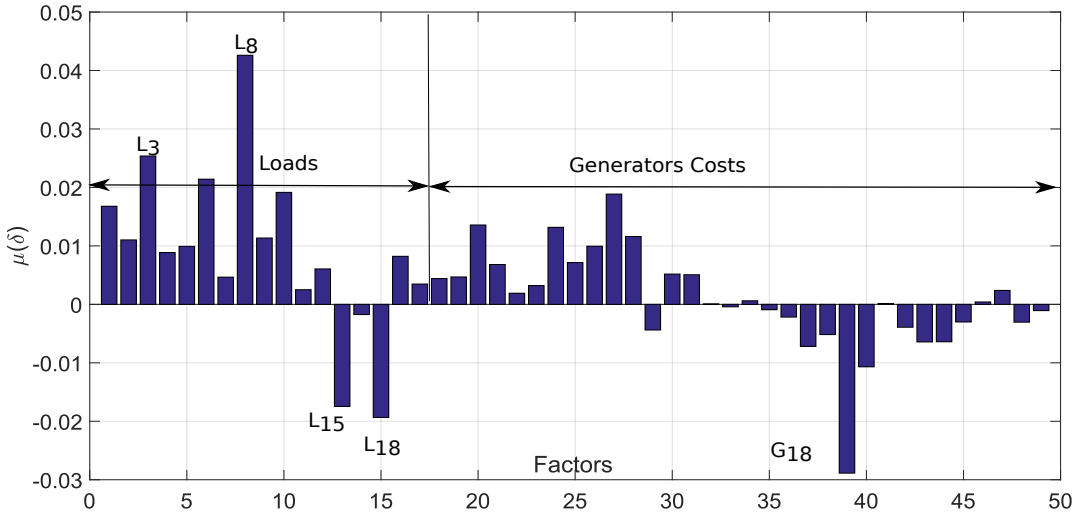

Figure 7.7: The tornado diagram presenting the mean o the elementary effects for the uncertain factors considered in case B.

Table 7.3: The most influencing factors for the line failure probability. Factors leading to a $S_i > 0.08$.

From	To node	Factors
7	8	L_7 , $G_7(1)$, $G_7(2)$
8	9	L_8
8	10	L_8
15	21	L_{18}, $G_{18}(1)$, $G_{21}(1)$
15	21	L_{18}, $G_{18}(1)$, $G_{21}(1)$
16	17	L_{18}
17	18	L_{18}, $G_{18}(1)$, $G_{21}(1)$
17	22	L_{18}, $G_{18}(1)$, $G_{21}(1)$
21	22	L_{18}, $G_{18}(1)$, $G_{21}(1)$

and better understand dependencies between output and factors.

Different system-level and component-level indicators have been evaluated using the cascading model. The selected metrics were the 95^{th} percentile of the DNS, the average total number of line failed and the frequency of line failure for each line. The IEEE RTS96 power grid has been selected as a representative case study and used to test the applicability of the methods to a real-world system. Two uncertainty cases (Case A and Case B) have been investigated, which were characterised by an increasing dimensionality of the aleatory space.

In the Case A, only load variability has been accounted for and the result suggested that two uncertainties in the loads in node 15 and 18 are the major contributors to the

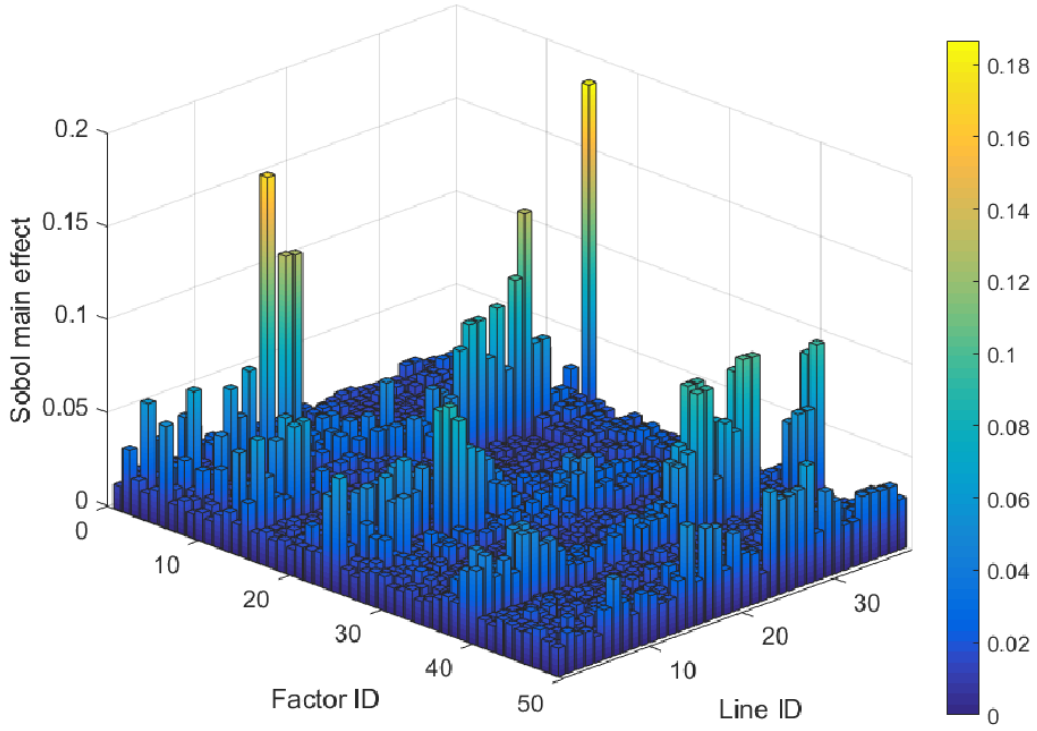

Figure 7.8: The S_i indices calculated for the 49 input factors and for the $P_{f,l}$ outputs. The factors from 1 to 17 are loads at different locations and last 32 are the generator costs.

extremes of the demand not served. A similar result is obtained for the average total number of line failed. Morris had the advantage of showing a negative relationship between the DNS and loads in nodes 15 and 18. In reality prices are indeed affected by uncertainty, so a sensitivity analysis that assumes fixed prices (and therefore fixed generator dispatch) might be misleading in identifying critical components in the power grid. Thus, in the uncertainty Case B, the variability of the generator costs and loads variability are both considered. The new economic setting changed the underling behaviour of the network and, consequently, of the cascading evaluation process. The Sobol's and Morris' analysis are fairly consistent in pointing out which among the load and generators costs are the most relevant for the system output. The results are quite different compared to case A, due to the difference in the economic setting of the generators. In addition, the sensitivity of the lines outage frequency has been computed.

This analysis was performed to investigate more in detail some cascading-relevant relationships between input loads, generators costs and line failures. The results are very interesting from an engineering perspective and at least 2 results can be highlighted which are helpful in a practical context:

- The vulnerable lines (i.e. prone to failure) and the most relevant factors affecting $P_{f,l}$ are identified (using sensitivity indices). This information can be helpful to

support reliability-related decision, for instance, in deciding on weather it is better to replace the line with one having higher capacity (i.e. if $P_{f,l}$ high and is similarly affected by all the input factor), or if it may be more useful to intervene on the factors affecting $P_{f,l}$ (i.e. if $P_{f,l}$ high and sensitive to just few factors);

- When the uncertainty in the loads is identified as highly relevant for a system-level indicator, it is advisable to consider actions such as allocation of distributed generators or adopt peak-shaving (load variance reduction) control methods. This can be beneficial to reduce the uncertainty in the reliability performance of the network (reducing its variance).

The framework proved to be flexible and computationally quite cheap which is a requirement for its application to more realistic large size power networks. This will be the focus of future analysis.

Chapter 8

Reinforcement Learning for Optimisation of Power Grid Operations and Maintenance

8.1 Abstract

In this chapter, we investigate Reinforcement Learning (RL) for managing Operation and Maintenance (O&M) of power grids equipped with Prognostic and Health Management (PHM) capabilities, which allow tracking the health state of the grid components. RL exploits this information to select optimal O&M actions on the grid components giving rise to state-action-reward trajectories maximising the expected profit. A scaled-down case study is solved for a power grid, and strengths and weaknesses of the framework are discussed.

8.2 Introduction

Modern power grids are complex systems, including many highly interconnected components. Maximising the grid productivity while ensuring a safe and reliable delivery of power is of uttermost importance for grid operators. This requires developing robust decision-making frameworks, which give account to both the complexity of the asset and the uncertainties on its operational conditions, component degradation, failure behaviours, external environment, etc.

Nowadays, the grid management issue is further challenged by the possibility of equipping grid elements with Prognostics and Health Management (PHM) capabilities, which allow tracking the health state evolution. This information can be exploited by grid operators to further increase the profitability of their assets [61,68,79,105,151,159].

Reinforcement Learning (RL) [142, 144] has been used in the last decades to solve a variety of realistic control and decision-making issues in the presence of uncertainty, including power grid management. In the RL paradigm, a controller (i.e. the decision maker) learns from the interaction with the environment (e.g. the grid) by observing states, collecting rewards and selecting actions to maximise the future revenues, considering the aleatory uncertainties in the environment behavior. The state-action-reward trajectories [42] can be gathered from direct interaction with the real system (e.g. [17]), or from its realistic simulation [142]. This makes RL suitable to power grid management optimization, as it can cope with both the complexity of the asset and the unavoidable uncertainties related to its operation.

In [151], an RL framework based on Q-learning is proposed to solve constrained load flow and reactive power control problems in power grids. Kuznetsova et al. [68] develop an optimisation scheme for consumers actions management in the microgrid contest and accounting for renewable volatility and environmental uncertainty. In [42], a comparison between RL and a predictive control model is presented for a power grid damping problem. In [79], the authors review recent advancements in intelligent control of micro grids including few attempts using RL methods. However, none of the revised works employs RL to find optimal combined Operation and Maintenance (O&M) policies for power grids with degrading elements.

We present an RL framework to support O&M decisions for power grids equipped with PHM systems, which seeks for the settings of the generator power outputs and the scheduling of preventive maintenance actions that maximize the grid load balance and expected profit over an infinite time horizon, while considering the uncertainty of power production from Renewable Energy Sources (RES), power loads and component

failure behaviors.

The rest of this work is organized as follows: Section 8.3 presents the RL framework for optimal decision making under uncertainty. A scaled-down power grid application is proposed in Section 8.4, whereas the results and limitations of RL are discussed in Sections 8.5 and 8.6, respectively. Section 8.8 closes the chapter.

8.3 Modelling framework for optimal decision making under uncertainty

As anticipated above, developing a RL framework for power grid O&M management requires defining the environment, the actions that the agent can take in every state of the environment, the state transitions the actions lead to and, finally, the rewards associated to each state-action-transition step.

8.3.1 State space

Consider a power grid made up of elements $C = \{1, ..., N\}$, physically and/or functionally interconnected, according to the given grid structure. Similarly to [30], the features of the grid elements defining the environment are the N^d degradation mechanisms affecting the degrading components $d \in D \subseteq C$ and the N^p setting variables of power sources $p \in P \subseteq C$. For simplicity, we assume $D = \{1, ..., |D|\}$, $P = \{|D| + 1, ..., |D| + |P|\}$ and $|D| + |P| \leqslant N$.

The degradation processes evolve independently on each other according to a Markov process defining the transition probability from state $s_i^d(t)$ at time t to the next state $s_i^d(t+1)$, where $s_i^d(t) \in \{1, ..., S_i^d\} \quad \forall t,\ d \in D, i = 1, ..., N^d$. Similarly, for the power sources production, a Markov process defines the probabilistic dynamic of power setting variables from $s_j^p(t)$ at time t to the next state $s_j^p(t+1)$, where $s_j^p(t) \in \{1, ..., S_j^p\} \quad \forall t$, $p \in P, j = 1, ..., N^p$. Then, system state vector $\mathbf{S} \in \mathcal{S}$ at time t reads:

$$\mathbf{S}(t) = \left[\ s_1^1(t), s_2^1(t), \ldots, s_{N^{|P|+|D|}}^{|P|+|D|}(t) \ \right] \in \mathcal{S} \tag{8.1}$$

8.3.2 Actions

Actions can be performed on the grid components $g \in G \subseteq C$ at each t. The system action vector $\mathbf{a} \in \mathcal{A}$ at time t is:

$$\mathbf{a}(t) = \left[\ a_{g_1}(t), \ldots, a_{g_\varrho}(t), \ldots, a_{|g|_{|G|}}(t) \ \right] \in \mathcal{A} \tag{8.2}$$

were action $a_{g_\varrho}(t)$ is selected for component $g_\varrho \in G$ among a set of mutually exclusive actions $a_{g_\varrho} \in \mathbf{A}_g$. The action set $\mathbf{A}_{g_\varrho}$ can include operational actions (e.g. closure of a valve, generator power ramp up, etc.) and maintenance actions (e.g. preventive and corrective). Constraints can be defined for reducing $\mathbf{A}_{g_\varrho}$ to a subset $\hat{\mathbf{A}}_{g_\varrho} \subseteq \mathbf{A}_{g_\varrho}$. For example, Corrective Maintenance (CM), cannot be taken on As-Good-As-New (AGAN) components and, similarly, it is mandatory action for failed components. In an optimistic view [30], both Preventive Maintenance (PM) and CM actions are assumed to restore the AGAN state for each component. An example of Markov process for a 4 degradation state component is presented in Fig.8.1, where circle markers indicate maintenance actions and squared markers indicate other actions, i.e. operational actions.

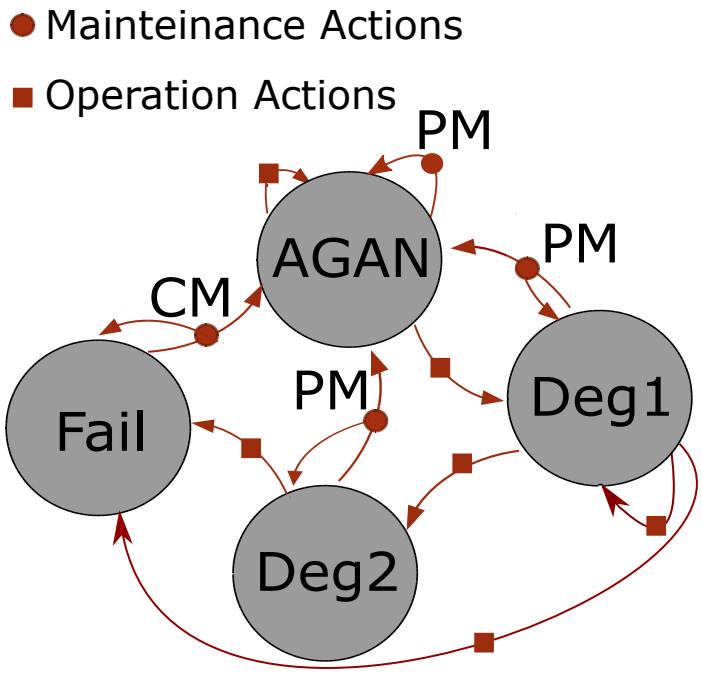

Figure 8.1: The Markov Decision Process associated to the health state of a degrading component.

8.3.3 Transition probabilities

Transition probability matrices are associated to each feature f of each component $c \in P \cup D$ and to each action $\mathbf{a} \in \mathcal{A}$, where $f \in \{1, .., N^d\}$ if $c \in D$ and $f \in \{1, .., N^p\}$ otherwise, as follows:

$$\mathcal{P}^{\mathbf{a}}_{c,f} = \begin{bmatrix} p_{1,1} & p_{1,2} & \cdots & p_{1,S^c_f} \\ p_{2,1} & p_{2,2} & \cdots & p_{2,S^c_f} \\ \vdots & \vdots & \ddots & \vdots \\ p_{S^c_f,1} & p_{S^c_f,2} & \cdots & p_{S^c_f,S^c_f} \end{bmatrix}^{\mathbf{a}}_{c,f} \tag{8.3}$$

where $p_{i,j}$ represents the probability of transition from state i to state j of feature f of component c and conditional to the action $\mathbf{a}$ in a time varying setting, i.e. $\mathcal{P}^{\mathbf{a}}_{c,f}(s_j|\mathbf{a}, s_i)$. The normalization propriety holds, i.e. $\sum_{j=1}^{n} p_{i,j} = 1$. In practice, element $p_{i,j}$ of the transition probability matrix $\mathcal{P}^{\mathbf{a}}_{c,f}$ can be estimated as the relative frequency of the measured component state to fall into the j^{th} state at time $t+1$ provided that it was at the i^{th} state in the previous time step when the action $\mathbf{a}$ was taken.

8.3.4 Rewards

Numerical rewards are case-specific and obtained by solving a physic-economic model of the system, which evaluates how good is the transition from one state to another given that $\mathbf{a}$ is taken:

$$R(t) = \mathfrak{F}\left(\mathbf{S}(t+1)\ ,\ \mathbf{a}(t)\ ,\ \mathbf{S}(t)\right)\ \ \in \mathbb{R}$$

Generally speaking, there are no restriction on the definition of a reward function. However, a well-suited reward function will indeed help the agent converging faster to an optimal solution [141]. Further specifications will depend strongly on the specific RL problem at hand and, thus, will be provided in section 8.4.3.

8.3.5 Reinforcement Learning and SARSA(λ) method

Generally speaking, the goal of RL methods for optimal control is to find the optimal action-value function $Q_{\pi*}(\mathbf{S}, \mathbf{a})$, which provides an estimation of future revenues when an action $\mathbf{a}$ is taken in state $\mathbf{S}$, following the optimal policy π*:

$$Q_{\pi*}(\mathbf{S}, \mathbf{a}) = \mathbb{E}_{\pi*}\left[\sum_{t=0}^{\infty} R(t)|\mathbf{S}(t), \mathbf{a}(t)\right] \tag{8.4}$$

Among the wide range of RL algorithms, we adopt SARSA(λ), which is a temporal difference learning methods (i.e. it changes an earlier estimate of Q based on how it

differs from a later estimate) employing eligibility traces to carry out backups over n-steps and not just over one step [142]. Details on SARSA(λ) are provided in Algorithm 4 in the Appendix.

8.4 Case study

A scaled-down power grid case study is used to test the RL decision making framework. The grid includes: 2 controllable generators; 5 cables for the power transmission; 2 non-controllable RES which are connected to 2 loads and provide them electric power depending on random weather conditions (Fig. 8.2). Then, $|C|$=11. Two traditional generators (Gen1 and Gen2) are installed as displayed in Fig. 8.2 and controlled to minimize power unbalances on the grid. We assume that the 2 controllable generators and links 3 and 4 are affected by degradation and, thus, are equipped with PHM capabilities to inform the decision-maker on their degradation states, then $D = \{1, 2, 3, 4\}$. The two loads and the two renewable generators define the grid power setting, $P = \{5, 6, 7, 8\}$

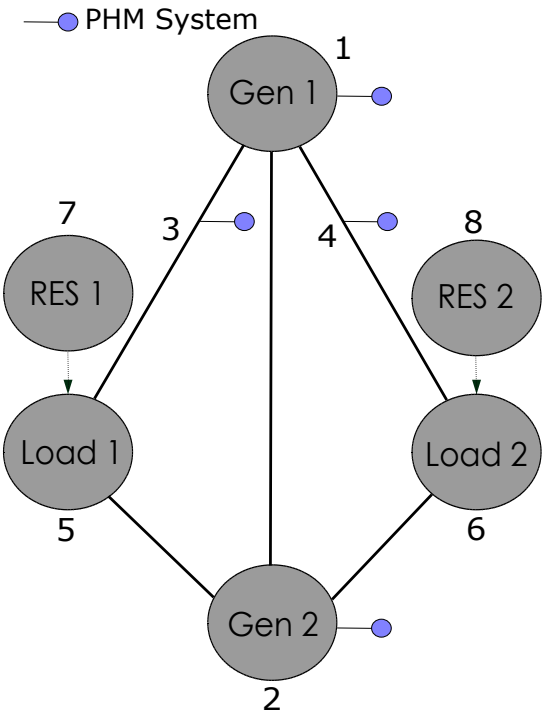

Figure 8.2: The power grid structure and the position of the 4 PHM capabilities, 2 renewable sources, 2 loads and 2 controllable generators.

8.4.1 States and actions

In the case study, we consider $N^d = 1$ degradation features, $d = 1, .., 4$ and $N^p = 1$ power features $p = 1, .., 4$. We consider 4 degradation states for the generators, $s_1^d = \{1, .., S_1^d = 4\}$ for $d = 1, 2$, whereas three states are associated to the power lines $s_1^d = \{1, .., S_1^d = 3\}$, $d = 3, 4$. State 1 refers to the AGAN conditions, state S_1^d to the failure state and states $1 < s_1^d < S_1^d$ to degraded states in ascending order. For each load, we consider 3 states of increasing power demand $s_1^p = \{1, .., S_1^p = 3\}$ for $p = 5, 6$ and three states of increasing power production are associated to renewable sources, $s_1^p = \{1, .., S_1^p = 3\}$ for $p = 7, 8$. Then, the total number of state vectors combinations is 11664 and the grid state vector at time t is defined as follows:

$$\mathbf{S}(t) = \{s_1^1, s_1^2, s_1^3, s_1^4, s_1^5, s_1^6, s_1^7, s_1^8\}$$

The agent can operate both generators with the aim to maximise the system revenue by minimizing unbalance between demand and production, while preserving the structural and functional integrity of the system, $g \in G = \{1, 2\}$. Other actions can be performed by other agents on other components (e.g. transmission lines), but being outside from the control domain of the first agent those are assumed included in the environment. Then, the action vector reads $\mathbf{a} = [a_1, a_2]$. Five O&M actions can be performed on each controllable generator, for a total of 25 combinations, thus giving rise to a 291600 state-action pairs. The action set for each generator is the following:

$$\mathbf{A}_g = \{1, .., 5\} \quad g \in \{1, 2\}$$

where the first 3 (operational) actions affect the power output of the generator, changing it to one of the 3 allowed power levels. The last 2 actions are preventive and corrective maintenance actions, respectively. It is assumed that CM is mandatory for failed generators. Furthermore, highly degraded generators (i.e. $S_g^d = 3,\ d = 1, 2$) are assumed degraded in their operational performance and only the lower power output can be obtained (only $a_g = 1$ action is allowed). Tables 8.1-8.3 display the costs for each action and the corresponding power output of the generator, the line electric parameters and the relation between state indices s_1^p and the power variable settings, respectively.

8.4.2 Probabilistic model

State transitions may occur from time t to the next time step $t + 1$ and are specifically defined for each feature of each component. The 2 loads have identical transition probability matrices and also the degradation of the transmission cables and generators are described by the same Markov process. Thus, for ease of notation, the component subscripts have been dropped. Each action $\mathbf{a} \in \mathcal{A}$ is associated to a specific transition probability matrix $\mathcal{P}_g^{\mathbf{a}}$ describing the evolution of the generator health state conditioned

Table 8.1: The power output of the 2 generators in [MW] associated to the 5 available actions and action costs in monetary unit [m.u.].

Action:	1	2	3	4	5
$P_{g=1}$ [MW]	40	50	100	0	0
$P_{g=2}$ [MW]	50	60	120	0	0
$C_{a,g}$ [m.u.]	0	0	0	10	500

Table 8.2: The transmission lines proprieties.

From	To	Am [A]	X
Gen 1	Load 1	125	0.0845
Gen 1	Load 2	135	0.0719
Gen 1	Gen 2	135	0.0507
Load 1	Gen 2	115	0.2260
Load 2	Gen 2	115	0.2260

Table 8.3: The physical values of the power settings in [MW] associated to each state S_1^p of component $p \in P$.

	State index s_1^p	1	2	3
$p = 5$	Demanded [MW]	60	100	140
$p = 6$	Demanded [MW]	20	50	110
$p = 7$	Produced [MW]	0	20	30
$p = 8$	Produced [MW]	0	20	60

by its operative state or maintenance action. It can be noticed that probabilities associated to operational actions, namely $a_g = 1, 2, 3$, affect differently the degradation of the component. For those actions, the bottom row corresponding to the failed state has only zero entries. This is to indicate that operational actions cannot be taken for failed generators, but only CM is allowed. The transition matrices for the considered features are defined as follows:

$$\mathcal{P}_d^{a_d=1} = \begin{bmatrix} 0.98 & 0.02 & 0 & 0 \\ 0 & 0.95 & 0.05 & 0 \\ 0 & 0 & 0.9 & 0.1 \\ - & - & - & - \end{bmatrix} \quad d = 1, 2 \qquad \mathcal{P}_d^{a_d=2} = \begin{bmatrix} 0.97 & 0.03 & 0 & 0 \\ 0 & 0.95 & 0.05 & 0 \\ - & - & - & - \\ - & - & - & - \end{bmatrix} \quad d = 1, 2$$

$$\mathcal{P}_d^{a_d=3} = \begin{bmatrix} 0.95 & 0.04 & 0.01 & 0 \\ 0 & 0.95 & 0.04 & 0.01 \\ - & - & - & - \\ - & - & - & - \end{bmatrix} \quad d = 1, 2$$

$$\mathcal{P}_d^{a_d=4} = \begin{bmatrix} 1 & 0 & 0 & 0 \\ 0.5 & 0 & 0.5 & 0 \\ 0.5 & 0 & 0 & 0.5 \\ - & - & - & - \end{bmatrix} \quad d = 1, 2 \qquad \mathcal{P}_d^{a_d=5} = \begin{bmatrix} - & - & - & - \\ - & - & - & - \\ - & - & - & - \\ 0.15 & 0 & 0 & 0.85 \end{bmatrix} \quad d = 1, 2$$

$$\mathcal{P}_d^{\mathbf{a}} = \begin{bmatrix} 0.9 & 0.08 & 0.02 \\ 0 & 0.97 & 0.03 \\ 0.1 & 0 & 0.9 \end{bmatrix} \forall\ \mathbf{a}, d = 3, 4 \qquad \mathcal{P}_p^{\mathbf{a}} = \begin{bmatrix} 0.4 & 0.3 & 0.3 \\ 0.3 & 0.3 & 0.4 \\ 0.2 & 0.4 & 0.4 \end{bmatrix} \forall\ \mathbf{a}, p = 5, 6$$

$$\mathcal{P}_7^{\mathbf{a}} = \begin{bmatrix} 0.5 & 0.1 & 0.4 \\ 0.3 & 0.3 & 0.4 \\ 0.1 & 0.4 & 0.5 \end{bmatrix} \forall\ \mathbf{a} \qquad \mathcal{P}_8^{\mathbf{a}} = \begin{bmatrix} 0.5 & 0.2 & 0.3 \\ 0.4 & 0.4 & 0.2 \\ 0 & 0.5 & 0.5 \end{bmatrix} \forall\ \mathbf{a}$$

8.4.3 Reward model

When the agent performs an action at time t; the environment provides a reward and leads the system to its state at time $t+1$. The reward is calculated as the sum of 4 different terms: (1) the revenue from selling electric power, (2) the cost of producing electric power by traditional generators, (3) the cost associated to the performed actions and (4) the cost of not serving energy to the customers. Mathematically, the reward reads:

$$R(t) = \sum_{p=5}^{6} (L_p(t) - ENS_p(t)/\Delta_t) \cdot C_{el} - \sum_{g=1}^{2} P_g \cdot C_g - \sum_{g=1}^{2} C_{a,g} - \sum_{p=5}^{6} ENS_p(T) \cdot C_{ENS} \quad (8.5)$$

where L_p is the power demanded by component p, C_{el} is the price paid by the loads for per-unit of electric power, P_g is the power produced by the generators, C_g is the cost of producing the unit of power, $C_{a,g}$ is the cost of the action a on the generator g, Δ_t is the time difference between the present and the next system state and it is assumed to be 1 h, ENS_p is the energy not supplied to the load p and is a function of the grid state vector and lines and generators electrical proprieties and availability, i.e. $\mathbf{ENS}(t) = \mathcal{G}(\mathbf{S}, \mathbf{Am}, \mathbf{X})$ where $\mathcal{G}$ defines the constrained DC power flow solver [132]. C_{ENS} is the cost of the energy not supplied. The costs C_{ENS}, C_g and C_{el} are set to 5, 4 and 0.145 monetary unit (m.u.) per-unit of energy or power, respectively.

8.5 Results and discussions

The SARSA(λ) algorithm (Algorithm 4 in the Appendix) has been used to provide an approximate solution to the decision problem. The stochastic grid model is used to sample control trajectories only, i.e. it provides a reward and a new state when an action and the old state is provided as input. The SARSA method has been run changing parameters setting and accumulating eligibility traces. The initial state $s = \mathbf{S}(t = 0)$ has been selected for the episodic loop randomly, using a degradation-

weighted probability mass function $f_S(s) \propto \sum_{d=1}^{|D|} s_1^d$. This sampling scheme is used to better estimate action-value functions in rarely visited sates (i.e. low-probability states with many failed/highly degraded components), which speeds up the convergence of the SARSA method. For validation, Bellman's optimality [15]- [54] has been solved to provide a reference optimal action-value function. The Bellman's results are in good agreement with the SARSA results, as it can be seen from Fig. 8.3.

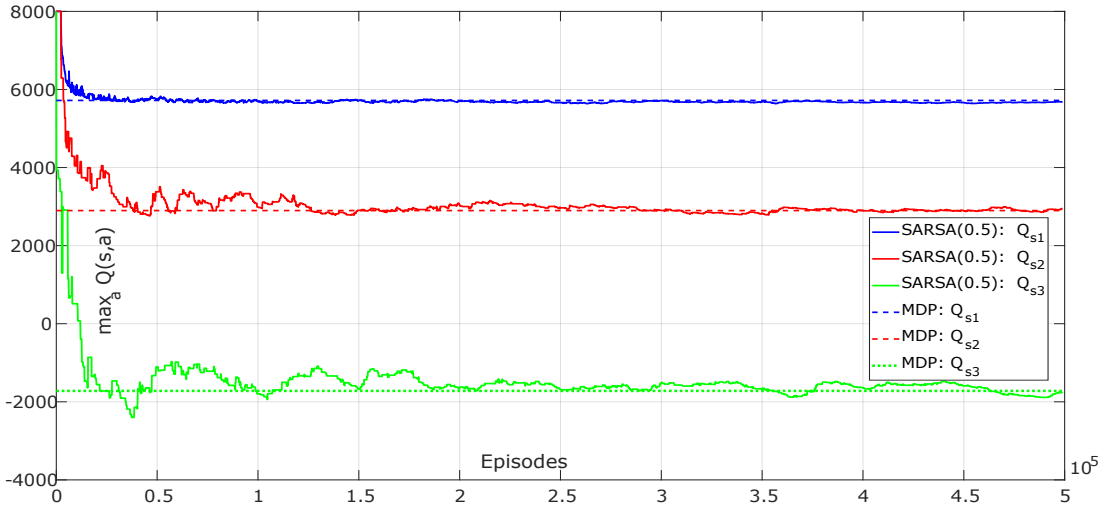

Figure 8.3: The plot shows a comparison of the maximum $Q_{\pi*}(\mathbf{S}, \mathbf{a})$ for 3 states indicative of the different state-action value levels, obtained by SARSA(0.5) algorithm and $T = 50$ (solid lines) and the reference Bellman's solution of the underlying Markov Decision Process (dashed lines).

The SARSA(λ) results are summarised in Fig. 8.4, where the curves provide a compact visualization of the distribution of $Q_{\pi*}(\mathbf{S}, \mathbf{a})$ over the states for the available 25 combinations of actions. Three clusters can be identified: on the far left, we find the set of states from which CM on both generators is performed; being CM a costly action, this leads to a negative expectation of the discounted reward. The second cluster (*C 2*) corresponds to the 8 combination of one CM and any other action on the operating generator. The final cluster (*C 1*) of 16 combinations of actions includes only PM and operational actions. If corrective maintenance is not performed, higher rewards are expected.

In Fig. 8.5, each sub-plot shows the the highest expected discounted power grid return, $Q_{\pi*}(\mathbf{S}, \mathbf{a})$, adopting the optimal policy, conditional to a specific degradation states of the generators and for increasing electric load demand. It can be noticed that if the generators are both healthy or slightly degraded (i.e. $\sum_{d=1}^{2} s_1^d = 2, 3, 4$) an increment in the overall load demand leads to an increment in the expected reward, due to the larger revenues from selling more electric energy to the customers. On the

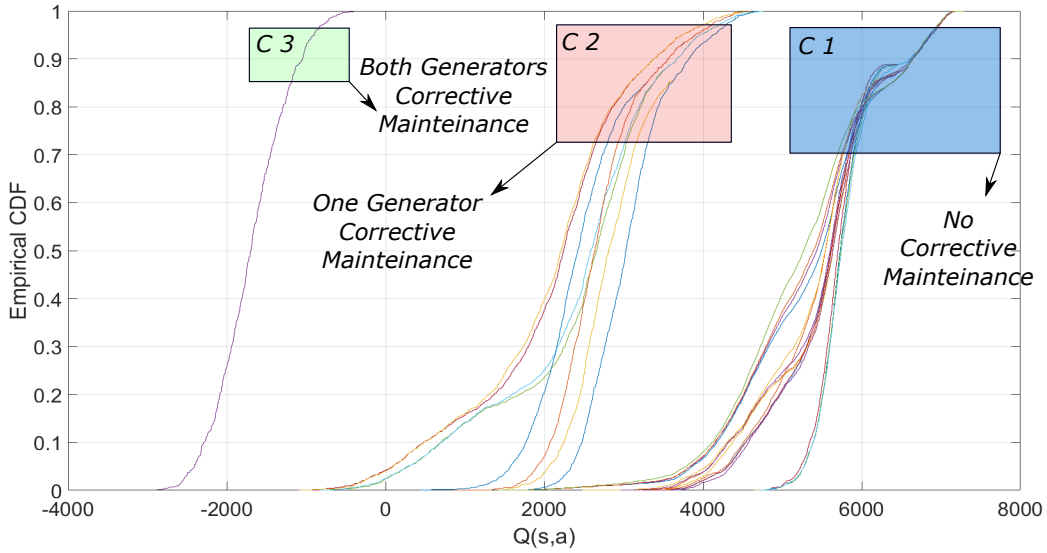

Figure 8.4: The $Q(s, a)$ values displayed using ECDFs and the 3 clusters.

other hand, if the generators are highly degraded or failed (i.e. $\sum_{d=1}^{2} s_1^d = 7, 8$), an increment in the load demand leads to a drop in the expected revenue. This is due to the increasing risk of load curtailments and associated cost (i.e. cost of energy not supplied), and to the impacting PM and CM actions costs.

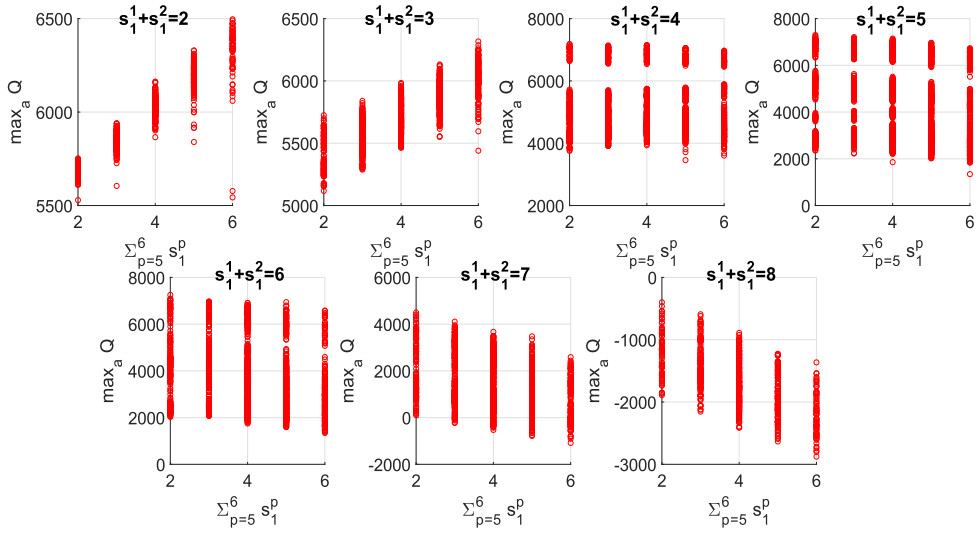

Figure 8.5: The maximum $Q_{\pi*}(\mathbf{S}, \mathbf{a})$ (i.e. maximum expected discounted cumulative reward) for increasing total load and different degrading condition of the generators.

8.5.1 Policies comparison

We have empirically found that SARSA(0.5) policies outperform SARSA(λ), $\lambda = 0$ and $\lambda = 1$. Thus, two SARSA(0.5) have been further investigated, by setting the truncation

Table 8.4: The MDP Bellman's optimality and the RL results compared with suboptimal policies.

	MDP	SARSA(0.5)		Q_{50rnd}	Q_{100rnd}
$Q_{\mathbf{S}_1}$	5719	5511	5555	4191	2028
$Q_{\mathbf{S}_2}$	2898	2577	2664	1297	-1229
$Q_{\mathbf{S}_3}$	-1721	-1816	-1813	-2956	-4288
Act top1	100 %	48.8 %	49.1 %	62.1%	24.8%
Act top3	100 %	66.5 %	66.5 %	71.4%	43.1%
$\mathbb{E}[R(t)]$	529.8	478.8	488.1	370.3	190.4
N_e	-	5e5	5e5	-	-
T	-	50	250	-	-

windows T to 50 and 250 time steps for each episode, respectively. Table 8.4 shows the results of the SARSA(λ) algorithms (columns 3 and 4, respectively) and compares them with the MDP (Bellman's optimality) solution (column 2) and 2 artificial suboptimal policies: Q_{50rnd} (column 5), which is artificially obtained randomizing the action to be selected in 50 % of the states and selecting the MDP optimal action for the remaining states and Q_{100rnd} (column 6), where all states have a random action associated with. Three representative system states $\mathbf{S}_1 = [1,1,1,1,1,1,1,1]$, $\mathbf{S}_2 = [4,1,1,1,1,1,1,1]$ and $\mathbf{S}_3 = [4,4,3,3,3,3,3,3]$ are used to compare the expected discounted return Q. The 3 states are associated with substantially different rewards as they have been selected from the 3 clusters *C 1*, *C 2* and *C 3*, respectively (see Fig. 8.4): $\mathbf{S}_1$ has both generators in the AGAN state, $\mathbf{S}_2$ has on generator out of service whilst $\mathbf{S}_3$ has both generators failed. *Act* is defined as the portion of actions taken from the SARSA(λ) policies that are equal to those taken using the reference MDP optimal policy in the corresponding states; $\mathbb{E}[R(t)]$ is the expected averaged non-discounted return, i.e. $\mathbb{E}\left[\frac{\sum_{t=1}^{T} R(t)}{T}\right]$, independent from the initial state of the system. It is interesting to notice that SARSA(0.5) provides better policies (i.e. higher expected discounted and non-discounted returns) compared to Q_{50rnd} and Q_{100rnd}. This is true even if Q_{50rnd} has higher *Act* compared to the SARSA policies, i.e. more than 60 % of the Q_{50rnd} actions are equal to the MDP actions whilst less than 50 % for the SARSA. This points out that the optimal policy is very sensitive to some of the state-action combinations and less to others. In other words, taking the wrong action in some states can lead to a catastrophic drop in the expected return, whilst in other cases a sub-optimal action affects less the expected revenue (e.g. making generator 1 produce power rather than generator 2 or vice versa).

Fig. 8.6 presents in details 2 control trajectories obtained selecting greedily actions with the MDP Bellman's policy (top plot) and the SARSA(λ) policy (bottom plot), rewards are displayed on the y-axis and actions and states (see Table 8.5) are associated to each time step. It is interesting to observe that by following an optimal policy, PM actions are sometimes recommended even if the generators are As-Good-As-New. This

might seem counter intuitive, but it can be explained considering the degradation model settings. A PM action taken in an AGAN degradation state will assure a transition to the AGAN state. In this sense, the MDP policy is ready to accept a slightly lower revenue (due to PM costs), but with the advantage of suspending the degradation process, especially when the power produced by RES can be used to minimise unbalances between power production and the 2 loads are small.

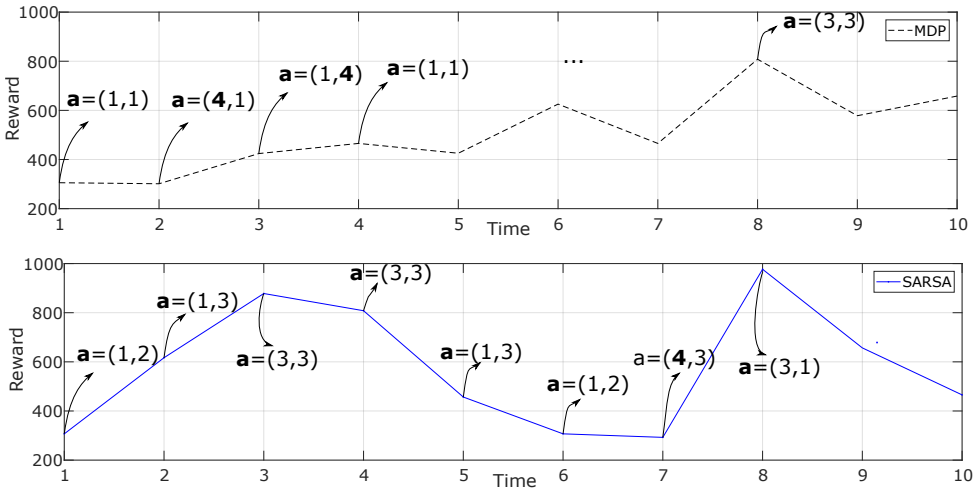

Figure 8.6: Actions taken in 2 separate control trajectories using MDP and SARSA policies. Initial state s_1 and next states are randomly generated by the underlying probabilistic model (see Table 8.5).

Table 8.5: The state vectors for the MDP and SARSA control trajectories in Figure 8.6.

MDP states trajectory							
Gens		Loads		RES		Lines	
s_1^1	s_1^2	s_1^5	s_1^6	s_1^7	s_1^8	s_1^3	s_1^4
1	1	1	1	1	1	1	1
1	1	1	1	3	1	1	1
1	1	1	2	2	3	1	1
1	1	2	1	3	2	1	1
1	1	1	2	3	1	1	1
1	1	3	1	3	3	3	1
2	1	2	1	3	2	1	1
2	2	2	3	1	2	1	1
2	2	2	2	1	1	1	1
2	2	1	3	1	2	1	1

SARSA states trajectory							
Gens		Loads		RES		Lines	
s_1^1	s_1^2	s_1^5	s_1^6	s_1^7	s_1^8	s_1^3	s_1^4
1	1	1	1	1	1	1	1
1	1	3	1	3	1	1	1
1	1	3	3	2	1	1	1
1	1	2	3	2	1	1	1
1	1	2	1	1	1	3	3
1	1	1	1	1	2	1	3
1	1	1	1	1	2	2	3
1	1	3	3	3	3	2	3
1	1	1	3	2	2	2	1
1	1	2	1	3	2	2	1

8.6 Limitations and extension to non-tabular method

While RL, like stochastic dynamic programming (DP), has in principle a very broad scope of application, it has to face computational issues when the state-action spaces of the control problem are very large. In such a case, RL has to be combined with regression techniques capable of interpolating over the state-action space the data obtained

from (relatively) few control trajectories [42]. Most of the research in this context has focused on parametric function approximators, representing either some (state-action) value functions or parameterized policies, together with some stochastic gradient descent algorithms (see e.g. [144] or [72]). The appendix presents an extension of the framework recently submitted for journal publication.
Further research work will focus on the development of enhanced RL algorithms, capable of dealing with imprecise rewards (e.g. due to unavailable/unreliable models), partial observability and issues related to scarcity of samples due to low-probability of specific state-action pairs.

8.7 Discussion on the uncertainty associated to PHM devices

Prognostics health management devices deal with predicting the health state of components and, possibly, future failures. The development of robust PHM devices is a challenging problem and is often device-dependent. Many authors developed computational methods for prognostics, both in the context of testing-based health management and condition-based health management. Robust systems will have to identify and explicitly account for various sources of uncertainty. Uncertainties in PHM systems are potentially very large and, although an in-depth discussion is beyond the scope of this work, a few examples of sources of uncertainty are reported here.

A robust condition-based health monitoring system will include a comprehensive list of failure mechanisms which are potentially harmful to the device. Indeed, each model will be subject to modeling uncertainty and there is always a potential risk of having identified just some of the most relevant mechanisms. Perhaps, multiple sensors and multiple signals can be collected from the device and their information content analyzed to extract useful health performance indicators. However, uncertainty will likely affect the signals and perhaps different signals might provide conflicting sources of evidence regarding the device health state. Once the signals are collected and uncertainty evaluated, a model-based, data-driven or hybrid procedure can be used to identify abnormality, e.g. degrading/warning states (i.e. outliers). Those will then be used, for instance, assign likelihood to the relevant failure mechanisms (damage classification) finally attempting to predict the remaining useful life.

8.8 Conclusion

A framework based on Reinforcement Learning for optimal decision making of power grid systems affected by uncertain operations and degradation mechanisms has been

investigated. Power grid models can include PHM devices, which are used to inform the agent about the health state of the system components. This information helps to select optimal O&M actions on the system components.
The SARSA(λ) method was used to solve a control problem for a scale down power grid with renewable and PHM capabilities. The RL results have been compared to the reference Bellman's optimality solution and are in good agreement, although inevitable approximation errors have been observed.
The framework proved to be flexible and effective in tackling a small but representative case study and future works will test its applicability to more realistic (larger) state-action spaces. To this aim, artificial neural networks will be used in future research work for state-action space regression to scale up to larger grids. This necessary verification for a possible future applicability of the method.

Appendix

Formally, a MDP is a tuple $\langle S,A,R,\mathcal{P}\rangle$, where S is a finite state set, $A(s)$ is a finite action set with $s \in S$, R is a reward function such that $R(s,a) \in \mathbb{R}, \forall s \in S, a \in A(s)$ and P is a probability function mapping the state action space:

$$\mathcal{P}_{s,a,s'} : S \times A \times S \mapsto [0,1]$$

A specific policy π is defined as a map from the state space to the action space $\pi : S \mapsto A$ with $\pi(s) \in A(s)\ \forall s \in S$ and it belongs to the set of possible policies Π. The action-value function $Q_\pi(s,a)$ is mathematically defined as **[141]**:

$$Q_\pi(s,a) = \mathbb{E}_\pi \left[\sum_{t=0}^{\infty} \gamma^t R(s_t, \pi(s_t)) | S_0 = s, A_0 = \pi(s_0) \right] \ s \in S$$

where $\gamma \in [0,1]$ is the discount factor and a $\gamma < 1$ is generally employed to avoid divergence of the cumulative rewards as well as to reflects the fact that is some cases earlier rewards are more valuable than future rewards. The Bellman's optimality equation provides an analytical expression for $Q_{\pi*}(s,a)$, which is the ation-value function for optimal policy π^*. The Bellman's optimality is defined by a recursive equation as follows [54]- [141]:

$$Q_{\pi*}(s_t,a_t) = \sum_{s_{t+1}} \mathcal{P}(s_{t+1}|s_t,a_t) \left[R(s_{t+1},a,s_t) + \underset{a_{t+1}}{max}\ \gamma Q_{\pi*}(s_{t+1},a_{t+1}) \right] \tag{8.6}$$

Equation 8.6 can be solved by Dynamic Programming such as policy iteration or value iteration [141].

The SARSA(λ) algorithm starts initializing the action-value function Q and eligibility traces Z tables. Then, the values for the learning rate α, the discount factor γ, the decay rate of the traces $\lambda \in [0, 1]$ and the greediness factor ϵ (or a policy π to be evaluated) are selected. After this initialization, the episodic loop starts with a random sample (or selection) of an initial state s_t, then, an action a_t is selected based on the adopted policy, e.g. ϵ-greedy or $\pi(\cdot|s_t)$. A ϵ-greedy policy consists of random actions, taken with probability ϵ, or greedy actions taken with probability 1-ϵ (i.e. actions for which Q is maximised). Once the initial state-action pair is obtained, the episode e is evaluated (i.e. a sequence of action-rewards-state-actions). Temporal difference errors δ_t at the time step t are calculated, traces replaced or accumulated and Q updated.

The episode terminates when a predefined truncation horizon T is reached (i.e. maximum time length of the episode). The procedure is iterated until a predefined number of events N_E is obtained. The SARSA(0) is guaranteed to convergence to an optimal action-value function for a Robbins-Monro sequence of step-sizes α_t, for further details regarding stopping criteria and convergence the reader is referred to [139]. RL approaches can tackle control problems with infinite optimisation horizon by approximating the solution with a T-stage approach. In this sense, windows of T time steps are used to truncating the time horizon, thus reducing the computational burdens [42]. The traditional SARSA method is sometimes referred as SARSA(0) as it corresponds to the SARSA(λ) algorithm when the decay rate of the traces $\lambda = 0$ (i.e. back up over 1-step). The SARSA(λ) with $\lambda = 1$ will perform complete backups over the full T of the episode (analogously to Monte Carlo learning).

The on-policy SARSA(λ) and the off-policy Q-learning algorithms work as follows [142]:

A non-tabular Reinforcement Learning algorithm

Generally speaking, the goal of Reinforcement Learning for strategy optimization is to maximize the action-value function $Q_{\pi*}(\mathbf{S}, \mathbf{a})$, which provides an estimation of cumulated discounted future revenues when action $\mathbf{a}$ is taken in state $\mathbf{S}$, following the optimal policy π^*:

$$Q_{\pi*}(\mathbf{S}, \mathbf{a}) = \mathbb{E}_{\pi*}\left[\sum_{t=0}^{\infty} \gamma^t R(t)|\mathbf{S}, \mathbf{a}\right] \tag{8.7}$$

We develop a Reinforcement Learning algorithm which uses an ensemble of ANNs to interpolate between state-action pairs, which helps to reduce the number of episodes needed to approximate the Q function. Figure 8.7 graphically displays an episode run within the algorithm.

Algorithm 4 The SARSA(λ) algorithm adopting replacing or accumulating eligibility traces settings.

Set $e = 1$, N_E, ϵ (or a policy π to be evaluated), α, γ, λ
Initialize $Q(s, a)$, for all $s \in S$ and $a \in A$, arbitrarily (e.g. $Q = 0$)
Initialize traces $Z(s, a) = 0$, for all $s \in S$ and $a \in A$
while $e < N_E$ (Episodic Loop) **do**
  Set $t = 1$ Initialize starting state s_t e.g. randomly
  Select action $a_t \in A(s_t)$ using policy derived from Q (e.g. ϵ-greedy) or $\pi(\cdot|s_t)$
  while $t < T$ (run an episode) **do**
    Take action a_t, observe s_{t+1} and reward R_t
    Select action $a_{t+1} \in A(s_{t+1})$ using policy derived from Q (e.g. ϵ-greedy) or $\pi(\cdot|s_{t+1})$
    Compute temporal difference δ_t and update traces:
    $\delta_t = R_t + \gamma Q(s_{t+1}, a_{t+1}) - Q(s_t, a_t)$
    $Z(s_t, a_t) = Z(s_t, a_t) + 1$ (accumulate traces) or
    $Z(s_t, a_t) = 1$ (replace traces)
    Update Q and Z for each s and a:
    $Q(s, a) = Q(s, a) + \alpha \delta_t Z(s, a)$
    $Z(s, a) = \gamma \lambda Z(s, a)$
    Set $t = t + 1$
  end while
  go to next episode $e = e + 1$
end while

Algorithm 5 The Q-learning algorithm.

Set $e = 1$, N_E, ϵ, α, γ;
Initialize $Q(s, a)$, for all $s \in S$ and $a \in A$, arbitrarily (e.g. $Q = 0$)
while $e < N_E$ (Episodic Loop) **do**
  Set $t = 1$ Initialize starting state s_t e.g. randomly
  Select action $a_t \in A(s_t)$ using policy derived from Q (e.g. ϵ-greedy) or $\pi(\cdot|s_t)$
  while $t < T$ (run an episode) **do**
    Take action a_t, observe s_{t+1} and reward R_t
    Compute temporal difference δ_t:
    $\delta_t = R_t + \gamma max_a Q(s_{t+1}, a_{t+1}) - Q(s_t, a_t)$
    Update $Q(s_t, a_t)$:
    $Q(s_t, a_t) = Q(s_t, a_t) + \alpha \delta_t$
    Set $t = t + 1$
  end while
  go to next episode $e = e + 1$
end while

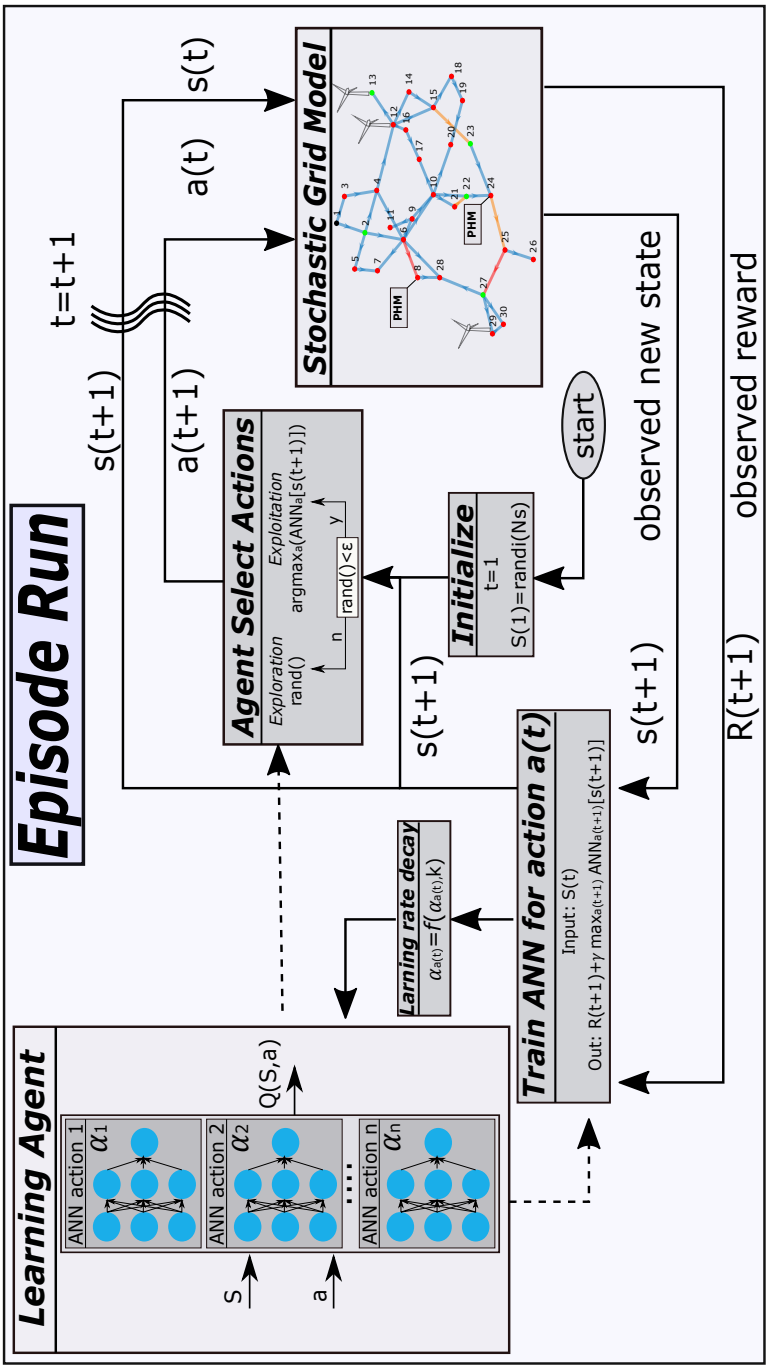

Figure 8.7: The flow chart displays an episode run and how the learning agent interacts with the environment (i.e. the power grid equipped with PHM devices) in the developed Reinforcement Learning framework; dashed-line arrows indicate when the learning agent takes part in the episode run.

In details, we estimate the value of $Q_\pi(\mathbf{S}_t, \mathbf{a}_t)$ using a different ANN for each action, with network weights $\boldsymbol{\mu}_1, \ldots, \boldsymbol{\mu}_{|\mathcal{A}|}$, respectively. Network $\mathcal{N}_l$, $l = 1, ...|\mathcal{A}|$, receives in input the state vector $\mathbf{S}_t$ and returns the approximated value $\hat{q}_l(\mathbf{S}_t|\boldsymbol{\mu}_l)$ of $Q_\pi(\mathbf{S}_t, \mathbf{a}_t = a_l)$. To speed up the training of the ANNs , we initially apply a standard supervised training over a batch of relatively large size n_{ei}, to set weights $\boldsymbol{\mu}_1, \ldots, \boldsymbol{\mu}_{|\mathcal{A}|}$. To collect this batch, we randomly sample the first state $\mathbf{S}_1$ and, then, move $n_{ei} + \Phi$ steps forward by uniformly sampling from the set of applicable actions and collecting the transitions $\mathbf{S}_t, \mathbf{a}_t \rightarrow \mathbf{S}_{t+1}, \mathbf{a}_{t+1}$ with the corresponding rewards $R_t, t = 1, ..., n_{ei} + \Phi - 1$. These transitions are provided by a model of the grid behavior.
Every network $\mathcal{N}_l, l \in \{1, \ldots, |\mathcal{A}|\}$, is trained on the set of states $\{\mathbf{S}_t | t = 1, ..., n_{ei}, \mathbf{a}_t = l\}$ in which the l-th action is taken, whereas the reward that the ANN learns is the Monte-Carlo estimate Y_t of $Q_\pi(\mathbf{S}_t, \mathbf{a}_t)$:

$$Y_t = \sum_{t'=t}^{t+\Phi} \gamma^{t'-t} \cdot R_{t'} \tag{8.8}$$

After this initial training, we apply Q-learning (e.g., [141], [144]) to find the ANN approximation of the optimal $Q_{\pi*}(\mathbf{S}_t, \mathbf{a}_t)$. Namely, every time the state $\mathbf{S}_t$ is visited, the action $\mathbf{a}_t$ is selected among all available actions according to the $\epsilon-$greedy policy π: the learning agent selects exploitative actions (i.e., the action with the largest value, maximizing the expected future rewards) with probability $1 - \epsilon$, or exploratory actions, randomly sampled from the other feasible actions, with probability ϵ.

The immediate reward and the next state is observed, and weights $\boldsymbol{\mu}_{\mathbf{a}_t}$ of network $\mathcal{N}_{\mathbf{a}_t}$ are updated: a single run of the back-propagation algorithm is done using $R_t + \gamma \cdot \max_{l \in \{1,...,|\mathcal{A}|\}} \hat{q}_l(\mathbf{S}_{t+1}|\boldsymbol{\mu}_l)$ as target value (Equation 8.9). This yields the following updating:

$$\boldsymbol{\mu}_{\mathbf{a}_t} \leftarrow \boldsymbol{\mu}_{\mathbf{a}_t} + \alpha_{\mathbf{a}_t} \cdot [R_t + \gamma \cdot \max_{l \in \{1,...,|\mathcal{A}|\}} \hat{q}_l(\mathbf{S}_{t+1}|\boldsymbol{\mu}_l) - \hat{q}_{\mathbf{a}_t}(\mathbf{S}_t|\boldsymbol{\mu}_{\mathbf{a}_t})] \cdot \nabla \hat{q}_{\mathbf{a}_t}(\mathbf{S}_t|\boldsymbol{\mu}_{\mathbf{a}_t}) \tag{8.9}$$

where $\alpha_{\mathbf{a}_t} > 0$ is the value of the learning rate associated to $\mathcal{N}_{\mathbf{a}_t}$ ([141]).
Notice that the accuracy of the estimates provided by the proposed algorithm strongly depends on the frequency at which the actions are taken in every state: the larger the frequency, the larger the information from which the network can learn the state-action value [141]. In real industrial applications, where systems spend most of the time in states of normal operation, this may entail a bias or large variance in the ANN estimations of $Q_\pi(\mathbf{S}_t, \mathbf{a}_t)$ for rarely visited states. To overcome this issue, we increase the exploration by dividing the simulation of the system, and its interactions with the environment and O&M decisions, into episodes of fixed length T. Thus, we run N_{ei} episodes, each one entailing T decisions; at the beginning of each episode, we sample

the first state uniformly over all states. This procedure increases the frequency of visits to highly degraded states and reduces the estimation error. At each episode $ei \in \{1, \ldots, N_{ei}\}$, we decrease the exploration rate $\epsilon = \epsilon_{ei}$ according to $\epsilon = \epsilon_0 \cdot \tau_\epsilon^{ei}$, and the learning rate $\alpha_l = \alpha_0 \cdot (\frac{1}{1+K_\alpha \cdot t_l})$, where α_0 is the initial value, K_α is the decay coefficient and t_l counts the number of times the network $\mathcal{N}_l$ has been trained ([141]).

The QL+ANN algorithm 7 consists of two phases: (1) an initialization phase of the ANNs ensemble and (2) the learning phase, where Q-learning algorithm is used in combination to the ANNs to learn an optimal decision-making policy.In phase (1) an ANN is associated with each action vector $\mathbf{a}$ and its architecture, i.e. number of layers and nodes per layer, is defined by the $\mathbf{N}_{layers}$ vector. Each network is first trained using the Levenberg-Marquardt algorithm, providing as input the state vectors and as output the estimator of Q obtained from the future rewards. In phase (2) the Reinforcement Learning algorithm run, Artificial Neural Networks select the actions and the ensemble is incrementally trained to improve its predictive performance. Notice that, whilst tabular Reinforcement Learning methods are guaranteed to convergence to an optimal action-value function for a Robbins-Monro sequence of step-sizes α_t, a generalized convergence guarantee for non-tabular methods has not been provided yet and an inadequate setup can lead to suboptimal, oscillating or even diverging solutions.Thus, an empirical convergence test has been designed to assess the the reliability of the results. For further details, please refer to Sutton98reinforcementlearning.

Algorithm 6 The value iteration algorithm (Bellman's optimality)

Initialize Q arbitrarily (e.g. $Q(s,a) = 0 \ \forall s \in \mathcal{S}, a \in \mathcal{A}$)
Define tolerance error $\theta \in \mathbb{R}^+$ and $\Delta = 0$
while $\Delta \geqslant \theta$ **do**
  for each $s \in \mathcal{S}$ **do**
    get constrained action set $\mathcal{A}_s$ in s
    for each $a \in \mathcal{A}_s$ **do**
      $q = Q(s,a)$
      $Q(s,a) = \sum_{s'} \mathcal{P}(s'|s,a) \left[R(s',a,s) + \max_{a'} \gamma Q(s',a') \right]$
      $\Delta = \max(\Delta, |q - Q(s,a)|)$
    end for
  end for
end while
Output a deterministic policy $\pi \approx \pi^*$
$\pi(s) = arg \max_{a \in \mathcal{A}_s} Q(s,a) \ \forall s \in \mathcal{S}$

Algorithm 7 The QL+ANN Algorithm.

Set $ei = 1$, n_{ei} N_{ei}, K_α, ϵ_0, α_0, γ, $\mathbf{N}_{layers}$;
Phase 1: Off-Line Training
Initialize Networks $\mathcal{N}_l$ and $t_l = 1$, $l = 1, ...|\mathcal{A}|$ with architecture $\mathbf{N}_{layers}$;
Sample transitions $\mathbf{S}_t, \mathbf{a}_t \rightarrow \mathbf{S}_{t+1}, \mathbf{a}_{t+1}$ and observe rewards R_t, $t = 1, ..., n_{ei}$;
Approximate Q by the MC estimate $Y_t = \sum_{t'=t}^{t+\Phi} \gamma^{t'-t} \cdot R_{t'}$
Train each $\mathcal{N}_l$ using $\{\mathbf{S}_t | t = 1, ..., n_{ei}, \mathbf{a}_t = l\}$ and the estimated Y_t (output);

Phase 2: Learning
while $ei < N_{ei}$ (Episodic Loop) **do**
  Set $t = 1$ initialize state $\mathbf{S}_t$ randomly
  $\epsilon = \epsilon_0 \cdot \tau_\epsilon^{ei}$
  while $t < T$ (episode run) **do**
    if $rand() < 1 - \epsilon$ (exploit)
      $\mathbf{a}_t = arg \max_{l \in \{1,...,|\hat{A}_{g_\varrho}|\}} \hat{q}_l(\mathbf{S}_t | \boldsymbol{\mu}_l)$
    else (explore)
      Select $\mathbf{a}_t$ randomly s.t. $\mathbf{a}_t \in \hat{A}_{g_\varrho}$
    end
    Take action $\mathbf{a}_t$, observe $\mathbf{S}_{t+1}$ and reward R_t
    Update network $\mathcal{N}_{\mathbf{a}_t}$ weights, ϵ and α
    $\boldsymbol{\mu}_{\mathbf{a}_t} \leftarrow \boldsymbol{\mu}_{\mathbf{a}_t} + \alpha_{\mathbf{a}_t} \cdot [R_t + \gamma \cdot \max_{l \in \{1,...,|\mathcal{A}|\}} \hat{q}_l(\mathbf{S}_{t+1} | \boldsymbol{\mu}_l) - \hat{q}_{\mathbf{a}_t}(\mathbf{S}_t | \boldsymbol{\mu}_{\mathbf{a}_t})] \cdot \nabla \hat{q}_{\mathbf{a}_t}(\mathbf{S}_t | \boldsymbol{\mu}_{\mathbf{a}_t})$
    $\alpha_{\mathbf{a}_t} = \alpha_0 \cdot (\frac{1}{1 + K_\alpha \cdot t_{\mathbf{a}_t}})$
    Set $t = t + 1$ and $t_{\mathbf{a}_t} = t_{\mathbf{a}_t} + 1$
  end while
  go to next episode $ei = ei + 1$
end while

Chapter 9

Conclusions and Future Work

In this dissertation, we presented novel computational frameworks for the assessment of the power grid reliability, vulnerability, and resilience by a rigorous quantification of all the relevant uncertainties. Several research questions motivated this work and each chapter presents an attempt to provide answer to those questions: When the available information suffice to answer a basic reliability, vulnerability and resilience question? How to assure computational tractability when advanced uncertainty quantification methods are adopted? What is the role of a vulnerable network topology and operations in the overall power grid security? How to properly select quantitative metrics for reliability, vulnerability and resilience assessment? How to realistically model cascading failures and domino effects? How to model extreme environmental conditions and interaction to the power grid resilience? How these environmental conditions link to components failures? How to learn better policies when gathering new data from a stochastic system-environment?
Those challenging questions have been addressed and novel computational frameworks, dedicated to analyse and quantify the uncertainty of power grid reliability, vulnerability and resilience metrics have been proposed. These models have been embedded within a generalized uncertainty quantification framework with the aim to better cope with situations affected by severe uncertainty, i.e. situations in which data is scarce, limited, qualitative or inconsistent. The proposed frameworks can be employed to assess the effect of extreme weather and cascading failures on the power grid resilience. These can be used also to identify outstanding sources of uncertainty which most heavily prevent a clear, well-defined quantification of security-related power grid metrics and they can be extremely valuable when computational time limitations prevent advanced uncertainty quantification analysis to be performed.

- When the available information suffice to answer a basic reliability, vulnerability and resilience question? How to assure computational tractability when advanced

uncertainty quantification methods are adopted?

In Chapter 4 we discussed limitations of 'exact' probabilistic model which generally requires a lot of data (possibly infinite) to be characterised. Unfortunately, a lack of information always affects engineering analysis and its extent cannot be quantified a priori. In general, the quality of the available information is context and scope-dependent, e.g. different systems performance indicators may react very differently to the same lack of data. The adopted methods provide a simple but effective way to assess a data deficiency by comparing the system reliability bounds (obtained through generalised probabilistic approaches) against single-valued probability indicators (obtained adopting classical probabilistic methods). If the lack of knowledge is not too large, the system reliability will result in relatively narrow bounds and always include the point reliability estimator. In this case, classical approaches will be well-suited to tackle the problem. Conversely, if the lack of data is severe, the reliability bounds will result very wide or, for extreme cases, even non-informative ([0,1]). Combination of pure probabilistic approaches (e.g. Monte Carlo Simulation) and generalised uncertainty quantification approaches (e.g. based on Dempster-Shafer structures and probability boxes), implemented in a common computational framework, are unavoidable tools for the industry which may rely on multiple accurate information qualification approaches. This will aid understanding if the data is of high quality or poor quality, with the aim of designing safer and more reliable systems and components. Two representative case study have been selected to showcase the capability of the adopted methods. Essential information was provided and the quality of the available data assessed.

- What is the role of a vulnerable network topology and operations in the overall power grid security? How does the choice of a specific vulnerability metric affect the result of power grid robustness analysis? What is the uncertainty associated with this selection and what are the effects on the contingency ranking results?

  In Chapter 5 we examined the role of topology and operations in defining vulnerability metrics for power grids. A novel framework for assessing power grids vulnerability has been presented. The vulnerability assessment framework was embedded to advanced uncertainty quantification methods used to quantify the level of epistemic and aleatory uncertainty on the results. Multiple line failures have been analysed and their vulnerability ranked with respect to topology-based metrics, flow-operations-based metrics and accounting for model tolerance imprecision and stochastic loads. Four spectral vulnerability metrics have been computed us-

ing four different weighting factors (taken from literature and newly defined) and used to assess the robustness of a modified version of the IEEE 24 nodes RTS. Different effects of epistemic and aleatory uncertainty on network operational weaknesses (i.e. AC and DC overflow cascading models) and structural vulnerabilities have been discussed and relevant differences in the contingency ranking have been pointed out. Major differences in ranking results are attributable to the different vulnerability metrics rather than to different line weights. In case that only one vulnerability metric have to be selected, the choice of metric must be done with a high degree of care and done so whilst accounting for all the relevant sources of uncertainty which may generate misleading results.

- How to properly select quantitative metrics for reliability, vulnerability and resilience assessment? How to realistically model cascading failures and domino effects? How to model extreme environmental conditions and interaction to the power grid resilience? How these environmental conditions link to components failures?

In Chapters 6 and 7 addressed the above mentioned research questions. In Chapters 6 we presented a generalised uncertainty quantification framework for power grid resilience assessment. The grid stochastic model accounts for interactions between severe weather conditions, transmission line failures and repairing crew working efficiency. One of the issue we faced in the probabilistic model design phase was the need to accurately estimate the model parameters as the data associated with rare weather conditions and failures was often limited or unavailable. Thus, the framework was extended adopting a generalised, non-intrusive uncertainty quantification method. An efficient solution has been proposed employing an Artificial Neural Network to emulate the grid solver. The surrogate accuracy was tested against the original model and pointed out its goodness. The effect of imprecision was tested by propagating nested Credal sets to the Expected-Energy-Not-Supplied. Results pointed out that the precision of the estimator decreases rapidly for increasing imprecision in the model parameters. To conclude, a global sensitivity analysis pointed out which among the wind, lightning and replacement related parameters are key drivers for the uncertainty in the proposed power grid resilience index.

In Chapters 7 variance-based global sensitivity analysis indices, i.e. Sobol's indices, have been computed to reveal which among the uncertainty sources is affecting the most the output variances of a realistic cascading failure model. The Morris screening indices were also obtained and compared to variance based indices to improve confidence in the results and better understand dependencies

between output and factors. This analysis was performed to investigate more in detail some cascading-relevant relationships between input loads, generators costs and line failures. The results pointed out some interesting features of the system. For instance, when the uncertainty in the loads was identified as highly relevant for cascading indicator, it is advisable to consider actions such as allocation of distributed generators or adopt peak-shaving (load variance reduction) control methods. This can be beneficial to reduce the uncertainty in the reliability performance of the network (i.e. reducing its variance). The framework proved to be flexible and computationally quite cheap which is a requirement for its application to more realistic large size power networks. This will be the focus of future analysis.

- How to learn better policies when gathering new data from a stochastic system-environment?

  In order to investigate the learning capability of complex stochastic systems, the conference paper presented in Chapter 8 was developed and future extensions and developments are expected. The framework, based on Reinforcement Learning, was developed for searching optimal decision-making policies for power grid systems affected by uncertain operations and degradation mechanisms. Power grid models can include prognostic health management devices, which are used to inform the agent about the health state of the system components. This information helps to select optimal Operational and Maintenance actions on the system components.
  The SARSA(λ) method was used to solve a control problem for a scale down power grid with renewable and PHM capabilities. The RL results have been compared to the reference Bellman's optimality solution and are in good agreement, although inevitable approximation errors have been observed.
  The framework proved to be flexible and effective in tackling a small but representative case study and future works will test its applicability to more realistic (larger) state-action spaces. To this aim, artificial neural networks will be used in future research work for state-action space regression to scale up to larger grids. This necessary verification for a possible future applicability of the method and can be considered the topic for further research.

9.1 Future Work

During my PhD, I contributed to the development of advanced uncertainty quantification frameworks which can work on top of any computational models. The applicability of this framework to power systems vulnerability, reliability and resilience assessment framework have been investigated but further work is necessary to enable the every-day

use of those powerful techniques. In these years, I also had the chance of working with some of the most recent and advanced machine learning methods such as, for instance, Deep Neural Networks and Reinforcement Learning. The applicability of these methods to complex systems and critical infrastructures have been investigated with the final goal of enhancing the overall reliability, robustness and resilience of the system, while and at the same time reducing operative and maintenance costs.

In this work, I adopted power grids as representative examples of complex systems and critical infrastructures due to their large size, many uncertainties associated, the complex interaction between components and the spatial and dynamic correlations between many uncertain factors/variables. However, the developed techniques are not limited to power grid systems and can find general applicability to a variety of cases, e.g. networked infrastructures such as heat district networks, transportation networks, gas networks, power plants, which are safety-critical systems and suffer from very similar uncertainty-related issues when compared to power grid systems. Uncertainties are ubiquitously affecting simulation models of systems, the available data and external environment often plays a key role (e.g. external weather conditions leading to load variability, failures, etc.). I believe further work has to be devoted to big data and also lack of data issues, such as e.g. data imprecision, poor design, expert judgement, missing information, censored data, tolerance imprecision.

To provide enhanced vulnerability/reliability/resilience models and better simulation tools and control policies, cope with uncertainty is uttermost important. This requires a robust characterization of the input uncertainty and a continuous updating of the model to embed new sources of information and evidence. For the quantification of the uncertainty in the output, advanced methods can be adopted which allow differentiating between what is considered lack of data (thus reducible uncertainty in principle) and what is considered aleatory uncertainty (i.e. inherent variability thus just quantifiable and not reducible). This is necessary to understand better, which are the risks and criticality of the system and networks. However, one of the main drawbacks of those methods is the lack of a common theoretical foundation, although some attempts to unify different mathematical theories have been made, and the limited practical use of these methods in everyday life situations. Limited practical applicability can be probably explained by the limited availability of easy-to-use software which allows the calculation to be performed efficiently and effectively on different cases and systems. Also, some misconception in the interpretation of the result can play a role. Further work should be dedicated to the development of computational tools and this can be considered part of my future research plan.

In classical probabilistic studies, sensitivity analysis methods have been widely applied with the aim of revealing key factors driving the aleatory uncertainty of the

output. Similarly, sensitivity analysis can be proposed to spot key drivers of epistemic uncertainty. However, just a few, although robust methods are nowadays available for this specific task. Novel methods for epistemic space sensitivity analysis should be proposed as this will help developing better decision-making policies and better understanding which factors have to be prioritised for data collection to obtain a substantial reduction in the output uncertainty. Also, non-probabilistic treatment of epistemic uncertainty can be very demanding computationally speaking, thus, methodological developments which allow reducing the computational effort of those demanding analysis will provide a valuable contribution to this research filed.

In my future research plan we can identify the following key elements:

1 **Networks Vulnerability, Reliability and Resilience as a unifying concept** Reliability is a well-defined concept for a power grid and it is used to assess the power grid long-run performance given that known disturbances can affect the system. For instance, the effect of a predefined list of N-k contingencies should be evaluated, where k is small (e.g. k=1,2,3) and defines the number of failed components out of the N available in a non-damaged situation. Reliability can be assessed using classical probabilistic methods and standard reliability indices. With similar aims, but differently for the reliability concept, power network vulnerability assessments try to analyse the impact of low-probability-high-consequence events, such as for instance a large disruption of the grid structure caused by extreme weather conditions or targeted malicious attacks. Vulnerability assessments generally require to evaluate the consequence of the most severe N-k contingencies, where the number of failed components k is relatively high. This type of analysis is generally supported by graph theory and complex network theory which provides a theoretical grounding for the analysis of the grid structure and its underlying graphical model. Differently, the resilience concept is relatively new in the power grids field and a generalised, well-accepted definition still has to be formulated. One example is 'the network ability to withstand high impact low probability events, rapidly recovering and improving operations and structures to mitigate the impact of similar events in the future'. I believe that future research should focus on providing a robust, widely accepted definition of network resilience. Furthermore, comprehensive metrics for the resilience quantification should be defined and account for the following key features:

   1. Include a robust quantification of all the relevant sources of uncertainty, from inherently variable inputs to small sample sizes (e.g. rare events), qualitative, vague and incomplete information (e.g. due to data protection, expert opinions or non-collaborative agents);

2. Distinguish between epistemic and aleatory uncertainty, therefore highlighting how much of the uncertainty on the resilience metric is reducible;
3. Include an evaluation of structural vulnerability and the consequence of low-probability-high-consequence events such as multiple-components outages, domino (network and network-network) cascading failures and account for weather-related effects and interconnected network of networks interactions;
4. Present and cost dimension, i.e. it should be conveniently adopted in cost-based optimisation problems by embedding an economic dimension;
5. Account for the system capacity to learn new optimal policies given that new data is made available (i.e. it should identify a system as more resilient if, given comparable vulnerability, reliability and self-healing performance, it displays a faster and/or better learning curve;

2 **Advanced imprecise probabilistic frameworks for the quantification of uncertainty**

Develop methods for a rigorous and efficient propagation of different forms of uncertainty through computational models was a fundamental task in this PhD work. In general, classical probabilistic methods rely upon a good characterisation of the uncertain factors and this usually requires a considerable body of empirical information to define well e.g. probability distributions, expectation, variance or higher moments. If the data is limited, prior assumptions on the distribution family may be required, which are generally hard to justify and can alter the quality of the available information and the final results of the analysis. More importantly, probability theory provides only a single measure for the uncertainty. This makes the uncertainty analyst unable to grasp how much of the uncertainty is due to inherent variability and to what extent the uncertainty is due to poor data quality (therefore reducible in principle). Advanced methods such as imprecise probabilistic methods allow epistemic uncertainty to be managed without the need for artificial probabilistic assumptions. However, many analysis tools which are based on probability theory do not simply translate to generalised probabilistic frameworks. Further research is needed to develop new tools (e.g. sensitivity analysis, uncertainty propagation, model updating, etc.) for robust and efficient analysis when the information is scarce or limited.

3 **Network-network inter-dependency and networks-environment coupling**

Future grids, also known as the smart grid, should provide reliable power supply at lower achievable cost, mitigating power losses and overall negative environmental impact. The present view on Smart Grid projects generally rates the power grid as the most prominent infrastructure whilst different systems (e.g. transportation and heat district networks) received a relatively limited consideration. In the last years, however, several researchers pointed out the benefits of combining analysis of power grids to different networked systems, which are inevitably linked and interconnected. For instance, integrated analysis of interconnected heat and power networks can provide better insights on systems collective behaviours and interactions. Similar conclusions can be obtained by analysis of the so-called multi-energy-systems (i.e. systems for which electricity, heating, cooling, fuels, transport optimally interact with each other at various levels). More research should be focused on improving and developing stochastic frameworks for combined multi-energy-systems analysis. Uncertain weather conditions deeply link to those critical infrastructures (e.g. renewable sources, extreme weather-induced failures, replacements delays). Their contribution can be extremely relevant for the overall multi-energy-system resilience and thus has to be properly modelled and quantified.

4 Learning capability in a stochastic environment, Reinforcement Learning and Bayesian Model Updating

Reinforcement Learning (RL) has been used in the last decades to solve a variety of realistic control and decision-making issues in the presence of uncertainty, including power grid management and robotics. In the RL paradigm, a controller (i.e. the decision maker) learns from the interaction with the environment (e.g. the grid) by observing states, collecting rewards and selecting actions to maximise the future revenues, considering the aleatory uncertainties in the environment behaviour. The state-action-reward trajectories can be gathered from direct interaction with the real system, from its realistic simulation or by a combination of both. This makes RL suitable to power grid management optimization, as it can cope with both the complexity of the asset and the unavoidable uncertainties related to its operation. In my research plan, I would like to further investigate network systems equipped with learning (e.g. Reinforcement Learning) capabilities. Indeed many are the challenges involved, for instance, the high dimensionality of the system will require some sort of regression function (e.g. Artificial Neural Networks) to be embedded within the RL framework. Also, partial observability of the underlying Markovian Process describing the system dynamic, i.e. the inability to fully characterize the state of the system due to missing information lack

of knowledge of relevant factors, is a challenging aspect. RL combined with regression tools (e.g. ANN) allows solving larger and more realistic decision-making problems in stochastic environments and I am planning to dedicate research time to explore more this topic in the future.

Bibliography

[1] Ebrahim Abiri, Farzan Rashidi, Taher Niknam, and Mohammad Reza Salehi. Optimal pmu placement method for complete topological observability of power system under various contingencies. *International Journal of Electrical Power & Energy Systems*, 61:585 – 593, 2014.

[2] Morteza Aien, Masoud Rashidinejad, and Mahmud Fotuhi-Firuzabad. On possibilistic and probabilistic uncertainty assessment of power flow problem: A review and a new approach. *Renewable and Sustainable Energy Reviews*, 37:883 – 895, 2014.

[3] Diego A. Alvarez and Jorge E. Hurtado. An efficient method for the estimation of structural reliability intervals with random sets, dependence modeling and uncertain inputs. *Computers & Structures*, 142:54 – 63, 2014.

[4] K. Alvehag and L. Soder. A reliability model for distribution systems incorporating seasonal variations in severe weather. *IEEE Transactions on Power Delivery*, 26(2):910–919, April 2011.

[5] N. Amjady and M. Ehsan. Evaluation of power systems reliability by an artificial neural network. *IEEE Transactions on Power Systems*, 14(1):287–292, Feb 1999.

[6] Badia Amrouche and Xavier Le Pivert. Artificial neural network based daily local forecasting for global solar radiation. *Applied Energy*, 130:333 – 341, 2014.

[7] Syed Mohammad Ashraf, Ankur Gupta, Dinesh Kumar Choudhary, and Saikat Chakrabarti. Voltage stability monitoring of power systems using reduced network and artificial neural network. *International Journal of Electrical Power & Energy Systems*, 87:43 – 51, 2017.

[8] Thomas Augustin. Optimal decisions under complex uncertainty - basic notions and a general algorithm for data-based decision making with partial prior knowledge described by interval probability. *Special Issue of ZAMM - Zeitschrift für Angewandte Mathematik und Mechanik*, 84(10–11):1–10, 2004.

[9] Thomas Augustin, Frank P. A. Coolen, Gert de Cooman, and Matthias C. M. Troffaes. *Introduction to Imprecise Probabilities*. Wiley Series in Probability and Statistics, 2014.

[10] Hamid Reza Baghaee, Mojtaba Mirsalim, G.B. Gharehpetian, and H.A. Talebi. Application of RBF neural networks and unscented transformation in probabilistic power-flow of microgrids including correlated wind/PV units and plug-in hybrid electric vehicles. *Simulation Modelling Practice and Theory*, 72:51 – 68, 2017.

[11] L. V. Barboza, G. P. Dimuro, and R. H. S. Reiser. Towards interval analysis of the load uncertainty in power electric systems. In *8th International Conference on Probabilistic Methods Applied to Power Systems*, pages 538–544, Sept 2004.

[12] Russell R. Barton and Martin Meckesheimer. Chapter 18 metamodel-based simulation optimization. In Shane G. Henderson and Barry L. Nelson, editors, *Simulation*, volume 13 of *Handbooks in Operations Research and Management Science*, pages 535 – 574. Elsevier, 2006.

[13] T. Bayes. An essay towards solving a problem in the doctrine of chances. *Philosophical Transactions of the Royal Society of London*, 53:370–418, 1763.

[14] Michael Beer, Scott Ferson, and Vladik Kreinovich. Imprecise probabilities in engineering analyses. *Mechanical Systems and Signal Processing*, 37(1â€“2):4 – 29, 2013.

[15] Richard Bellman. A markovian decision process. *Journal of Mathematics and Mechanics*, 6(5):679–684, 1957.

[16] Yakov Ben-Haim. Robust rationality and decisions under severe uncertainty. *Journal of the Franklin Institute*, 337(2â€“3):171 – 199, 2000.

[17] Dimitri P. Bertsekas and John N. Tsitsiklis. *Neuro-Dynamic Programming*. Athena Scientific, 1st edition, 1996.

[18] J. Bialek, E. Ciapessoni, D. Cirio, E. Cotilla-Sanchez, C. Dent, I. Dobson, P. Henneaux, P. Hines, J. Jardim, S. Miller, M. Panteli, M. Papic, A. Pitto, J. Quiros-Tortos, and D. Wu. Benchmarking and validation of cascading failure analysis tools. *IEEE Transactions on Power Systems*, 31(6):4887–4900, Nov 2016.

[19] Blazhe Gjorgiev Bing Li and Giovanni Sansavini. A genetic algorithm based calibration approach on validating cascading failure analysis. In *IEEE PES general meeting*, July 2017.

[20] Ettore Bompard, Di Wu, and Fei Xue. Structural vulnerability of power systems: A topological approach. *Electric Power Systems Research*, 81(7):1334 – 1340, 2011.

[21] Emanuele Borgonovo and Elmar Plischke. Sensitivity analysis: A review of recent advances. *European Journal of Operational Research*, 248(3):869 – 887, 2016.

[22] Michel Bruneau, Stephanie E. Chang, Ronald T. Eguchi, George C. Lee, Thomas D. O'Rourke, Andrei M. Reinhorn, Masanobu Shinozuka, Kathleen Tierney, William A. Wallace, and Detlof von Winterfeldt. A framework to quantitatively assess and enhance the seismic resilience of communities. *Earthquake Spectra*, 19(4):733–752, 2003.

[23] Francesco Cadini, Gian Luca Agliardi, and Enrico Zio. A modeling and simulation framework for the reliability/availability assessment of a power transmission grid subject to cascading failures under extreme weather conditions. *Applied Energy*, 185, Part 1:267 – 279, 2017.

[24] O. Cangul, R. Rocchetta, E. Patelli, and M. Fahrioglu. Financially optimal solar power sizing and positioning in a power grid. In *2018 IEEE International Energy Conference (ENERGYCON)*, pages 1–6, June 2018.

[25] J.J. Chen, Y.B. Zhuang, Y.Z. Li, P. Wang, Y.L. Zhao, and C.S. Zhang. Risk-aware short term hydro-wind-thermal scheduling using a probability interval optimization model. *Applied Energy*, 189:534 – 554, 2017.

[26] L. Chen, S. Matoba, H. Inabe, and T. Okabe. Surrogate constraint method for optimal power flow. *IEEE Transactions on Power Systems*, 13(3):1084–1089, Aug 1998.

[27] Qiming Chen and J. D. McCalley. Identifying high risk n-k contingencies for online security assessment. *IEEE Transactions on Power Systems*, 20(2):823–834, May 2005.

[28] Jianye Ching and Yi-Chu Chen. Transitional markov chain monte carlo method for bayesian model updating, model class selection, and model averaging. *Journal of engineering mechanics*, 133(7):816–832, 2007.

[29] E. Ciapessoni, D. Cirio, G. Kjølle, S. Massucco, A. Pitto, and M. Sforna. Probabilistic risk-based security assessment of power systems considering incumbent threats and uncertainties. *IEEE Transactions on Smart Grid*, 7(6):2890–2903, Nov 2016.

[30] Michele Compare, Paolo Marelli, Piero Baraldi, and Enrico Zio. A markov decision process framework for optimal operation of monitored multi-state systems. *Proceedings of the Institution of Mechanical Engineers Part O Journal of Risk and Reliability*, 02 2018.

[31] Gabriel J. Correa and JosÃ© M. Yusta. Grid vulnerability analysis based on scale-free graphs versus power flow models. *Electric Power Systems Research*, 101:71 – 79, 2013.

[32] Gabriel J. Correa and JosÃ© M. Yusta. Structural vulnerability in transmission systems: Cases of Colombia and Spain. *Energy Conversion and Management*, 77:408 – 418, 2014.

[33] Noel Cressie. The origins of kriging. *Mathematical Geology*, 22(3):239–252, 1990.

[34] Lucas Cuadra, Sancho Salcedo-Sanz, Javier Del Ser, Silvia JimÃ©nez-FernÃ¡ndez, and Zong Woo Geem. A critical review of robustness in power grids using complex networks concepts. *Energies*, 8(9):9211, 2015.

[35] S. Cvijic and M. Ilic. On limits to the graph-theoretic approaches in the electric power systems. In *2011 North American Power Symposium*, pages 1–6, Aug 2011.

[36] Marco de Angelis, Edoardo Patelli, and Michael Beer. Advanced line sampling for efficient robust reliability analysis. *Structural Safety*, 52, Part B:170 – 182, 2015. Engineering Analyses with Vague and Imprecise Information.

[37] Arthur P. Dempster. *A Generalization of Bayesian Inference*, pages 73–104. Springer Berlin Heidelberg, Berlin, Heidelberg, 2008.

[38] Tao Ding, Yanling Lin, Zhaohong Bie, and Chen Chen. A resilient microgrid formation strategy for load restoration considering master-slave distributed generators and topology reconfiguration. *Applied Energy*, 199:205 – 216, 2017.

[39] I. Dobson, B. A. Carreras, V. E. Lynch, and D. E. Newman. An initial model fo complex dynamics in electric power system blackouts. In *Proceedings of the 34th Annual Hawaii International Conference on System Sciences*, pages 710–718, Jan 2001.

[40] W. Dong and H.C. Shah. Vertex method for computing functions of fuzzy variables. *Fuzzy Sets and Systems*, 24(1):65–78, 1987.

[41] Patelli Edoardo. *COSSAN: A Multidisciplinary Software Suite for Uncertainty Quantification and Risk Management*, pages 1–69. Springer International Publishing, Cham, 2016.

[42] D. Ernst, M. Glavic, F. Capitanescu, and L. Wehenkel. Reinforcement learning versus model predictive control: A comparison on a power system problem. *IEEE Transactions on Systems, Man, and Cybernetics, Part B (Cybernetics)*, 39(2):517–529, April 2009.

[43] SebastiÃ¡n Espinoza, Mathaios Panteli, Pierluigi Mancarella, and Hugh Rudnick. Multi-phase assessment and adaptation of power systems resilience to natural hazards. *Electric Power Systems Research*, 136:352 – 361, 2016.

[44] SebastiÃ¡n Espinoza, Mathaios Panteli, Pierluigi Mancarella, and Hugh Rudnick. Multi-phase assessment and adaptation of power systems resilience to natural hazards. *Electric Power Systems Research*, 136:352 – 361, 2016.

[45] Ernesto Estrada, Naomichi Hatano, and Michele Benzi. The physics of communicability in complex networks. *Physics Reports*, 514(3):89 – 119, 2012. The Physics of Communicability in Complex Networks.

[46] Yi Ping Fang and Enrico Zio. Unsupervised spectral clustering for hierarchical modelling and criticality analysis of complex networks. *Reliability Engineering & System Safety*, 116:64 – 74, 2013.

[47] E. Ferrario, N. Pedroni, and E. Zio. Evaluation of the robustness of critical infrastructures by hierarchical graph representation, clustering and monte carlo simulation. *Reliability Engineering & System Safety*, 155:78 – 96, 2016.

[48] Scott Ferson. Estimating rare-event probabilities without data. In *Proceedings of the 12th International Conference on Structural Safety & Reliability (ICOSSAR)*, page 1, 6-10 , August 2017, Wien, Austria.

[49] Scott Ferson, Vladik Kreinovich, Lev Ginzburg, Davis S Myers, and Kari Sentz. *Constructing probability boxes and Dempster-Shafer structures*, volume 835. Sandia National Laboratories, 2002.

[50] Scott Ferson and W. Troy Tucker. Sensitivity analysis using probability bounding. *Reliability Engineering & System Safety*, 91(10â€“11):1435 – 1442, 2006. The Fourth International Conference on Sensitivity Analysis of Model Output (SAMO 2004)SAMO 2004The Fourth International Conference on Sensitivity Analysis of Model Output (SAMO 2004).

[51] Alberto Fichera, Mattia Frasca, and Rosaria Volpe. Complex networks for the integration of distributed energy systems in urban areas. *Applied Energy*, 193:336 – 345, 2017.

[52] M. Fortier, R. Rebba, P. Koch, A. Karl, M. Broggi, and L. Wright. Challenge in uncertainty quantification. *Bench Mark, The International Magazine for Engineering Designers & Analysis from NAFEMS, Medical Modelling*, pages 40–43, October 2014.

[53] C. Grigg, P. Wong, P. Albrecht, R. Allan, M. Bhavaraju, R. Billinton, Q. Chen, C. Fong, S. Haddad, S. Kuruganty, W. Li, R. Mukerji, D. Patton, N. Rau, D. Reppen, A. Schneider, M. Shahidehpour, and C. Singh. The ieee reliability test system-1996. a report prepared by the reliability test system task force of the application of probability methods subcommittee. *IEEE Transactions on Power Systems*, 14(3):1010–1020, Aug 1999.

[54] Eitan Gross. On the bellman's principle of optimality. *Physica A: Statistical Mechanics and its Applications*, 462:217 – 221, 2016.

[55] W.K. Hastings. Monte carlo sampling methods using markov chains and their applications. *Biometrika*, 82:711–732, 1970.

[56] Paul Hines, Eduardo Cotilla-Sanchez, and Seth Blumsack. Do topological models provide good information about electricity infrastructure vulnerability? *Chaos: An Interdisciplinary Journal of Nonlinear Science*, 20(3):033122, 2010.

[57] Aurélien Hot, Thomas Weisser, and Scott Cogan. An info-gap application to robust design of a prestressed space structure under epistemic uncertainties. *Mechanical Systems and Signal Processing*, 91(Supplement C):1 – 9, 2017.

[58] Guang-Bin Huang, Qin-Yu Zhu, and Chee-Kheong Siew. Extreme learning machine: Theory and applications. *Neurocomputing*, 70(1):489 – 501, 2006. Neural Networks.

[59] IEEE. Guide for electric power distribution reliability indices. *IEEE Std 1366-2003 (Revision of IEEE Std 1366-1998)*, pages 1–50, May 2004.

[60] JGCM: 101: 2008. *Evaluation of measurement data – Supplement 1 to the "Guide to the expression of uncertainty in measurement" – Propagation of distributions using a Monte Carlo method.*

[61] Junchen Jin and Xiaoliang Ma. Hierarchical multi-agent control of traffic lights based on collective learning. *Engineering Applications of Artificial Intelligence*, 68:236 – 248, 2018.

[62] P. Kaplunovich and K. Turitsyn. Fast and reliable screening of n-2 contingencies. *IEEE Transactions on Power Systems*, 31(6):4243–4252, Nov 2016.

[63] Alexander Karlsson, Ronnie Johansson, and Sten F. Andler. *An Empirical Comparison of Bayesian and Credal Set Theory for Discrete State Estimation*, pages 80–89. Springer Berlin Heidelberg, Berlin, Heidelberg, 2010.

[64] Yakup Koç, Martijn Warnier, Piet Van Mieghem, Robert E. Kooij, and Frances M.T. Brazier. The impact of the topology on cascading failures in a

power grid model. *Physica A: Statistical Mechanics and its Applications*, 402:169 – 179, 2014.

[65] Yakup Koç, Martijn Warnier, Piet Van Mieghem, Robert E. Kooij, and Frances M.T. Brazier. A topological investigation of phase transitions of cascading failures in power grids. *Physica A: Statistical Mechanics and its Applications*, 415:273 – 284, 2014.

[66] Deepak Kumar, S.R. Samantaray, and G. Joos. A reliability assessment based graph theoretical approach for feeder routing in power distribution networks including distributed generations. *International Journal of Electrical Power & Energy Systems*, 57:11 – 30, 2014.

[67] P. Kundur, J. Paserba, V. Ajjarapu, G. Andersson, A. Bose, C. Canizares, N. Hatziargyriou, D. Hill, A. Stankovic, C. Taylor, T. Van Cutsem, and V. Vittal. Definition and classification of power system stability IEEE/CIGRE joint task force on stability terms and definitions. *IEEE Transactions on Power Systems*, 19(3):1387–1401, Aug 2004.

[68] Elizaveta Kuznetsova, Yan-Fu Li, Carlos Ruiz, Enrico Zio, Graham Ault, and Keith Bell. Reinforcement learning for microgrid energy management. *Energy*, 59:133 – 146, 2013.

[69] Sarah LaRocca, Jonas Johansson, Henrik Hassel, and Seth Guikema. Topological performance measures as surrogates for physical flow models for risk and vulnerability analysis for electric power systems. *Risk Analysis*, 35(4):608–623, 2015.

[70] Bing Li, G. Sansavini, S. Bolognani, and F. Dörfler. Linear implicit ac pf cascading failure analysis with power system operations and automation. In *2016 IEEE Power and Energy Society General Meeting (PESGM)*, pages 1–5, July 2016.

[71] Guoqing Li, Rufeng Zhang, Tao Jiang, Houhe Chen, Linquan Bai, Hantao Cui, and Xiaojing Li. Optimal dispatch strategy for integrated energy systems with CCHP and wind power. *Applied Energy*, 192:408 – 419, 2017.

[72] H. Li, T. Wei, A. Ren, Q. Zhu, and Y. Wang. Deep reinforcement learning: Framework, applications, and embedded implementations: Invited paper. In *2017 IEEE/ACM International Conference on Computer-Aided Design (ICCAD)*, pages 847–854, Nov 2017.

[73] Y.F. Li, G. Sansavini, and E. Zio. Non-dominated sorting binary differential evolution for the multi-objective optimization of cascading failures protection in complex networks. *Reliability Engineering & System Safety*, 111:195 – 205, 2013.

[74] Chung-Shou Liao, Tsung-Jung Hsieh, Xian-Chang Guo, Jian-Hong Liu, and Chia-Chi Chu. Hybrid search for the optimal pmu placement problem on a power grid. *European Journal of Operational Research*, 243(3):985 – 994, 2015.

[75] Haibin Liu, Rachel A. Davidson, and Tatiyana V. Apanasovich. Spatial generalized linear mixed models of electric power outages due to hurricanes and ice storms. *Reliability Engineering & System Safety*, 93(6):897 – 912, 2008.

[76] I M. Sobol. Sensitivity estimates for nonlinear mathematical models. 2, 01 1990.

[77] Y. Zee Ma and Paul R. La Pointe, editors. *Uncertainty Analysis and Reservoir Modeling*. American Association of Petroleum Geologists, 2011.

[78] W.R Madych and S.A Nelson. Polyharmonic cardinal splines. *Journal of Approximation Theory*, 60(2):141 – 156, 1990.

[79] Magdi S. Mahmoud, Nezar M. Alyazidi, and Mohamed I. Abouheaf. Adaptive intelligent techniques for microgrid control systems: A survey. *International Journal of Electrical Power & Energy Systems*, 90:292 – 305, 2017.

[80] Marzio Marseguerra and Enrico Zio. *Basics of the Monte Carlo Method with Application to System Reliability*. LiLoLe - Verlag GmbH (Publ. Co. Ltd.), Hagen, Germany, 2002. ISBN 3-934447-06-6.

[81] F. Massey. The kolmogorov-smirnov test for goodness of fit. *Journal of the American Statistical Association*, 46(253):68–78., 1951.

[82] MaruÅ¡a Matko, Mojca GolobiÄ, and Branko KontiÄ. Reducing risks to electric power infrastructure due to extreme weather events by means of spatial planning: Case studies from slovenia. *Utilities Policy*, 44:12 – 24, 2017.

[83] M. A. Matos and E. Gouveia. The fuzzy power flow revisited. In *2005 IEEE Russia Power Tech*, pages 1–7, June 2005.

[84] J. McCalley, S. Asgarpoor, L. Bertling, R. Billinion, H. Chao, J. Chen, J. Endrenyi, R. Fletcher, A. Ford, C. Grigg, G. Hamoud, D. Logan, A. P. Meliopoulos, M. Ni, N. Rau, L. Salvaderi, M. Schilling, Y. Schlumberger, A. Schneider, and C. Singh. Probabilistic security assessment for power system operations. In *Power Engineering Society General Meeting, 2004. IEEE*, pages 212–220 Vol.1, June 2004.

[85] J. McCalley, S. Asgarpoor, L. Bertling, R. Billinion, H. Chao, J. Chen, J. Endrenyi, R. Fletcher, A. Ford, C. Grigg, G. Hamoud, D. Logan, A.P. Meliopoulos, M. Ni, N. Rau, L. Salvaderi, M. Schilling, Y. Schlumberger, A. Schneider, and C. Singh. Probabilistic security assessment for power system operations. In

Power Engineering Society General Meeting, 2004. IEEE, pages 212–220 Vol.1, June 2004.

[86] John. J. McKeown, Fabio Stella, and Gary Hall. Some numerical aspects of the training problem for feed-forward neural nets. *Neural Networks*, 10(8):1455 – 1463, 1997.

[87] R. Mena, E. Zio, and M. Hennebel. Sensitivity analysis of a simulation model for evaluating renewable distributed generation on a power network. In *2014 International Conference on Probabilistic Methods Applied to Power Systems (PMAPS)*, pages 1–6, July 2014.

[88] Rodrigo Mena, Martin Hennebel, Yan-Fu Li, Carlos Ruiz, and Enrico Zio. A risk-based simulation and multi-objective optimization framework for the integration of distributed renewable generation and storage. *Renewable and Sustainable Energy Reviews*, 37:778 – 793, 2014.

[89] Rodrigo Mena, Martin Hennebel, Yan-Fu Li, and Enrico Zio. A multi-objective optimization framework for risk-controlled integration of renewable generation into electric power systems. *Energy*, 106:712 – 727, 2016.

[90] Leslie H. Miller. Table of percentage points of kolmogorov statistics. *Journal of the American Statistical Association*, 51(273):111–121, 1956.

[91] D. Moens and D. Vandepitte. A survey of non-probabilistic uncertainty treatment in finite element analysis. *Computer Methods in Applied Mechanics and Engineering*, 194(12-16):1527–1555, 2005.

[92] B. Möller, W. Graf, and M. Beer. Fuzzy structural analysis using α-level optimization. *Computational Mechanics*, 26(6):547–565, 2000.

[93] Ramon Moore and Weldon Lodwick. Interval analysis and fuzzy set theory. *Fuzzy Sets and Systems*, 135(1):5 – 9, 2003.

[94] Amin Moradkhani, Mahmood R. Haghifam, and Mohsen Mohammadzadeh. Failure rate estimation of overhead electric distribution lines considering data deficiency and population variability. *International Transactions on Electrical Energy Systems*, 25(8):1452–1465, 2015. ETEP-13-0523.R2.

[95] Max D. Morris. Factorial sampling plans for preliminary computational experiments. *Technometrics*, 33(2):161–174, 1991.

[96] Dusko P. Nedic, Ian Dobson, Daniel S. Kirschen, Benjamin A. Carreras, and Vickie E. Lynch. Criticality in a cascading failure blackout model. *International Journal of Electrical Power & Energy Systems*, 28(9):627 – 633, 2006. Selection of Papers from 15th Power Systems Computation Conference, 2005.

[97] M. Ni, J.D. McCalley, V. Vittal, and T. Tayyib. Online risk-based security assessment. *IEEE Transactions on Power Systems*, 18(1):258–265, 2003. cited By 243.

[98] J.W. Nims, A.A. El-Keib, and R.E. Smith. Contingency ranking for voltage stability using a genetic algorithm. *Electric Power Systems Research*, 43(1):69–76, 1997.

[99] Council of European Energy Regulators. Ceer benchmarking report 6.1 on the continuity of electricity and gas supply. *C18-EQS-86-03*, 2015.

[100] Min Ouyang, Zhezhe Pan, Liu Hong, and Lijing Zhao. Correlation analysis of different vulnerability metrics on power grids. *Physica A: Statistical Mechanics and its Applications*, 396:204 – 211, 2014.

[101] Giuliano Andrea Pagani and Marco Aiello. From the grid to the smart grid, topologically. *Physica A: Statistical Mechanics and its Applications*, pages –, 2015.

[102] M. Panteli and P. Mancarella. Modeling and evaluating the resilience of critical electrical power infrastructure to extreme weather events. *IEEE Systems Journal*, 11(99):1–10, 2015.

[103] M. Panteli, C. Pickering, S. Wilkinson, R. Dawson, and P. Mancarella. Power system resilience to extreme weather: Fragility modelling, probabilistic impact assessment, and adaptation measures. *IEEE Transactions on Power Systems*, PP(99):1–1, 2017.

[104] Mathaios Panteli and Pierluigi Mancarella. Influence of extreme weather and climate change on the resilience of power systems: Impacts and possible mitigation strategies. *Electric Power Systems Research*, 127:259 – 270, 2015.

[105] M. Papageorgiou, C. Diakaki, V. Dinopoulou, A. Kotsialos, and Yibing Wang. Review of road traffic control strategies. *Proceedings of the IEEE*, 91(12):2043–2067, Dec 2003.

[106] E. Patelli, D.A. Alvarez, M. Broggi, and M. De Angelis. Uncertainty management in multidisciplinary design of critical safety systems. *Journal of Aerospace Information Systems*, 12(1):140–169, 2015.

[107] E. Patelli, M. Broggi, M. Angelis, and M. Beer. Opencossan: An efficient open tool for dealing with epistemic and aleatory uncertainties. In *Vulnerability, Uncertainty, and Risk*, pages 2564–2573–. American Society of Civil Engineers, June 2014.

[108] E. Patelli, S. Tolo, H. G. Williams, J. Sadeghi, R. Rocchetta, M. de Angelis, and M. Broggi. Opencossan 2.0: an efficient computational toolbox for risk, reliability and resilience analysis. In *Proceedings of the joint ICVRAM ISUMA UNCERTAINTIES conference Florianopolis, SC, Brazil*, April 8-11 2018.

[109] Edoardo Patelli, Diego A Alvarez, M Broggi, and Marco de Angelis. An integrated and efficient numerical framework for uncertainty quantification: application to the nasa langley multidisciplinary uncertainty quantification challenge. *16th AIAA Non-Deterministic Approaches Conference (SciTech 2014)*, pages 2014–1501, 2014.

[110] Edoardo Patelli, Diego A Alvarez, Matteo Broggi, and Marco de Angelis. Uncertainty management in multidisciplinary design of critical safety systems. *Journal of Aerospace Information Systems*, 12(1):140–169, 2014.

[111] Edoardo Patelli, Helmut J. Pradlwarter, and Gerhart I. SchuÃ«ller. Global sensitivity of structural variability by random sampling. *Computer Physics Communications*, 181(12):2072 – 2081, 2010.

[112] Guan Sheng Peng and Jun Wu. Optimal network topology for structural robustness based on natural connectivity. *Physica A: Statistical Mechanics and its Applications*, 443:212 – 220, 2016.

[113] W. Pirie. *Spearman Rank Correlation Coefficient*. John Wiley & Sons, Inc., 2004.

[114] Elmar Plischke, Emanuele Borgonovo, and Curtis L. Smith. Global sensitivity measures from given data. *European Journal of Operational Research*, 226(3):536 – 550, 2013.

[115] H.J. Pradlwarter and G.I. Schuëller. The use of kernel densities and confidence intervals to cope with insufficient data in validation experiments. *Computer Methods in Applied Mechanics and Engineering*, 197(29â€“32):2550 – 2560, 2008. Validation Challenge Workshop.

[116] Z. Qiu, Y. Xia, and J. Yang. The static displacement and the stress analysis of structures with bounded uncertainties using the vertex solution theorem. *Computer Methods in Applied Mechanics and Engineering*, 196(49-52):4965–4984, 2007. cited By 56.

[117] A. B. Owen R. Liu. Estimating mean dimensionality of analysis of variance decompositions. *JASA*, 101(474):712–721, 2006.

[118] R. Rocchetta, L. Bellani, M. Compare, E. Zio, and E. Patelli. A reinforcement learning framework for optimal operation and maintenance of power grids. *Applied Energy*, 241:291 – 301, 2019.

[119] R. Rocchetta, M. Broggi, Q. Huchet, and E. Patelli. Likelihoods comparison in a bayesian updating procedure for fatigue crack detection. In *Safety and Reliability of Complex Engineered Systems (ESREL 2015)*, Sep 2015.

[120] R. Rocchetta, M. Broggi, and E. Patelli. Efficent epistemic-aleatory uncertainty quantification: Application to the nafems challenge problem. In *NAFEMS World Congress 2015, At San Diego, CA*, 2015.

[121] R. Rocchetta, M. Compare, E. Patelli, and E. Zio. A reinforcement learning framework for optimisation of power grid operations and maintenance. In *workshop on Reliable Engineering Computing 2018*, 2018.

[122] R. Rocchetta, Y.F. Li, and E. Zio. Risk assessment and risk-cost optimization of distributed power generation systems considering extreme weather conditions. *Reliability Engineering & System Safety*, 136(0):47 – 61, 2015.

[123] R. Rocchetta and E. Patelli. A simulation-based probabilistic risk assessment of electric vehicles control strategies accounting for renewable energy sources. In *13th International Probabilistic Workshop (IPW 2015)*, pages 183–198, Nov 2015.

[124] R Rocchetta and E Patelli. Imprecise probabilistic framework for power grids risk assessment and sensitivity analysis. In *Risk, Reliability and Safety: Innovating Theory and Practice*, pages 2789–2796, 2016.

[125] R. Rocchetta and E. Patelli. Power grid robustness to severe failures: Topological and flow based metrics comparison. In *ECCOMAS Congress 2016 - Proceedings of the 7th European Congress on Computational Methods in Applied Sciences and Engineering*, volume 3, pages 6121–6135, 2016.

[126] R. Rocchetta and E. Patelli. An efficient framework for reliability assessment of power networks installing renewable generators and subject to parametric p-box uncertainty. In *Safety and Reliability. Theory and Applications (ESREL 2017)*. Taylor and Francs, 2017.

[127] R. Rocchetta and E. Patelli. Stochastic analysis and reliability-cost optimization of distributed generators and air source heat pumps. In *2017 2nd International Conference on System Reliability and Safety (ICSRS)*, pages 31–35, Dec 2017.

[128] R. Rocchetta, E. Patelli, M. Broggi, and S. Schewe. Robust probabilistic risk/safety analysis of complex systems and critical infrastructures. *Master of Research in Decision Making Under Risk and Uncertainty, Liverpool University, 2015*, 21, September 2015.

[129] R. Rocchetta, E. Patelli, B. Li, and G. Sansavini. Effect of load-generation variability on power grid cascading failures. In *European Safety and Reliability Conference (ESREL 2018)*, 2018.

[130] Roberto Rocchetta, Matteo Broggi, Quentin Huchet, and Edoardo Patelli. On-line bayesian model updating for structural health monitoring. *Mechanical Systems and Signal Processing*, 103:174 – 195, 2018.

[131] Roberto Rocchetta, Matteo Broggi, and Edoardo Patelli. Do we have enough data? robust reliability via uncertainty quantification. *Applied Mathematical Modelling*, 54(Supplement C):710 – 721, 2018.

[132] Roberto Rocchetta and Edoardo Patelli. Assessment of power grid vulnerabilities accounting for stochastic loads and model imprecision. *International Journal of Electrical Power & Energy Systems*, 98:219 – 232, 2018.

[133] Roberto Rocchetta, Enrico Zio, and Edoardo Patelli. A power-flow emulator approach for resilience assessment of repairable power grids subject to weather-induced failures and data deficiency. *Applied Energy*, 210:339 – 350, 2018.

[134] Andrea Saltelli, Paola Annoni, Ivano Azzini, Francesca Campolongo, Marco Ratto, and Stefano Tarantola. Variance based sensitivity analysis of model output. design and estimator for the total sensitivity index. *Computer Physics Communications*, 181(2):259 – 270, 2010.

[135] G. Sansavini, R. Piccinelli, L.R. Golea, and E. Zio. A stochastic framework for uncertainty analysis in electric power transmission systems with wind generation. *Renewable Energy*, 64:71 – 81, 2014.

[136] G. Shafer. *A Mathematical Theory of Evidence*. Princeton University Press, Princeton, 1976.

[137] Alex S. Silva, Ricardo C. dos Santos, Fernando B. Bottura, and MÃ¡rio Oleskovicz. Development and evaluation of a prototype for remote voltage monitoring based on artificial neural networks. *Engineering Applications of Artificial Intelligence*, 57:50 – 60, 2017.

[138] Bernard W Silverman. *Density estimation for statistics and data analysis*, volume 26. CRC press, 1986.

[139] Satinder Singh, Tommi Jaakkola, Michael L. Littman, and Csaba Szepesvári. Convergence results for single-step on-policy reinforcement-learning algorithms. *Machine Learning*, 38(3):287–308, Mar 2000.

[140] P. M. Subcommittee. Ieee reliability test system. *IEEE Transactions on Power Apparatus and Systems*, PAS-98(6):2047–2054, Nov 1979.

[141] Richard S. Sutton and Andrew G. Barto. Reinforcement learning i: Introduction, 2017.

[142] Richard S. Sutton, Doina Precup, and Satinder Singh. Between mdps and semi-mdps: A framework for temporal abstraction in reinforcement learning. *Artificial Intelligence*, 112(1):181 – 211, 1999.

[143] Angeliki L.A. Syrri and Pierluigi Mancarella. Reliability and risk assessment of post-contingency demand response in smart distribution networks. *Sustainable Energy, Grids and Networks*, 7:1 – 12, 2016.

[144] Csaba Szepesvari. *Algorithms for Reinforcement Learning*. Morgan and Claypool Publishers, 2010.

[145] R. J. Sánchez-García, M. Fennelly, S. Norris, N. Wright, G. Niblo, J. Brodzki, and J. W. Bialek. Hierarchical spectral clustering of power grids. *IEEE Transactions on Power Systems*, 29(5):2229–2237, Sept 2014.

[146] Fulvio Tonon. Using random set theory to propagate epistemic uncertainty through a mechanical system. *Reliability Engineering & System Safety*, 85(1â€“3):169 – 181, 2004. Alternative Representations of Epistemic Uncertainty.

[147] P. Turati, N. Pedroni, and E. Zio. Dimensionality reduction of the resilience model of a critical infrastructure network by means of elementary effects sensitivity analysis. page 457, 2017.

[148] E.R. van Dam and R.E. Kooij. The minimal spectral radius of graphs with a given diameter. *Linear Algebra and its Applications*, 423(2):408 – 419, 2007.

[149] D. Van Hertem, J. Verboomen, K. Purchala, R. Belmans, and W.L. Kling. Usefulness of dc power flow for active power flow analysis with flow controlling devices. In *AC and DC Power Transmission, 2006. ACDC 2006. The 8th IEE International Conference on*, pages 58–62, March 2006.

[150] P. Verma, P. Singh, K.V. George, H.V. Singh, S. Devotta, and R.N. Singh. Uncertainty analysis of transport of water and pesticide in an unsaturated layered soil profile using fuzzy set theory. *Applied Mathematical Modelling*, 33(2):770 – 782, 2009.

[151] J. G. Vlachogiannis and N. D. Hatziargyriou. Reinforcement learning for reactive power control. *IEEE Transactions on Power Systems*, 19(3):1317–1325, Aug 2004.

[152] Fei Wang, Hanchen Xu, Ti Xu, Kangping Li, Miadreza Shafie-khah, and JoÃ£o. P.S. CatalÃ£o. The values of market-based demand response on improving power system reliability under extreme circumstances. *Applied Energy*, 193:220 – 231, 2017.

[153] Robert C. Williamson and Tom Downs. Probabilistic arithmetic. i. numerical methods for calculating convolutions and dependency bounds. *International Journal of Approximate Reasoning*, 4(2):89 – 158, 1990.

[154] P. Wong, P. Albrecht, R. Allan, R. Billinton, Q. Chen, C. Fong, S. Haddad, W. Li, R. Mukerji, D. Patton, A. Schneider, M. Shahidehpour, and C. Singh. The ieee reliability test system-1996. a report prepared by the reliability test system task force of the application of probability methods subcommittee. *Power Systems, IEEE Transactions on*, 14(3):1010–1020, Aug 1999.

[155] Allen J. Wood and Bruce F. Wollenberg. *Power Generation, Operation, and Control, 2nd Edition.* pp. 104, 112, 119, 123-124, 549, ohn Wiley & Sons, NY, Jan 1996.

[156] Fei Xiao. *Risk based multi-objective security control and congestion management.* Retrospective Theses and Dissertations,Paper 15848., 2007.

[157] Fei Xiao and J.D. McCalley. Power system risk assessment and control in a multiobjective framework. *Power Systems, IEEE Transactions on*, 24(1):78–85, Feb 2009.

[158] M. Yang, J. Wang, H. Diao, J. Qi, and X. Han. Interval estimation for conditional failure rates of transmission lines with limited samples. *IEEE Transactions on Smart Grid*, PP(99):1–1, 2016.

[159] R. Yousefian, R. Bhattarai, and S. Kamalasadan. Transient stability enhancement of power grid with integrated wide area control of wind farms and synchronous generators. *IEEE Transactions on Power Systems*, 32(6):4818–4831, Nov 2017.

[160] Haoyu Yuan and Fangxing Li. Hybrid voltage stability assessment VSA for N-1 contingency. *Electric Power Systems Research*, 122:65 – 75, 2015.

[161] Hao Zhang, Hongzhe Dai, Michael Beer, and Wei Wang. Structural reliability analysis on the basis of small samples: An interval quasi-monte carlo method. *Mechanical Systems and Signal Processing*, 37(1â€“2):137 – 151, 2013.

[162] Huai zhi Wang, Gang qiang Li, Gui bin Wang, Jian chun Peng, Hui Jiang, and Yi tao Liu. Deep learning based ensemble approach for probabilistic wind power forecasting. *Applied Energy*, 188:56 – 70, 2017.

[163] Tang Zhong. Graph theory based expert system to form de-icing route in changsha power grid. *International Journal of Electrical Power & Energy Systems*, 43(1):1318 – 1321, 2012.

[164] R. D. Zimmerman, C. E. Murillo-Sanchez, and R. J. Thomas. Matpower: Steady-state operations, planning, and analysis tools for power systems research and education. *IEEE Transactions on Power Systems*, 26(1):12–19, Feb 2011.

[165] R. D. Zimmerman, C. E. Murillo-Sanchez, and R. J. Thomas. Matpower: Steady-state operations, planning, and analysis tools for power systems research and education. *IEEE Transactions on Power Systems*, 26(1):12–19, Feb 2011.

[166] E. Zio. A study of the bootstrap method for estimating the accuracy of artificial neural networks in predicting nuclear transient processes. *IEEE Transactions on Nuclear Science*, 53(3):1460–1478, 2006.

[167] Enrico Zio. Challenges in the vulnerability and risk analysis of critical infrastructures. *Reliability Engineering & System Safety*, 152:137 – 150, 2016.

[168] Boris A. ZÃ¡rate, Juan M. Caicedo, Jianguo Yu, and Paul Ziehl. Bayesian model updating and prognosis of fatigue crack growth. *Engineering Structures*, 45:53 – 61, 2012.